Targeted delivery of nucleic acids to skin using microneedles

A thesis submitted for the degree of

Doctor of Philosophy (PhD)

by

Rosalind Hui Ee Chong, MPharm (Hons)

School of Medicine and

School of Pharmacy and Pharmaceutical Sciences

Cardiff University

November 2013

Declaration

This work has not previously been accepted in substance for any degree and is not concurrently submitted in candidature for any degree.

Signed ……..…… (Rosalind Hui Ee Chong) Date: 01/11/2013

STATEMENT 1

This thesis is being submitted in partial fulfillment of the requirements for the degree of PhD

Signed ……..…… (Rosalind Hui Ee Chong) Date: 01/11/2013

STATEMENT 2

This thesis is the result of my own independent work/investigation, except where otherwise stated. Other sources are acknowledged by explicit references.

Signed ……..…… (Rosalind Hui Ee Chong) Date: 01/11/2013

STATEMENT 3

I hereby give consent for my thesis, if accepted, to be available for photocopying and for inter-library loan, and for the title and summary to be made available to outside organisations.

Signed ……..…… (Rosalind Hui Ee Chong) Date: 01/11/2013

Acknowledgements

First and foremost, I express my greatest gratitude to my supervisors, Professor James Birchall, Dr Sion Coulman and Miss Rachel Hargest for their invaluable insights, advice, encouragement, support and presence throughout my post-graduate studies.

I must thank Dr Roger Kaspar, Dr Christopher Contag, Dr Emilio Gonzalez-Gonzalez, Dr Maria Fernanda Lara and Dr Tycho Speaker for facilitating and contributing to the *in vivo* delivery work at Stanford University and Transderm Inc. in California, USA.

I also thank Cardiff University Central Biotechnology Services (CBS; http://medicine.cf.ac.uk/cbs) for performing RNA extraction from skin samples and the quality of RNA analyses.

I must also thank the Bowel Disease and Research Foundation, Royal College of Surgeons and Cardiff University for co-funding the research.

I deeply appreciate all current and past members of the research group, supervisors and research assistants at the School of Pharmacy, especially Dr Barbara Torrisi, Dr Christopher Martin, Dr Marc Pearton, Dr Baljinder Bains, Dr. Daniela Tatovic, Marion, Xin and Harsha for their support, kind help, guidance and sincere friendship over the last 3 years.

I am greatly indebted to my parents for their love and financial support, without which this experience would not have been possible. I would also like to thank my partner and the rest of my family for their continued support and encouragement.

Last but not least, my utmost respect and appreciation go to every authors and researchers whom I have referenced for their insightful thoughts and work that contributed to the comprehensive writing of this thesis.

Summary

Nucleic acid therapies may have significant potential for effectively treating genetic, hyper-proliferative or malignant skin conditions caused by aberrant gene expression. To be effective, the restorative pDNA or inhibitive siRNA must access the viable skin layers and cells in a stable and functional form, preferably without painful administration. Microneedles are able to penetrate the stratum corneum skin barrier in a minimally invasive manner to allow targeted delivery of therapeutic macromocules. To date, there are limited studies reporting the delivery of nucleic acids, particularly siRNA, to the skin using microneedle devices.

A range of *in vitro*, *ex vivo* and *in vivo* skin models was developed to characterise nucleic acid delivery and functional response. *In vitro* studies conducted in both continuous and primary keratinocyte cultures provided proof-of-concept of efficient and non-toxic cell uptake and gene silencing with siRNA and moderately efficient gene expression with pDNA. In initial studies, pDNA and siRNA was pre-complexed with lipid-based transfection reagents, however, in the case of siRNA, coating of the lipoplexes onto microneedles resulted in a reduction in functionality. Hence, modified self-delivery (sd) siRNA formulations were used in subsequent microneedle delivery experiments.

Stainless steel microneedles coated with reporter pDNA or sd-siRNA were successful in penetrating the stratum corneum barrier of *ex vivo* viable human breast skin. It was difficult to demonstrate equivocally both plasmid gene expression and functional gene silencing in the skin explants, which only remain viable for short periods. Delivery of pDNA and sd-siRNA to *in vivo* mouse skin however, resulted in demonstrable gene expression and gene silencing, particularly evident at the protein level, in an established transgenic reporter mouse skin model.

Overall, these investigations generally support the use of the coated steel microneedles for the simple and potentially self-administrable delivery of nucleic acids to the skin.

Abbreviations

%	Percent
× *g*	Gravitational force (Relative centrifugal force)
°C	Degrees celcius
3D	Three dimensional
$A_{260/280}$	Ratio of absorbance at wavelengths 260 μm and 280 μm
ANOVA	Analysis of variance
APC	Allophycocyanin
bp	Base pair
BCA	Bichichonic acid
BSA	Bovine serum albumin
CBL	Click beetle luciferase
cm	Centimetre
CMV	Cytomegalovirus
CO_2	Carbon dioxide
Cu	Copper
D-PBS	Dulbecco's phosphate buffered saline
Da	Dalton
diH2O	Deionised water
DMEM	Dulbecco's modified eagle medium
DMSO	Dimethyl sulfoxide
DNA	Deoxyribonucleic acid
DNase	Deoxyribonuclease
DOPE	Dioleoylphosphatidyl ethanolamine
DOTAP	1,2-dioleoyl-3-triammonium-tropane
dsRNA	Double stranded RNA
EB	Epidermolysis bullosa
EDM	Electrical discharge machining
EDTA	Ethylenediaminetetraacetic acid
EGF	Epidermal growth factor
EGFP	Enhanced green fluorescent protein
FACS	Fluorescence activated cell sorting

FDA	Food and drug administration
Fe	Iron
FITC	Fluorescein isothiocyanate
g	Gram
GFP	Green fluorescent protein
h	Hour
H&E	Haematoxylin and eosin
HCl	Hydrochloric acid
HKGS	Human Keratinocyte Growth Supplement
hMGFP	Humanised monster green fluorescent protein
K1	Cytokeratin-1
K10	Cytokeratin-10
K14	Cytokeratin-14
K5	Cytokeratin-5
L	Litre
LB	Luria broth
M	Molar
MEAs	Microenhancer arrays
MFI	Mean fluorescent intensity
min	Minute
miRNA	MicroRNA
mL	Millilitre
mRNA	Messenger RNA
MTS	(3-(4,5-dimethylthiazol-2-yl)-5-(3-carboxymethoxyphenyl)-2-(4-sulfophenyl)-2H-tetrazolium
MTT	[3-(4,5-dimethylthiazol-2-yl)-2,5-diphenyltetrazolium bromide]
n	Number of replicates
NaCl	Sodium chloride
NaOH	Sodium hydroxide
nM	NanoMolar
nm	Nanometre
non-sd-siRNA	Non self-delivery siRNA
O_2	Oxygen
OCT	Optical coherence tomography

OCT medium	Optimal cutting temperate medium
p	Value of significance
PAD	Protrusion array device
PBS	Phosphate buffered saline
PCR	Polymerase chain reaction
pDNA	Plasmid DNA
PEI	Polyethylenimine
PFA	Paraformaldehyde
qPCR	Quantitative PCR
RF	Radiofrequency
RISC	RNA-induced silencing complex
RNA	Ribonucleic acid
RNAi	RNA interference
RT	Reverse transcription
s	Second
SD	Standard deviation
sd-siRNA	Self-delivery siRNA
SECosomes	Surfactant-ethanol-cholesterol-osomes
SEM	Standard error of the mean
shRNA	Small hairpin RNA
siRNA	Small interfering RNA
ssRNA	Single stranded RNA
TBE	Tris-borate EDTA
UHW	University Hospital of Wales
UK	United Kingdom
USA	United States of America
UV	Ultraviolet
V	Volt
v/v	Volume per volume
w/v	Weight per volume
w/w	Weight per weight
X-gal	4-bromom-5-chloro-3-indoyl-β-D-galactopyrosanide
µg	microgram
µL	microlitre

μM	microMolar
μm	micrometre

Contents

CHAPTER 1

General introduction

1 General introduction

Genetic manipulation in the skin is appealing because the skin is the largest, outermost organ of the body rendering it highly accessible to local therapeutic interventions. It is possible to specifically treat a confined skin area and monitor the treated region for clinical improvement or adverse effects, which can be surgically removed if necessary. Effective delivery of therapeutic nucleic acid across the cellular membrane is one of the greatest challenges in gene therapy. In the skin, this challenge is further compounded by the presence of the stratum corneum, a non-viable outermost barrier layer. The stratum corneum serves as protective interface between the body and external environment to prevent infiltration of harmful chemicals and pathogens as well as to prevent the loss of endogenous substances. The presence of the skin barrier layer limits transdermal entry of therapeutic substances to high potency molecules of low molecular weight (less than 500 Daltons) and high lipophilicity (log P above 1). Nucleic acids are hydrophilic, negatively charged molecules that pose significant challenge not only for delivery across the skin barrier but also across the negatively charged cellular membrane.

With the advances in gene therapy research, scientists have managed to elucidate candidate genes for a variety of skin conditions. However, effective gene delivery to the skin remains a challenge and the ability to develop a method for efficient and convenient nucleic acid delivery to the skin and skin cells for localised gene expression or gene silencing would provide the opportunity to treat a variety of debilitating genetic, hyper-proliferative or malignant skin conditions. Therefore, the research in this thesis aims to optimise methods for delivering nucleic acid, in particular plasmid DNA (pDNA) and small interfering ribonucleic acid (siRNA), to the skin via a coated steel microneedle system. This introductory chapter describes the structure and function of the human skin, gene therapy with emphasis on cutaneous gene therapy and non-viral cutaneous gene delivery approaches as well as the concept of microneedles as a physical skin disruption method for delivery of nucleic acid and other therapeutic molecules to the skin.

1.1 The human skin

The human skin (Figure 1.1) consists of two layers, the epidermis and the dermis. Below the dermis is a fatty layer of adipose tissue called the subcutaneous layer (McGrath et al. 2004). Other parts of the skin include the hair follicles, which are present in up to 0.1% of the total skin surface (Otberg et al. 2004) and the eccrine sweat glands, which are present in every region of the body in densities of 16 to 530 glands per cm^2 and form pores on the skin surface (Taylor and Machado-Moreira 2013).

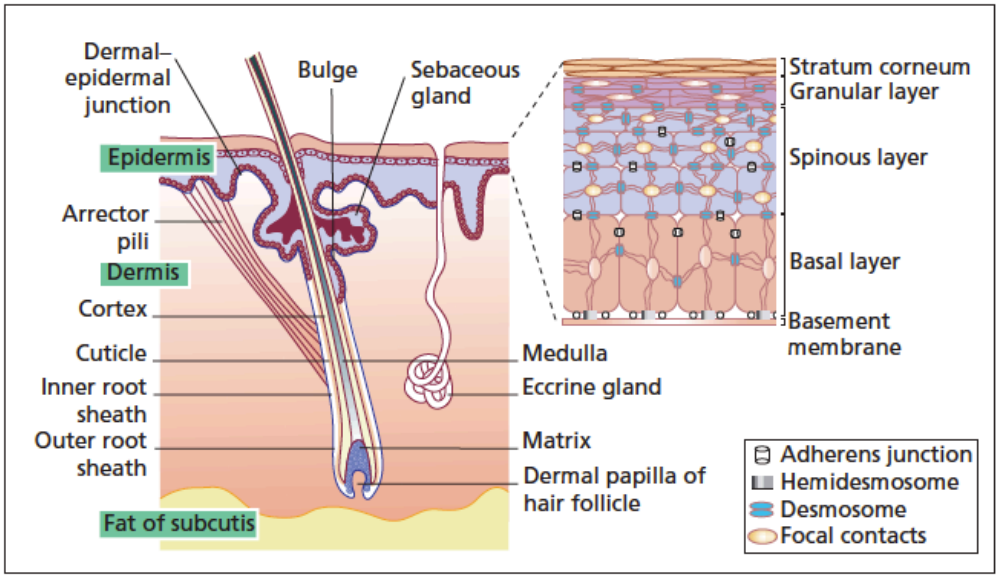

Figure 1.1: A cross-section schematic representation of the skin (taken from McGrath et al. 2004)**.**

1.1.1 Dermis

The dermis is composed of a combination of cell populations including the fibroblasts, mast cell and histiocytes such as monocytes and macrophages. The dermis acts as a supporting matrix and is highly capable of water retention due to presence of macromolecules produced by linkage of polysaccharides and proteins. Two kinds of protein fibres are present in the dermal matrix – collagen, which provides tensile strength, and to a lesser extent elastin. The dermal layer also has a rich blood supply and nerve fibre bundles that provide sensory perception (McGrath et al. 2004).

The skin's blood supply is provided by a deep plexus that lies at the dermal-subcutaneous junction and a superficial papillary plexus that lies at the overlying dermal

tissue, approximately 1 to 1.5 mm from the skin surface. Nutrients and oxygen are supplied to the skin via capillaries that extend from the superficial papillary plexus into the epidermal ridges to form the dermal papillary loops (Braverman 1997). Therefore, skin penetration of sharp objects, such as hypodermic needles into deeper skin layers impacts upon the dermal papillary loops and will inevitably cause skin bleeding (Coulman et al. 2006a).

The cutaneous presence of nerve fibre bundles that are important for the perception of various stimuli, including pain, is believed to be present in the papillary dermis, alongside capillaries and lymphatic vessels. Although there is evidence that nerve fibres also exist in all cells of the viable epidermis, the role of the epidermis as a sensory tissue is still unclear (Boulais and Misery 2008; Hilliges et al. 1995). Penetration of sharp objects of micron dimensions restricted to the uppermost layers of the skin, avoiding the highly innervated dermal tissue, should be pain free or cause negligible pain upon insertion (Coulman et al. 2006a).

1.1.2 Dermal-epidermal junction

The skin epidermis is attached to the dermis through the cutaneous basement membrane, known as the dermal-epidermal junction. The dermal-epidermal junction allows epidermal-dermal adherence through anchoring protein filaments found in the basal cell membrane called hemidesmosomes. The dermal-epidermal junction also has the function of providing the epidermis with mechanical support and being a partial barrier for cells and macromolecules to exchange across the junction (Briggaman and Wheeler 1975; Burgeson and Christiano 1997).

There are multiple protein components that are present in the dermal-epidermal junction and they play an important role in morphogenesis, wound healing and skin remodelling (Burgeson and Christiano 1997). When the proteins are mutated and the dermal-epidermal junction structures have been disrupted, inherited skin disorders and skin diseases manifest (Figure 1.2). An example of such skin diseases is epidermolysis bullosa, which is a group of heritable skin disorders characterised by skin blistering and mucous membranes (Burgeson and Christiano 1997; Christiano and Uitto 1996).

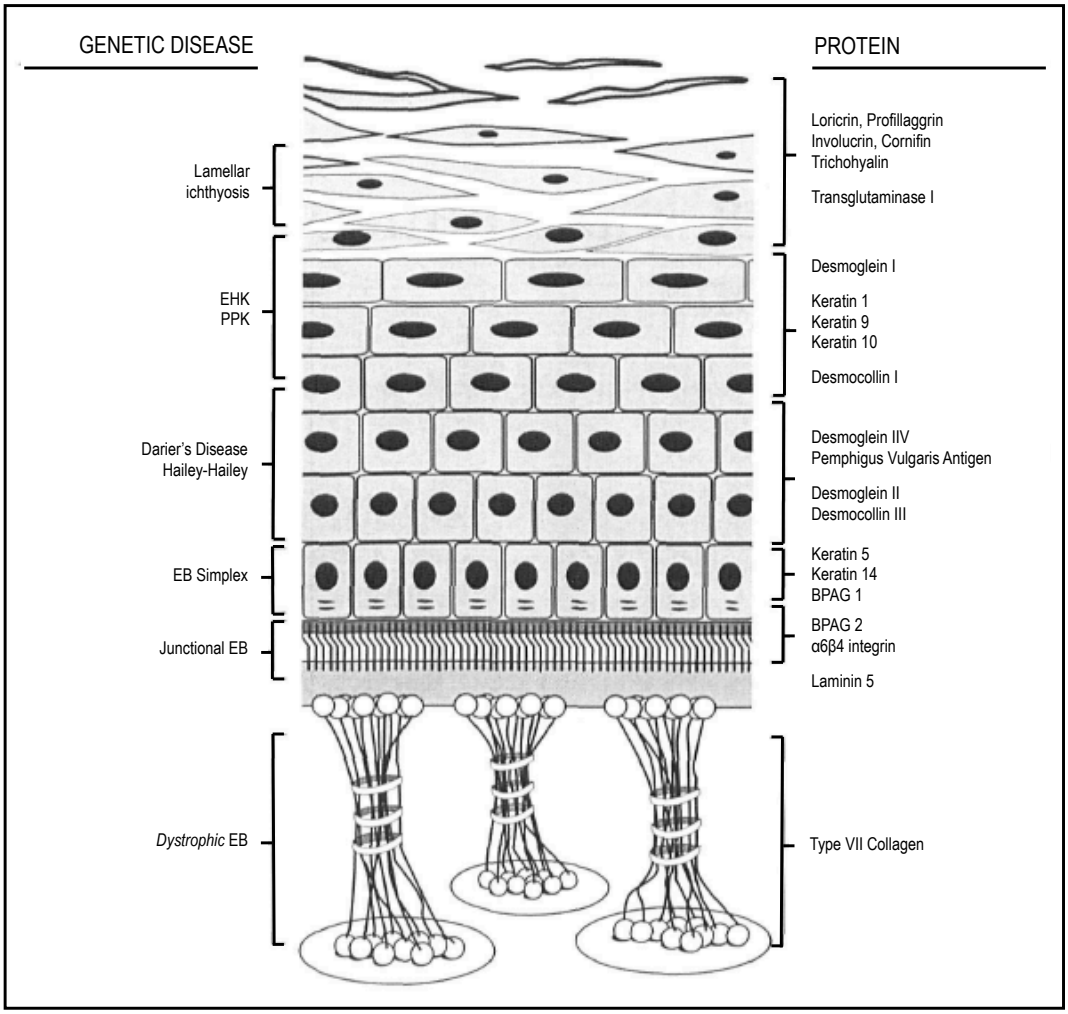

Figure 1.2: A schematic representation of cell layers in the epidermis and dermal-epidermal junction, with indication of genetic diseases that affect the skin layers. The genetic diseases are listed on the left, and the specific gene products, the proteins are listed on the right. (EB: epidermolysis bullosa; EHK: epidermolytic hyperkeratosis; PPK: palmoplantar keratosis; and BPAG: bullous pemphigoid antigen) (taken from Christiano and Uitto 1996)

1.1.3 Epidermis

The human skin epidermis can be considered as a two-layered structure of viable epidermis and stratum corneum. The viable epidermis is a stratified squamous epithelium of approximately 50 to 100 μm in thickness. The viable epidermis, composed mainly of keratinocytes, is formed by cell division in the basal layer and the progressive differentiation and maturation of cells as they migrate towards the stratum corneum (Bickenbach 2001; McGrath et al. 2004; Preat and Dujardin 2001). This results in several distinguishable layers of epidermal cells. The cells in the viable

epidermis are connected intercellularly to adjacent and overlying cells to form a 3-dimensional (3D) lattice through membrane junctions called desmosomes and hemidesmosomes (Eckert 1989; Menon 2002).

Apart from the durable and cohesive keratinocyte cells, several other cell populations exist, such as the melanocyte cells which have a role in ultraviolet protection, the Langerhans' cells which have a role in immunological functions and the Merkel cells, which are important for sensation (Bressler and Bressler 1989; McGrath et al. 2004; Odland 1958). The outermost layer of the skin, the stratum corneum is the main barrier for transdermal drug delivery.

1.1.3.1 Viable epidermis

The aim of the thesis is to optimise delivery of nucleic acids across the stratum corneum and to analyse subsequent transgene expression or gene silencing within the cells in the viable epidermis of the skin. Therefore, it is important to understand the role and characteristics of cells in each sublayer of the epidermis. The stratified epidermis of human skin is divided into four distinct layers: stratum basale, stratum spinosum and stratum granulosum in the viable epidermis, and the non-viable stratum corneum. Keratinocyte cells in the viable epidermis differentiate and mature to ultimately form the stratum corneum (Menon 2002).

The stratum basale is a monolayer of columnar basal cells located immediately above the dermal-epidermal junction, which is anchored to the basement membrane via adhesion molecules known as integrins, forming a specialised adhesion structure known as hemidesmosomes (Sonnenberg et al. 1991). In the epidermis, only cells within the basal layer are actively dividing due to the presence of highly proliferative stem cells and transit amplifying cells (Kaur and Li 2000). These basal cells express the K5 and K14 keratin filaments (Nelson and Sun 1983); differentiate after a number of divisions, detach from the basement membrane and migrate into the suprabasal layers (Kaur and Li 2000). The tissue renewal and barrier function of the skin is maintained by the regeneration of the proliferative basal cells (Fuchs 1990; Kaur and Li 2000). In order to successfully manipulate gene expression, it is crucial to deliver nucleic acid to the appropriate target cells (Mulligan 1993). The major intracellular barrier to gene therapy

is the nuclear envelope (Dean et al. 2005). In dividing cells, such as basal keratinocytes, the nuclear envelope breaks down, allowing nuclear translocation of exogenous nucleic acid for proficient gene expression (Nicolau and Sene 1982). Therefore, cells within the stratum basale should be the prime targets for cutaneous gene delivery

The stratum spinosum is a suprabasal layer located above the stratum basale. This layer of cells has a spiny appearance due to the abundance of desmosomes joining adjacent cells (Eckert 1989). The cells in this layer are non-dividing but metabolically active, synthesising the K1 and K10 keratin filaments (Eichner et al. 1986; Fuchs 1990). Lamellar bodies that are rich in lipids are also present in the stratum spinosum (Menon 2002). When compared to cells in the stratum basale, cells in the stratum spinosum are larger and appear flattened (Eckert 1989; Eichner et al. 1986; Fuchs 1990).

The stratum granulosum consist of cells rich in keratohylin granules that have high electron density and are composed of profillaggrin, K1 and K10 keratin filaments and other proteins (Eckert 1989; Menon 2002). There is an increased synthesis and accumulation of keratin, which contributes to the cells appearing progressively flattened and larger, as they differentiate and migrate towards the upper layers of the viable epidermis (Menon 2002). Even as the stratum granulosum cells undergoes the final keratinisation steps, the cells contain organelles and are metabolically active, rendering this a viable cell layer (Eckert 1989). Lipogenesis is also increased, resulting in the increased presence of lipid rich lamellar bodies that eventually fuse with the cell membrane within the upper layers of cells in the stratum granulosum and their lipid content is eventually released into the extracellular matrix (Eckert 1989; Elias et al. 1988; Menon 2002). Cell viability within the upper layers begins to be compromised when essential cell organelles are degraded prior to the process of cornification to form terminally differentiated cells in the stratum corneum (Menon 2002).

1.1.3.2 Stratum corneum

As the outermost organ of the human body, the main biological function of the skin is as a physical barrier for preventing permeation by harmful chemicals and pathogens as well as for protecting the body from the loss of endogenous materials. This physical barrier is provided by the non-viable outermost layer above the viable epidermis, the

stratum corneum. The stratum corneum is an extremely thin layer (approximately 10 to 20 μm in thickness) consisting keratin-filled corneocyte cells that are without nuclei, anchored in a lipophilic matrix (Bouwstra and Honeywell-Nguyen 2002; Christophers 1971; Naik et al. 2000; Scheuplein and Blank 1971). The corneocyte cells are keratinocytes, which have been terminally differentiated and are constantly being produced, maintained and renewed by the viable epidermis (Bouwstra and Honeywell-Nguyen 2002; Menon and Elias 2001). The stratum corneum cells form a very densely cross-linked protein structure, often described as the 'brick and mortar' structure where the 'bricks' represents corneocyte cells with hydrated keratin that are interspersed within a 'mortar' matrix composed of multiple lipid bilayers of ceramides, fatty acids and cholesterol (Elias 1983, 1988). Although the stratum corneum is non-viable and unable to regenerate, it is in a dynamic state. It is continuously being renewed and maintained by different enzymes and continuous shedding of the outer stratum corneum layers (Elias et al. 1988; Menon and Elias 2001).

1.1.4 Transdermal drug entry routes

The stratum corneum is a sophisticated lipophilic molecular architecture that functions as a physical barrier against permeation of water, penetration of exogenous substances and invasion of microbes and parasites (Menon and Elias 2001). The penetration of drug molecules through the lipid rich matrix surrounding corneocytes in the stratum corneum and in between epidermal cells in the viable epidermis represents the intercellular lipidic route of transdermal delivery (Figure 1.3). Experimental data and modelling of skin penetration by passive diffusion have shown that increasing molecular weight more than 500 Dalton (Da) or decreasing log P below 1 (decreasing lipophilicity) strongly decreases transdermal delivery (Bos and Meinardi 2000; Idson 1971). There are approximately 20 drug molecules approved by the FDA that are currently available in the market as 40 transdermal products (patches) and all the molecules are highly potent and relatively lipophilic with molecular weights below 400 Da (Kim et al. 2012b; van der Maaden et al. 2012). Therefore, macromolecules that are hydrophilic like protein, peptide and nucleic acid do not penetrate the skin through the transdermal pathway.

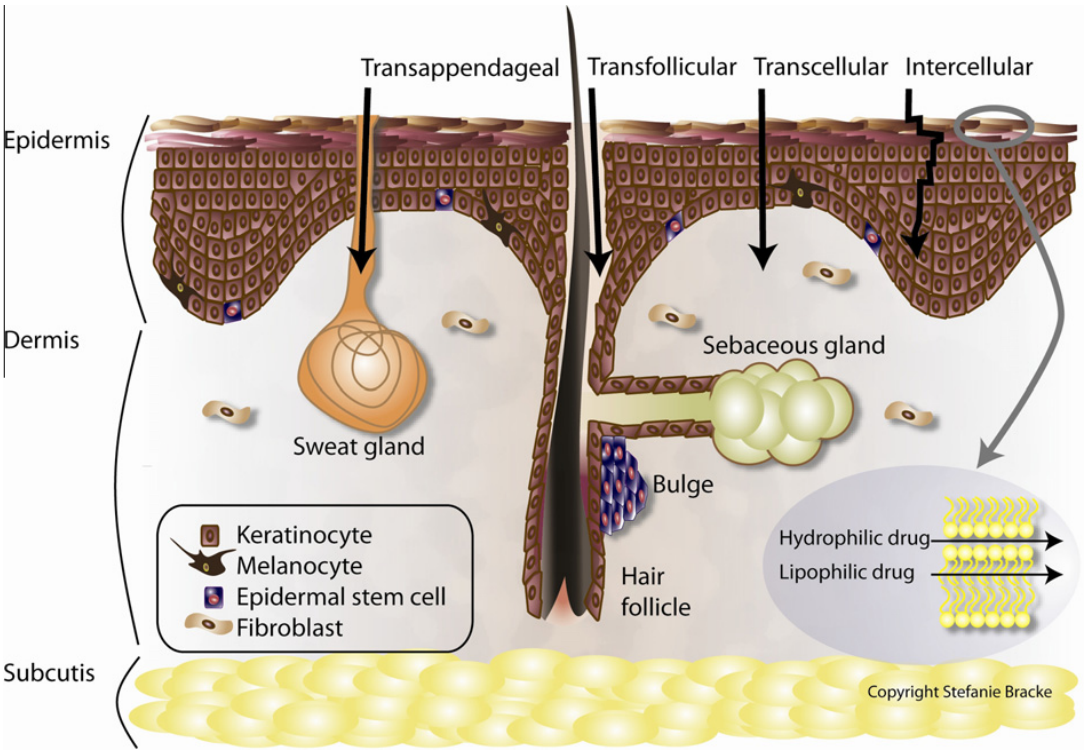

Figure 1.3: A cross-sectional diagram of the skin, with indication of transdermal drug penetration routes including the transappendageal, transfollicular, transcellular and intercellular pathways (taken from Geusens et al. 2011).

Although the stratum corneum constitutes a major barrier to drug penetration, the existence of both sweat glands and the pilosebaceous unit (sebaceous gland and hair follicle) in the skin is believed to provide pathways through which small lipophilic molecules and vesicular systems diffuse into the skin (El Maghraby and Williams 2009; Otberg et al. 2008). The size of the follicular opening in human skin range an average of between 70 and 170 μm in a density of between 14 follicles per cm^2 (calf) and 455 follicles per cm^2 (lateral forehead), depending on gender and ethnicity (Mangelsdorf et al. 2006; Otberg et al. 2004). However, the role of the transappendageal route for transdermal drug delivery is debatable as they are only present in less than 0.1% (Otberg et al. 2004) of total skin surface area (Geusens et al. 2011). A study reported that microparticles applied locally to the skin were found in the hair follicle and the upper layer of stratum corneum but not into the viable epidermis (Lademann et al. 1999). Another route through which drugs may enter is the transcellular route but it is unclear whether the transcellullar pathway contributes to transdermal drug penetration

(Geusens et al. 2011) as the complexity of the skin layers and cell membrane bilayer probably prevents free movement of drugs in and out of cells.

As permeability of drug substances across the stratum corneum of healthy skin is restricted, different strategies have been developed to improve penetration of hydrophilic and large molecules across the skin for both therapeutic and cosmetic purposes (Barry 2001; Brown et al. 2006). Ideally, a drug delivery enhancer should be able to disrupt the stratum corneum in a reversible manner to increase skin permeability for a short period of time and provide an additional force to transfer drugs into and through the skin, whilst avoiding injury to the tissues in the treatment area (Prausnitz and Langer 2008). Based on these strategies, various chemical and physical methods have been developed for use alone or in combination to increase transdermal penetration as reviewed by numerous authors (Barry 2001; Brown et al. 2006; Cross and Roberts 2004; Prausnitz and Langer 2008; Preat and Dujardin 2001). Examples of chemical methods are chemical enhancers such as surfactants and liposomes; and biochemical enhancers such as peptides. Chemical enhancers are able to modify skin barrier by disrupting the stratum corneum and also enhance drug solubility, which improves drug delivery driven by an increase in drug concentration gradient (Prausnitz and Langer 2008; Preat and Dujardin 2001). A few physical methods that have been exploited include iontophoresis, electroporation, cavitational ultrasound, microneedle devices, skin abrasion, skin puncture and perforation, needleless injection, suction ablation and skin stretching (Barry 2001; Brown et al. 2006; Cross and Roberts 2004; Prausnitz and Langer 2008; Preat and Dujardin 2001; Villemejane and Mir 2009). The use of chemical and physical enhancers to improve nucleic acid penetration across the skin and into cells is described further in section 1.3.

1.2 Skin gene therapy

1.2.1 Gene therapy

Morgan and Anderson (1993) defined gene therapy as "the introduction of an exogenous genetic material to the cells of an individual to achieve therapeutic benefit" (Morgan and Anderson 1993). This is a broad definition of gene therapy, which reflects on the potentially wide application of gene therapy including but not exclusive to (i) gene replacement to re-introduce a defective or missing gene, for example in monogenic recessive genetic disorders such cystic fibrosis, (ii) gene therapeutics to introduce gene expressing a protein with specific pharmacological effect, for example growth factors (iii) gene encoding a suicidal enzyme, for example in cancer treatment (iv) DNA vaccination to deliver gene encoding specific antigens to create an adaptive immune response and (v) RNA interference to destruct or inhibit translation of messenger RNA (mRNA), thus preventing expression of targeted genes to curb diseases caused by dominant negative mutation or to combat viral infections (Gong et al. 2005; Preat and Dujardin 2001). Initial research on gene therapy mainly targeted monogenic diseases but it is now apparent that gene therapy may be applied for many polygenic and multi-factorial disorders. Treatment of monogenic disorders is relatively straightforward, where gene therapy can be applied to target the pre-identified defective gene but the choice of gene to treat multi-factorial disease is less apparent.

Apart from identifying a candidate gene, the greatest challenge in gene therapy is perhaps the effective delivery of therapeutic gene into human cells. In order to be effective, a gene delivery system should fulfil certain criteria. Firstly, an ideal gene delivery system should be able to protect the therapeutic nucleic acid against degradation by cellular nucleases. Next, it should be able to efficiently deliver genetic materials into a sufficiently large population of cells within targeted diseased tissues so that a biological effect can be achieved and gene expression is mediated for a sustained period of time. Equally as important, a gene delivery system should be safe and not adversely affect the recipient (Gao et al. 2007; Ledley 1994; Preat and Dujardin 2001). It has been a challenge to identify a gene delivery system that meets all of these criteria.

In order to deliver a gene into a cell, viral and non-viral vectors have been developed over several decades. Viruses represent an ideal model for gene delivery, as they are

capable of carrying out each of the required steps for gene delivery into a cell with high efficiency for long-term gene expression (Gao et al. 2007; Walther and Stein 2000). Examples of medical disorders, which have demonstrated clinical successes using viral gene therapy, include severe combined immunodeficiency (SCID) (Cavazzana-Calvo et al. 2000), haemophilia (Powell et al. 2003) and retinal degeneration (Cideciyan et al. 2013). Several classes of viral gene delivery vectors widely researched and employed are herpex simplex virus, adeno-associated virus, adenovirus, retrovirus and lentivirus (Howarth et al. 2010; Vannucci et al. 2013; Walther and Stein 2000).

One of first gene therapy clinical trials on human involved the use of retroviral vectors to introduce the adenosine deaminase (ADA) gene into the T cells of children with SCID (Blaese et al. 1995). Thereafter, several other viral gene therapy clinical trials were also performed using retroviral vectors but serious adverse reactions such as acute immune response, immunogenicity, and insertional mutagenesis were reported (Hacein-Bey-Abina et al. 2008; Howe et al. 2008; Vannucci et al. 2013). Another example of viral vector that has been tested in human is the adenovirus vectors, whereby it was used for the treatment of ornithine transcarbamylase deficiency. The study reported death of an 18-year old male patient due to multiple organ failure as a result of severe anti-adenovirus vector immune response caused by over-dosage of the viral vector (Raper et al. 2003).

There are advantages and disadvantages to using different classes of viral vectors, which has recently been reviewed by Vannucci et al. (2013) and Howarth et al. (2010). Several viral vectors such as adenovirus, adeno-associated virus and lentiviral vectors are capable of transducing both non-dividing and dividing cells whilst retroviral vectors only transduce dividing cells. Adenovirus and poxvirus vectors are highly immunogenic but adeno-associated viral vectors and retroviral vectors have low immunogenicity. Retroviral and lentiviral vectors cause integration of the vector genome into the host cell genome, enabling stable long-term gene expression in transduced cells whereas adenovirus, herpes simplex virus and poxvirus vectors do not integrate into the host cell genome. The use of viral vectors is also limited by the size of the genetic material that recombinant viruses are able to encode and biosafety concerns associated with the production of viral vectors (Howarth et al. 2010; Vannucci et al. 2013).

The limitations and clinical safety issues associated with viral gene delivery have motivated the development of non-viral gene delivery systems. The advantages of non-viral gene delivery are low toxicity, low immune response and are easy to synthesise but are compromised by being less efficient *in vivo* and having short duration of gene expression (Hart 2010; Wang et al. 2013). Non-viral gene delivery methods can be subdivided into physical and chemical approaches. The physical approaches of non-viral gene delivery involve carrier-free gene delivery of naked nucleic acid and uses a physical force to permeate the cell membrane and aid cellular gene transfer (Gao et al. 2007). Examples of physical approaches include needle injection (Wolff et al. 1990), electroporation (Neumann et al. 1982), gene gun (Yang et al. 1990), ultrasound (Kim et al. 1996) and hydrodynamic delivery (Liu et al. 1999). The chemical approaches of non-viral gene delivery uses synthetic or naturally occurring compounds, including cationic lipid or polymer as carriers to introduce therapeutic genetic materials into cells (De Smedt et al. 2000; Felgner et al. 1987; Zhang et al. 2004; Zhang et al. 2007).

1.2.2 Gene therapy targeted to the skin

Gene therapy in the skin is appealing as the skin has a large and readily accessible surface area that permits nucleic acid access to target cells within the skin (Khavari et al. 2002; Naik et al. 2000; Preat and Dujardin 2001). Nucleic acid delivery to the skin can easily be confined to the affected skin area and the treated region can conveniently be monitored visually or with biopsy. If an unwanted side effect is encountered during treatment, aberrant tissue can be surgically removed (Geusens et al. 2009b; Preat and Dujardin 2001). Nucleic acid has low lipophilicity, therefore systemic absorption of nucleic acid applied to the skin is minimal and should result in negligible systemic toxicity (Fattal and Bochot 2008).

There are several limitations to gene therapy targeted to the skin, which has previously been reviewed by Coulman et al (2006a). Cutaneous gene expression or silencing is usually short-term and inefficient due to continuous epidermal regeneration over 2 to 4 weeks, resulting in gene expression or silencing effect that declines over a 2 to 7 day period (Coulman et al. 2006a; Hengge 2006; Preat and Dujardin 2001). Gene therapy aimed at cells within the skin epidermis (mainly keratinocyte cells) has a limited targeting range, as the viable epidermis is a thin region of cells approximately 50 to 100

μm in thickness below the stratum corneum (Coulman et al. 2006a). Localised delivery of nucleic acids, deposited extracellularly, also necessitates diffusion through tightly packed skin cells to reach enough defective cells for clinically effective genetic correction (Coulman et al. 2006a). Gene delivery systems used for cutaneous gene therapy should avoid stimulation of immune response to be clinically safe for use (Burnett and Rossi 2012; Coulman et al. 2006a). These limitations need to be addressed for safe and effective clinical application of localised cutaneous gene therapy (Burnett and Rossi 2012; Coulman et al. 2006a; Hengge 2006).

Both viral and non-viral vectors have been exploited for nucleic acid delivery to the skin. A number of viral vectors that have been considered for cutaneous gene delivery include adenovirus, adeno-associated virus, retrovirus and lentivirus (Ferrari et al. 2005; Teo et al. 2009). Adenoviral or adeno-associated vectors are highly efficient but gene expression with these vectors is short-term due to rapid loss from continually renewing epidermis and cell division in human skin cells (Ferrari et al. 2005; Teo et al. 2009). Retroviruses have also been investigated for cutaneous gene delivery but the use of retrovirus for gene therapy became undesirable when clinical trials revealed serious adverse effects caused by random retroviral integration into the host chromosome resulting in insertional oncogenesis (Hacein-Bey-Abina et al. 2008; Hacein-Bey-Abina et al. 2003; Howe et al. 2008). Thereafter, significant interest developed in using lentiviral vectors for cutaneous gene therapy. Lentiviral vectors are reportedly efficient and result in long-term expression in both dividing and non-dividing human skin cells (Ferrari et al. 2005; Serrano et al. 2003; Teo et al. 2009) as well as in *in vivo* human skin equivalent grafted onto immunodeficient mice (Woodley et al. 2004). However, safety concerns associated with viral gene delivery have hindered the clinical progress of lentiviral vectors (Vannucci et al. 2013). Due to the risk and disadvantages associated with viral gene delivery, the research in this thesis involves only non-viral approaches for nucleic acid delivery to the skin.

1.2.3 Medical conditions with potential for cutaneous gene therapy

The knowledge on skin pathobiology is ever increasing and recent advancement in molecular genetics is leading to a greater understanding towards the genetic basis of various skin conditions. Localised gene therapy could offer an effective personalised

treatment for many skin conditions including inheritable skin diseases, skin cancer and wound healing. Nucleic acid-based therapy can be used for the treatment of genetic skin disorders that could potentially be corrected through genetic modification.

Monogenic recessive disorders occur as a consequence of gene mutation that results in deletion of a particular gene essential for maintaining normal cell or tissue function. Examples of monogenic recessive disorders that manifest in the skin are xeroderma pigmentosum, simplex and dystrophic forms of epidermolysis bullosa and x-linked ichthyosis (Del Rio et al. 2004; Uitto 2009; Uitto and Richard 2004). Monogenic recessive disorders could potentially be treated by non-viral insertion of a normal copy of gene through pDNA generated using recombinant DNA technologies for expression of the missing gene to restore gene function (Kikuchi et al. 2008).

Dominant negative disorders occur when gene mutation results in aberrant expression of protein that adversely affects the function of its normal counterpart (Carretero et al. 2006; Geusens et al. 2009b). Examples of dominant negative skin disorders are the recessive form of epidermolysis bullosa simplex, the recessive form of dystrophic epidermolysis bullosa, hemidesmosomal epidermolysis bullosa and pachyonychia congenita (Leachman et al. 2008; Uitto 2009; Uitto and Richard 2004). Dominant negative disorders can be treated by supressing the mutated gene through RNA interference (RNAi) or by increasing the expression of the normal gene in a controlled manner to counteract the activity of the overexpressed counterpart (Carretero et al. 2006). Other skin conditions caused by aberrant gene expression which may be treated with gene silencing therapy include allergic skin diseases (Inoue et al. 2007; Ishimoto et al. 2008; Ritprajak et al. 2008), alopecia (Nakamura et al. 2008), skin malignancy (Hoeflich et al. 2006; Matsumoto et al. 2006; Nakai et al. 2010; Nakai et al. 2007; Sharma et al. 2005; Tao et al. 2005; Tran et al. 2008), psoriasis (Funding et al. 2006; Jakobsen et al. 2009; Johansen et al. 2006), hyperpigmentation (Kim et al. 2012a), and wound healing (Thanik et al. 2007).

The skin also has great potential as a target for DNA immunisation due to the presence of Langerhans cells in the viable epidermis and dermal dendritic cells that could acquire antigens expressed in cells after DNA vaccination and then migrate to the regional lymph node area to stimulate immune responses (Falo Jr 1999; Larregina and Falo

2005; Peachman et al. 2003; Tuting et al. 1998). DNA vaccines can be delivered to the skin in the form of pDNA encoding for exogenous antigenic protein, mainly to keratinocyte cells in the epidermis (Larregina and Falo 2005). Transgenic antigens that are subsequently expressed are taken up by neighbouring Langerhans cells to stimulate an immune response (Larregina and Falo 2005).

1.2.4 RNA interference (RNAi)

In comparison with gene therapy that leads to gene expression, gene silencing is a relatively new concept, having been introduced only 15 years ago (Fire et al. 1998). In a Nobel prize winning discovery, it was found that double-stranded RNA (dsRNA) was considerably more effective than single stranded RNA (ssRNA) at inducing RNAi in *Caenorhabditis elegans* (a nematode) (Fire et al. 1998). However, dsRNA used in initial studies were long (more than 30 nucleotides), which renders them potent inducers of an interferon response in more complex organisms (Stark et al. 1998), therefore preventing the translation of the initial results into human. Shortly thereafter, small interfering RNA (siRNA) described as 'small antisense RNA' was discovered (Hamilton and Baulcombe 1999). The first successful introduction of synthetic siRNA to induce RNAi in mammalian cell was reported in a paper published in 2001, whereby 21-nucleotide synthetic siRNA complexed to lipid based transfection reagents was delivered to human embryonic kidney and HeLa cells (Elbashir et al. 2001a).

This initial sequence of discoveries caused an increased interest in RNAi research and there are countless publications that have described the potential of siRNA *in vitro* and *in vivo* (Grimm 2009). Following the first successful delivery of siRNA to mice *in vivo* (McCaffrey et al. 2002) and numerous other pre-clinical studies in small animals, RNAi therapies, mainly with siRNAs have entered Phase I, II and III clinical trials for diseases such as wet age-related macular degeneration, diabetic macular oedema, intraocular hypertension, respiratory syncytial virus infection, familial adenomatous polyposis, hepatitis C, acquired immune deficiency syndrome (AIDS), solid tumours and pachyonychia congenita (Burnett and Rossi 2012; Castanotto and Rossi 2009). Results from the clinical trials (Table 1.1) were mixed and the clinical progress of the RNA-based therapies is impeded by issues such as efficiency and specificity of delivery, stability of the RNA drug, prolonged duration of drug action, off target toxicity,

immunogenicity (Burnett and Rossi 2012). These issues could be overcomed by refining the biochemical properties of siRNA and its delivery vectors for more efficient and tissue-specific delivery (Burnett and Rossi 2012).

Table 1.1: An overview of anti-miRNA and siRNA/shRNA therapeutics in clinical trials (taken from Burnett and Rossi 2012).

Disease	Drug	Delivery route	Target	Vehicle	Company	Phase	Status
Advanced solid cancer	Atu027	IV	PKN3	siRNA-lipoplex	Silence Therapeutics	I	Ongoing
AKI and DGF	I5NP	IV	P53	Naked siRNA	Quark Pharma	II	Ongoing
AMD	AGN-745	IVT	VEGF-R1	Naked siRNA	Allergan/Sirna	II	Terminated
AMD/DME	Bevasiranib	IVT	VEGF	Naked siRNA	Opko Health	III	Terminated
AMD/DME	PF-655	IVT	RTP801	Naked siRNA	Quark/Pfizer	II	Completed
Asthma	Excellair	Inhalation	Syk kinase	unknown	ZaBeCor	II	Ongoing
CML	Bcr-Abl siRNA	IV	Bcr-Abl	Anionic liposome	University Duisburg	I	Completed
Dry eye syndrome	SYL1001	Ophthalmic drops	TRPV1	Naked siRNA	Sylentis	I	Ongoing
FAP/colon cancer	CEQ508	Oral	Beta catenin	tkRNAi in E. Coli	Marina Biotech	I	Ongoing
HCV	SPC3649 (LNA)	SC	mir-122	Naked LNA	Santaris	IIa	Ongoing
HIV	Tat/Rev shRNA	Ex vivo transplant	HIV Tat and Rev	Lentivirus	City of Hope/Benitec	0	Ongoing
Hypercholesterolemia	TKM-ApoB	IV	Apo B	SNALP	Tekmira	I	Terminated
Intraocular pressure	SYL040012	Ophthalmic drops	ADRB2	Naked siRNA	Sylentis	II	Ongoing
Metastatic melanoma	iPsiRNA	Ex vivo intradermal injection	LMP2, LMP7, MECL1	Transfection	Duke University	I	Ongoing
NAION	QPI-1007	IVT	Caspase 2	Naked siRNA	Quark Pharma	I	Ongoing
Pachyonychia congenita	TD101	Intralesional injection	KRT6A(N171K)	Naked siRNA	TransDerm/IPCC	Ib	Completed
PDAC	siG12D LODER	EUS biopsy needle	KRASG12D	LODER polymer	Silenseed Ltd	I	Ongoing
RSV	ALN-RSV01	Nebulisation or intranasal	RSV Nucleocapsid	Naked siRNA	Alnylam/Cubist	IIb	Ongoing
Solid tumours	TKM-PKL1	IV	PLK1	SNALP	Tekmira	I	Ongoing
Solid tumours	ALN-VSP02	IV	KSP and VEGF	SNALP	Alnylam/Tekmira	I	Completed
Solid tumours	CALAA-01	IV	RRM2	Cyclodextrin nanoparticle, TF and PEG	Calando Pharma	I	Ongoing
Solid tumours	FANG vaccine	Ex vivo IV	Furin and GM-CSF	Electroporation	Gradalis Inc.	II	Ongoing
TTR-mediated amyloidosis (ATTR)	ALN-TTR01	IV	TTR	SNALP	Alnylam	I	Ongoing

AKI = acute kidney injury; DGF = delayed graft function; AMD = age-related macular degeneration; DME = diabetic macular oedema; CML = chronic myeloid leukaemia; FAP = familial adenomatous polyposis; HCV = hepatitis C virus; HIV = human immunodeficiency virus; NAION = optic nerve-related visual loss; PDAC = pancreatic ductal adenocarcinoma; RSV = respiratory syncytial virus; TTR = transthyretin; IV = intravenous; IVT = intravitreal; SC = subcutaneous; EUS = endoscopic ultrasound; PKN3 = protein kinase N3; VEGF = vascular endothelial growth factor; VEGF-R1 = vascular endothelial growth factor receptor-1; RTP801 = proangiogenic factor; Syk = spleen tyrosine kinase; Bcr-Abl = fusion oncogene expressed in CML; TRPV1 = transient receptor potential cation channel subfamily V member 1; mir-122 = microRNA-122; ADRB2 = beta-2 adrenergic receptor; LMP = immunoproteasome subunit; KRT6A = keratin 6a gene; KRASG12D = KRAS oncogene; PLK1 = polo-like kinase 1; KSP = kinesin spindle protein; RRM2 = ribonucleotide reductase; GM-CSF = granulocyte-macrophage colony stimulating factor; tkRNAi = TransKingdom RNA interference; LNA = locked nucleic acid; SNALP = stable nucleic acid lipid particle; LODER = Local Drug EluteR; TF = transferrin; PEG = polyethylene glycol.

1.2.4.1 Small double stranded RNAs

siRNAs or silencing RNAs are a group of small dsRNA molecules that is usually 20 – 25 nucleotides in length and are designed with specific sequences that is homologous to sequences in the target mRNA. siRNA has many biological functions and its most notable function is in the RNA interference (RNAi) pathway (Figure 1.4). Through RNAi, siRNA interferes with the expression of a target gene to cause silencing of gene expression (Elbashir et al. 2001c; Hamilton and Baulcombe 1999; Hammond et al. 2000; Pei and Tuschl 2006; Zamore et al. 2000).

Besides siRNA, another class of small RNA molecules that acts through similar RNAi pathway is the microRNA (miRNA). Whilst naturally occurring siRNAs are generated by degradation of long dsRNAs, miRNAs are endogenous RNA molecules that do not code for protein and are derived from hairpin shaped precursors (Bartel 2004). The production of miRNAs are encoded for by genes in the organism genome (Bartel 2004). Both siRNA and miRNA are of similar nucleotide length but siRNA sequences are fully complementary to their target mRNAs leading to target mRNA cleavage and degradation whereas miRNAs sequences are not fully complementary to their target mRNA recognition sites and downregulate gene expression either by inducing degradation of target mRNA or translational inhibition (Bartel 2004; Shabalina and Koonin 2008).

To exogenously exploit the miRNA machinery, small hairpin RNA (shRNA) can be produced by cellular gene expression machinery using DNA vector-based technology. shRNA can be delivered to cells through transfection of pDNA construct that encodes for shRNA or infection of cells with viral vectors for stable integration of exogenous DNA into the host genome (Moore et al. 2010; Rao et al. 2009; Yu et al. 2002). Following transcription in the nucleus, shRNA sequence is exported to the cell cytoplasm, recognised by the enzyme Dicer and then processed into siRNA duplexes (Lund et al. 2004; Moore et al. 2010; Rao et al. 2009).

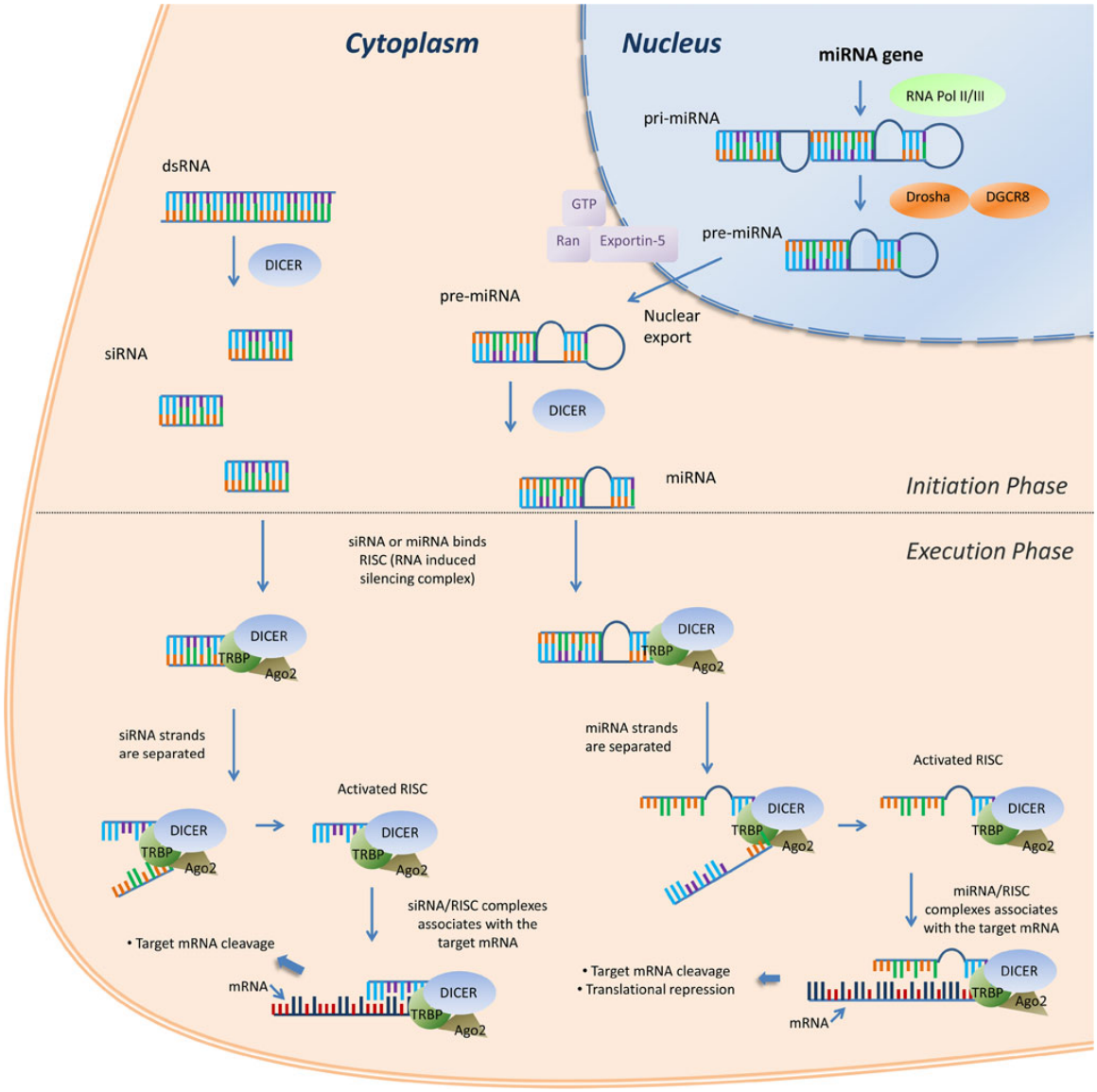

Figure 1.4: **RNA interference pathway (taken from Vicentini et al. 2013).** The initiation phase involves production of effector molecules such as siRNA and miRNA. In the nucleus, miRNA synthesis occurs, whereby the miRNA gene is transcripted by RNA Pol II/III to form primary miRNA (pri-miRNA). pri-miRNA is then processed into miRNA precursor (pre-miRNA) by Drosha and DGCR8, and then exported to the cytoplasm by exportin-5. In the cytoplasm, an enzyme called Dicer fragments dsRNA and pre-miRNA into siRNA and miRNA, respectively. The execution phase involves loading of effector molecules into RISC protein complexes to promote gene silencing. RISC is composed of Dicer, TRBP and Ago2. siRNA or miRNA strands are unravelled and the guide strand is bound to the RISC complex, which activates the complex to search for the target mRNA. Association of the active RISC complex with target mRNA promotes either mRNA degradation or translational inhibition.

1.2.4.2 RNAi pathway and mechanism of action

The RNAi pathway is depicted and explained in Figure 1.4. With specific reference to siRNA, RNAi is initiated when an enzyme called Dicer (ribonuclease III) (Bernstein et al. 2001) recognises long dsRNA molecules and fragments the molecule into small RNA duplexes of approximately 20 nucleotides in length (Hamilton and Baulcombe 1999; Zamore et al. 2000). The short RNA duplexes, also known as small interfering RNA (siRNA) are then unravelled into single stranded RNAs (ssRNAs) of the guide strand and passenger strand. A protein complex known as the RNA-induced silencing complex (RISC) is preferentially loaded with the guide strand to form an active RISC complex and the passenger strand is degraded. The active RISC complex is capable of finding potential target mRNA that has a sequence homologous to the guide ssRNA (Hammond et al. 2000) and then cleaves the target mRNA (Meister and Tuschl 2004) with an endonuclease or the ‘slicer’, which has been identified as Argonaute protein found in the RISC complex (Hammond et al. 2001; Meister et al. 2004).

1.3 Non-viral cutaneous gene delivery systems

Localised delivery of nucleic acid to the skin faces two major barriers, the skin's physical barrier, the stratum corneum and the intracellular barrier of the target cell. For therapeutic nucleic acid to effectively express or silence a gene, it has to be efficiently delivered to the cell cytoplasm, in the case of siRNA for gene silencing (Tseng et al. 2009; Wang et al. 2010), or the cell nucleus, in the case of pDNA for gene expression (Capecchi 1980; James and Giorgio 2000). Treatment of inherited skin disorders requires lifelong integration of a corrective nucleic acid sequence in the form of DNA or siRNA. However, due to the continuous differentiation and desquamation of epidermal keratinocyte cells, longevity of gene expression or silencing can only last for as long as the epidermal turnover rate which is two to four weeks. Targeting of stem cells within the epidermis provides the possibility of long-term gene correction as transgenes can be selectively and stably integrated into permanently residing epidermal stem cells (Alonso and Fuchs 2003).

Current cutaneous gene delivery approaches can be classified as *ex vivo* and *in vivo* gene delivery (Kikuchi et al. 2008). *Ex vivo* gene delivery involves removing a skin biopsy from a patient to harvest cells for *in vitro* culture, inserting correctional gene into those cultured cells and then subsequent re-grafting the genetically modified cells on to the same patient (Ferrari et al. 2005). *In vitro* gene insertion is efficient and large areas of skin can be treated with the *ex vivo* approach of gene delivery (Coulman et al. 2006a; Ferrari et al. 2005; Kikuchi et al. 2008). However, *ex vivo* gene therapy is expensive, time-consuming and technically challenging to perform in clinical practice (Coulman et al. 2006b). This approach may be more suited for skin conditions like epidermolysis bullosa, where the condition manifests in large skin areas (Dellambra et al. 2000). On the other hand, *in vivo* gene transfer is generally less complicated and more direct as it delivers therapeutic gene directly to the patient's skin. However, this approach may be restricted to skin disorders that manifest in isolated skin areas (Choate and Khavari 1997). Various viral and non-viral vectors and physical methods have been developed to improve *in vivo* targeting of skin cells and to assist *in vivo* and *in vitro* cellular uptake of exogenous genetic materials, however only non-viral approaches will be discussed in this thesis.

1.3.1 Non-viral vectors for cellular delivery of nucleic acid

Nucleic acids are negatively charged hydrophilic macromolecules that do not permeate negatively charged cellular membrane efficiently (Singer and Nicolson 1972; Watson and Crick 1953). In fact, *in vitro* cell treatment with naked DNA or unmodified siRNA has low delivery efficiency resulting in almost undetectable transgene expression or gene silencing (Bains et al. 2010; Basner-Tschakarjan et al. 2004; Elbashir et al. 2002). In order to facilitate cellular gene transfer, a variety of non-viral vectors have been developed. Most vectors used for non-viral gene delivery can be broadly classified as cationic lipids or cationic polymers.

1.3.1.1 Cationic lipid/DNA complexes (lipoplexes)

Cationic lipid-based vectors for nucleic acid delivery are well characterised and comprehensively reviewed in literature (Elouahabi and Ruysschaert 2005; Lv et al. 2006; Ma et al. 2007; Niculescu-Duvaz et al. 2003; Pedroso de Lima et al. 2003; Rao 2010; Rehman et al. 2013; Spagnou et al. 2004; Tranchant et al. 2004; Tseng et al. 2009; Wasungu and Hoekstra 2006; Zhang et al. 2004; Zhi et al. 2010; Zuhorn et al. 2007). A broad range of cationic lipids with different structures has been developed over the years for a wide range of applications. The chemical components that are common to all cationic lipids are the positively charged headgroup and hydrophobic domains with two aliphatic chains or cholesterol-type group (Niculescu-Duvaz et al. 2003).

When preformed cationic lipids and nucleic acids are mixed in an aqueous solution, a spontaneous process occurs, which condenses nucleic acid with extensive rearrangement to produces small lipoplexes (Caracciolo et al. 2005; Pedroso de Lima et al. 2003). The formation of a lipoplex is driven by electrostatic interactions between the positively charged cationic lipid headgroups and the negatively charged phosphate DNA backbones (Elouahabi and Ruysschaert 2005). The use of lipoplex formulations for nucleic acid delivery is advantageous over naked DNA as condensation of nucleic acid in lipoplexes protects nucleic acid from extracellular and intracellular nuclease degradation and improves interaction with the cellular membrane for more efficient cellular uptake through endocytosis (Gershon et al. 1993; Niculescu-Duvaz et al. 2003; Xu et al. 1999).

Some cationic liposomal formulations incorporate “helper lipid” with non-charged phospholipids like dioleoylphosphatidyl ethanolamine (DOPE) or cholesterol to form liposomes with improved transfection efficiencies (Gao et al. 2007; Ramezani et al. 2009; Xu and Anchordoquy 2008). The analogues of DOPE and other phospholipids have been shown to facilitate lipoplex interaction with cell membranes and aid nucleic acid escape from endosomes (Felgner et al. 1994; Hoekstra et al. 2007; Zuhorn et al. 2007). Liposomal formulations can also be formulated with cholesterol to form a very stable bilayer that provides rigidity and stability to the lipoplexes in the presence of serum, which usually causes lipoplex disintegration (Templeton et al. 1997; Zhang and Anchordoquy 2004). It has been said that the presence of cholesterol domains in lipoplexes reduces serum protein binding and improves membrane interaction to result in enhanced transfection efficiency (Xu and Anchordoquy 2008).

Many of the more efficient cationic transfection reagents have become commercially available such as Lipofectamine™ by Invitrogen, DOTAP and FuGENE® distributed by Roche, and Escort™ by Sigma-Aldrich (Pedroso de Lima et al. 2003). Furthermore, some of the liposomal formulations have also been employed in clinical trials for gene therapy of cancer and other genetic disorders (Zhi et al. 2010). Lipid-based nucleic acid complex formulations are potentially convenient and inexpensive vectors that have demonstrated limited success in the delivery of exogenous genetic material across the stratum corneum barrier without significant skin disruption (Geusens et al. 2011; Geusens et al. 2010; Raghavachari and Fahl 2002).

Although lipoplexes have conventionally been thought to cause less immunologic reaction than viral vectors, there have been reports of toxicity associated with gene delivery by lipoplexes (Lv et al. 2006). Some of these have proved more toxic than others and toxicity is dependant on the cationic lipid structure and dose used both *in vivo* (Ruiz et al. 2001; Scheule et al. 1997; Song et al. 1997) and *in vitro* (Fischer et al. 2003). In an *in vivo* experiment, mice that were treated with intravenous injection of N-(2,3-dioleoyloxy)propyl-N,N,N-trimethylammonium chloride (DOTMA) and 1,2-dioleoyloxy-3-trimethylammonium propane (DOTAP) lipoplexes at a dose higher than 50 μg DNA per mouse or higher cationic to lipid ratio of 48:1 nmol:μg with 25 μg DNA per mouse have suffered from liver inflammation that resulted in animal death 20 to 48 h after injection (Song et al. 1997). In mice (Scheule et al. 1997) and human (Ruiz et al.

2001) studies investigating *in vivo* pulmonary delivery, pDNA lipoplex reportedly caused pulmonary inflammation, increased expression of pro-inflammatory cytokines and short-term increase in inflammatory cells (Ruiz et al. 2001; Scheule et al. 1997). The studies have also demonstrated that the immune response was mainly caused by lipoplexes, with administration of individual components of the lipoplex formulation having minimal or undetectable effect, suggesting that combination of cationic lipid and DNA were synergistic in causing toxicity (Ruiz et al. 2001; Scheule et al. 1997). The studies suggested that improvement in cationic liposomal formulation that could target tissue and cells with specificity at a low dose is required (Ruiz et al. 2001; Scheule et al. 1997) before gene delivery with lipoplex formulation could progress to widespread clinical use (Rehman et al. 2013).

1.3.1.2 Cationic polymer/DNA complexes (polyplexes)

Similar to cationic lipids, synthetic and naturally occurring polymers have been widely used as carriers for gene delivery (Gary et al. 2007; Lungwitz et al. 2005; Luten et al. 2008; Zhang et al. 2004; Zhang et al. 2007). Over the years, numerous cationic polymers have been explored and synthesised for *in vitro* and *in vivo* gene delivery, including polyethylenimine (PEI) (Boussif et al. 1995; Chemin et al. 1998; Goula et al. 1998; Kwok and Hart 2011; Rudolph et al. 2000), polyamidoamine dendrimers (Haensler and Szoka 1993; Rudolph et al. 2000; Tang et al. 1996), polypropylamine dendrimers (Schatzlein et al. 2005), polyallylamine (Nimesh et al. 2006), cationic dextran (Hosseinkhani et al. 2004; Nimesh et al. 2006), chitosan (Erbacher et al. 1998; Lee et al. 1998; Leong et al. 1998), cationic proteins and peptides like polylysine (Wu and Wu 1988), protamine (Park et al. 2003) and histones (Balicki and Beutler 1997; Balicki et al. 2002).

Cationic polymers are different from cationic lipids as cationic polymers do not have a hydrophobic moiety, are completely water soluble and are more efficient in condensing DNA than cationic lipids (Ruponen et al. 1999). Moreover, the polymeric nature of cationic polymers allows easy manufacturing manipulation of polymer lengths, geometry (linear or branched), and presence of functional groups (Elouahabi and Ruysschaert 2005). Similar to cationic lipids, condensation of DNA with cationic polymers protects DNA from degradation and facilitates membrane interaction for

cellular uptake through endocytosis (Rejman et al. 2005). Although cationic polymer-based nucleic acid delivery systems are advantageous in terms of formulation reproducibility, DNA condensing efficiency and formulation biocompatibility, its value in cutaneous gene therapy is limited as it is inefficient in delivering nucleic acid across the skin barrier layers (Raghavachari and Fahl 2002).

1.3.2 Nucleic acid delivery across the skin barrier

In vivo delivery of nucleic acid across the skin barrier can be achieved through specialised chemical formulation for non-invasive topical application or through physical skin disruption methods, sometimes in combination with non-viral vectors such as cationic lipids. There are advantages and limitations associated to every cutaneous gene delivery method. Several factors such as proposed application, cost effectiveness and patient compliance should be considered when selecting a particular method (Geusens et al. 2009b).

1.3.2.1 Non-invasive topical application

Non-invasive topical cutaneous application of naked nucleic acid is an attractive and simple approach for delivering therapeutic gene to large areas of skin. As previously mentioned, the presence of stratum corneum in healthy skin provides a significant physical barrier against permeation of naked DNA or siRNA. Formulation approaches that use cationic lipid and chemical enhancers to improve skin permeability of nucleic acid following topical application has been reported but was of limited success (Meykadeh et al. 2005). A recent review on lipid-mediated cutaneous gene delivery systems has indicated that numerous studies investigating topical application of pDNA lipoplexes to animal skin, predominantly *in vivo* mouse skin, resulted in reporter gene expression in hair follicles (Geusens et al. 2011). A study investigating siRNA delivery reported an ultraflexible siRNA-containing lipoplex formulation called SECosomes (surfactant-ethanol-cholesterol-osomes) capable of penetration into keratinocytes in the epidermis of freshly excised intact human skin but the gene silencing effect of the delivery system in the skin has not been shown (Geusens et al. 2010).

More recent studies reported success in functional siRNA delivery to the skin *in vivo*. A study reported that the use of skin penetrating and cell entering (SPACE) peptide in the

lightly shaved back of mice resulted in partial gene silencing (Hsu and Mitragotri 2011). An earlier study using a cream-emulsified siRNA formulation to target dendritic cells on murine ear skin showed a marked decrease in the target gene (Ritprajak et al. 2008). Another study developed an agarose matrix system for delivery of a siRNA-liposomal transfection complex to a cutaneous mouse wound model that resulted in local gene silencing (Thanik et al. 2007). An *in vivo* gene silencing study using a proprietary lipid and alcohol-based GeneCream formulation containing functional siRNA resulted in suppression of the development of arthritic symptoms when topically applied to the paws of a mouse rheumatoid arthritis model (Takanashi et al. 2009). The GeneCream formulation, probably similar in concept to the SECosomes formulation (Geusens et al. 2009a), is an interesting prospect for non-invasive topical cutaneous delivery of siRNA therapeutics. Another study has demonstrated the ability of GeneCream formulated with food grade dye to penetrate through the stratum corneum into lower layers of the epidermis and into the dermis (up to a depth of 100 μm) in a human volunteer with healthy skin and also the callused or noncallused skin region of a patient with pachyonychia congenita (Ra et al. 2011). It will be interesting to observe the progress of the GeneCream formulation to clinical application and the gene silencing efficiency of the formulation in human skin.

1.3.2.2 Physical disruption methods

Despite promising progress in non-invasive topical gene delivery to the skin, physical approaches are more widely used to enhance nucleic acid permeation across the skin barrier. The different commonly used invasive and minimally invasive physical gene delivery techniques in active research include intradermal injection, electroporation, ultrasound, particle and jet acceleration and microneedles. The skin is a unique organ and despite the complexity associated with gene delivery through multiple skin layers to cells within the viable epidermis and subsequently across cellular barriers to its target site, many studies have reported success in naked pDNA delivery when delivered in combination with some of the physical approaches.

1.3.2.2.1 Intradermal injection

Intradermal injection is the most commonly used and effective method to achieve localised gene expression in epidermal keratinocytes following nucleic acid delivery

(Gonzalez-Gonzalez et al. 2010a; Hengge et al. 1995; Hengge et al. 1996; Sawamura et al. 2002; Wolff and Budker 2005). The potential of direct intradermal injection of naked pDNA for cutaneous gene expression has long been established in extensive studies using murine, porcine and excised human skin (Hengge et al. 1995; Hengge et al. 1996). In human and porcine skin, reporter gene expression was localised in cells surrounding the injection site, throughout the epidermal layer, mainly in keratinocytes in the stratum spinosum layer within 4 h post-treatment (Hengge et al. 1996). This was the first study to report gene expression following naked pDNA delivery in freshly excised human skin, cultured in an *ex vivo* environment, and also highlights the interspecies differences or similarity in cutaneous gene expression patterns between human, porcine and mouse (Hengge et al. 1996).

A study attempting to characterise pDNA distribution and gene expression following intradermal delivery revealed that at 4 h post-injection with rhodamine-labelled plasmid, the fluorescent plasmid was found in most epidermal cells but transgene expression was only detected in a small proportion of cells in the back of rat skin (Sawamura et al. 2002). *In vivo* gene delivery faces many extracellular and intracellular barriers (Barry et al. 1999; Khalil et al. 2006; Ruponen et al. 2003). Even if the therapeutic gene has been delivered to the extracellular matrix, naked pDNA faces repulsion from the negatively charged cellular membrane and clearance from the skin tissue. A recent study has suggested that cellular entry of exogenous DNA in the skin following intradermal injection is driven by increased interstitial pressure (Gonzalez-Gonzalez et al. 2010a). Assuming successful cellular entry, a non-mitotic cell, including suprabasal keratinocytes would need to be exposed to at least 100000 copies of plasmids to overcome nuclease degradation and to ensure a few copies translocate into the cell nucleus for gene expression (Lechardeur and Lukacs 2006; Lechardeur et al. 2005; Tseng et al. 1997). This suggests that intradermal injection alone may not be able to facilitate cellular entry of sufficient nucleic acid copies for efficient gene expression or gene silencing in the epidermis. Intradermal injection is often used in combination with other strategies such as electroporation to improve cell permeation of injected nucleic acid (Drabick et al. 2001; Ferraro et al. 2009; Hirao et al. 2008).

Conventional intradermal injection has the advantage of being able to overcome the stratum corneum barrier with certainty to deliver relatively large and precise volumes of

aqueous nucleic acid formulation. It is often the standard to which other cutaneous gene delivery techniques are compared. However, with respect to gene delivery targeted to the upper layers of the skin, injection administration by different administrators causes variation in the depth where the needle penetrates and the drug deposits. The thickness of the skin is also variable according to body sites, individual differences and differences between the species of animals tested, which may potentially lead to subcutaneous rather than intradermal delivery (Hengge et al. 1996; Morton et al. 2001; Sandby-Moller et al. 2003). The smallest size of hypodermic syringe needle recommended for intradermal injection is 28 gauge (G) and has nominal outer diameter of 362 μm, which creates an average skin penetration hole diameter of between 410 μm and 710 μm (Baxter and Mitragotri 2005). This means that drugs are not delivered exclusively to the viable layer of the epidermis (thickness of approximately 50 to 100 μm below stratum corneum) but to deeper layers of the skin as well.

Hypodermis needle injection also causes considerable pain, with a study showing that approximately 53% of insertions with a 27 G hypodermic syringe needle caused pain in healthy volunteers (Arendt-Nielsen et al. 2006). The pain sensation may be potentiated at the site of cutaneous manifestation in certain skin disorders, where topical gene treatment is usually targeted. In the first human skin phase I clinical trial for siRNA treatment, pain from intradermal delivery has hampered further clinical progress of siRNA drug treatment for pachynychia congenita (inherited dominant skin disorder) even though the treatment resulted in callus regression in a patient (Leachman et al. 2009). Some of the risks and unwanted effects associated with intradermal injections are infection, phlebitis, haematoma, thrombosis and the potential for needle stick injury during administration or disposal. Hypodermic needles have proven clinical effectiveness but they are unfavourable to both children and adults because they are painful, cause anxiety to the recipients and they are difficult to use (Deacon and Abramowitz 2006; Gill and Prausnitz 2007c; Hanas 2004). Therefore, minimally invasive methods that could improve patient compliance are actively being pursued for delivery of nucleic acids to the skin.

1.3.2.2.2 Electroporation

The use of electroporation for gene delivery is also called gene electrotransfer. It involves the application of short (50 μs to 400 ms) high voltage (>400 V) or low voltage (<400 V) electrical pulse to cells or across tissue to create pores that open temporarily to allow tissue and cellular entry of otherwise impermeable molecules such as nucleic acids and other macromolecules of up to 40 kDa (Lombry et al. 2000; Neumann et al. 1982; Wells 2010). Theoretically, electroporation can be applied in any tissues where a pair of electrodes can be inserted and reviews have shown that this physical method can be used in various tissues *in vitro* and *in vivo* (Gothelf and Gehl 2010; Wells 2010).

Compared to direct DNA injection alone, gene electrotransfer shows less variable gene delivery efficiency between different animal species (McMahon and Wells 2004). Factors such as nucleic acid dose and tissue distribution of injected dose before electroporation affect transfection efficiency (McMahon and Wells 2004; Molnar et al. 2004). A study reported that the use of electroporation in a hairless mouse model following intradermal injection resulted in improved cutaneous naked DNA delivery by a few hundred times when compared to intradermal injection alone (Zhang et al. 2002). However, attempts to combine lipid-DNA lipoplexes with electroporation to improve skin transfection proved futile, as a study has shown that electroporation following intradermal and intramuscular injection of naked pDNA resulted in a higher increase in gene expression compared to electroporation following injection of DNA lipoplexes (Mignet et al. 2010).

There are several drawbacks to *in vivo* cutaneous application of gene electrotransfer. Firstly, the technique may not be effective for cell transfection in a large tissue area because the range in between which the electrodes are effective is limited (Ferraro et al. 2011; Heller et al. 2010). Secondly, electrotransfer alone does not sufficiently increase stratum corneum permeability (Chen et al. 1999) to allow entry of topically applied macromolecules like nucleic acids, thus requiring intradermal injection of therapeutic gene before electroporation (Gothelf and Gehl 2010) and hence it is also associated with the inconveniences of gene transfer through intradermal injection. Thirdly, applying

high voltage to tissues may induce thermal heating, resulting in irreversible tissue damage (Durieux et al. 2004; Ferraro et al. 2011).

In a Phase 1 dose escalation pDNA delivery with electroporation clinical trial, intratumoral injection of pDNA encoding interleukin 12 (IL-12) followed by electroporation in patients with metastatic melanoma was reported to be safe and effective, with increased IL-12 protein expression as well as marked reduction in tumour size (Daud et al. 2008). However, patients who received electroporation suffered from transient pain at the treatment site (Daud et al. 2008). This again highlights the importance in developing more patient friendly methods for delivery of nucleic acids to the skin.

1.3.2.2.3 Ultrasound

In vivo gene delivery facilitated by ultrasound has received considerable research interest in recent years (Escoffre et al. 2013; Newman and Bettinger 2007). The combination of low ultrasound waves with gas microbubbles that are usually incorporated in a drug formulation creates transient permeability across tissue and cell membranes in a process known as sonoporation to allow enhanced entry of small molecules and nucleic acids (Delalande et al. 2013; Escoffre et al. 2013). Sonoporation occurs when the frequency of ultrasound is near the frequency where microbubbles resonate, leading to oscillation of the microbubbles, which causes pore formation (approximately 100 nm in size) in surrounding cell membranes (Delalande et al. 2013; Morgan et al. 2000; van Wamel et al. 2006; Zhou et al. 2009). Pore formation could either be due to the shear stress as a result of microbubble collapse (Dijkmans et al. 2004; Tachibana and Tachibana 2001) or due to the physical interaction between the microbubbles and cell membrane (van Wamel et al. 2006). This phenomenon facilitates intracellular gene delivery as nucleic acid can passively diffuse across the pores formed in the cell membrane (Kim et al. 1996; Koch et al. 2000).

Although promising, direct application of ultrasound alone for cutaneous gene therapy still requires optimisation as, similar to electroporation, skin pores formed by ultrasound application are not sufficient for permeation of large nucleic acid molecules like pDNA (estimated sizes between 3000 to 6000 kDa) across the stratum corneum. Application of

ultrasound in the skin reportedly lead to pore formation in the stratum corneum (Wu et al. 1998) to allow transdermal entry of proteins such as insulin (6 kDa) and erythropoietin (48 kDa) (Mitragotri et al. 1995) but ultrasound-mediated transdermal delivery of nucleic acids with molecular weights in the order of mega Daltons has not been shown.

1.3.2.2.4 Particle and jet acceleration

In principle, particle and jet acceleration involves the use of devices to propel particles (Yang et al. 1990) or expel stream of liquid drug formulation at high speed (Schramm-Baxter and Mitragotri 2004) through the stratum corneum into the skin. An example of a well-studied particle acceleration method uses a device called the gene gun, which has been shown to be effective for skin immunisation through delivery of pDNA vaccine-coated particles to the upper layers of the skin (Dileo et al. 2003; Fynan et al. 1993; Haynes et al. 1996; Lin et al. 2000; Peachman et al. 2003; Pertmer et al. 1995; Tang et al. 1992). The gene gun particle acceleration method has also been used to deliver cDNA and mRNA for wound healing (Nanney et al. 2000; Sohn et al. 2001) and cDNA for suppression of skin malignancy (Oshikawa et al. 2001). Nucleic acids are usually coated onto the surface of gold particles and accelerated to a high velocity by a high voltage discharge or pressurised gas to enable efficient expulsion and penetration of target organs, tissues or single cells. The momentum generated also allows DNA release from the surface of gold particles resulting in DNA deposition into cells that are in the path of tissue penetration (Gao et al. 2007; O'Brien and Lummis 2002; Yang et al. 1990).

Several prototypes of particle acceleration gene delivery devices have been developed and tested in early phase clinical trials for DNA vaccination against hepatitis (Roberts et al. 2005) and influenza (Dean and Chen 2004; Jones et al. 2009). The most recent Phase 1b clinical trial delivering Trivalent DNA vaccine for influenza consisting of three plasmids coated onto microscopic (1–3 μm in diameter) gold beads using particle mediated epidermal delivery (PMED™) system reported vaccine delivery to the epidermis but the level of efficiency was less than that of trivalent inactivated influenza vaccine, with substandard serological responses (Jones et al. 2009). No serious adverse events were reported in the study and the most common adverse reactions were

application site burning, headache and application site stinging. The study concluded that optimisation to the gene delivery system is needed in order to compete with conventional influenza vaccines (Jones et al. 2009).

The use of ballistic devices is reportedly safe and effective in delivery of exogenous gene to the skin (Dean and Chen 2004; Jones et al. 2009; Roberts et al. 2005). However the use of gene gun as a cutaneous gene delivery tool is limited by several factors such as the lack of control over successful penetration of particles through the stratum corneum and variability in the depth of particle penetration in the skin (Kendall et al. 2004). Gold particles are non-biodegradable, hence it is unclear whether these particles are cleared from the tissue. Treatment with accelerated particles may also result in cell death (Raju et al. 2006). There is also a limitation in dose of nucleic acid that can be loaded onto particles, necessitating the need for frequent immunisation and the particle acceleration method requires the use of devices that may not be readily available (Peachman et al. 2003).

Jet injection uses air or spring injector to drive pressurised liquid at a speed of more than 100 m s^{-1} into the skin to allow delivery of macromolecules such as insulin, human growth hormone and vaccines (Baxter and Mitragotri 2005; Kim and Prausnitz 2011; Mitragotri 2006). Jet injection creates micron-sized channels that are proportionate in diameter to the ejected stream of approximately 100 μm and depth of skin penetration (up to 10 mm) depends on the injection volume (Baxter and Mitragotri 2005). Several studies have indicated the potential of jet injection for cutaneous gene therapy (Aguiar et al. 2001; Cui et al. 2003; Mumper and Cui 2003; Sawamura et al. 1999) and a phase 1 clinical trial has reported safety and efficiency of intratumoral jet-injection for gene delivery using β-galactosidase-expressing pDNA (pCMVβ) in patients with metastasised skin cancer and breast cancer (Walther et al. 2009).

1.3.2.2.5 Microneedles

Over recent years, microneedles have been investigated as a means of cutaneous drug and vaccine delivery (Kim et al. 2012b). A microneedle array is a device with multiple repeated structures that are micron size in dimension (usually less than 1 mm in length) protruding from a base (Figure 1.5) and can be of different shapes, size and needle

density (Donnelly et al. 2010). Upon skin insertion, microneedles create micron-sized channels for delivery of macromolecules across the stratum corneum (Badran et al. 2009; Chabri et al. 2004; Henry et al. 1998; Wang et al. 2006). Microneedles have several advantages over other physical skin disruption methods. The design of microneedles can easily be adapted for various applications. There is a potential for microneedles to be self-administered due to their simplicity; they do not depend upon the use of devices that are expensive, complex, relatively large and require training to use. Skin penetration with microneedles is reportedly pain-free (Gill et al. 2008; Haq et al. 2009) and the micron-scaled dimensions of microneedles should more acceptable to patients and could improve patient compliance to treatment (Gill and Prausnitz 2007c). Large-scale manufacture of microneedles is cost-effective and microneedles can easily be distributed due to their small size (Coulman et al. 2006a; Kim et al. 2012b). The use of microneedles for nucleic acid delivery to the skin is discussed in section 1.4.

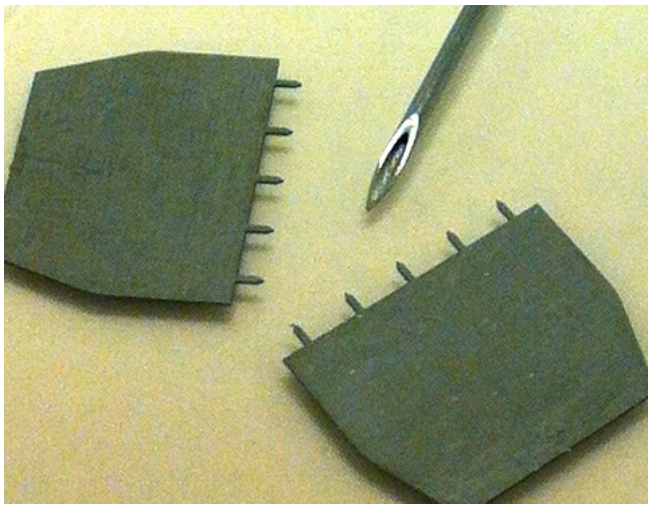

Figure 1.5: Digital image of two in-plane steel microneedle arrays of 700 µm in length (5 needles per array) in comparison with the tip of a 23G hypodermic syringe needle.

1.3.2.2.6 Other stratum corneum disruption methods

Apart from the major methods discussed, there are very few reports on successful cutaneous gene delivery. Other methods that have been used to disrupt the stratum corneum for cutaneous gene delivery are the tape stripping method (Choi et al. 2004; Vandermeulen et al. 2009) and radio frequency ablation method (Birchall et al. 2006). Tape stripping is a simple and inexpensive method that uses repeated taping and

stripping of the tape to remove stratum corneum but the technique has poor reproducibility and is highly variable between individuals and within individuals depending on skin site, state of skin hydration, age, gender and ethnicity (Choi et al. 2004; Geusens et al. 2009b). Tape stripping has been exploited for skin vaccination (Choi et al. 2004; Mitragotri 2005; Peachman et al. 2003) but is disadvantageous because this method requires high doses of DNA to achieve immunisation and is a harsh method because stratum corneum have to be completely removed for effective delivery (Liu et al. 2001; Peachman et al. 2003). A recent study suggested the potential of tape stripping as an adjuvant to electroporation as mice that were tape-stripped following intradermal injection and electroporation elicited significantly higher immune responses (Vandermeulen et al. 2009).

Radio frequency (RF) ablation can be performed using a device called ViaDerm™. Micron-sized channels are created by RF ablation whereby the skin is exposed to an array of densely spaced microelectrodes under an alternating electrical current (Sintov et al. 2003). The microchannels created permit entry of macromolecules across the stratum corneum and into the underlying skin layers (Birchall et al. 2006; Sintov et al. 2003). Radiofrequency ablation has been used to deliver reporter pDNA to excised human skin resulting in gene expression (Birchall et al. 2006). The ViaDerm™ system has also been tested in early phase clinical trials for delivery of hormones and insulin (Arora et al. 2008).

1.4 Microneedles for cutaneous gene delivery

1.4.1 Microneedles concept

Although the concept of using micron sized devices for administration of therapeutic molecules were described nearly 40 years ago (Gerstel and Place 1976), it was not until near the turn of the millennium that the technology required to microfabricate these devices were available (Henry et al. 1998). Since the first paper describing the use of microneedles for drug delivery was published in 1998 (Henry et al. 1998), microneedle-based research has attracted significant interest from both academic and industrial groups (Kim et al. 2012b). This has resulted in an exponential increase in publications with progress to clinical trials and the availability of a few products that have been approved for medical and cosmetic applications (Kim et al. 2012b).

The use of microneedles is appropriate for targeting cells in the upper layers of epidermis as the stratum corneum is only approximately 10 to 20 μm in thickness (Kim et al. 2012b). Microneedles are able to penetrate through the stratum corneum and into the skin up to a limited depth, thus potentially avoiding nerve fibres and blood vessels in the dermis that causes pain and bleeding (Gill et al. 2008; Haq et al. 2009). Microneedle devices when applied to human skin are considered minimally invasive and are reported to be significantly less painful than conventional hypodermic needle injection (Gill et al. 2008; Haq et al. 2009; Kaushik et al. 2001). There is however, increased pain associated with longer microneedles with length of up to 1450 μm (Gill et al. 2008). Increase in the number of microneedles in an array also caused a minimal increase in pain sensation but pain was not affected by the thickness, tip angle and width of the microneedles (Gill et al. 2008). It has been reported that application of longer microneedles resulted in minor bleeding at the treatment site but the incidence of bleeding was not associated with infection or subsequent scarring (Widera et al. 2006).

Studies have shown that microneedles are capable of increasing delivery of a range of therapeutic substances across the skin barrier including small molecules (Li et al. 2010; Wermeling et al. 2008) and biotherapeutics such as DNA (Birchall et al. 2005; Coulman et al. 2006b; Mikszta et al. 2002; Pearton et al. 2008), RNA (Gonzalez-Gonzalez et al. 2010b), oligonucleotide (Lin et al. 2001), peptide (Cormier et al. 2004), protein (Davis et al. 2005; Torrisi et al. 2013), vaccines (Kim et al. 2010; Matriano et al. 2002; Mikszta

et al. 2002; Pearton et al. 2010) and other materials. The first microneedles were fabricated out of silicon (Henry et al. 1998) and since then, various bio-degradable and non-biodegradable materials including metal (Chong et al. 2013; Gill and Prausnitz 2007a; Khandan et al. 2012; Matriano et al. 2002), polymer (Gonzalez-Gonzalez et al. 2010b; Park et al. 2010; Park et al. 2007), sugar (Donnelly et al. 2009; Li et al. 2009; Martin et al. 2012), glass (Wang et al. 2006) and ceramic (Bystrova and Luttge 2011) have been used in the fabrication of microneedles with a variety of shapes and sizes, as needed for different applications (Figure 1.6). Different techniques that have been used to fabricate microneedles include silicon etching (Henry et al. 1998), laser cutting (Davis et al. 2005), metal electroplating (A Fomani and Mansour 2011) and micromoulding (Donnelly et al. 2011; Park et al. 2005) or a combination of techniques (Choi et al. 2010).

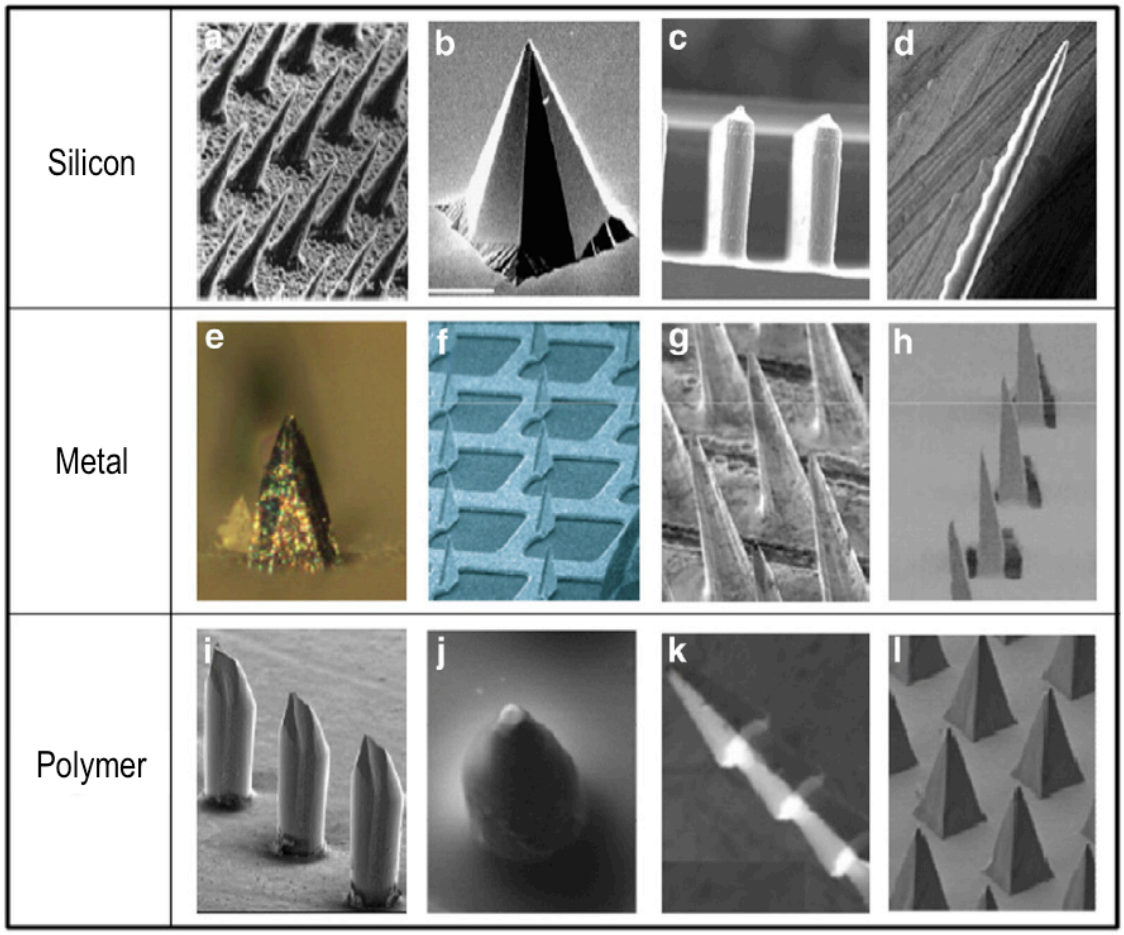

Figure 1.6: Microscopic images of various solid microneedles that are made of silicon (a–d), metal (e–h) and polymer (i–l) (taken from Kim et al. 2012b).

The use of different types of microneedles for delivery of a broad range of therapeutic substances to the skin and various other applications has been thoroughly reviewed by several authors (Bariya et al. 2012; Chandrasekhar et al. 2013; Kim et al. 2012b; Tuan-Mahmood et al. 2013; van der Maaden et al. 2012). For the purpose of narrowing interest in this thesis, this introductory section on microneedles focuses on the general concept of microneedle delivery to the skin and the historical progress of studies involving microneedles for delivery of nucleic acid to the skin.

With specific regards to nucleic acid delivery, microneedles have actively been studied for cutaneous gene transfer and DNA vaccination through delivery of pDNA (Alarcon et al. 2007; Birchall et al. 2005; Chabri et al. 2004; Coulman et al. 2006a; Coulman et al. 2006b; Gill et al. 2010; Gonzalez-Gonzalez et al. 2011; Kim et al. 2012b; Pearton et al. 2008; Pearton et al. 2012). In early 2010 (at the beginning of the work contained in this thesis), the use of microneedles for cutaneous siRNA delivery had never been reported (Geusens et al. 2009b). Since then, the potential of microneedles for delivery of siRNA to the skin has been demonstrated by both this research group and others (Chong et al. 2013; Gonzalez-Gonzalez et al. 2010b; Lara et al. 2012).

1.4.2 Microneedle application methods

In general, methods of drug delivery using microneedles can be categorised into four approaches (i) solid microneedles for skin pre-treatment: pre-applying solid microneedles before drug application to create channels through which drugs can pass the stratum corneum barrier, (ii) drug-coated microneedles: microneedles that are dry-coated with drugs, which dissolve upon skin insertion, (iii) dissolving microneedles: integrating drug into dissolving or biodegradable microneedles, which completely dissolve in the skin upon skin insertion, leading to release of the drug payload and (iv) hollow microneedles: injecting liquid drug formulation through hollow microneedles (Figure 1.7) (Kim et al. 2012b).

The first publication on microneedles described the use of solid silicon microneedles of approximately 150 μm in length as a skin pre-treatment to allow skin permeation of calcein, a model drug with molecular weight of 623 Da by more than 10000 fold compared to intact human skin in *in vitro* diffusion studies (Henry et al. 1998). In the

solid microneedles for skin pre-treatment approach, microneedles are used to form micron-sized channels through the stratum corneum for enhanced delivery of drugs across the skin. Drugs can be applied directly to the skin in the form of aqueous formulation or ointment, or formulated in a transdermal drug delivery patch. Therapeutic formulations that are applied to the skin could produce local effects or can be taken up by skin capillaries for systemic effect. Several other methods for solid microneedle application have since been reported including drug-coated microneedles for delivery of dry-coated drug formulation (Cormier et al. 2004; Gill and Prausnitz 2007a; Matriano et al. 2002) and drug incorporation into the matrix of dissolvable microneedles (Park et al. 2005; Park et al. 2007).

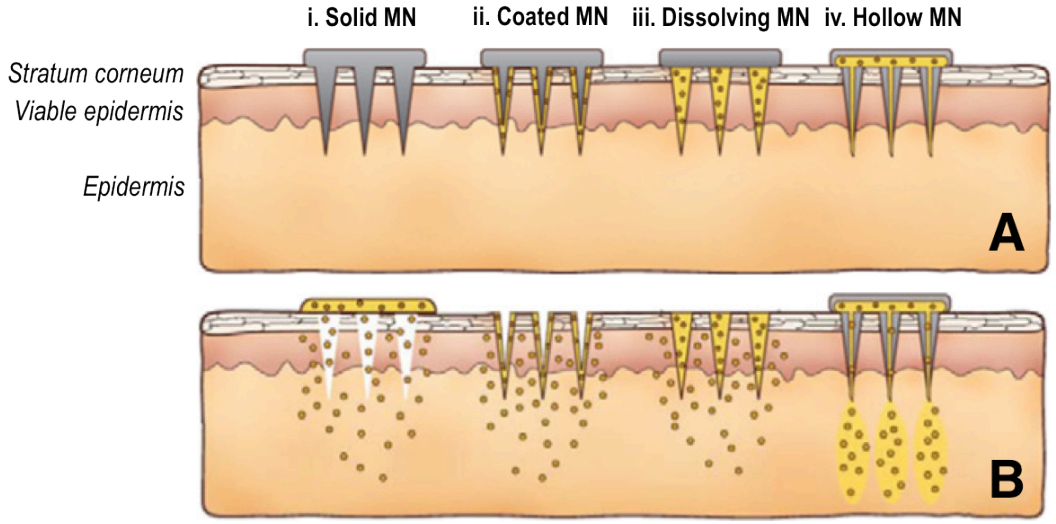

Figure 1.7: A schematic representation of the skin and drug-delivery approaches using microneedles. Different types of microneedles are applied to the skin (A), after which drug is delivered and deposited in the skin (B). (i. Solid MN: solid microneedle for skin pre-treatment; ii. Coated MN: drug-coated microneedles; iii. Dissolving MN: dissolving microneedles; iv. Hollow MN: hollow microneedles) (taken from Kim et al. 2012b).

Hollow microneedles are capable of precise microinjection of liquid drug formulation in the skin dermis through defined channels within their micron-sized structure, similar to intradermal injection with a hypodermic syringe needle (Wang et al. 2006). The use of hollow microneedles for intradermal injection is advantageous because the limited micron length of hollow microneedles allows improved control of injection depth and the injected dose is delivered to the dermis with precision (Van Damme et al. 2009).

The needles on a hollow microneedle device are almost invisible to the naked eye and therefore they appear to be less intimidating to patients than a hypodermic syringe needle (Van Damme et al. 2009). Hollow microneedles are an ideal substitute for intradermal injection with syringe needles but delivery of liquid formulation into the dermis is not ideal for gene delivery targeted to epidermal cells.

1.4.3 Current limitations and mitigation strategies

Despite numerous advantages associated with the use of microneedles as a minimally invasive skin disruption method, there are several limitations that need to be addressed before wide scale use of the devices in clinical practice. In some of the microneedle delivery systems, it is difficult to deliver reproducible and accurate doses because manual loading and application of the devices is subjected to variation dictated by the skills and technique of the person handling these devices (Verbaan et al. 2008). There are also variations in the skin thickness at different sites of the body and between individuals (Sandby-Moller et al. 2003). Factors such as difference in stratum corneum thickness and skin hydration could affect or impede the penetration of microneedles (Bariya et al. 2012). A degree of care needs to be employed while manipulating these devices to avoid loss of material on the skin surface or reduced penetration that may reduce the delivery of the intended dose to the target site (Bariya et al. 2012). There are also risks of microneedle tip rupture upon insertion and the deposition of fragments of the needle within the skin upon removal of the device (Bariya et al. 2012).

The issue with inconsistent manual delivery is being addressed with the use of applicators to achieve reproducible penetration and penetration depth to ensure that patients receive the same and required dose during each administration (Singh et al. 2011; van der Maaden et al. 2012). Several examples of microneedle applicators include the microneedle roller (Park et al. 2010), an impact applicator device with a microprotrusion membrane called Macroflux® (Trautman and Keenan 2005), a hand-held device with a planar side for microneedle application and an actuation unit on the opposing side (Yuzhakov 2007; Yuzhakov 2010), and a pen type device that includes a drug cartridge filled with liquid drug formulation, a plunger and a drive mechanism for liquid drug ejection (Petits et al. 2009).

1.4.4 Non-viral nucleic acid delivery to the skin using microneedles

One of the initial reports of nucleic acid delivery with microneedles described delivery of antisense oligonucleotide formulated in 2% (w/v) hydroxyethyl cellulose gel using a microprojection patch (Macroflux®) consisting of stainless steel microneedles with a length of 430 μm (Lin et al. 2001) to hairless guinea pig skin *in vivo*. This study investigated systemic delivery of oligonucleotide through the transdermal route following microprojection patch application using a radioactively labelled oligonucleotide. Delivery with microprojection patches reportedly achieved therapeutically relevant dose of oligonucleotide systemically and was compared to iontophoresis (similar in concept to electrophoresis), which delivered oligonucleotides at doses that were several orders of magnitude lower than the dose required for therapeutic efficacy. This study did not show functional efficacy of the delivered oligonucleotide (Lin et al. 2001).

Shortly after, functional delivery of reporter pDNA and pDNA encoding hepatitis B antigen in liquid PBS formulation to shaved mouse skin *in vivo*, after skin pre-treatment with microenhancer arrays (MEAs) was reported (Mikszta et al. 2002). The skin was treated with the pDNA solution and microneedles by placing the MEA with blunt tip silicon microneedles (length of up to 200 μm) in contact with the DNA solution and then moving the MEA laterally across the skin surface several times to cause dermal abrasion. This method of pDNA delivery resulted in up to 2800 times increase in reporter luciferase gene expression compared to topical delivery controls and also induced immune response following skin immunisation with DNA vaccine that was less variable and significantly greater than intramuscular and intradermal injections (Mikszta et al. 2002).

The first human skin studies describing functional nucleic acid delivery to excised skin through microneedles, which resulted in successful reporter plasmid expressions were performed by the research group in Cardiff (Birchall et al. 2005; Coulman et al. 2006b). Solid silicon microneedles of up to 280 μm in length were used to create microchannels in the excised human skin stratum corneum of approximately 20 to 50 μm in diameter, through which pre-applied liquid formulation of reporter pDNA was delivered. This resulted in gene expression in viable epidermal cells proximal to the microneedle

penetration site (Birchall et al. 2005; Coulman et al. 2006b). However, both studies reported unpredictable gene expression, as only a minority of the created microchannels stained positive for reporter gene expression (Birchall et al. 2005; Coulman et al. 2006b). Further attempts to improve consistency in the extent of gene expression in human skin, including the use of pDNA formulated in a prolonged release hydrogel formulation applied to the skin after silicon microneedles pre-treatment, failed to achieve more consistent reporter gene expression (Pearton et al. 2008). Nevertheless, these studies were important in describing the ability to deliver nucleic acid to human skin through microneedles that resulted in detectable transgene expression.

The use of pDNA coated microneedles to achieve hepatitis C DNA vaccination (Gill et al. 2010) and reporter transgene expression (Gonzalez-Gonzalez et al. 2011) *in vivo* has also been reported. A study comparing the delivery of pDNA encoding for hepatitis C virus protein from microneedles with the gene gun and also intramuscular injection demonstrated that significantly lower doses of plasmid coated onto stainless steel microneedles of 700 μm in length (8 μg) and plasmid delivered using gene gun technology (4 μg) was required to achieve an immune response in mice that was comparable to intramuscular injection dose of 100 μg (Gill et al. 2010). It was estimated that microneedles delivered 90% of the coated dose (Gill and Prausnitz 2007a). Another study compared the use of steel microneedles, similar to the ones used in the DNA vaccination study (Gill et al. 2010), with dissolvable microneedles made of polyvinyl alcohol, termed the protrusion array device (PAD), for delivery of coated reporter pDNA to mouse paws (Gonzalez-Gonzalez et al. 2011). The study demonstrated the ability to load higher doses of pDNA on the steel microneedles than PADs (3 μg for steel microneedles; 0.1 μg for PAD microneedles), which correspondingly resulted in higher reporter gene expression.

More remarkably, functional siRNA delivery to the paws of a transgenic mouse model (Gonzalez-Gonzalez et al. 2009) with siRNA coated onto PAD microneedles was reported (Gonzalez-Gonzalez et al. 2010b). PAD microneedles were used to deliver siRNA that had been modified for stability and to enter cells passively without a transfection reagent. This resulted in gene silencing in the paws of the transgenic mouse model (Gonzalez-Gonzalez et al. 2010b). However, PADs deliver only 10% of the coated drug payload in mouse skin (Gonzalez-Gonzalez et al. 2010b), which represents

significant wastage in the coated materials. Nonetheless, this study is the first study to demonstrate functional siRNA delivery through microneedles. The ability to target delivery of siRNA to a cell population within human skin using microneedles is an attractive minimally invasive treatment option for localised gene treatment of a plethora of skin disorders caused by aberrant gene expressions.

1.5 Thesis aim and objectives

Thesis aim

The aim of this thesis was to understand gene expression and gene silencing in *in vitro*, *ex vivo* and *in vivo* skin models employing various gene detection systems to realise the potential of targeted nucleic acid delivery to the skin using microneedles.

Thesis objectives

The objectives of the thesis were:

- To optimise the culture of relevant *in vitro* and *ex vivo* human skin models for nucleic acid delivery studies
- To characterise the appearance of solid steel microneedle devices and develop a manual coating technique that allows estimation of coating dose and quantification of delivered dose
- To learn and optimise pre-validated techniques for delivery and detection of gene expression following non-viral delivery of pDNA to human skin models
- To develop assays to detect siRNA mediated gene silencing at the mRNA and protein levels as well as to quantify and visualise cellular delivery of siRNA in *in vitro* human skin models
- To determine the suitability of coating siRNA onto steel microneedles by investigating biological functionality of siRNA formulations following coating and recovery from microneedles
- To visualise physical skin disruptions caused by application of steel microneedles in human volunteers and in excised human skin
- To develop methods to quantify delivery of siRNA and detection of siRNA mediated gene silencing in *ex vivo* human skin as a pre-clinical model to test potential siRNA therapeutics targeted to human skin
- To determine *in vivo* functionality of nucleic acids, delivered to established mouse models *via* drug-coated steel microneedle system, using different gene detection systems

CHAPTER 2

Human skin models and characterisation of microneedle devices

2 Human skin models and characterisation of microneedle devices

2.1 Introduction

The human skin is a structurally complex multilayer tissue, with its outermost layer, the stratum corneum, acting as physical barrier that limits entry of therapeutic molecules to potent lipophillic small molecules. Nucleic acids are highly negatively charged macromolecules that do not cross the skin barrier. In order to penetrate the stratum corneum barrier, microneedle devices were explored as a means to overcome the skin barrier in a minimally invasive and pain-free manner to deposit therapeutic nucleic acid to the skin. Microneedle length and delivery depth can be manipulated to potentially target either the epidermis or the dermis to treat a plethora of inherited skin disorders or skin conditions caused by aberrant gene expression. Local delivery of therapeutic gene allows concentration of nucleic acid where it is required so that clinically relevant doses can be delivered for local gene correction whilst avoiding systemic side effects.

2.1.1 Human skin models

In order to investigate delivery of nucleic acid to the skin, the development of suitable human skin models to perform gene delivery and expression studies was necessary. The target area for cutaneous nucleic acid delivery is the epidermis due to the abundance of keratinocytes in this cellular layer of the skin. Gene therapy targeted to epidermal keratinocytes is appealing because human keratinocytes can be harvested from a small skin biopsy and cultured *in vitro* for the *ex vivo* approach of cutaneous gene therapy (Del Rio et al. 2004). In gene therapy targeted to *in vivo* human skin, gene expression or gene silencing is usually short-term (Coulman et al. 2006a; Hengge 2006; Preat and Dujardin 2001) but could potentially be clinically relevant with the development of efficient gene delivery systems and targeting of appropriate cell populations like epidermal stem cells (Del Rio et al. 2004). An immortalised cell line and primary keratinocytes, isolated from excised human skin, are therefore often used as *in vitro* models of the human skin.

2.1.1.1 *In vitro* human skin models

HaCaT cells are spontaneously immortalised human keratinocytes obtained from the distant periphery of a melanoma of a 62-year-old male patient (Boukamp et al. 1988).

The HaCaT cell line is non-tumorigenic, despite having an *in vitro* phenotype alteration that enables colonies formation and proliferation on plastic and agar. Chromosomal alterations occur in HaCaT cells that are in long-term culture but cells continue to differentiate normally (Boukamp et al. 1988; Boukamp et al. 1997).

Primary keratinocytes are cells isolated from excised human skin samples and selectively cultured *in vitro* under a controlled environment of keratinocyte specific growth medium. One of the oldest and most commonly used method (Daniels et al. 1996) for isolating and culturing primary keratinocytes was described by Rheinwald and Green in 1975 (Rheinwald and Green 1975). This method involves the trypsinisation of skin sample to yield a variety of cell types and then growing the cells in medium supplemented with epidermal growth factor (EGF) and hydrocortisone, on a growth-arrested or lethally irradiated 3T3 feeder layer, which functions as a growth suppressor of dermal fibroblasts and provides the matrix for keratinocyte attachment (Rheinwald and Green 1975, 1977). Over the years, various methods have been explored and serum-free medium specific for growth of primary keratinocytes is commercially available.

The method that has been adapted for use in this thesis uses commercially available, defined keratinocyte specific and serum-free medium that does not require the 3T3 feeder layer for cell attachment and proliferation (Aasen and Izpisua Belmonte 2010; Richards et al. 2008; Zellmer and Reissig 2002). Eliminating the need for the 3T3 feeder layer reduces risk of fibroblast contamination and avoids laborious work preparing the feeder layer. The commercially available serum-free mediums used for culture of primary keratinocytes are supplemented with bovine serum albumin, hydrocortisone, insulin or insulin-like growth factor-I, EGF and prostaglandin E_2. A combination of EGF, insulin and hydrocortisone has been shown to be essential for stimulation of keratinocytes growth in long-term culture of more than 5 days (Formanek et al. 1996).

2.1.1.2 Excised human skin

For the ultimate goal of delivering therapeutic nucleic acid to human subjects, it was important to perform nucleic acid delivery experiments on a more representative model of the *in vivo* environment of human skin. Although animal models may be used,

excised human skin cultured in a controlled *ex vivo* setting would provide the closest physiological resemblance to the human skin (Hengge et al. 1996). Previously, an *ex vivo* human skin culture protocol has been developed and pre-validated in the research laboratory for analysis of gene expression (Birchall et al. 2005; Coulman et al. 2006b; Ng et al. 2009).

2.1.2 Microneedle devices

As previously mentioned, drug delivery using microneedles can be categorised into four general approaches (i) solid microneedles for skin pre-treatment, (ii) drug-coated microneedles, (iii) dissolving microneedles and (iv) hollow microneedles (Kim et al. 2012b; Prausnitz 2004). Of the four approaches, drug coated solid microneedles is appealing as a drug delivery system because drugs coated on the surface of microneedles may have enhanced stability in a solid state and pre-coated microneedle devices are particularly attractive as a one step delivery device that may be developed as a simple self-administrable drug delivery option (Gill and Prausnitz 2007a). A study examining desmopressin coating onto microneedles reported that 98% of the coated drug remained intact when stored under nitrogen at 25°C for 6 months or more (Cormier et al. 2004). Coated microneedles have been widely investigated for skin vaccination as antigens that are released in the skin following microneedle application are taken up by Langerhans cells in the epidermis and dendritic cells in the dermis to induce a potent immune response (Babiuk et al. 2000; Pearton et al. 2010; Song et al. 2010). Due to the versatility of the drug-coated microneedle system, it is also being explored as a delivery system for a broad range of drugs (for review, refer to Kim et al. 2012b) and therapeutic nucleic acids (refer to section 1.4.4). Besides delivery of dry drug-coated microneedles, the ability to coat and deliver a liquid formulation of protein to the skin using pocketed metal microneedles has recently been shown (Torrisi et al. 2013).

In order to deliver an effective dose of a therapeutic substance using the drug-coated microneedle system, it is important to ensure consistent coating of material onto the surface of solid microneedles for subsequently effective skin penetration performance and efficient targeted drug deposition (Gill and Prausnitz 2007a, b; Kim et al. 2012b). There are several features that should be considered when coating sensitive

biotherapeutics (Gill and Prausnitz 2007a). The microneedle coating process should (i) be able to produce uniform coating and avoid drug deposition onto the base of the microneedle arrays to achieve reproducible dosage whilst minimising drug loss, (ii) not be performed at high temperatures, to avoid drug degradation, (iii) be able to load sufficiently high doses of drugs per microneedle and (iv) be able to coat drugs that adhere well onto the surface of microneedles and yet be able to rapidly dissolve upon skin insertion or formulated for controlled release (Gill and Prausnitz 2007a). The coating formulation should be aqueous to prevent the degradation of biotherapeutics and to enable drugs to dissolve following microneedle insertion into the skin (Gill and Prausnitz 2007a; Pearton et al. 2012). The formulation also needs to be sufficiently viscous with low surface tension so that materials are uniformly coated on the surface of microneedles (Gill and Prausnitz 2007a).

Several coating process such as dip-coating, spray-coating and roll-coating have been used for coating objects (Bierwagen 1992). Of these methods, the method that is suitable for coating microneedles is dip-coating because it is a simple to perform and is capable of coating objects with complex shapes (Gill and Prausnitz 2007a). An object is dip-coated by immersing into a coating solution and then withdrawing. This allows adherence of a continuous liquid film on the object, which upon drying forms a uniform coating (Gill and Prausnitz 2007a). Although effective, surface tension plays a dominant role when coating micron-scale objects like microneedles and it is difficult to precisely coat specific sections of microneedles with close spacing in between needles (Beebe et al. 2002; Gill and Prausnitz 2007a). Therefore, an improved technique for manual coating of microneedles with clinically relevant doses of therapeutic substances is necessary.

2.1.3 Aim and objectives

The aim of this chapter was to develop and optimise human skin models for nucleic acid delivery and to characterise microneedle devices for the delivery of nucleic acids to the skin. The objective of the experiments were:

- To successfully culture and maintain HaCaT cells for *in vitro* nucleic acid delivery optimisation studies.
- To compare epidermal sheet separation methods for successful isolation of viable cells from the skin.
- To optimise a method for selective culture of primary keratinocytes *in vitro*.
- To maintain viability of excised human skin within organ culture, in an *ex vivo* environment.
- To develop an optimised manual technique for dip-coating steel microneedles.
- To characterise steel microneedle devices in terms of appearance, coating and cargo release following delivery of liquid-loaded or dry-coated substances to both mouse and human skin.

2.2 Methods

Unless specified, all other reagents and materials including tissue culture vessels were obtained from Thermo Fisher Scientific, UK.

Cell and organ cultures were maintained in an incubator at 37°C in a humidified atmosphere containing 5% CO_2 in air unless specified otherwise.

2.2.1 Aseptic procedures

Where necessary, materials were sterilised by autoclaving at 121°C for 15 min. Aseptic techniques were performed as required and carried out in a class 2 biosafety cabinet with 70% (v/v) ethanol in water used as the general disinfectant.

2.2.2 Cell culture

2.2.2.1 Cell culture medium

HaCaT cell lines were cultured using Dulbecco's modified Eagle medium (DMEM) (Life Technologies, UK) supplemented with 10% foetal bovine serum (FBS) (Life Technologies, UK), 100 unit mL^{-1} penicillin and 100 mg mL^{-1} streptomycin (Life Technologies, UK).

2.2.2.2 Culturing from frozen stock

HaCaT cells (passage 47 and passage 58), a gift from Professor Mark Gumbleton (School of Pharmacy and Pharmaceutical Sciences, Cardiff University), were maintained as 1 mL aliquots of cells suspension at -80°C until use. The frozen cells were thawed at 37°C in a water bath and 10 mL growth medium was added slowly (drop-wise) to dilute the cells with continuous gentle shaking. The cells were then centrifuged (Beckman Coulter, UK) at 180 × *g* for 10 min at room temperature and seeded in a 25 cm^2 tissue culture flask. Cells were then incubated to allow adherence to the bottom of the culture vessel and proliferation until approximately 90% confluency before subculture as described in section 2.2.2.3.

2.2.2.3 Routine subculture

Firstly, confluent cells were rinsed three times with PBS (Life Technologies, UK) and then incubated with 1mL (equivalent to 40 μL cm^{-2} growth area) of 0.05% Trypsin-0.53 mM EDTA (Life Technologies, UK) at 37°C for 5 to 10 min. Then, cells were removed from the growth surface by tapping the culture vessel against the edge of a bench top. Growth medium with serum was then added to the flask to inhibit the enzymatic action of trypsin-EDTA. The cells were then centrifuged at 300 × *g* for 5 min at room temperature. The supernatant was discarded and the cell pellet was re-suspended in growth medium. Cells were disaggregated by passing through the serological pipette several times and then seeded in sufficient density by splitting the cells approximately in ratios of 1 in 5 to 1 in 10, for a new passage. Cells were maintained in an incubator and fluid changed with growth medium every 48 to 72 h. Cell subcultures were performed every 4 to 5 days. If a $75cm^2$ tissue culture flask was used, reagents were scaled up accordingly.

2.2.2.4 Determination of cell count

Cell count was performed using a Neubauer haemocytometer (Paul Marienfield, Germany). A 20 μL aliquot of cell samples was removed from the tissue culture vessel and disaggregated as described in section 2.2.2.3 were diluted 1:1 with trypan blue solution (Sigma Aldrich, UK). Then, 10 μL sample of the trypan blue diluted cell suspension was loaded into each counting chamber of the haemocytometer for counting under a light microscope. Only viable cells that were not stained with trypan blue were included in the count.

2.2.2.5 Cryopreservation of cells

Cells were occasionally frozen to maintain stock for future use. Cells that have been removed from the tissue culture vessel and disaggregated as described in section 2.2.2.3 were suspended in DMEM supplemented with 20% FBS and 10% DMSO at a cell density of 10^6 cells per mL. Cell suspensions were divided into 1mL aliquots in cryogenic tubes and frozen at -80°C in an isopropyl alcohol bath setup (Mr. Frosty Freezing Container; Nalgene, Thermo Fisher Scientific, UK) to achieve a rate of cooling of approximately -1°C per min, the optimal rate for cell preservation.

2.2.3 Excised human breast skin organ culture

2.2.3.1 Organ culture medium

Organ culture medium was prepared using DMEM supplemented with 100 mg mL^{-1} penicillin and 100 unit mL^{-1} streptomycin. Amphotericin B (Life Technologies, UK) at a concentration of 2.5 µg mL^{-1} was added to cultures that are maintained for more than 2 days.

2.2.3.2 Acquisition of skin samples

Human breast skin samples were obtained from subjects of breast reduction and mastectomy following informed consent and with full ethical approval from South East Wales Local Research Ethics Committee (reference 08/WSE03/55). After surgical removal, breast skin tissue was placed into organ culture medium and transported to the laboratory on ice. Upon arrival at the laboratory, the skin tissue was stored at 2 to 8°C until use. Subcutaneous adipose tissue was removed with surgical scissors. The excised skin was briefly rinsed in sterile PBS and was then stretched and pinned using 1 cm push pins (Staples, UK) on a planar corkboard with the epidermal side facing up. Skin samples were then treated or cut to required size before being cultured in an organ culture setting as described in section 2.2.3.3.

2.2.3.3 *Ex vivo* skin culture

The viability of skin samples were maintained at the air-liquid interface of a Trowell-type organ culture (Trowell 1954) to simulate *in vivo* conditions. A lens cleaning tissue paper was wrapped around a metal gauze platform before being inserted into a 6-well plate. The well was then filled with 6 mL organ culture medium, which was quickly drawn up by the lens tissue paper. Skin samples were then placed epidermal side up and dermal side in contact with the soaked lens tissue paper (Figure 2.1). Skin samples were then maintained in an incubator for the required duration of time.

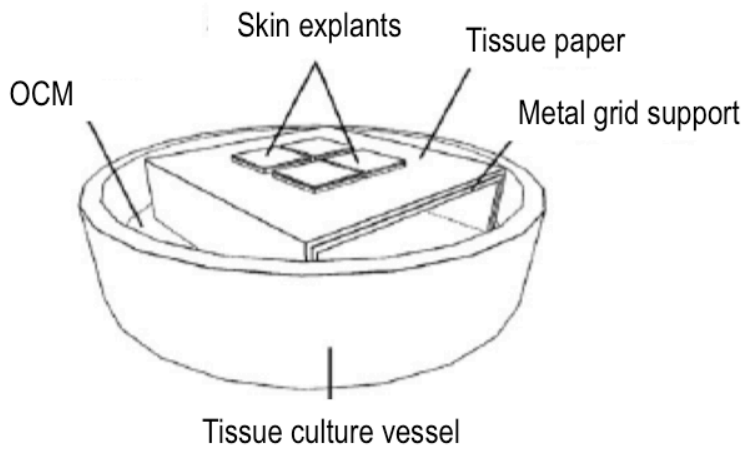

Figure 2.1: A schematic diagram of the Trowell-type organ culture setup. (OCM = organ culture medium) (taken from Ng et al. 2009)

Alternatively, skin viability was maintained by suspension at the air-liquid interface of a hanging insert organ culture setup (Figure 2.2). Organ culture medium of 700 μL per well was added to the wells of 24-well plate. Skin samples cut using 8 mm diameter biopsy punch (KAI medical, Japan) were suspended in a de-membraned 6 mm diameter hanging cell culture insert (Millipore (UK) Ltd, UK) with the epidermal side up and dermal side in contact with the organ culture medium. Skin samples were then incubated for the required duration of time.

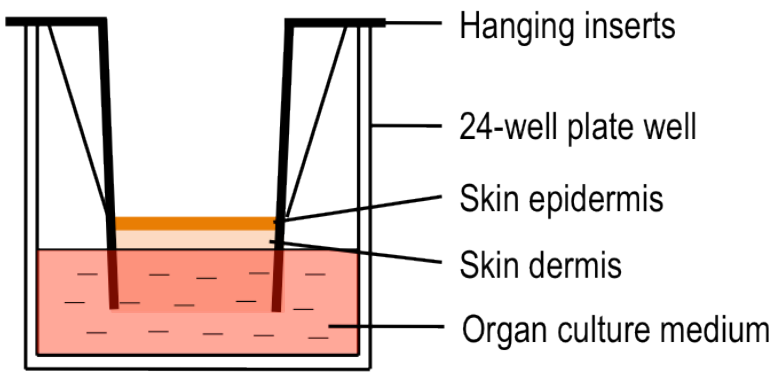

Figure 2.2: A schematic diagram of the hanging insert organ culture setup.

2.2.4 Primary keratinocyte isolation and culture

2.2.4.1 Primary keratinocyte specific culture medium

Primary keratinocyte cell lines were cultured in EpiLife® Medium supplemented with Human Keratinocyte Growth Supplement (HKGS) (Life Technologies, UK) and 100 unit mL^{-1} penicillin and 100 mg mL^{-1} streptomycin. Amphotericin B at a concentration of 2.5 μg mL^{-1} was also added to freshly isolated primary cells.

2.2.4.2 Epidermal sheet separation

Freshly excised (within 6 h of surgery) breast skin tissue (section 2.2.3.2) was placed into a rinse solution of D-PBS (Life Technogies, UK) with an antibiotic cocktail containing 100 unit mL^{-1} penicillin and 100 mg mL^{-1} streptomycin, 50 μg mL^{-1} gentamicin (Life Technologies, UK) and 2.5 μg mL^{-1} amphotericin B, for approximately 30 min. The skin tissue was then divided using a 6 mm diameter biopsy punch. To improve reagent penetration into the tissue during enzymatic separation, a significant portion of the dermis was mechanically removed before treatment using either:

i. a 2.4 caseinolytic units mL^{-1} solution of Dispase II (Life Technologies, UK) dissolved in D-PBS supplemented with 100 unit mL^{-1} penicillin, 100 mg mL^{-1} streptomycin and 2.5 μg mL^{-1} amphotericin B. This was incubated at 4°C for 16 h and then at 37°C for 20 min before separation or

ii. an enzyme cocktail solution containing 2 caseinolytic units mL^{-1} solution of Dispase II, 197 units mL^{-1} solution of Collagenase D (Life Technologies, UK) and 20 units mL^{-1} solution of Deoxyribonuclease (DNase) I from bovine pancreas (Sigma Aldrich, UK) in RPMI medium (Sigma Aldrich, UK) at 37°C for 40 min.

For chemical separation of the epidermal sheets, skin tissue pieces were incubated in 3.8% (w/v) ammonium thiocyanate (Sigma Aldrich, UK) in PBS at room temperature for 40 min. After incubation in dispase, enzyme cocktail or ammonium thiocyanate, the epidermal layer of human skin was separated from the dermis using forceps. Epidermal sheets for primary cells isolation were then handled as described in section 2.2.4.3.

2.2.4.3 Isolation of primary epidermal cells

Epidermal sheets separated using dispase were transferred into a 15 mL centrifuge tube containing 5 mL of 0.25% Trypsin-0.53 mM EDTA (Life Technologies, UK). The sheets were then incubated at 37°C for 30 min, during which it was aspirated using a 1 mL serological pipette every 10 min to aid cell dissociation. Following incubation, trypsin activity was inhibited by addition of an equal volume of soybean trypsin inhibitor (Life Technologies, UK) at a final concentration of 1 mg mL^{-1} dissolved in D-PBS and sterile filtered prior to use. The cell suspension was transferred to a fresh 50 mL centrifuge tube through a 70 μm cell strainer and rinsed with 5 mL PBS, after which it was centrifuged at 300 × *g* for 5 min at room temperature. The resulting cell pellet was gently re-suspended in complete keratinocyte specific medium and centrifuged again at 300 × *g* for 5 min at room temperature.

The cell pellet was gently re-suspended in 5 mL of complete keratinocyte specific medium and the concentration of basal keratinocytes was determined using a haemocytometer. Primary cells were seeded into 25 cm^2 tissue culture flasks at a density of approximately 4 × 10^4 cell cm^{-1} in complete keratinocyte specific medium with amphotericin B. The primary cultures were incubated and fluid changed with fresh complete keratinocyte specific medium every 48 to 72 h.

2.2.4.4 Secondary culture of human epidermal keratinocytes

Upon reaching 60% to 75% confluency, the culture medium was removed and the cell monolayer was rinsed twice with PBS before incubation in 1 mL (equivalent to 40 μL cm^{-2} growth area) TrypLE™ Express (Life Technologies, UK) at 37°C for 5 to 10 min. Following the enzymatic treatment with TrypLE™ Express, cells were removed from the growth surface by tapping the culture vessel against the edge of a bench top.

When approximately 90% of the cells have detached, the enzymatic activity was stopped by the addition of 200 μL cm^{-2} growth area (5 times dilution) of PBS. The cell suspension was transferred to a sterile 50 mL centrifuge tube and centrifuged at 300 × *g* for 5 min at room temperature. The supernatant was discarded and cell pellet was re-suspended in keratinocyte specific medium and seeded into a fresh tissue culture flask at a density of approximately 3 × 10^4 cells cm^{-2} in keratinocyte specific medium. The

primary cultures were maintained in an incubator and fluid changed with fresh complete keratinocyte specific medium every 2 to 3 days until the cells reached 80% confluency, after which it was further sub-cultured. Primary cells were cultured in keratinocyte specific medium without amphotericin B in subsequent passages. If a 75cm^2 tissue culture flask was used, reagents were scaled up accordingly.

Primary keratinocytes after the initial passage were also grown on glass coverslips and subjected to immunofluorescence staining with anti-cytokeratin-14-FITC antibody (Abcam, UK) to determine purity of the keratinocyte cell population as described in section 2.2.4.6.

2.2.4.5 Cryopreservation of primary keratinocyte cells

Cells were counted and re-suspended from routine subculture, at 3×10^6 cells per mL, in FBS, supplemented with 10% dimethyl sulfoxide (DMSO). Cell suspensions were divided into 1mL aliquots in cryogenic tubes and frozen at -80°C in an isopropyl alcohol bath setup to achieve a rate of cooling of approximately -1°C per minute, the optimal rate for cell preservation.

2.2.4.6 Immunofluorescence staining for confocal microscopy

Prior to confocal microscopy, cells grown on glass coverslips in the wells of 12-well plates were fixed and stained with primary antibodies and fluorescently conjugated secondary antibodies. Firstly, growth medium was removed and cells were rinsed 3 times with PBS. Then, paraformaldehyde (PFA) 3% (w/v) dissolved in PBS was added to the cells as a fixative agent for 15 min at room temperature. The cells were rinsed 3 times with PBS. Ammonium chloride 50mM in PBS was added to the cells to remove any traces of PFA for 5 min at room temperature. The cells were rinsed 3 times with PBS. Triton X-100 0.2% (w/v) in PBS was added to the cells to permeabilise cell membranes for 5 min at room temperature. The cells were then rinsed 3 times with PBS. Subsequently, the cells were incubated in 500 μL blocking solution made of 2% (v/v) foetal bovine serum (FBS) and 2% (w/v) bovine serum albumin (BSA), for 30 min at room temperature. Primary antibodies were diluted in blocking solution according to manufacturer's recommended concentration for immunofluorescence. The cells were incubated in the diluted primary antibodies for 30 min at room temperature. The cells

were rinsed 3 times with triton X-100 0.2% (w/v) in PBS and then once with PBS. AlexaFluor conjugated secondary antibodies (Life Technologies, UK) were diluted 1:400 in blocking solution. The washed cells were incubated in the diluted secondary antibodies for 30 min at room temperature and then rinsed 3 times with triton X-100 0.2% (w/v) in PBS and once with PBS. The cells were then incubated in Hoechst 33258 or 33342 (Sigma Aldrich, UK), a fluorescent nuclei counterstain, at a concentration of 1 $\mu g\ mL^{-1}$ in PBS for 15 min at room temperature and then rinsed 3 times with PBS.

Each coverslip was lifted and excess fluid was removed using filter paper, without damaging the cells, before being mounted on a drop of Dako fluorescence mounting medium (Dako, UK) on a microscope slide. The coverslips mounted on oil were allowed to dry for 2 h at room temperature before the sides of the coverslips were sealed with a clear coat of nail varnish (Boots UK Ltd, UK). The slides were kept at 4°C until further use for up to 4 weeks.

A Leica DMI6000B confocal microscope (Leica Microsystems (UK) Ltd, UK) with the LAS AF software (Leica Microsystems (UK) Ltd, UK) system was used to visualise and capture micro-images of the fixed and stained cells. The images saved were then analysed using the Image J computer software (United States National Institute of Health, USA).

2.2.4.7 Cryosectioning and immunohistochemistry staining

Skin samples were embedded in optimal cutting temperature (OCT) medium (Tissue-Tek® OCT™ Compound, Sakura Finetek Europe B.V.), frozen on dry-ice and then stored at -80°C. The samples embedded in OCT blocks were sectioned using the Leica CM3050S Cryostat (Leica Microsystems (UK) Ltd, UK). Skin sections of 10 to 14 μm were captured on Superfrost Plus® microscope slides. Selected slides were washed in PBS for 5 min to remove residual OCT embedding medium and subjected to haematoxylin and eosin (H&E) staining to assist visualisation of the epidermal architecture. Briefly, the skin sections were immersed in Harris' haematoxylin solution for 45 to 90 s, rinsed under running tap water for 1 min, differentiated in 0.3% (v/v) hydrochloric acid in ethanol (acid alcohol) for 10 s, rinsed under running tap water for 2 min, immersed in 1% eosin solution for 1 s, and then rinsed under running tap water for

2 min. The stained cryosections were then dehydrated in an ethanol gradient by consecutive immersion in 30%, 50%, 70%, 90% and 100% ethanol for 2 min each immersion, respectively. The stained and dehydrated cryosections were then immersed in xylene for 5 min before permanent mounting with Histomount™ mounting solution (National Diagnostics, USA) and cover-slipped. For long-term storage, the side of the coverslips were sealed with a clear coat of nail varnish.

Specimens were observed using the Olympus® BX-50 or IX-50 microscopes (Olympus (UK) Ltd, UK) and images were captured using the DP-10 digital camera (Olympus (UK) Ltd, UK).

2.2.5 Characterisation of microneedle devices

Steel microneedle devices manufactured and fabricated by Cardiff University and Georgia Institute of Technology, USA were characterised by imaging under a microscope (section 2.2.5.3). The microneedles were also coated with nucleic acid and allowed to dry after which the nucleic acid was recovered with a small volume of buffer and then quantified. These microneedle devices were then utilised for *ex vivo* and *in vivo* experiments to deliver methylene blue to mouse skin (section 2.2.5.4), FITC conjugated oligonucleotide (section 2.2.5.5), pDNA (Chapter 3) and siRNA (Chapter 5) to excised human skin as well as, pDNA and siRNA to mouse skin (Chapter 6).

2.2.5.1 Microneedle fabrication

Microneedle devices of various needle densities and dimensions manufactured by Cardiff University were fabricated by wire electrical discharge machining (EDM) from a stainless steel sheet (Chong et al. 2013). Other microneedle devices (5 needles per array or 10 × 5 needles per array; 700 μm in length), manufactured and provided by Georgia Institute of Technology, were fabricated using laser cutting followed by electropolishing (Gill and Prausnitz 2007a).

2.2.5.2 Microneedle coating

Before coating, microneedle devices were pre-conditioned by rinsing in buffer solutions and were then allowed to dry at room temperature. Steel microneedles were coated

using the dip-coating method depicted in Figure 2.3 (Chong et al. 2013). A volume, *V,* of concentrated solution, *C,* was loaded into a pipette tip as a reservoir for coating. Microneedles were coated by repeated immersions of the needles into the reservoir, with 30 s air drying time in between each immersion until the reservoir was exhausted. More than one microneedle device (*N*) was coated at a time. The coated microneedles were then allowed to dry further at 4°C.

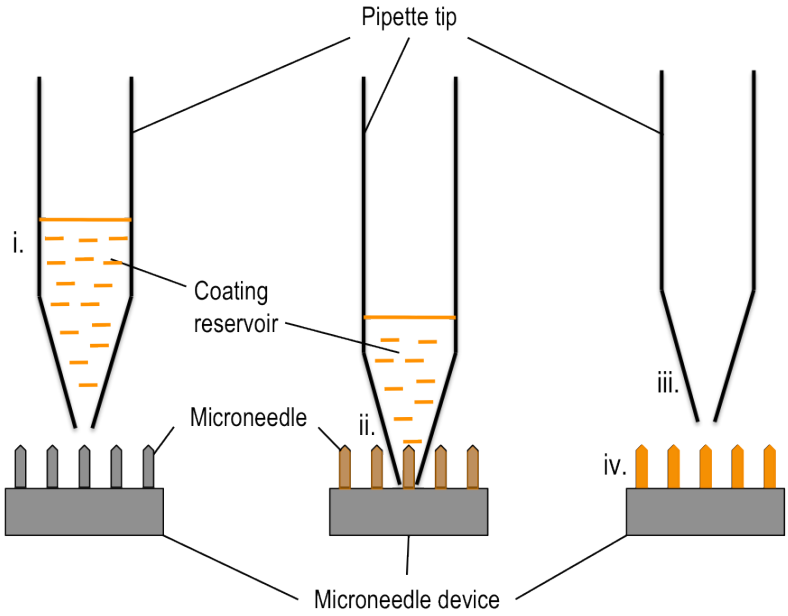

Figure 2.3: **A schematic illustration of the microneedle coating method (Chong et al. 2013).** (i) A volume of solution of known concentration was loaded into a pipette tip as a reservoir for coating. (ii) Microneedles were coated by repeated immersions of the needles into the reservoir, with 30 s of air-drying time between each immersion. (iii) Microneedles were coated until the reservoir was exhausted. (iv) Coated microneedles were allowed to dry further at 4 °C.

The estimated mass of material coated onto each microneedle device, x, was then calculated using the formula below:

$$x = \frac{C \times V}{N}$$

2.2.5.3 Imaging of microneedle devices

Microneedle devices were imaged *en face* using the Maplin USB digital microscope (Maplin Electronics, UK) and at greater magnification using the VWR BI 500 light

microscope (VWR International, UK). Fluorescent images of coated microneedles were imaged using Leica DM IRB epifluorescence microscope (Leica Microsystems (UK) Ltd, UK) with Openlab imaging software (Perkin Elmer, UK).

2.2.5.4 Delivery of a liquid-loaded formulation from microneedles

Microneedles were coated by a single immersion of each microneedle in the array in 2% (w/v) methylene blue with 10% (v/v) glycerol in water using the method described in section 2.2.5.2. The methylene blue coated microneedles were not allowed to dry (liquid-loaded) but immediately applied to dead mouse skin with the mouse hair having been chemically removed using Veet® Hair Removal Cream (Boots, UK). Prior to microneedle application, skin at the proposed area of treatment was pulled taught and then the coated microneedles were manually inserted with enough force to puncture the surface of the mouse skin and were left in place for 5 min.

2.2.5.5 Delivery of a dry-coated formulation from microneedles

Microneedles were coated with fluorescein isothiocyanate (FITC) conjugated oligonucleotide 10 mg mL^{-1} using the method described in section 2.2.5.2. The microneedles were coated through repeated immersions (20 times per microneedle) in the coating reservoir and were allowed to dry at 4°C for 16 h (dry-coated). Microneedles were imaged before and after insertion into excised human skin. The treated skin samples were embedded in OCT medium, frozen on dry ice and cryosectioned using the method described in section 2.2.4.7. The transverse sections of sample collected on microscope slides were not H&E stained but kept frozen until imaging using the Leica DM IRB epifluorescence microscope with Openlab imaging software. The epidermal sheets were separated from some of the treated samples using ammonium thiocyanate, as described in section 2.2.4.2, and imaged using the Leica DM IRB epifluorescence microscope with Openlab imaging software.

2.3 Results and discussion

2.3.1 Cell culture of the HaCaT cell line

Routine subculture was successfully performed with the HaCaT cell line. HaCaT cells used in all the experiments were between passage 50 and 75.

2.3.2 Epidermal sheet separation, primary keratinocyte isolation and culture

2.3.2.1 Epidermal sheet separation

Epidermal sheet from freshly excised human breast skin tissue was successfully separated from the dermis using different chemical and enzymatic reagents. For skin tissue incubated in ammonium thiocynate, the average incubation time was approximately 30 min at room temperature to achieve separation. As ammonium thiocynate is a chemical compound, it is not suitable for primary culture work. However, ammonium thiocynate is useful for sheet separation in a short period of time and is reportedly the preferred method for extracting RNA of high quality for transcriptional analysis of skin tissues (Clemmensen et al. 2009; Trost et al. 2007).

The more popular methods of choice for epidermal sheet separation where viable cells are required for subsequent processes are the enzymatic methods using dispase (Green et al. 1979; Kitano and Okada 1983) or thermolysin (Walzer et al. 1989). Both dispase and thermolysin are protease enzymes that act at the basal cell attachment level by disrupting the hemidesmosomes to cause epidermal-dermal separation (Green et al. 1979; Poumay et al. 1994; Spurr and Gipson 1985; Walzer et al. 1989). Albeit having slightly varied protocols, these enzymatic methods of epidermal sheet separation have been widely applied to isolate cells from skin tissues for primary cell cultures (Germain et al. 1995; Hybbinette et al. 1999; Normand and Karasek 1995; Rakhorst et al. 2006).

Epidermal sheet separations were initially attempted using published methods by incubating in dispase for 16 h at 4°C (Kitano and Okada 1983; Normand and Karasek 1995) or thermolysin for 2 h at 37°C (Germain et al. 1993). However, the skin tissues incubated in thermolysin at 37°C for 2 h were difficult to handle and epidermal separation was challenging as the dermal tissues disintegrated. Separation of epidermal sheets after 16 h incubation in dispase was possible but separation was not always

complete with small segments of epidermal sheet proving inseparable around the centre of the skin tissue.

However, consistent epidermal sheet separations were achieved by incubating tissues in dispase for 16 h at 4°C and then 20 min at 37°C prior to separation (Rakhorst et al. 2006). Incubation at 4°C overnight seemed to be gentle enough to allow the enzymes to fully penetrate the tissues into the dermal-epidermal junction without disintegrating the tissue. A short incubation at 37°C provided the optimum condition for the enzymes to work efficiently at the junction and allowed dermal-epidermal separation with ease.

Whilst epidermal sheet separation with dispase alone was successful in the culture of primary cells (section 2.3.2.2), this enzymatic separation method requires overnight incubation time which was not suitable for epidermal cell extraction for flow cytometry analysis. An alternative protocol using an enzyme cocktail solution with dispase, collagenase and DNase was employed, which required a shorter incubation time of 40 min. This separation method extracts epidermal cells in a shorter period of time, which was more suitable for viable cell extraction for flow cytometry.

2.3.2.2 Isolation of epidermal keratinocytes and culture

After several initial attempts, primary keratinocyte cells were successfully isolated and cultured from human epidermis. Upon seeding in the culture flask, some smaller cells immediately settled and stuck to the culture flask while larger cells remained afloat (Figure 2.4 A). The following day some cells were fully attached to the bottom of the culture vessel, whilst many large rounded cells had adhered to the bottom of the culture vessel but failed to fully attach, even after 4 days (Figure 2.4 B). The cells capable of attachment during this phase were probably basal cells, whereas the majority of larger, more differentiated cells remained in an arrested state (Staiano-Coico et al. 1986; Zellmer et al. 2001). Attached cells started proliferating after 3 to 4 days and formed colonies of 20 to 30 cells after 4 to 7 days in culture (Figure 2.4 B). By day 8 to 10 cell confluency was approximately 70%, with cells clusters of 70 to 80, and the culture was therefore split at this point.

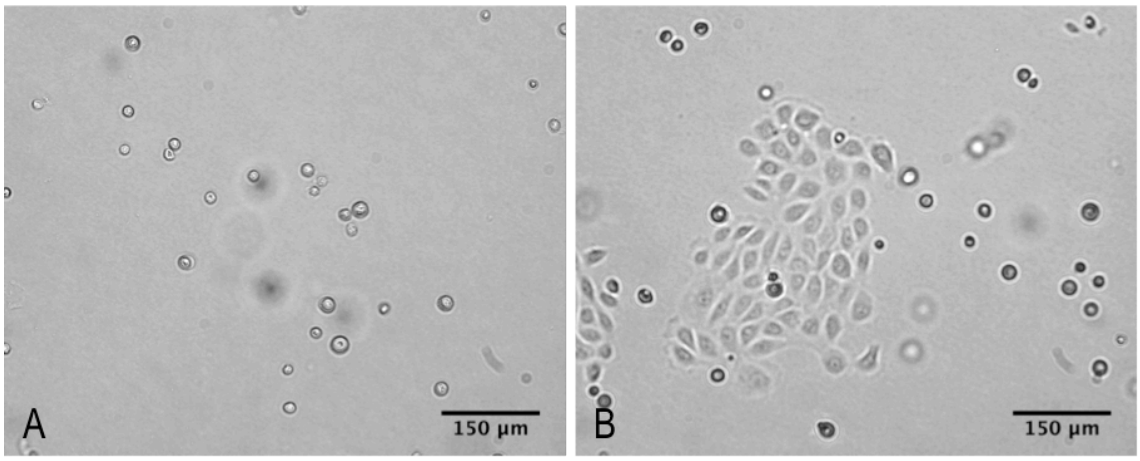

Figure 2.4: Representative bright-field micrographs of primary keratinocyte cells post-isolation (Passage 0). A. Non-adherent rounded cells on Day 1. B. Cell colony with approximately 20 to 30 cells and visible rounded cells, which adhered but did not fully attach or proliferate on Day 4.

Several studies have reported that keratinocyte cells that are present in the skin can be classified into three subpopulations of cells with different sizes and cell cycle kinetics (Barrandon and Green 1987; Staiano-Coico et al. 1986; Watt and Green 1981). Keratinocyte cells deriving from the basal layer of epidermis are small and have the greatest capacities to form colonies if cultured *in vitro*. These basal keratinocytes are called the holoclone and are likely the stem cells (Barrandon and Green 1987). These cells were observed in the cultures as the smaller sized cells, which easily attached and proliferated in the culture vessel (Zellmer et al. 2001).

In contrast, suprabasal keratinocytes found in the upper layer of epidermis are larger in size and are less efficient at forming colonies *in vitro*. The suprabasal cells are meroclone, a clone of cells with mixed composition and paraclone, which consists of matured keratinocytes (Barrandon and Green 1987). The keratinocyte cells in the skin increase in size as they differentiate from haloclone to meroclone to paraclone as synthesis of involucrin and large keratin filaments begin at different stages of keratinocyte maturation (Watt and Green 1981). Therefore, primary keratinocytes isolated from adult human breast skin tissue may contain a majority of differentiated or terminally differentiated cells that do not adhere or divide in the culture vessel (rounded non-adhering cells in Figure 2.4 B). The duration of keratinocytes propagation in cell culture has been said to decline with the age of donor (Rheinwald and Green 1975) due

to changes in relative levels of the three clonal types (Barrandon and Green 1985) but insufficient samples were processed in this study to be able to support this claim.

Subcultures of primary keratinocytes were attempted with various cell-seeding densities. When cells were seeded at low density, initial proliferation was remarkably slow, sometimes did not proliferate enough for subsequent subculture and were abandoned. Based on daily observations, cells seeded at higher density following subculture attached to the culture vessel and proliferated. Larger cells that did not attach well during these cultures were washed away when the culture medium was refreshed. At higher seeding density, primary keratinocytes reached 80% confluency and were ready for further subculture after 4 to 6 days (Figure 2.5). Primary keratinocyte cells should always be seeded at higher cell density for growth and proliferation to avoid issues such as apoptosis at low density (Aasen and Izpisua Belmonte 2010; Zellmer and Reissig 2002).

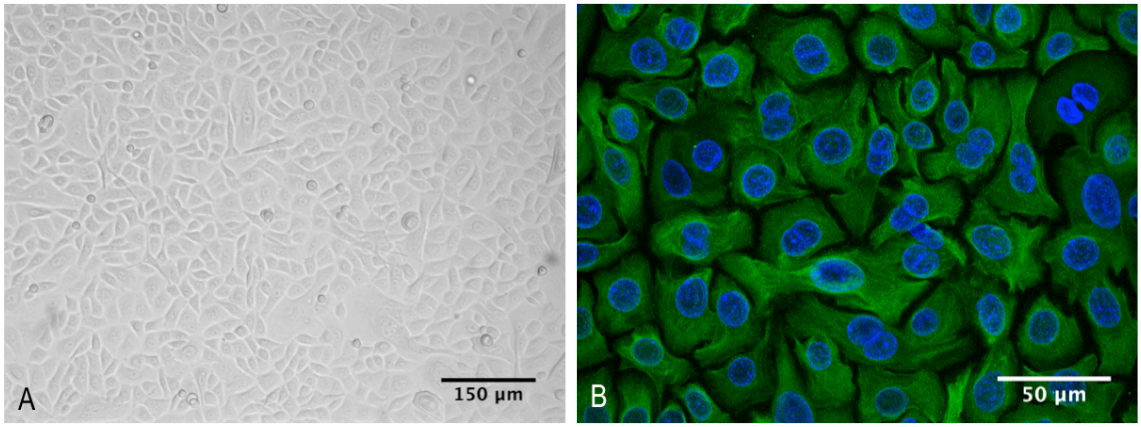

Figure 2.5: Representative bright-field (A) and fluorescent confocal (B) micrograph of confluent primary keratinocyte cells after subculture. A. Primary keratinocyte cells assumed the distinct "cobble stone" morphology and the proliferating cells were visibly of different sizes. B. Primary keratinocyte cells were stained with anti-cytokeratin-14-FITC antibody and pseudo-coloured green. Nuclei were counterstained with Hoecsht 33342 and pseudo-coloured blue. The confocal image is a z-stacked projection of 20 slices of images taken over a cell layer thickness of approximately 12 µm.

Generally, keratinocyte cells display distinct "cobble stone" morphology and are easily distinguished from other cell types present in the human skin such as fibroblasts, which usually display spindle morphology upon reaching confluency (Tomakidi et al. 1999).

Therefore, it was easy to monitor that primary keratinocyte cells were proliferating in the cultures instead of other populations of cells. Primary keratinocytes also expresses K14 protein (Figure 2.5 B), which can be used as a marker to identify the proliferating cells through immunofluorescence (Aasen and Izpisua Belmonte 2010). Primary culture was exploited to investigate the plausibility of delivering nucleic acids to cells similar to those found in human skin under controlled culture environment. The results from work with primary cells would facilitate or support transition of future work to excised human skin.

2.3.3 *Ex vivo* Human Skin

Excised human skin samples were successfully cultured *ex vivo* and remained viable for the duration of time required for gene manipulation studies described in Chapter 3 and 5. The protocol for culture of excised human skin maintained for up to 72 h has been previously optimised for pDNA delivery (Ng et al. 2009) and therefore the same organ culture protocol was employed for all *ex vivo* skin studies with pDNA. An example of the Trowell-type organ bath is depicted in Figure 2.6.

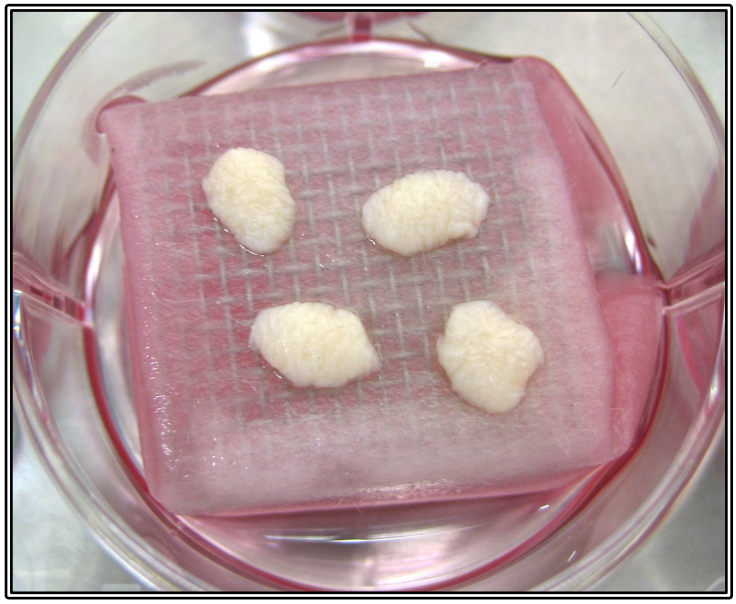

Figure 2.6: **A representative image of the Trowell-type organ culture setup**. The skin samples were punch biopsies of human breast skin resting on an air-liquid interface with the dermis in direct contact with the lens tissue paper wrapped around a metal grid platform, drawing up culture medium from the reservoir in the culture vessel.

An alternative *ex vivo* culture model using the hanging insert organ culture setup was employed in subsequent siRNA delivery experiments. This hanging insert organ culture setup requires less organ culture volume and involves less processing steps. The viability of excised human skin cultured in hanging inserts has previously been validated by a colleague, who demonstrated high epidermal cell viability through flow cytometry for culture of up to 5 days (results not published). An example of the hanging insert organ culture setup is depicted in Figure 2.7.

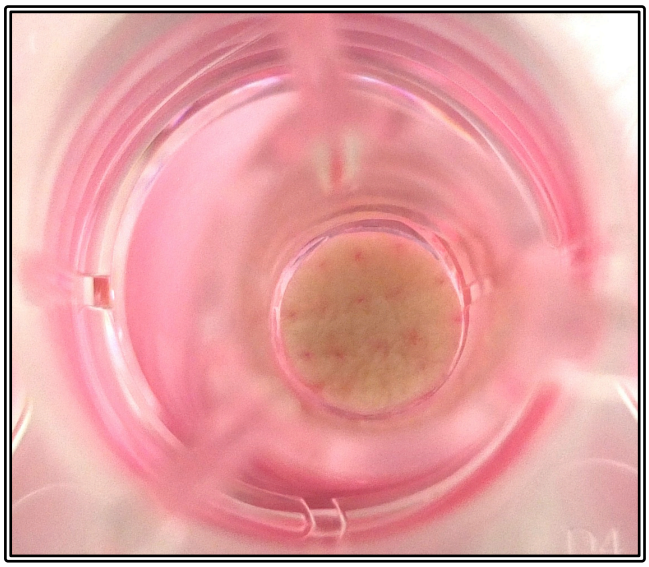

Figure 2.7: A representative image of the hanging insert organ culture setup. The skin sample was a punch biopsy of microneedle-treated human breast skin resting on an air-liquid interphase with the dermis in direct contact with culture medium in the culture vessel.

2.3.4 Characterisation of microneedle devices

Microneedle devices used in this research were made of stainless steel and were manufactured and fabricated by Georgia Institute of Technology, USA or Cardiff University, UK (Figure 2.8). The microneedle devices have different needle shapes (blade, concave, serrated), heights (500 or 750 μm) and spatial densities (5 or 10 needles per array).

5 × 700 μm (Georgia Institute of Technology, USA)

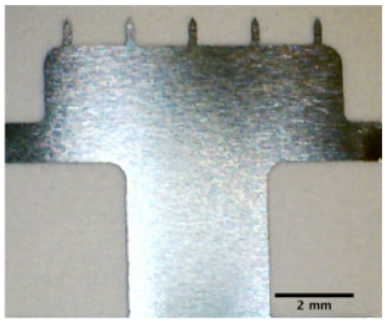

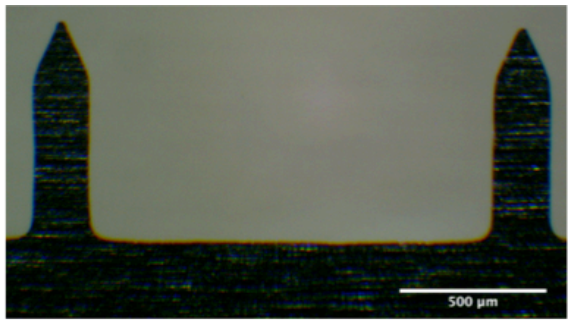

5 × 700 μm Regular (Cardiff University, UK)

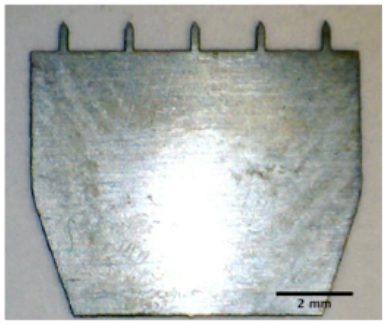

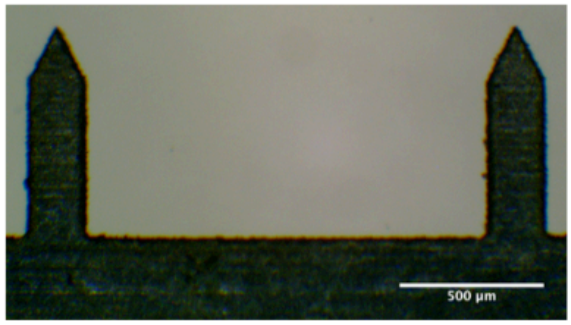

10 × 700 μm Regular (Cardiff University, UK)

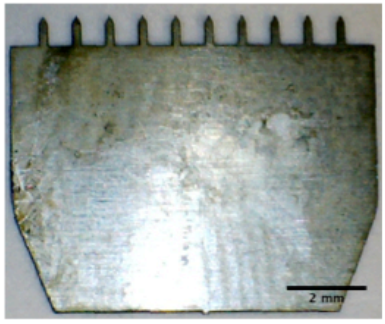

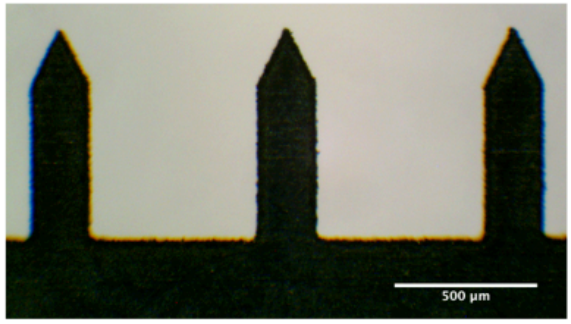

5 × 700 μm Concave (Cardiff University, UK)

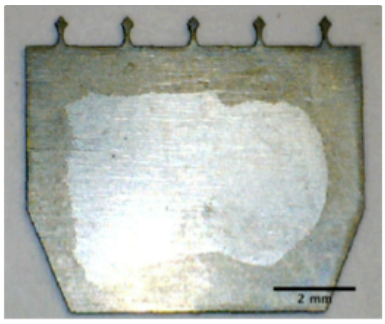

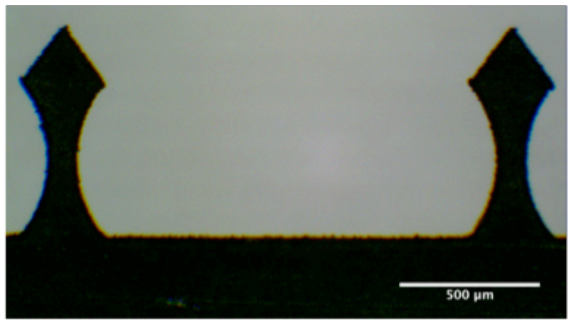

5 × 700 μm Serrated (Cardiff University, UK)

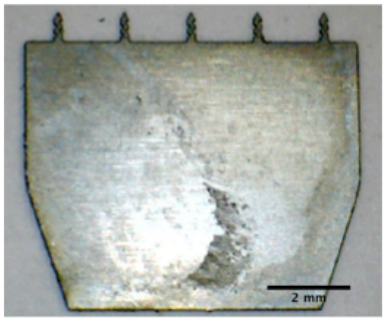

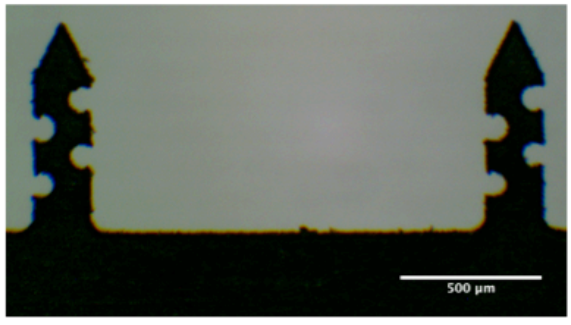

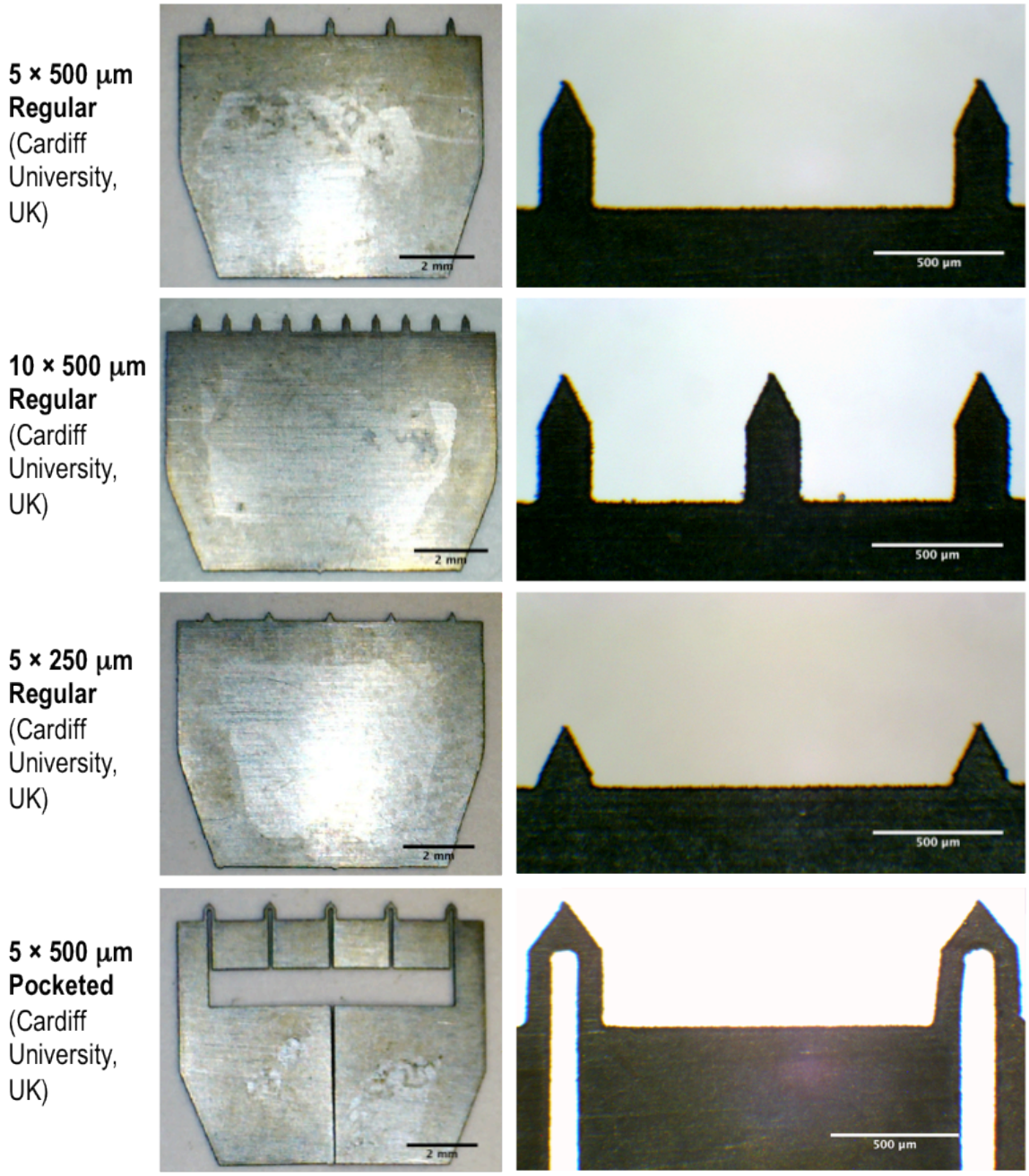

Figure 2.8: Images of stainless steel microneedle devices of different needle heights, shapes and spatial densities.

Previously, in-plane steel microneedle arrays in the laboratory were coated using a specially designed micro-dip-coating device (Figure 2.9). The device has a solution reservoir that is covered by a thin sheet of plastic with micron-sized holes of the same spacing as the needles in an array of in-plane metal microneedle device. This served to prevent solution contact with the base of the microneedles on insertion into the reservoir (Gill and Prausnitz 2007a). The aforementioned micro-dip-coating device is useful when coating microneedles with a single coat of potent drug solution with precision.

However when manually coating microneedles multiple times the shape of the thin sheet cover distorts over time causing the micron-sized holes to expand. This can lead to deposition of drug substance on the base of the microneedle array. The dip-coating device is cleaned after use and reused, which raises the concern of residual contaminants from previous experiments. Most importantly, the device also has a dead volume of 10 μL, which causes wastage of materials such as proteins, nucleic acids and other expensive biologic drugs.

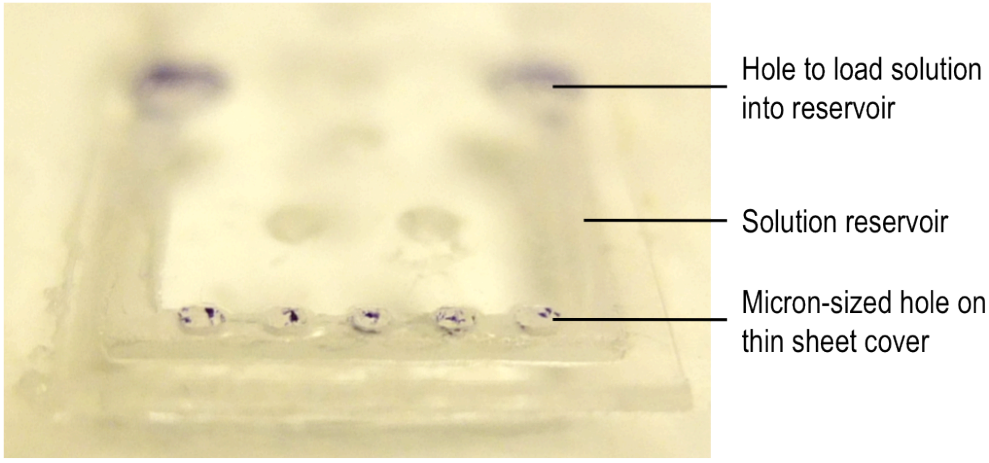

Figure 2.9: Digital image of the micro-deep-coating device.

An optimised technique for dip-coating microneedles was developed as depicted in Figure 2.3. Albeit a slower coating process than using the dip-coating device, this technique improves coating precision and dosage accuracy. The depth of microneedle immersion into the coating reservoir can be manually manipulated when coating under the inspection microscope. Coating fluid in the reservoir can be fully utilised to avoid wastage of material as well as provide theoretical estimation of drug quantity coated on the microneedles if the volume and concentration of drug formulation loaded into the reservoir was known. Microneedles of any shape, spatial density and dimension may be coated as the end of a pipette tip can be cut to reveal larger hole if necessary. As pipette tips are inexpensive and readily available in laboratories, the tips are for single use ensuring coating material purity. This technique is inexpensive and can be performed in any laboratory setting.

Initial skin penetration studies using these steel microneedles were performed using methylene blue (Figure 2.10) and FITC conjugated oligonucleotide (Figure 2.11 and

2.12) delivered to dead mouse skin and excised human skin, respectively. These studies aim to determine the ability of steel microneedles to penetrate both the mouse and human skin and deliver their cargo using simple, easily detectable reagents. The characteristics of cargo delivery with formulations that were either liquid loaded or dry-coated onto microneedles were then evaluated to determine a system suitable for nucleic acid delivery.

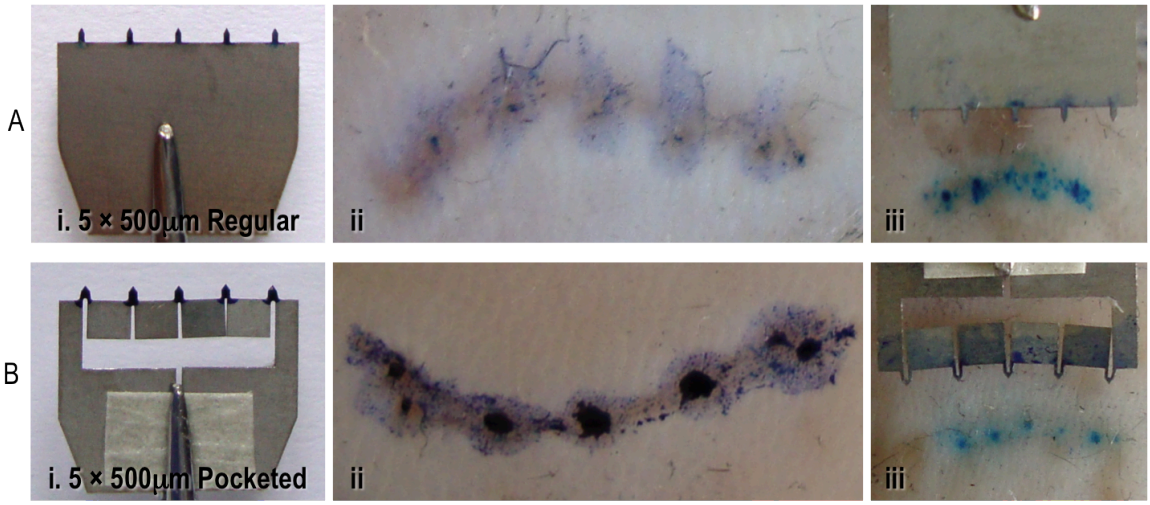

Figure 2.10: Images of stainless steel microneedles liquid-loaded with methylene blue and mouse skin that have been treated by the microneedle devices. Microneedle devices (A: 5 regular needles per array and B: 5 pocketed needles per array, both with 500 μm needle length) were (i) coated with 2% (w/v) methylene blue + 10% glycerol, (ii) delivered to mouse skin and (iii) imaged with used devices beside the corresponding penetration sites on the mouse skin.

Methylene blue is a water-soluble compound that does not penetrate the highly lipophilic stratum corneum of intact skin. Methylene blue solution dries quickly on the surface of microneedles, therefore glycerol was added to the formulation in this experiment to investigate the delivery of liquid-loaded methylene blue solution to mouse skin. As depicted in Figure 2.10, methylene blue in a glycerol solution, liquid-loaded onto the surface of steel microneedles, resulted in penetration of the mouse skin stratum corneum and deposition of methylene blue on the surface of the skin. The pocketed microneedles showed higher liquid loading capacity than the regular microneedles. However, the majority of the methylene blue solution was deposited on the surface of the skin instead of in the skin penetration site. The delivery of liquid-

loaded formulations using microneedles also resulted in a visible amount of liquid formulation adhering to the microneedle base plate after they were removed from the skin. Although liquid-loaded formulations do not enable the microneedle to fully deliver its cargo into the skin, but rather on the surface of the skin, this approach may be advantageous as it avoids the dissolution step required in formulations that have been dry-coated onto microneedles.

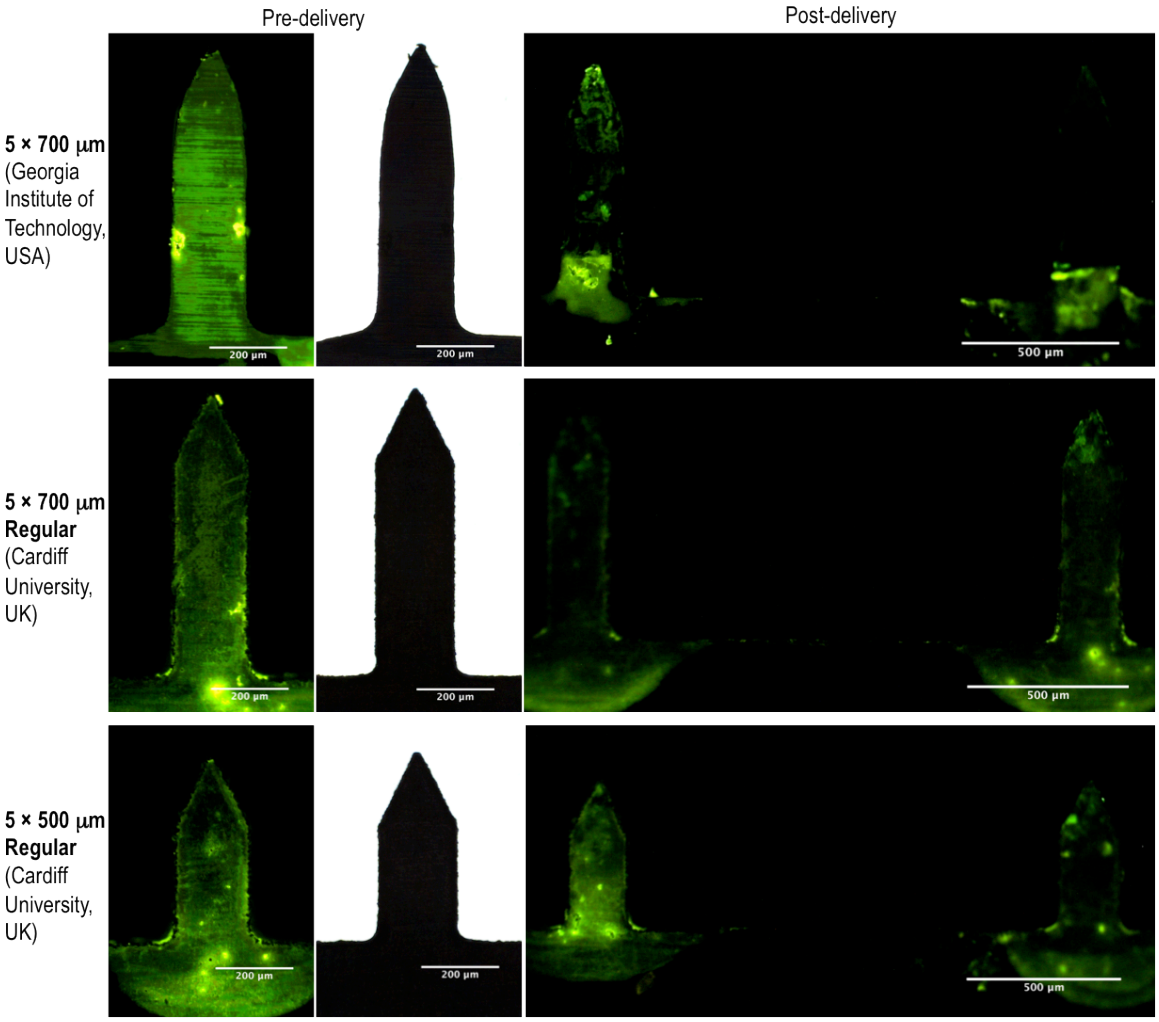

Figure 2.11: Representative fluorescent and bright-field micrographs of stainless steel microneedle devices coated with FITC-conjugated oligonucleotide before (pre-delivery) and after (post-delivery) insertion into human skin. (FITC fluorescence was pseudo-coloured green)

The ability to deliver high molecular weight compounds into the skin using dry-coated microneedles was then investigated using FITC conjugated oligonucleotide. The surfaces of microneedles of different needle lengths and from different manufacturers

were evenly coated with the fluorescent material (Figure 2.11 “pre-delivery”). There was a visible amount of material coated on the base of the microneedle arrays, which could be improved by controlling the depth of microneedle immersion into the coating reservoir. Following insertion of coated microneedles into human skin (Figure 2.11 “post-delivery”), the fluorescence signal was reduced along the length of the Georgia Institute of Technology microneedles (Figure 2.11). It is presumed that the coated material has been deposited in the human skin during microneedle administration. However, there was a notable amount of coating material left on both the microneedle arrays manufactured by Cardiff University (Figure 2.11).

The treated skin samples were cryosectioned and transverse sections of the microneedle penetration sites were examined microscopically (Figure 2.12). More FITC conjugated oligonucleotide was deposited on skin sample treated with the microneedles from Georgia Institute of Technology, consistent with the observation of less fluorescence remaining on the microneedles post-delivery compared to the microneedles manufactured at Cardiff School of Engineering. The fluorescent oligonucleotide was also deposited in human skin treated with the microneedles manufactured in Cardiff University but to a lesser extent, which corresponds to the notable fluorescence signal that remained on the surface of microneedles post-delivery.

The steel microneedle devices manufactured by Georgia Institute of Technology, USA were surface-electropolished (Gill and Prausnitz 2007a) whilst the microneedle devices manufactured by Cardiff University, UK were not. This could be one of the factors affecting the ability of steel microneedle devices to release its coated cargo. As visible from the scanning electron micrographs published by Gill and Prausnitz in 2007 (Figure 2.13), there are vast differences in microneedle surface smoothness and tip sharpness following electropolishing. The effect of the different microneedle surfaces on the ability to release its coated cargo was investigated further with pDNA in Chapter 3 and siRNA in Chapter 4.

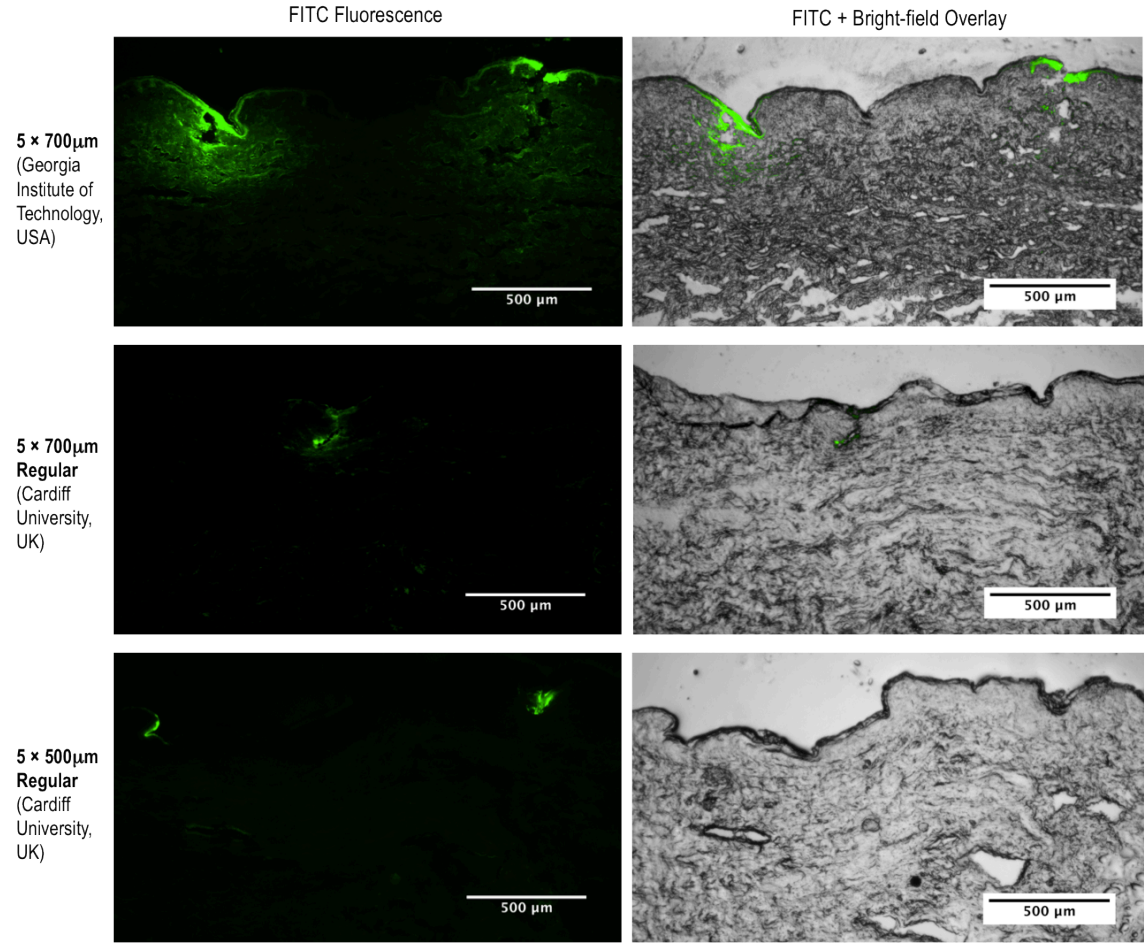

Figure 2.12: Representative fluorescent and bright-field micrographs of human skin sections, which have been microneedle-treated with dry-coated FITC-conjugated oligonucleotide. FITC fluorescence was pseudocoloured green.

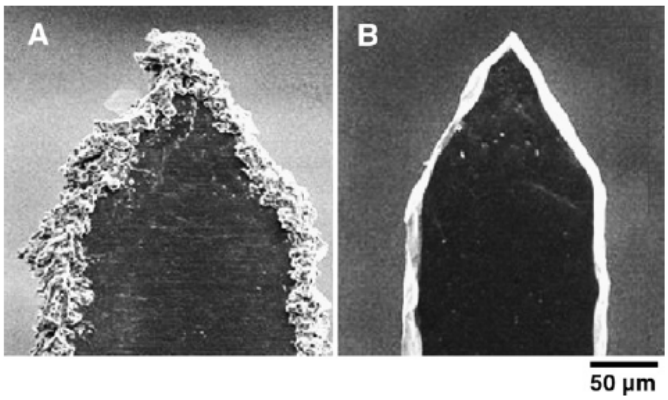

Figure 2.13: Scanning electron micrograph showing the effect of electropolishing on the surface of steel microneedle. (A) A microneedle tip after cleaning with detergent powder appears to have debris residue and slag. (B) A microneedle tip after electropolishing reveals a cleaner, sharper and smoother surface that is free from debris and slag (taken from Gill and Prausnitz 2007a).

2.4 Conclusion

In this method development and optimisation chapter, several culture models of human skin were successfully developed and optimised. The availability and ability to maintain these culture models was essential to future nucleic acid delivery work in later chapters. Microneedles of various shape, dimension and spatial densities were also characterised microscopically. More importantly, a simple and precise manual coating technique was successfully developed and used for coating nucleic acid onto steel microneedles in later chapters. Preliminary skin penetration studies showed the ability of the various coated steel microneedles to breach the stratum corneum barrier and subsequently deposit coated materials in the skin proximal to the microneedle penetration site.

CHAPTER 3

Non viral delivery of plasmid DNA to human skin

3 Non viral delivery of plasmid DNA to human skin

3.1 Introduction

According to the "central dogma" of molecular biology, expression of genetic information occurs from the direction of nucleic acids to proteins (Crick 1970). Gene expression to produce proteins involves transcription of sequence specific DNA to corresponding mRNA. The subsequent translation of mRNA into amino acids, which are then folded into proteins, is essential for the regulation of cellular function. Genetic diseases are caused by failure in gene regulation, resulting in over-, under- or non-expression of functional protein in the body. For genetic manipulation to occur, therapeutically relevant genetic material needs to be delivered across the cellular membrane and introduced to the target site in a safe and effective manner. In the skin, this challenge is further complicated by the presence of the physical barrier of the tissue, the stratum corneum. Despite the presence of the stratum corneum barrier, gene delivery to the skin is advantageous as it is the largest organ of the human body and is readily accessible for treatment. Non-viral gene therapy uses plasmid DNA (pDNA) to allow introduction of a missing gene to correct monogenic recessive disorders (Kikuchi et al. 2008). This chapter describes introduction of nucleic acid to both *in vitro* and *ex vivo* humans skin models, in the form of pDNA that expresses a reporter gene, as the first steps to understanding cutaneous gene delivery and gene expression.

3.1.1 Non-viral delivery of nucleic acids

The ability to deliver naked reporter pDNA to excised human skin and observe transgene expression has been shown previously (Hengge et al. 1996) and is a useful tool to investigate pre-clinical functional genetic manipulation in human skin. Although delivery of naked pDNA to human skin models using skin disruption techniques such as intradermal injection (with or without electroporation), ballistic approaches and microneedles have been widely reported in the literature (refer to Chapter 1 for comprehensive literature review), naked DNA does not cross the cellular barrier in monolayer cell culture *in vitro* and requires vectors for cellular delivery (Felgner et al. 1987).

As previously discussed in the general introduction chapter, certain viral vectors are ideal for gene delivery as they allow permanent introduction of genetic material into the

cells. However, viral gene delivery is associated with risks of life threatening adverse effects such as acute immune response, immunogenicity, and insertional mutagenesis (Hacein-Bey-Abina et al. 2008; Howe et al. 2008; Vannucci et al. 2013). The use of non-viral vectors, if executed optimally, provides a safe and effective alternative method of gene delivery to the skin. Non-viral vectors such as cationic lipids can be used to deliver nucleic acids to *in vitro* keratinocyte cells, which can be re-grafted back to a patient in an *ex vivo* approach of cutaneous gene delivery (Del Rio et al. 2004; Ferrari et al. 2005). The ability to improve cellular delivery of nucleic acid with a non-viral vector could also potentially improve *in vivo* gene delivery and subsequent gene expression in human skin.

3.1.2 Reporter plasmid DNA

Plasmid DNA exists naturally as supercoiled small circular double-stranded DNA molecules that is not a part of genomic DNA (extra-chromosomal) and replicates independently in a cell. Naturally occurring plasmids in bacteria carry auxiliary genes that can be exchanged between bacterial cells. For example, some bacteria contains fertility factor that allows gene transfer between one bacterium to another through conjugation, known as the F-plasmids (Lederberg et al. 1952); and some bacteria gain antibiotic resistance through pDNA exchange between different strains, known as the R-plasmids (Christie et al. 1987). Synthetic plasmids are capable of multiplying rapidly in bacterial culture for extraction and purification (Prazeres et al. 1998). Recombinant DNA technology allows insertion of a gene sequence that encodes a visual marker into a synthetic plasmid construct, which is expressed as reporter gene when introduced to cells. pDNA expressing reporter genes are commonly used to identify and quantify gene expression in cells as reporter gene expression can easily be detected using established detection methods or assays. The expression of a reporter gene from a plasmid is used in proof-of-concept studies to indicate successful gene transfer resulting in gene expression. Therefore, it is important to select reporter gene that is not endogenously expressed in the target cells or organism. Two examples of commonly used reporter pDNAs are pEGFP-N1 and pCMVβ.

3.1.2.1 pEGFP-N1

The pEGFP-N1 reporter plasmid (GenBank accession number U55762) is a 4733 base pair (bp) vector construct that encodes a red-shifted variant of wild-type green fluorescent protein (GFP), called the enhanced GFP (EGFP). When expressed in cells and visualised through fluorescence microscope with a blue light, green fluorescence emitted by EGFP (excitation maximum at 488 nm; emission maximum at 507 nm) is more intense than wild-type GFP. The pEGFP-N1 vector has been optimised for enhanced expression in mammalian cells and contains a kanamycin/neomycin resistance region as a selectable bacterial propagation marker (ClontechLaboratories 2002). The green fluorescent protein reporter system is simple to analyse as it does not require a substrate to stimulate detection and is therefore widely utilised in gene therapy studies (van Roessel and Brand 2002). Besides fluorescence microscopy, a fluorescence detector within a flow cytometry system can also detect the expression of EGFP within living cells.

3.1.2.2 pCMVβ

The pCMVβ (or pCMV-LacZ) reporter plasmid (GenBank accession number: U02451) is a 7165 bp vector construct that encodes bacterial (*Escherichia coli*) β-galactosidase. The pCMVβ uses human cytomegalovirus (CMV) immediate early gene promoter to drive expression of β-galactosidase in mammalian cells (MacGregor and Caskey 1989). The hydrolysis of galactosides into monosaccharides is catalysed by β-galactosidase, a hydrolase enzyme. One of the galactoside substrates, 5-bromo-4-chloro-3-indolyl-D-galactoside (X-gal) is converted by the β-galactosidase enzyme to galactose and an intermediate, which readily oxides to form a water-insoluble blue pigment visible to the naked eye when expressed in tissue or under the light microscope when expressed in monolayer cell culture. The plasmid vector also has an ampicillin resistance gene as a selectable bacterial propagation marker (ClontechLaboratories 2004).

3.1.3 Cationic liposomal transfection reagents

The use of microneedle devices has previously been shown to facilitate functional delivery of naked reporter pDNA expressing the β-galactosidase enzyme in excised human skin (Birchall et al. 2005; Coulman et al. 2006b; Ng et al. 2009). For gene

expression to occur from a plasmid vector, the exogenous DNA molecule needs to cross the cell membrane, avoid degradation in the cytoplasm and translocate into the cell nucleus. This renders naked pDNA a vulnerable candidate, as naked DNA is prone to degradation by intracellular and extracellular nucleases. Furthermore, naked DNA does not cross intact cell membranes easily because DNA has a negative charge and is repelled by the negatively charged cell membrane (Gao et al. 2007; Lechardeur and Lukacs 2006).

To overcome nuclease degradation and repulsion from the cell membrane, lipid based transfection reagents are commercially available and widely used to protect DNA from degradation and to facilitate uptake *in vitro*. However, the use of lipid based transfection reagents in the skin has resulted in varying degrees of success. Studies have been performed in murine models, porcine skin model, injured skin and reconstructed human epidermis (Branski et al. 2010; El Maghraby et al. 2008; Jeschke et al. 2000; Raghavachari and Fahl 2002; Steinstraesser et al. 2007). Nucleic acid uptake and subsequent gene expression varies between species (Hengge et al. 1996). Reconstructed human skin equivalent is also more permeable than *in vivo* human skin, which could exaggerate the effect of transdermal drug delivery (El Maghraby et al. 2008). Therefore, the use of lipid based transfection reagent in *ex vivo* human skin could provide great pre-clinical insights to the potential of such reagents for the delivery of nucleic acid to *in vivo* human skin.

Liposomes used for non-viral nucleic acid delivery are usually positively charged (cationic) and are complexed with negatively charged DNA to form lipoplexes. Liposomes are normally used in excess charge ratio over DNA to form lipoplexes with a net positive charge, which enhances interaction of lipoplexes with cellular membrane (Felgner et al. 1987; Sakurai et al. 2000). Lipoplexes are taken up by cells through the endocytosis pathway, whereby they are internalised through fusion with cell membrane and formation of endosomes (Almofti et al. 2003; Rejman et al. 2005). Encapsulation of DNA in liposomes to form lipoplexes also protects DNA from enzymatic degradation by nucleases (Gershon et al. 1993). The mechanism of DNA release from endosomes upon cellular internalisation, which is a critical step for efficient transfection, is still unclear but it has been proposed that the interaction of cationic lipids with anionic lipids of endosome membrane destabilises and induces a “flip-flop” of the endosomal lipids to

allow DNA escape into cytoplasm (Hoekstra et al. 2007; Xu et al. 1999; Xu and Szoka Jr 1996). Differences in liposome structures and composition are said to affect cellular uptake and cellular toxicity in a cell-type specific and transfection condition specific manner and should be optimised (Yamano et al. 2010).

3.1.4 Aim and objectives

The aim of this chapter was to develop and optimise techniques for non-viral delivery and analyse gene expression in human skin models using microneedle devices. The objective of the experiments were:

- To propagate *Escherichia coli* bacteria transformed with reporter plasmids and then isolate purified reporter plasmids pEGFP-N1 and pCMVβ.
- To identify a liposomal DNA formulation capable of enhancing delivery of pDNA to an *in vitro* cell monolayer with minimum toxicity.
- To characterise steel microneedle devices in terms of pDNA coating ability and the stability of pDNA coated microneedles during storage.
- To demonstrate reproducible functional pDNA delivery to *ex vivo* human skin using various disruption methods, including microneedles.
- To visualise epidermal localisation of reporter gene expression in *ex vivo* human skin.

3.2 Methods

Unless specified, the suppliers of all reagents and materials have previously been mentioned or were obtained from Thermo Fisher Scientific, UK.

3.2.1 Plasmid DNA preparation

3.2.1.1 Colony selection

Frozen transformed pEGFP-N1 and pCMVβ *Escherichia coli* bacteria were gifts from Dr Marc Pearton and Dr Keng Wooi Ng (previously School of Pharmacy and Pharmaceutical Sciences, Cardiff University).

Luria agar (Sigma Aldrich, UK) (40 mg mL^{-1}) and Luria broth (Sigma Aldrich, UK) (25 mg mL^{-1}) were prepared according to manufacturer's instruction in deionised water and autoclaved. Luria agar was cooled to approximately 50°C before 50 μg mL^{-1} kanamycin (Life Technologies, UK) or 100 μg mL^{-1} ampicillin (Sigma Aldrich, UK) were respectively added to the molten agar as selective antibiotics for propagation of bacteria containing pEGFP-N1 or pCMVβ plasmids, respectively. Molten luria agar with antibiotics were poured into sterile petri dishes and allowed to cool and solidify at room temperature. A volume of 100 μL transformed bacterial culture was transferred on to the agar. The culture was sequentially streaked across the agar surface using a sterile inoculation loop, in a pattern shown in Figure 3.1, to achieve dilution of the culture. The agar plate was incubated at 37°C for 18 h.

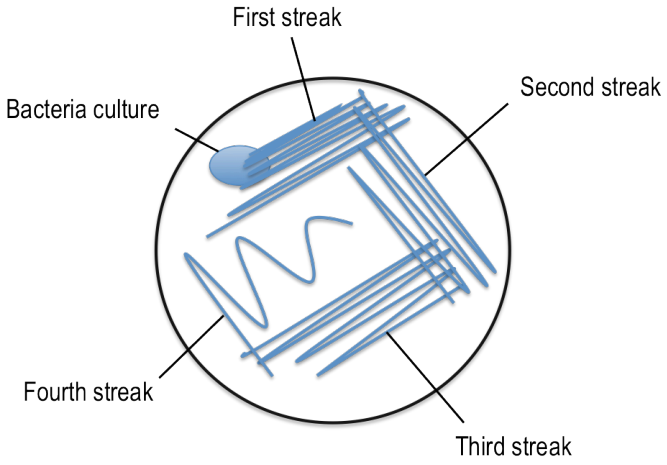

Figure 3.1: A schematic representation of the bacteria culture streak pattern on agar.

3.2.1.2 Bacterial propagation

At the end of the incubation period, a single isolated bacterial colony on the agar plate was selected and isolated using a sterile inoculation loop and added to 5 mL Luria broth containing the selective antibiotic in a McCartney bottle. The broth was then incubated at 37°C with shaking at 140 rpm in the Orbi-Safe shaking incubator (Sanyo E&E, UK) for 6 h.

3.2.1.3 Plasmid amplication

After initial incubation, 1 mL of bacterial culture was transferred into each of the four 125 mL Luria broths with a selective antibiotic, in a 500 mL conical flask, respectively (total of 500 mL Luria broth volume in four flasks). The broths were incubated at 37°C with shaking at 140 rpm in the Orbi-Safe shaking incubator for a further 18 h.

3.2.1.4 Plasmid isolation and purification

Plasmid from the bacterial culture was isolated and purified using the Qiagen® Plasmid Mega Kit (Qiagen, UK) according to a protocol supplied with the kit. Briefly, the inoculated broths were centrifuged (Beckman Coulter, UK) at 6000 × *g* at 4°C for 15 min to create a bacterial pellet. The supernatant was discarded while the bacterial pellet was re-suspended and subsequently lysed by pre-formulated buffers supplied with the kit to lyse bacteria cells based on a modified alkaline lysis procedure (Birnboim and Doly 1979). The lysate was collected by centrifuging at 20000 × *g* for 30 min at 4°C. The supernatant containing pDNA was removed promptly and kept while the lysate pellet was discarded. The QIAGENtip 2500 anion-exchange column was pre-conditioned to the appropriate low-salt and pH conditions by equilibrating with one of buffers supplied with the kit. The supernatant containing pDNA was then eluted through the column, which retained the pDNA through binding with resin in the column and a medium-salt wash buffer was added to remove protein, RNA and other impurities. A high-salt buffer was then added to eluate the pDNA and the eluate was collected in a sterile tube.

Isopropanol was added to the eluate to concentrate and desalt the pDNA through precipitation and the precipitate was centrifuged at 15000 × *g* for 30 min at 4°C. The

supernatant was carefully decanted without disturbing the DNA pellet. The pellet was then air-dried for 10 to 20 min and re-dissolved in 1 mL of tris-EDTA (TE) buffer, pH 8.0. The pDNA solution was frozen at -20°C until further use.

3.2.1.5 Quantification of nucleic acid

The concentration and purity of nucleic acid was measured using a NanoVue Plus spectrophotometer (GE Healthcare, UK) or NanoDrop spectrophotometer (Thermo Fisher Scientific, USA). The baseline absorbance was obtained by measuring absorbance of 2 μL of buffer. The concentration of nucleic acid sample was then determined by measuring 2 μL of the sample undiluted or diluted up to 1:100 with buffer. The concentration of the nucleic acid sample and a ratio of absorbance, at wavelengths 260 μm and 280 μm ($A_{260/280}$) were recorded. If the sample was diluted, the concentration was calculated by multiplying the value obtained with the dilution factor. The $A_{260/280}$ value was used to determine the purity of the nucleic acid sample.

3.2.1.6 Analysis of plasmid DNA

pDNA was analysed by agarose gel electrophoresis. Agarose gel 1% (w/v) was prepared by dissolving 1 g of agarose powder in 100 mL tris-borate-EDTA (TBE) buffer and heated using the microwave at 800 watt (W) for 1 min and 5 s. The agarose solution was allowed to cool to approximately 50°C before a drop of ethidium bromide was added to the solution. The molten agarose solution containing ethidium bromide was poured into an electrophoresis tray fitted with a gel comb and allowed to solidify at room temperature for 30 min. The gel comb was then removed to reveal wells for sample loading and the gel setting was placed in an electrophoresis tank filled with TBE buffer.

A loading buffer containing bromophenol blue was added to an aliquot of DNA sample containing 0.5 μg pDNA diluted in deionised water and a supercoiled DNA molecular weight marker (New England Biolabs, UK). The samples were loaded into the wells and electrophoresis was carried out at 100 V for 30 to 45 min. After electrophoresis, the gel was imaged with the Bio-rad ChemiDoc™ XRS+ gel imaging system (Bio-rad, UK).

3.2.2 Preparation of DNA-liposome complexes

3.2.2.1 DOTAP liposomes

For the preparation of 1,2-dioleoyl-3-trimethylammonium-propane (chloride salt) (DOTAP) (Avanti Polar Lipids, USA) liposomes 10 mg DOTAP powder was measured and transferred into a 50 mL round-bottom flask. Chloroform was added to dissolve the DOTAP powder and the solvent was subsequently evaporated using the Rotavap R110 (BÜCHI Labortechnik AG, Switzerland) rotary evaporater. The round bottom flask was fitted to the rotary evaporator and was lowered into a 37°C water bath. The condenser was filled with running tap water as coolant and partial vacuum was induced. The flask was rotated at approximately 60 rpm for 2 to 3 min and when the chloroform had evaporated, a thin film lining the inner wall of the flask was observed. Full vacuum and rotation speed was set to operate for 90 min. Then, 10 mL of sterile deionised water, pre-warmed to 37°C, was added to the flask, resulting in a 1mg mL^{-1} DOTAP solution, Alternatively, the headspace of the flask was purged with N_2, stoppered and sealed with paraffin film and stored at 4°C for short-term storage.

To proceed, the flask with DOTAP and water was placed on the vortex to disperse the film and create an aqueous suspension of DOTAP vesicles. The suspension was incubated in water bath at 37°C for 30 min before liposome extrusion through a 100 nm Nuclepore® polycarbonate filter membrane (Millipore (UK) Ltd, UK) within The Extruder™ (Lipex Biomembranes Inc., Canada), for a total of 10 extrusions. The size of the DOTAP liposomes was determined by photon correlation spectroscopy using the N4 Plus submicron particle size analyser (Beckman Coulter (UK) Ltd, UK) and the Coulter counter software (Beckman Coulter (UK) Ltd, UK). If the extruded liposomes were not of the satisfactory size, the extrusion process was repeated. Extruded liposomes of satisfactory size (≤120 nm) were kept in small sterile glass vials with the headspace of the vials purged with N_2, capped, sealed with paraffin film and refrigerated at 4°C for use within 3 days.

DOTAP and pDNA lipoplexes were assembled within 2 h of use using the formulation outlined in Table 3.1 and 3.2. Sterile deionised water was added to dilute the pDNA. Then, protamine sulphate (grade X from salmon sperm; Sigma Aldrich, UK) was added to the diluted DNA solution and then incubated for 10 min at room temperature. The

preceding incubation step was repeated after the addition of DOTAP. Finally, DMEM was added to the formulation. For formulations containing protamine sulphate, the mass ratio of DOTAP, protamine sulphate and DNA was kept at 3:2:1 (Birchall et al. 2000).

Table 3.1: Formulation of DOTAP lipoplexes with protamine sulphate (per well of 24 well plate)

Components	Volume (μL)
Plasmid DNA (1 mg mL^{-1})	0.5
Sterile deionised water	99.5
Protamine sulphate (1 mg mL^{-1})	1.0
DOTAP (1 mg mL^{-1})	1.5
DMEM	897.5

Table 3.2: Formulation of DOTAP lipoplexes without protamine sulphate (per well of 24 well plate)

Components	Volume (μL)
Plasmid DNA (1 mg mL^{-1})	0.5
Sterile deionised water	99.5
DOTAP (1 mg mL^{-1})	1.5
DMEM	898.5

3.2.2.2 Lipofectamine™ Reagent

Lipofectamine™ (Life Technologies, UK) transfection reagent is a 3:1 (w/w) liposome formulation of the polycationic lipid 2,3-dioleyloxy-N-[2(sperminecarboxamido)ethyl]-N,N-dimethyl-1-propanaminium trifluoroacetate (DOSPA), and the neutral lipid dioleoyl phosphatidylethanolamine (DOPE) in membrane-filtered water. Lipofectamine™ (Life Technologies, UK) lipoplexes were formulated and prepared within 2 h of use, using the formulation outlined in Table 3.3. The complexation method was adapted from the supplier's recommended protocol. For each transfection well, pDNA was diluted to 25 μL with Opti-MEM® and mixed gently. Lipofectamine™ reagent was gently mixed before use and then diluted to 25 μL with Opti-MEM® and mixed gently. The diluted DNA and diluted Lipofectamine™ was combined, gently mixed and then incubated at room temperature for 30 to 45 min. The complexes were further diluted by adding 150 μL of Opti-MEM® and gently mixed.

Table 3.3: Formulation of Lipofectamine™ lipoplexes (per well of 24 well plate)

Components	Volume (μL)
Plasmid DNA (1 mg mL^{-1})	0.5
Lipofectamine™ reagent	1.5
Opti-MEM® I Reduced Serum Medium	198.0

3.2.2.3 Lipofectine™ Reagent

Lipofectine™ (Life Technologies, UK) transfection reagent is a water-based 1:1 (w/w) liposome formulation of the cationic lipid N-[1-(2,3- dioleyloxy)propyl]-N,N,N-trimethylammonium chloride (DOTMA) and neutral lipid dioleoyl phosphatidylethanolamine (DOPE) in membrane-filtered water. Lipofectine™ lipoplexes were formulated and prepared within 2 h of use, using the formulation outlined in Table 3.4. The complexation method was adapted from the supplier's recommended protocol. For each transfection well, pDNA was diluted to 25 μL with Opti-MEM® and mixed gently. Lipofectine™ reagent was gently mixed before use and then diluted to 25 μL with Opti-MEM®. The diluted reagent was gently mixed and allowed to stand at room temperature for 30 to 45 min. The diluted DNA and diluted Lipofectine™ was combined, gently mixed and then incubated at room temperature for 10 to 15 min. The complexes were further diluted by adding 150 μL of Opti-MEM® and gently mixed.

Table 3.4: Formulation of Lipofectine™ lipoplexes (per well of 24 well plate)

Components	Volume (μL)
Plasmid DNA (1 mg mL^{-1})	0.5
Lipofectine™ reagent	1.5
Opti-MEM® I Reduced Serum Medium	198.0

3.2.2.4 Lipofectamine™ 2000 Reagent

Lipofectamine™ 2000 (Life Technologies, UK) transfection reagent is a proprietary formulation. Lipofectamine™ 2000 lipoplexes were formulated and prepared within 2 h of use, using the formulation outlined in Table 3.5. The complexation method was adapted from the supplier's recommended protocol. For each transfection well, pDNA

was diluted to 50 μL with Opti-MEM® and mixed gently. Lipofectamine™ 2000 reagent was gently mixed before use. It was then diluted to 50 μL with Opti-MEM®, gently mixed and incubated at room temperature for 5 min. The diluted DNA and diluted Lipofectamine™ 2000 was combined, gently mixed and then incubated at room temperature for 20 min.

Table 3.5: Formulation of Lipofectamine™ 2000 lipoplexes (per well of 24 well plate)

Components	Volume (μL)
Plasmid DNA (1 mg mL^{-1})	0.5
Lipofectamine™ 2000 reagent	2.0
Opti-MEM® I Reduced Serum Medium	97.5

3.2.2.5 Lipofectamine™ LTX and PLUS™ Reagent

Lipofectamine™ LTX (Life Technologies, UK) transfection reagent is a proprietary formulation. Lipofectamine™ LTX lipoplexes were formulated and prepared within 2 h of use, using the formula as outlined in Table 3.6. The complexation method was adapted from the supplier's recommended protocol. For each transfection sample, pDNA was diluted in 97.5 μL Opti-MEM® and mixed thoroughly. PLUS™ reagent (Life Technologies, UK) was gently mixed before being added directly to the diluted DNA. The solution was gently mixed and incubated at room temperature for 5 min. Lipofectamine™ LTX was gently mixed before being added directly to the diluted DNA and mixed thoroughly. The complexes were incubated for 30 min at room temperature to allow the lipoplexes to form.

Table 3.6: Formulation of Lipofectamine™ LTX lipoplexes (per well of 24 well plate)

Components	Volume (μL)
Plasmid DNA (1 mg mL^{-1})	0.5
PLUS™ reagent	0.5
Lipofectamine™ LTX reagent	1.5
Opti-MEM® I Reduced Serum Medium	97.5

3.2.3 HaCaT Cell Transfection

One day before transfection, HaCaT cells were seeded at 5×10^4 cells cm^{-2} in a 24-well plate, so that the cells were at least 70% confluent at the time of transfection, and allowed to adhere to the bottom of the plate surface overnight. For cells transfected with Lipofectamine 2000, cells were seeded at 7.5×10^4 cells cm^{-2} so that the cells were at least 90% confluent at the time of transfection. Cells were seeded in 0.5 mL of growth medium without antibiotics. Cells were then treated in triplicate or quadruplicate wells as described in sections 3.2.3.1, 3.2.3.2 and 3.2.3.3. The plates were gently rocked back and forth for 30 s to ensure thorough mixing of the well contents. The cells were incubated at 37°C in a humidified atmosphere containing 5% CO_2 in air for 5 h to allow sufficient time for lipoplex entry into cells. After the initial incubation, the transfection media was replaced with 500 μL of DMEM with serum to reduce cell toxicity and cell death. Cells were then further incubated and transgene expression was tested 48 h post-transfection. As negative controls, cells were treated with formulation equivalents of each transfection reagents minus the pDNA. As a non-lipoplex control, cells were treated with the same concentration of pDNA without transfection reagents.

3.2.3.1 DOTAP lipoplexes

The cell growth medium was removed from the wells and the cells were washed twice with PBS. Thereafter, 1 mL of the DOTAP lipoplexes (transfection media) was added to each well.

3.2.3.2 Lipofectamine™ and Lipofectine™ lipoplexes

The cell growth medium was removed from the wells and the cells were washed twice with Opti-MEM® I Reduced Serum Medium and replaced with 200 μL of Opti-MEM® I Reduced Serum Medium and 200 μL of the diluted Lipofectamine™ and Lipofectine™ lipoplexes in each well.

3.2.3.3 Lipofectamine™ 2000 and Lipofectamine™ LTX lipoplexes

For transfection with Lipofectamine™ 2000 or Lipofectamine™ LTX lipoplexes, 100 μL of the lipoplexes was added to each well.

3.2.4 Primary keratinocyte transfection

Primary keratinocytes were isolated from excised human breast skin of a 38-year-old female patient using methods described in section 2.2.4.

3.2.4.1 Lipofectamine™ 2000 reagent and DNA lipoplexes

Lipofectamine™ 2000 lipoplexes were formulated and prepared within 2 h of use, using the formula as outlined in Table 3.7 and described in section 3.2.2.4, except that keratinocyte specific culture medium without antibiotics was used in place of Opti-MEM®.

Table 3.7: Formulation of Lipofectamine™ 2000 lipoplexes (per well of 24 well plate)

Components	Volume (μL)
Plasmid DNA (1 mg mL^{-1})	0.5
Lipofectamine™ 2000 reagent	2.0
Keratinocyte specific culture medium	97.5

3.2.4.2 Lipofectamine™ LTX with PLUS™ reagent and DNA lipoplexes

Lipofectamine™ LTX lipoplexes were formulated and prepared immediately (up to 2 h) before use, using the formula as outlined in Table 3.8 and described in section 3.2.2.5, except that keratinocyte specific culture medium without antibiotics was used in place of Opti-MEM®.

Table 3.8: Formulation of Lipofectamine™ LTX lipoplexes (per well of 24 well plate)

Components	Volume (μL)
Plasmid DNA (1 mg mL^{-1})	0.5
PLUS™ reagent	0.5
Lipofectamine™ LTX reagent	1.5
Keratinocyte specific culture medium	97.5

3.2.4.3 Primary keratinocyte cell transfection

Cell transfection was performed on primary keratinocytes at passage 4. One day before transfection, cells were seeded at 5×10^4 cell cm^{-2} in a 24-well plate, so that the cells were at least 80% confluent at the time of transfection and allowed to adhere to the bottom of the plate surface overnight. Cells were seeded in 0.5 mL of keratinocyte specific culture medium without antibiotics.

Thereafter, 100 μL of the Lipofectamine™ 2000 and Lipofectamine™ LTX lipoplexes were added to each well, respectively. Cells were treated in quadruplicate wells. The plates were gently rocked back and forth for 30 s to ensure thorough mixing of the well contents. The cells were incubated at 37°C in a humidified atmosphere containing 5% CO_2 in air for 5 h. After the initial incubation, the media was replaced with 500 μL of keratinocyte specific medium without antibiotics to reduce cell toxicity and cell death. Cells were then further incubated and transgene expression was tested 48 h post-transfection.

3.2.5 Characterisation of plasmid DNA coating onto steel microneedles

3.2.5.1 Nucleic acid coating and quantification

Microneedles were coated with nucleic acid using the method described in section 2.2.5.2. Following drying and/or application of these microneedle devices, the mass of nucleic acid coated or deposited was quantified by determining the mass of nucleic acid left on the devices. Nucleic acid was recovered from the surface of microneedle devices by washing in a small volume, V, of buffer (50–150 μL) for 5 min with agitation. The concentration, C of nucleic acid was then quantified using the NanoVue or NanoDrop spectrophotometer, as described in section 3.2.1.5. The mass of nucleic acid recovered was calculated using the formula below:

$$m = C \times V$$

3.2.5.2 Re-using microneedle devices

Steel microneedle devices were re-used following thorough removal of previously coated material by sonication in deionised water for 15 min and a rinse in deionised

water. The 'clean' microneedle devices were then rinsed with 70% ethanol and air dried before next use.

3.2.5.3 Plasmid DNA coating functional assay

An assay was performed to determine functional stability of pDNA following coating and recovery from steel microneedles by coating, drying and recovering the pEGFP-N1 pDNA, as detailed in section 3.2.5.1. An aliquot of 2 μL pEGFP-N1 at a concentration of 6.5 μg μL^{-1} in TE buffer was loaded into a pipette tip reservoir for coating. Stainless steel microneedle devices (4 devices per treatment group; each with 5 microneedles per array and 700 μm needle length) were coated with pDNA using the dip-coating method described in section 2.2.5.2. A set of four coated devices was allowed to dry at 4°C for 24 h and the other set of four MNDs for 96 h before pDNA was recovered from the surface of the devices by washing in 100 μL TE buffer for 5 min and the buffers containing recovered pDNA were stored at -20°C until use.

On the day of transfection, the mass of pEGFP-N1 recovered from the microneedles was quantified and the pDNA was complexed with Lipofectamine™ 2000 reagent, as detailed in section 3.2.2.4. The pDNA solution and Opti-MEM® volumes were adjusted to maintain the mass of pEGFP-N1 to 0.5 μg per transfection well. The lipoplexes were then used to transfect HaCaT cells using the method described in section 3.2.3.

3.2.6 Excised human skin transfection

Excised human skin samples were acquired and prepared as described in section 2.2.3.2. The disruption methods as detailed in section 3.2.6.1.1, 3.2.6.1.2, 3.2.6.1.3, 3.2.6.1.4 and 3.2.6.1.5 were performed on the excised skin. The treated skin was cut into samples measuring 1 cm^2 using surgical scissors or cut using a 6 mm diameter biopsy punch and were cultured at the air-liquid interface in a Trowel-type system, in organ culture medium containing DMEM supplemented with 5% FCS, 100 mg mL^{-1} penicillin and 100 unit mL^{-1} streptomycin and 2.5 μg mL^{-1} amphotericin B at 37°C in a 5 % CO_2/95 % air humidified incubator for 24 h. Gene expression was determined 24 h post-transfection using the method detailed in section 3.2.7.3.

3.2.6.1 Microneedle abrasion

A 10 μL pDNA formulation containing either (i) naked pCMVβ 6 mg mL^{-1} in TE buffer, (ii) naked pCMVβ 1 mg mL^{-1}, (iii) naked pCMVβ 2.5 mg mL^{-1}in TE buffer, (iv) pCMVβ 1 mg mL^{-1} complexed with 50% (v/v) Lipofectamine™ 2000 in TE buffer, or (v) pCMVβ 2.5 mg mL^{-1} complexed with 50% (v/v) Lipofectamine™ 2000 in TE buffer was topically applied to the skin surface either before or after abrasion. The skin surface was abraded by inserting a stainless steel microneedle array (10 × 5 needles; 700 μm length) (Georgia Technologies, USA) into the skin and subsequently moving it laterally (5 mm) through the area of skin that was in contact with the liquid formulation. This action was repeated 5 times.

3.2.6.2 Tape-stripping

The skin surface was tape-stripped 40 times using D-squame® discs (CuDerm Corporation, USA). A 10 μL pDNA formulation containing naked plasmid pCMVβ 6 mg mL^{-1} in TE buffer was then applied to the skin surface and the treated area of skin was occluded with Vaseline® gauze (Covedien AG, USA).

3.2.6.3 Liquid cyanoacrylate strip

A drop of liquid cyanoacrylate (Loctite, UK & Ireland) was applied to either the tape-stripped skin or non-tape-stripped skin surface. A glass microscope slide was placed on the treated area for 5 min, allowing the liquid cyanoacrylate to dry, and the slide was subsequently removed in a single motion. A 10 μL pDNA formulation containing naked plasmid pCMVβ 6 mg mL^{-1} in TE buffer was then applied to the treated area. The treatment area was occluded with Vaseline gauze. PBS was applied on the treated skin surface instead of the pDNA formulation as a negative control. Alternatively, 10 μL of 2% (w/v) methylene blue in water solution was applied to the treated area to determine whether the stratum corneum barrier has been breeched following application of the liquid cyanoacrylate stripping method.

3.2.6.4 Multiple liquid cyanoacrylate strip

The liquid cyanoacrylate stripping method described in section 3.2.6.1.3 was repeated 2 to 4 times. A 10 μL pDNA formulation containing naked plasmid pCMVβ 6 mg mL^{-1}

in TE buffer was then applied to the skin surface. The treatment area was occluded with Vaseline gauze.

3.2.6.5 Multiple liquid cyanoacrylate strip and microneedles abrasion

The liquid cyanoacrylate stripping method described in section 3.2.6.1.3 was repeated 3 times. A stainless steel microneedle array (10 × 5 needles; 700 μm length) was inserted into the skin and moved laterally (5 mm) from the microneedle insertion site, across the area of skin 5 times. A 10 μL pDNA formulation containing 6 mg mL^{-1} naked plasmid pCMVβ in TE buffer was then applied to the skin surface. The treatment area was occluded with Vaseline gauze.

3.2.7 Analysis of transgene expression

3.2.7.1 Detection of GFP expression

3.2.7.1.1 Fluorescent microscopy

The expression of EGFP in cell monolayers was examined by fluorescence microscopy under blue laser light, which excited GFP at its peak excitation wavelength of 488 nm. Representative images were captured using the Olympus® DP-10 digital camera attached to the Olympus IX 50 microscope with the TH-3 halogen lamp, U-RFL-T fluorescence illuminator (Olympus (UK) Ltd, UK) or Leica DM IRB epifluorescence microscope with the Openlab imaging software.

3.2.7.1.2 Flow cytometry

The transfection efficiency of pEGFP-N1 in cells was determined by flow cytometry using the FACSCalibur™ or FACSCanto II flow cytometry systems (BD Biosciences, UK). The following procedure was performed on ice to reduce any cell activities past the incubation period and to keep cells viable for analysis. First, the cells were washed twice with chilled PBS and then trypsinised by incubating at 37°C for 10 min with trypsin-EDTA, to liberate the cells from the culture vessels. The cells were then re-suspended in growth medium, centrifuged (Thermo Fisher Scientific, UK) at 300 × *g* for 3 min, and then re-suspended in 200 μL chilled PBS. The cell suspensions were transferred into polysterene flow cytometry tubes (Elkay Laboratory Products (UK) Ltd,

US), stored on ice and analysed immediately by flow cytometry. If the flow cytometer was not immediately available, pelleted cells were resuspended in 100 μL flow cytometry buffer containing 1% (w/v) bovine serum albumin (Sigma Aldrich, UK) and 0.1% (w/v) sodium azide (Sigma Aldrich, UK) in PBS and transferred into flow cytometry tubes. The cells were fixed with 200 μL fixing buffer containing 1% (w/v) paraformaldehyde and 0.1% (w/v) sodium azide in PBS and analysed by flow cytometry within a week.

The flow cytometric analysis was performed as recommended by the instrument manual. The frequency of fluorescent cells in the FL1 channel (corresponding to green fluorescence), out of a total of at least 10^5 events analysed per sample was recorded. The data collected was analysed with the FlowJo Flow Cytometry Analysis Software for Mac Version 8.8 (Tree Star Inc., USA). A representative cell population excluding cell debris was selected from the dot plot of side-scattering (SSC-H) *vs.* forward-scattering (FSC-H). Then, within the selected population, a histogram of number of events against fluorescence intensity (FL1-H) was obtained. A software gate was created to define significant fluorescence intensity to indicate cells with the presence of fluorescence. Fluorescent signal from cells was considered significant when the fluorescence signal intensity is above the baseline fluorescence (autofluorescence), where ≤1% of cells in the negative control (untreated cells) samples was gated. The percentage of gated cells in each sample indicates the proportion of cells with fluorescence.

3.2.7.2 Confocal microscopy

For cells transfected with pEGFP-N1, and expressing GFP, an established fixation method to preserve GFP fluorescence was used (Brock et al. 1999). Briefly, growth medium was removed and cells were washed 3 times with PBS. The cells were initially fixed with 3% (w/v) paraformaldehyde (PFA) in PBS at 4°C for 5 min and at room temperature for 10 min and then washed 3 times with PBS. Thereafter, cells were fixed and permeabilised with ice-cold methanol, pre-chilled in a -20°C freezer, at 4°C for 6 min and washed 3 times with PBS. Each coverslip was lifted and excess fluid was carefully removed using filter paper, before being mounted on a drop of fluorescence mounting medium (Dako, UK) or PBS on a microscope slide. The edges of the

coverslips mounted on PBS were immediately sealed with nail varnish. The coverslips mounted in oil were allowed to dry at room temperature for 2 h before the edge of the coverslips were sealed with nail varnish. The slides were kept at 4°C until further use within a week. Cells were then imaged using the Leica DMI6000B confocal microscope system and analysed using the method described in section 2.2.4.6.

3.2.7.3 Detection of β-galactosidase expression

For detection of β-galactosidase expression in monolayer cell culture, cells were incubated with solutions in the Invitrogen β-gal Staining Kit (Life Technologies, UK) according to the protocol supplied with the kit. The cells were rinsed twice in PBS and fixed in 2 % (v/v) formaldehyde and 0.2 % (v/v) glutaraldehyde in PBS at room temperature for 10 min. The cells were then rinsed twice with PBS and were then incubated in X-gal staining solution at 37°C for 2 h. Again, the cells were rinsed twice in PBS and remain in PBS for visualisation under the Olympus® IX-50 microscope. Representative images were captured using the Olympus® DP-10 digital camera attached to the microscope.

For detection of β-galactosidase in excised human skin, an optimised protocol according to Coulman (2006) was adapted for use (Coulman 2006). Skin samples were washed twice in PBS and then fixed in 2% (v/v) glutaraldehyde in PBS at 4°C for 2 h. The fixed skin samples were then rinsed twice in PBS supplemented with 4 mM $MgCl_2$ for 30 min each rinse. The skin samples were then incubated in the X-gal staining solution, prepared according to the formula shown in Table 3.9, at 37°C for up to 16 h. The samples were then washed in PBS and visualised under the Leica Zoom 2000 stereomicroscope (Leica Microsystems (UK) Ltd, UK) with illumination from the Schott KL1500 Electronic fibre optic light source lamp (Schott AG, UK) for any blue pigmentation. *En face* images of the skin sample were captured using the VisiCam 5.0 digital camera (VWR International, UK) attached to the stereomicroscope.

Relevant skin samples were then frozen in OCT embedding medium, cryosectioned and transverse sections with visible epidermal β-galactosidase expression were subjected to H&E staining using the methodology detailed in section 2.2.4.7. Skin sections were

visualised using the Olympus® IX 50 microscope and images were captured using the DP-10 digital camera attached to the microscope.

Table 3.9: Formulation of X-gal staining solution (per 50 mL) used for the detection of β-galactosidase in excised human skin

Components	Volume (mL)
Deionised water	21.56
Tris-HCl (200 mM)	25
Magnesium chloride (1 M)	0.1
Potassum ferrocyanide ($K_4Fe(CN)_6$, 600 mM)	0.42
Potassum ferricyanide ($K_3Fe(CN)_6$, 600 mM)	0.42
X-gal stock solution (5-bromo-4-chloro-indolyl-β-D-galactopyranoside, 40 mg mL^{-1})	2.5

3.2.8 Cell viability assay

For MTT (3-[4,5-dimethylthiazol-2-yl]-2,5-diphenal tetrazolium bromide) or MTS (3-[4,5-dimethylthiazol-2-yl]-5-[3-carboxymethoxyphenyl]-2-[4-sulfophenyl]-2H-tetrazolium) assay cell toxicity studies, cell transfections as described in section 3.2.3 were scaled-down and performed in 96-well plates. As the surface area of each well in 96 well plates was approximately 5 times less than that of 24-well plate, all the materials were scaled down 5 times.

MTT (3-[4,5-dimethylthiazol-2-yl]-2,5-diphenal tetrazolium bromide) is a tetrazolium salt, which forms an insoluble purple formazan crystal when it is cleaved by mitochondrial enzymes in viable cells. Acidified isopropanol solution can be added to solubilise the formazan crystals to a purple solution, which can be measured using a spectrophotometer (Edmondson et al. 1988). When compared to untreated controls, an increase or decrease in absorbance due to changes in the concentration of formazan indicates the degree of cytotoxicity caused by test materials.

MTT reconstituted with PBS to a concentration of 5 mg mL^{-1} was added to each well in an amount equal to 10% of the culture medium volume 48 h post transfection. The side of the 96-well plate was gently tapped for 15 s to thoroughly mix the well contents. The cultures were then returned to the incubator for 4 h. After the incubation period, the culture medium was carefully removed from the wells using a syringe needle, without

disturbing the formazan crystals that had formed. The resulting formazan crystals were dissolved by adding an amount of MTT Solubilization Solution equal the original culture medium volume. The side of the 96-well plate was gently tapped for 60 s and the plate was allowed to stand at room temperature for 15 min to equilibrate the temperature and thoroughly dissolve the crystals. The absorbance was measured at a wavelength of 570 nm using the Titerback Sunrise™ plate reader with pre-measurement shaking of 90 s.

Alternatively, MTS assay was performed by adding an amount of MTS reagent at a concentration of 1.9 mg mL^{-1} (CellTiter® 96 AQueous One Solution Reagent; Promega, UK) equal to 20% of the culture medium volume to fresh culture medium without FBS and antibiotics. Growth medium was removed from the wells of 96 well-plate with treated cells and replaced with culture medium containing MTS reagent (Patel et al. 2005). The cultures were then returned to the incubator for 4 h. The plate was allowed to stand at room temperature for 30 min before the absorbance was measured at a wavelength of 490 nm using the Labtech LT-5000MS plate reader (Labtech International Ltd, UK) with Manta PC software (Dazdaq Ltd, UK). If the absorbance reading was above the optimum value of approximately 1, the samples were diluted up to 10 times with PBS.

3.2.9 Data processing and statistical analysis

Image processing including scale bar inclusion was performed using the ImageJ software (National Institute of Health, USA). Raw numerical data was processed using the Microsoft® Excel for Mac 2011 software (Microsoft Corporation, USA). Graphs were generated and statistical analysis was performed using Prism® 5 for Mac OS X (GraphPad Software Inc. USA). Unless stated otherwise, one-way ANOVA followed by Tukey's multiple comparison test was performed to compare multiple groups against a reference group with significant differences indicated by p-values of less than 0.05 ($p<0.05$), less than 0.01 ($p<0.01$) or less than 0.001 ($p<0.001$). Results are summarised as mean ± standard deviation (SD) and error bars on graphs represents SD unless stated otherwise.

3.3 Results and discussion

3.3.1 DNA preparation

pEGFP-N1 and pCMVβ pDNA were successfully propagated and quantified. The concentrations of the purified pDNA were between 2.5 and 6.5 mg mL^{-1} with $A_{260/280}$ values of above 1.8. The acceptable DNA purity values ($A_{260/280}$) are reported to be between 1.8 and 2.0 (Sambrooks and Russell 2001). The identity of both the reporter plasmids has previously been confirmed through restriction analysis by the donor (Ng 2010). To determine the success of the extraction method in obtaining purified pDNA, agarose gel electrophoresis was performed. Gel analysis of one of the pEGFP-N1 plasmid samples revealed a single distinct band at approximately 4733 kilobase pairs (kbp), Band 1 and presence of 2 weak bands, Band 2 and 3 (Figure 3.2), thus confirming the purity of pDNA obtained through the extraction method.

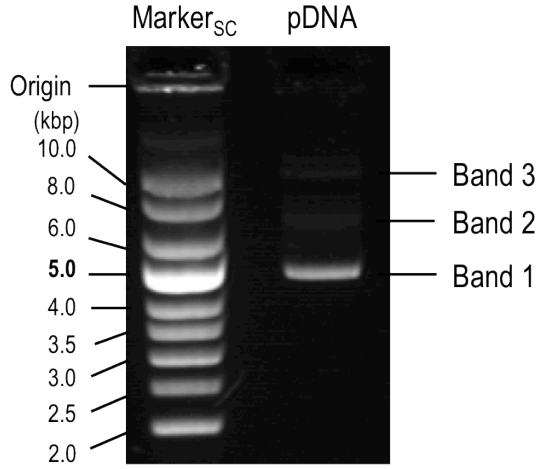

Figure 3.2: Agarose gel image of electrophoretically separated pEGFP-N1 pDNA. ($Marker_{sc}$ = molecular weight marker of supercoiled DNA; pDNA = pEGFP-N1; kbp = kilobase pairs)

On agarose gels, DNA is resolved according to its molecular weight and its conformation. Like other pDNAs, the pEGFP-N1 plasmid was predominantly isolated in its supercoiled conformation (Middaugh et al. 1998), which corresponded to the brightest band, Band 1. However, pDNA also undergoes major degradative pathways both *in vivo* and *in vitro* as the phosphodiester backbone is cleaved through the depurination and β-elimination processes (Lindahl 1993; Middaugh et al. 1998). The pDNA backbone cleavage causes the conversion of supercoiled plasmid to open circular

and linear forms of the DNA, as observed by the faint bands, and is a major limiting factor to the aqueous stability of pDNA (Cherng et al. 1999; Middaugh et al. 1998; Voordouw et al. 1978).

3.3.2 Preparation of DNA-Liposome complexes

DOTAP liposomes were prepared and extruded. The average size of the freshly extruded liposomes was 117.0 nm, with a standard deviation (SD) of 39.0 nm. All the transfection reagents, including DOTAP, Lipofectamine™, Lipofectamine™ 2000, Lipofectamine LTX™ and Lipofectine™, were complexed with pEGFP-N1 or pCMVβ. All cell transfections with the lipoplexes resulted in expression of either the green fluorescent protein (GFP) or beta-galactosidase (β-gal).

3.3.3 HaCaT cell transfection

Numerous transfection reagents are currently commercially available. An attempt to determine and compare the efficiency and toxicity of commercially available transfection reagents in human keratinocyte cells was made by transfecting HaCaT cells with pEGFP-N1 reporter pDNA complexed with various transfection reagents (lipoplexes). HaCaT cells that were transfected with the pEGFP-N1 reporter pDNA lipoplexes resulted in expression of GFP (Figure 3.3). All negative controls failed to express any GFP.

Flow cytometry analysis was performed to quantify and compare GFP expression of cells treated with different lipoplexes (Figure 3.4). There was no significant difference in the percentage of fluorescent cells in the untreated cells and cells incubated with naked pEGFP-N1. This indicates negligible or no GFP expression in cells treated with naked pEGFP-N1 ($p > 0.05$), which was confirmed by visual inspection through fluorescence microscopy (Figure 3.3). For each lipoplex formulation containing 0.5μg pEGFP-N1 per well, respectively, GFP expression was significantly greater than autofluorescence (gated at ≤1%; $p < 0.01$ for each lipoplex formulations compared against untreated samples) with the exception of the lipoplex formulation containing DOTAP only, which was not significantly different than untreated cells.

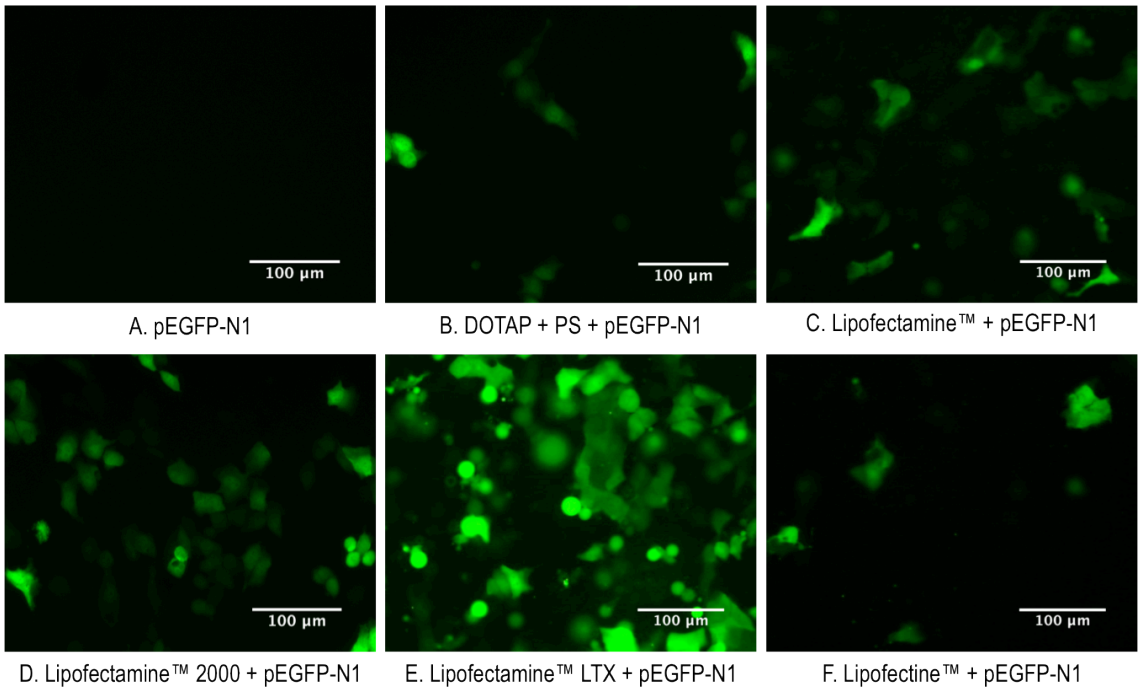

Figure 3.3: Representative fluorescence micrographs of HaCaT cells treated with naked pEGFP-N1 (A) or lipoplexes (B-F) of pEGFP-N1. In each treatment group, pEGFP-N1 pDNA amount was 0.5 µg. GFP fluorescence was pseudocoloured green. (PS = protamine sulphate)

When the mass of pDNA remained constant, the highest GFP expression was observed when cells were transfected with pEGFP-N1 complexed with Lipofectamine™ LTX (37.0 ± 1.5%; n = 3), followed by Lipofectamine™ 2000 (26.63 ± 2.69%; n = 4), Lipofectamine™ (26.0 ± 0.76%; n = 3), DOTAP with protamine suphate (6.603 ± 0.29%; n = 4), Lipofectine™ (4.2 ± 0.39%; n = 3) and DOTAP without protamine suphate (2.045 ± 0.19%; n = 4). Increasing the amount of pDNA by 60% (0.8 µg instead of 0.5 µg) complexed to the same concentration of Lipofectamine™ 2000 transfection reagent did not result in significant increase in the GFP expression level (0.8 µg pEGFP-N1 + Lipofectamine™ 2000 mean: 26.0 ± 1.48%; n = 4; $p > 0.05$). When protamine sulphate was added to the DOTAP formulation, significantly enhanced gene expression was observed ($p < 0.01$).

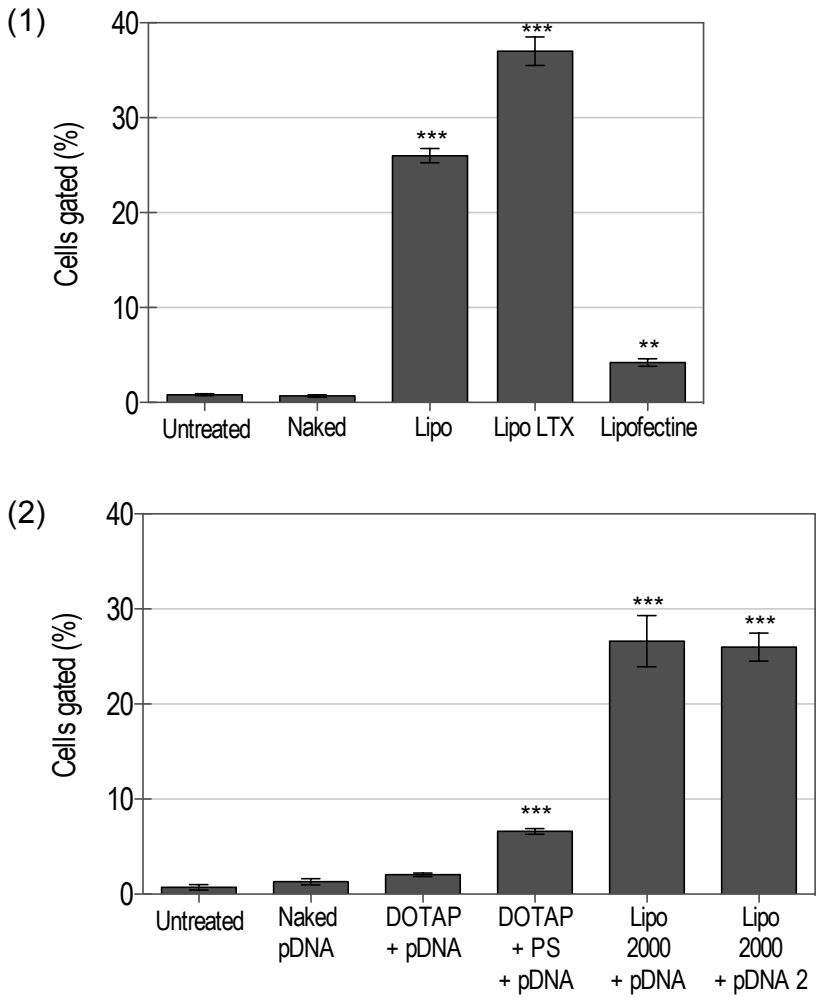

Figure 3.4: Transfection efficiency of pEGFP-N1 lipoplexes in HaCaT cells. (pDNA = 0.5 μg pEGFP-N1; pDNA 2 = 0.8 μg pEGFP-N1; Lipo = Lipofectamine™; PS = protamine sulphate; experiment (1): n = 3; experiment (2): n = 4; error bar = standard deviation; ** = $p<0.01$; *** = $p<0.001$ compared to untreated)

Whilst cell viability studies were not performed, visual observation under the light microscope indicated that cell viability decreased with increased transfection efficiency (data not shown). Similar observations were reported in the literature by Yamano et al. (2010), whereby studies were performed comparing six commercially available nonviral transfection reagents on nine different cells lines. Lipofectamine™ 2000 was efficient in transfecting HEKn human epidermal keratinocytes resulting in significant level of β-galactosidase expression. Gene expression was significantly enhanced under serum free conditions. However, amongst the six transfection reagents tested by Yamano et al., Lipofectamine™ 2000 showed the lowest cell viability (69.1 ± 17.8%)(Yamano et al. 2010).

In an unpublished study using HaCaT cells where the transfection efficiency of a range of transfection reagents at the same pEGFP-N1 to lipid ratio and concentration were compared, similar findings with transfection efficiency were found. Lipofectamine™ LTX gave the highest transfection efficiency (46.2 ± 1.969%, n = 4) and DOTAP with protamine sulphate the lowest transfection efficiency (6.7 ± 1.552%, n = 4) (Ng 2010). Another study compared different ratios of 5 commercially available transfection reagents, including Lipofectine™ complexed to pDNA expressing GFP, in keratinocyte cells extracted from the skin. At a ratio of pDNA to Lipofectine™ of 1:4 using 0.4 µg pDNA, the study found low transfection efficiency with Lipofectine™ lipoplexes (3.55 ± 0.62%; n = 3) (Dickens et al. 2010). The transfection efficiency achieved with Lipofectine™ containing 0.5 µg pDNA, at a ratio of pDNA to Lipofectine™ of 1: 3, was 4.2 ± 0.39% (Figure 3.4; n = 3). The low transfection efficiency of Lipofectine™ lipoplexes in keratinocyte cells suggests that the reagent is unsuitable for the cell line. Transfection related cell toxicity was not reported in both of the aforementioned studies (Dickens et al. 2010; Ng 2010).

As the formulations were kept at similar DNA to lipid ratios and the same mass of pDNA was used in each transfection experiment, the observed differences in transfection efficiency and toxicity were most likely due to the differences in the chemical structures and compositions of the cationic lipids. When complexed with pDNA, different chemical structures (Zhang et al. 2004; Zhi et al. 2010) and lipid compositions of transfection reagents are known to form lipoplexes of various sizes and molar charge ratios, which affects transfection efficiency and toxicity (Lv et al. 2006; Masotti et al. 2009). Several authors have proposed the lipid-mixing hypothesis and suggested that interactions between cationic lipids and cell membranes and other cell organelle membranes, such as the mitochondrial membranes may result in membrane charge alteration that affects function of membrane receptors and ion channels, leading to toxicity. These membrane changes may also affect cell attachment resulting in cell detachment from the culture vessel (Felgner et al. 1994; Xu and Szoka Jr 1996).

Based on observation under the light microscope, cells treated with Lipofectamine™, Lipofectamine™ LTX and Lipofectamine™ 2000 pDNA lipoplexes showed morphological and cell number changes, which indicated cell toxicity (data not shown).

Cells treated with naked pDNA and the respective transfection reagents controls appeared normal and healthy. In the absence of additional physical disruption like electroporation, naked pDNA does not enter the cells efficiently (Basner-Tschakarjan et al. 2004; Wattiaux et al. 2000). Any naked pDNA that manages to penetrate the cell membrane, presumably through endocytosis is not likely to escape from the endosomes and is thereby degraded by nucleases in the lysosomes (Lechardeur and Lukacs 2006; Lechardeur et al. 2005; Wattiaux et al. 2000). In lipoplexes, the presence of cationic lipids has been postulated to aid endosomal release of pDNA through interaction of cationic lipids with the anionic lipids of endosomal membrane (Hoekstra et al. 2007; Xu et al. 1999; Xu and Szoka Jr 1996). Since cell membranes are composed of lipids, interactions of uncomplexed cationic lipids with cellular lipids are unlikely to cause significant harm to cells. Several *in vivo* studies have also reported that DNA and cationic lipids in a lipoplex formulation can have a synergistic effect on the toxicity observed (Ruiz et al. 2001; Scheule et al. 1997). The studies performed established the efficiency of various commercially available transfection reagents on HaCaT cells, which enabled the selection of these reagents for functional assay studies in monolayer cell cultures.

In a separate study, HaCaT cells were transfected with pCMVβ to determine the functionality of the plasmid for use in skin transfection studies. Lipofectamine™ 2000 transfection reagent was used and expression of β-galactosidase was detected, confirming the functionality of the pCMVβ plasmid (Figure 3.5). A MTT assay was also performed to determine the toxicity of the lipoplexes and there was insignificant reduction in cell viability in the pDNA lipoplexes treatment groups (Figure 3.6). These results show that the isolated and purified pCMVβ reporter pDNA was functional and suitable for use in skin experiments.

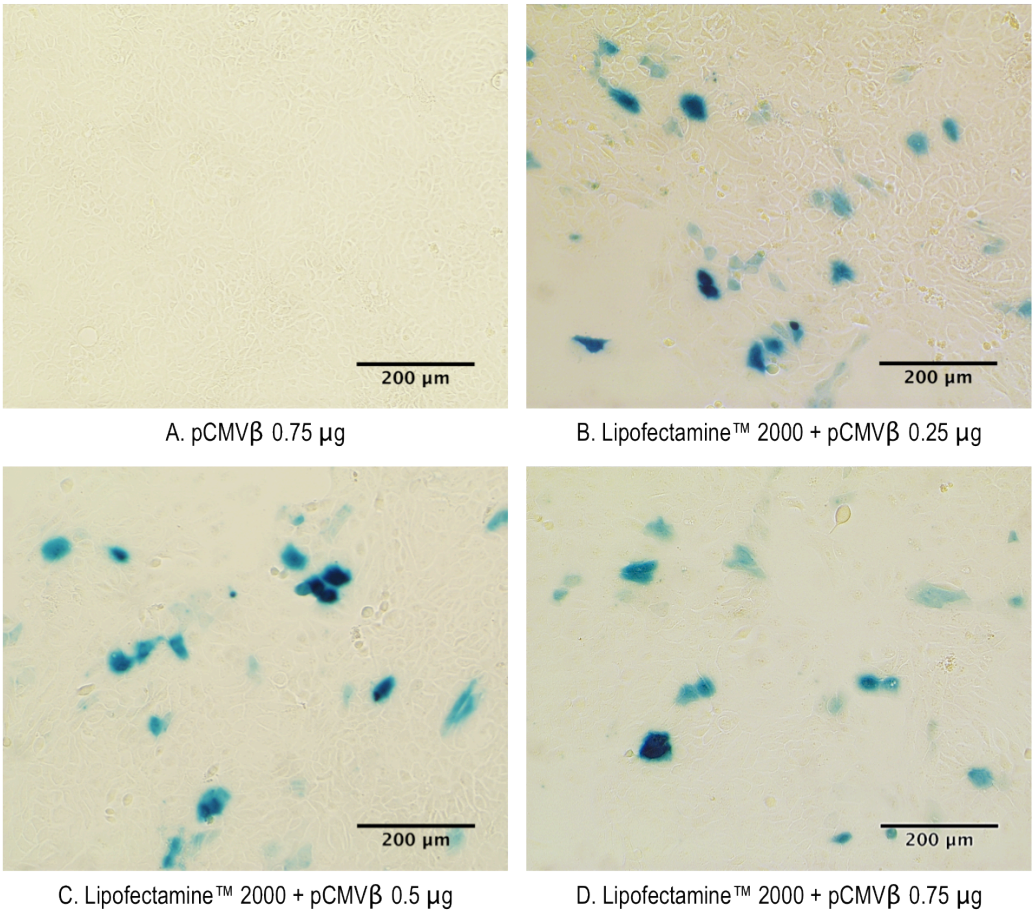

A. pCMVβ 0.75 µg

B. Lipofectamine™ 2000 + pCMVβ 0.25 µg

C. Lipofectamine™ 2000 + pCMVβ 0.5 µg

D. Lipofectamine™ 2000 + pCMVβ 0.75 µg

Figure 3.5: Representative bright-field micrographs of HaCaT cells treated with naked pCMVβ (A) and lipoplexes (B-D). In each treatment group with lipid transfection reagent, Lipofectamine™ 2000 amount was constant.

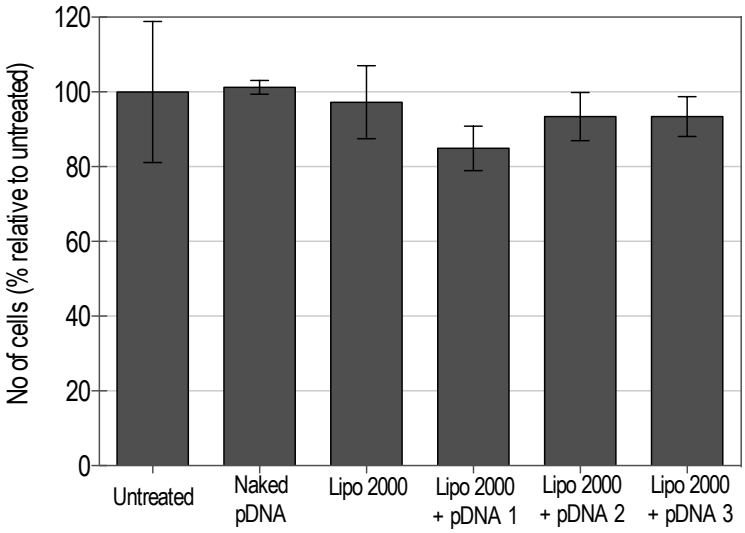

Figure 3.6: Cell viability (MTT assay) following treatment with pCMVβ lipoplexes in HaCaT cells. The percentage viability was relative to normalised untreated cells. (pDNA 1 = 0.25 µg pCMVβ; pDNA 2 = 0.5 µg pCMVβ; pDNA 3 = 0.75 µg pCMVβ; Lipo = Lipofectamine™; n = 4; error bar = standard deviation)

3.3.4 Primary keratinocyte transfection

The relative ease of growth of HaCaT cells helped in preliminary and optimisation experiments while the primary keratinocytes cultured in a controlled monolayer environment provide closer biological proximity to keratinocyte cells in human skin. Therefore, primary keratinocyte cells, isolated from the excised skin of a 38-year-old subject, were transfected with pEGFP-N1 complexed with Lipofectamine™ 2000 or Lipofectamine™ LTX transfection reagents (Figure 3.7), the reagents with the highest transfection efficiencies amongst the previously tested reagents (Figure 3.4)

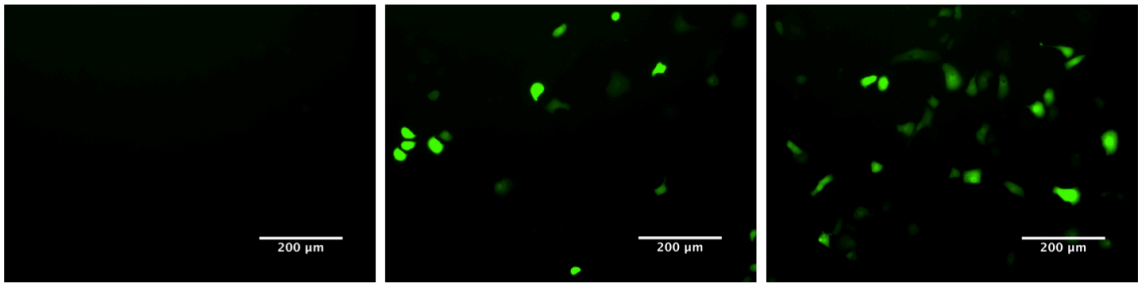

Figure 3.7: Representative fluorescence micrographs of primary keratinocyte cells treated with naked pEGFP-N1 (A) or lipoplexes (B and C). In each treatment group, pEGFP-N1 mass was constant at 0.5 µg. GFP fluorescence was pseudocoloured green.

Primary cells are usually said to be difficult to transfect with pDNA using a non-viral delivery system due to their slower rate of proliferation. When compared with dividing cells, transfection efficiencies in non-dividing cells are generally lower (Mortimer et al. 1999) as the nuclear envelope is regarded as the major intracellular barrier to delivery of nucleic acid (Dean et al. 2005). During mitosis, the nuclear membrane breaks down, thus allowing entry of pDNA and subsequent gene expression (Escriou et al. 2001; Nicolau and Sene 1982; Wilke et al. 1996). Nevertheless, in non-proliferating cells, nuclear translocation of DNA is thought to still occur, probably as a result of passive movement through the nuclear pore complex (Mattaj and Englmeier 1998; Stoffler et al. 1999; Wilson et al. 1999). The size of a nuclear pore is approximately 55 Å in diameter, which allows free diffusion of small molecules (less than 40 kDa) but it is unlikely that pEFGP-N1 pDNA of 4733 bp (approximately 3000 kDa) could enter the nucleus through the nuclear pore complex (Escriou et al. 2001). Primary keratinocytes used in this study were transfected between passage 2 and 6, when the cells were highly

proliferative. This is consistent with a study that reported the successful transfection of highly proliferating primary keratinocytes with a reporter gene and subsequent expression for up to 2 weeks in culture (Zellmer et al. 2001).

Flow cytometry analysis was performed to compare the efficiency of lipoplex treatment and subsequent gene expression in primary keratinocyte cells (Figure 3.8). GFP expressions in cells treated with both lipoplexes were significantly greater than autofluorescence of untreated cells and naked pDNA (both $p<0.001$). GFP expression was significantly higher when cells were transfected with pEGFP-N1 complexed with Lipofectamine™ LTX (19.25 ± 2.58%; n = 4) compared to Lipofectamine™ 2000 (6.37 ± 0.65%; n = 4, $p<0.001$). The level of GFP expression in primary keratinocytes treated with both the lipoplexes were lower than the expression in HaCaT cells (Figure 3.4), where GFP expressions were 47.9% and 76.1% lower in Lipofectamine™ LTX and Lipofectamine™ 2000 lipoplex treated groups, respectively. The lower transfection efficiencies seen in primary keratinocytes can be attributed to a lower rate of cell division, compared to HaCaT cells.

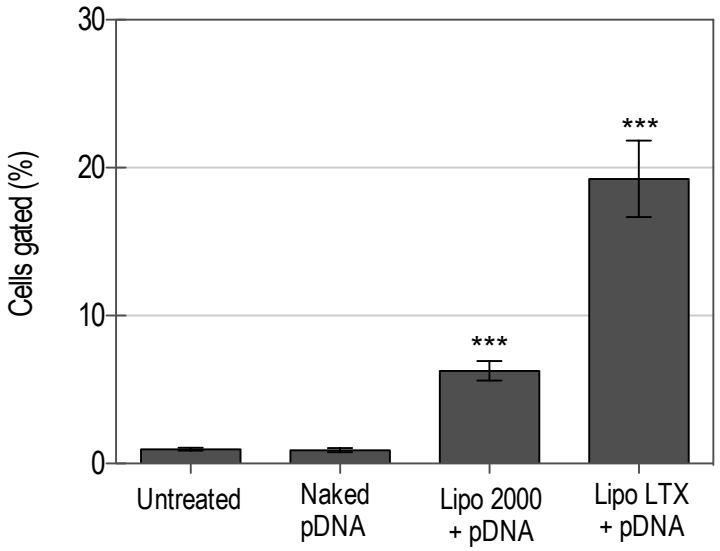

Figure 3.8: Transfection efficiency following treatment with pEGFP-N1 lipoplexes in primary keratinocyte cells. (pDNA = 0.5 µg pEGFP-N1; Lipo = Lipofectamine™; n = 4; error bar = standard deviation; *** = $p<0.001$ compared to untreated)

Confocal microscopy was used to capture fluorescence micrographs of the primary keratinocyte cells expressing GFP and the images taken sequentially were stacked (z-

stack projection) to provide an in depth view of GFP expression in the cells (Figure 3.9). Primary keratinocyte cells were seeded on glass coverslips and transfected the following day with pEGFP-N1 and Lipofectamine™ LTX lipoplexes. The cells were fixed using the combined PFA/Methanol method (Brock et al. 1999). Alternatively, cells were unfixed and mounted on a microscope slide in PBS. However, unfixed live cells had to be analysed immediately. Fixing and then mounting cells on glycerol-based mounting buffer containing anti-fading agent provides the benefit of anti-bleaching effect, preservation of signal intensity and improve the durability of the sample (Longin et al. 1993; Ono et al. 2001).

Despite the advantages of glycerol-based mounting, cells mounted in this solution face problems of receptor redistribution (Brock et al. 1999). The commonly used cell fixation method, with PFA, fixes cells through cross-linking with cellular proteins (Kiernan 2000). However when cells are mounted on a glycerol-based mounting buffer, membrane integrity is compromised due to cellular redistribution of receptors (Brock et al. 1999). On the other hand, methanol fixation precipitates cellular proteins but washes out soluble cellular proteins and free GFP (Brock et al. 1999; Kalejta et al. 1997). The combined PFA/methanol method of fixation combines the advantages of both the procedures and can be used to fix both transmembrane and soluble proteins as well as to preserve GFP fluorescence following mounting on glycerol-based buffer (Brock et al. 1999).

From the z-stack projection micrographs of fixed (Figure 3.9 A) and unfixed cells (Figure 3.9 B), it is obvious that GFP protein expression occurred both in the nucleus and cytoplasm of the cells. Cell fixation with PFA/methanol seemed to have precipitated the fluorescent proteins in cross-linked structure, as fluorescence distribution appeared fibrous when compared to the even expression of fluorescence found in unfixed cells. This is an interesting technical observation and highlights the importance in understanding how various cell fixing methods could affect fluorescence distribution in cells.

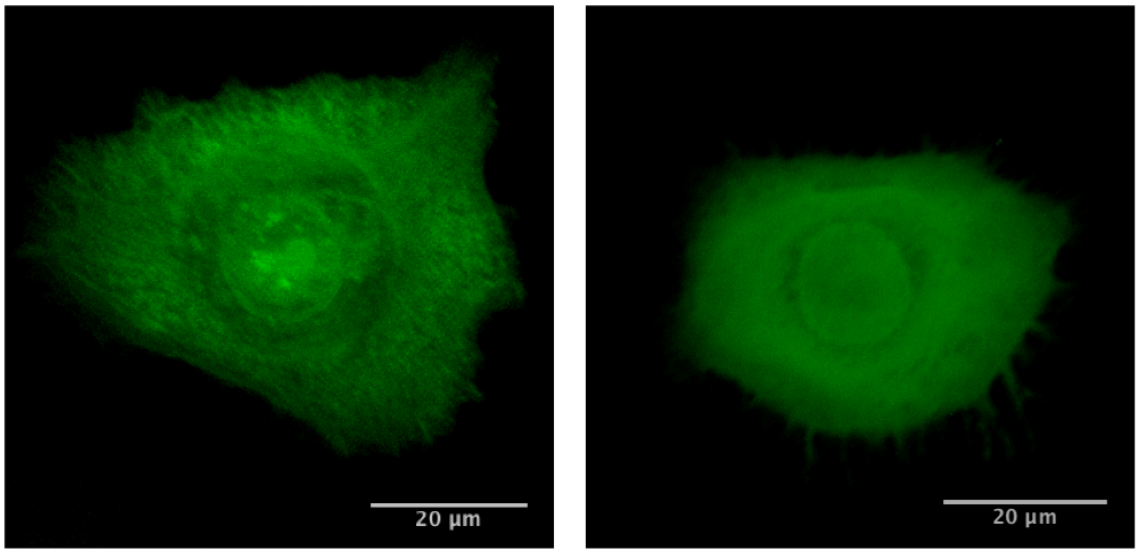

A. Fixed with PFA/methanol and mounted on fluorescent mounting medium

B. Unfixed, mounted on PBS

Figure 3.9: Fluorescence z-stack confocal micrographs of primary keratinocyte cells transfected with pEGFP-N1 and Lipofectamine™ LTX transfection reagent complexes. The green fluorescent protein was excited with laser at 488 nm and pseudocoloured green. Cells were grown on glass cover slips *in vitro* appeared to be flattened out against the culture surface. The confocal image is a z-stacked projection of 20 slices of images taken over a cell layer thickness of approximately 15 µm (Transfection volume = 1200 µL; pDNA = pEGFP-N1; LTX = Lipofectamine™ LTX transfection reagent)

3.3.5 Characterisation of plasmid DNA coating onto steel microneedles

Steel microneedles have the ability to penetrate the stratum corneum and deposit dry coated materials in the skin as demonstrated in Chapter 2. In this study, the ability to coat stainless steel microneedle devices with pDNA was evaluated. Using the optimised coating method described in section 2.2.5.2, two sets of 4 microneedle devices (5 × 700 µm regular, Cardiff University, UK) were evenly coated with 13 µg of pEGFP-N1 pDNA each set. This approximates to a theoretical maximum loading of 3.25 µg pDNA coated per device and 0.65 µg pDNA coated per microneedle. Following drying, the average mass of pDNA recovered in 100 µL of TE buffer from each device was 2.78 ± 0.54 µg (n = 4) after a 24 h drying time and 2.28 ± 0.69 µg (n = 4) after a 96 h drying time. This was an average of 14.5% and 30.1% reduction in the mass of pDNA recovered from the microneedles, compared to the theoretical maximum loading dose after 24 h and 96 h drying times respectively.

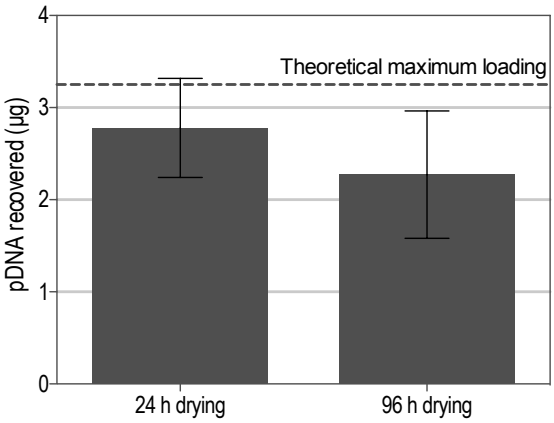

Figure 3.10: pDNA coating onto steel microneedles. A theoretical maximum mass of 3.25 µg of pDNA per microneedle device was loaded onto two sets of 4 microneedle devices (5 × 700 µm Regular, Cardiff University, UK). pDNA from 4 random devices was recovered at the drying time points. (pDNA = pEGFP-N1; h = hour; n = 4; error bar = standard deviation)

The reduction in the mass of pDNA recovered could be due to less than 100% efficient loading from the theoretical maximum loading dose. If the full loading dose was coated, reduction in recovered pDNA mass could be due to retention of coated materials on the surface of microneedles or shedding of dry-coated pDNA from the microneedles during storage and handling. pDNA is relatively stable in solid state; therefore it is not expected to be degraded within the 96 h drying time. The mass reduction seemed to have increased with time suggesting that the increased drying time may have resulted in significant dehydration of the coated material and subsequent difficulty re-dissolving it from the surface of microneedles in the small volume of buffer used and with minimum agitation. Furthermore, unpolished steel microneedles were used and it is possible that dehydrated pDNA adhered more strongly to the rough microneedle surface. In chapter 2 (section 2.3.4), electropolished microneedles from Georgia Institute of Technology, USA resulted in higher skin deposition (Figure 2.12) of coated materials from the FITC-oligonucleotide coated microneedles (Figure 2.13), compared to unpolished microneedles. pDNA dissolution from electropolished microneedles has not been tested concurrently, but the results indicate that the surface property of steel microneedles affects the adherence and dissolution of the pDNA coat.

A transfection assay was performed on the recovered pDNA to determine if plasmid DNA remained functional after coating and drying. Lipofectamine™ 2000 or DOTAP with protamine sulphate were used as transfection reagents to form lipoplexes with the recovered pEGFP-N1. Gene expression was observed (Figure 3.11) and flow cytometry was performed to quantify and compare GFP expression between different treatment groups (Figure 3.12 A). An MTT assay was also performed to determine cell viability post-transfection (Figure 3.12 B).

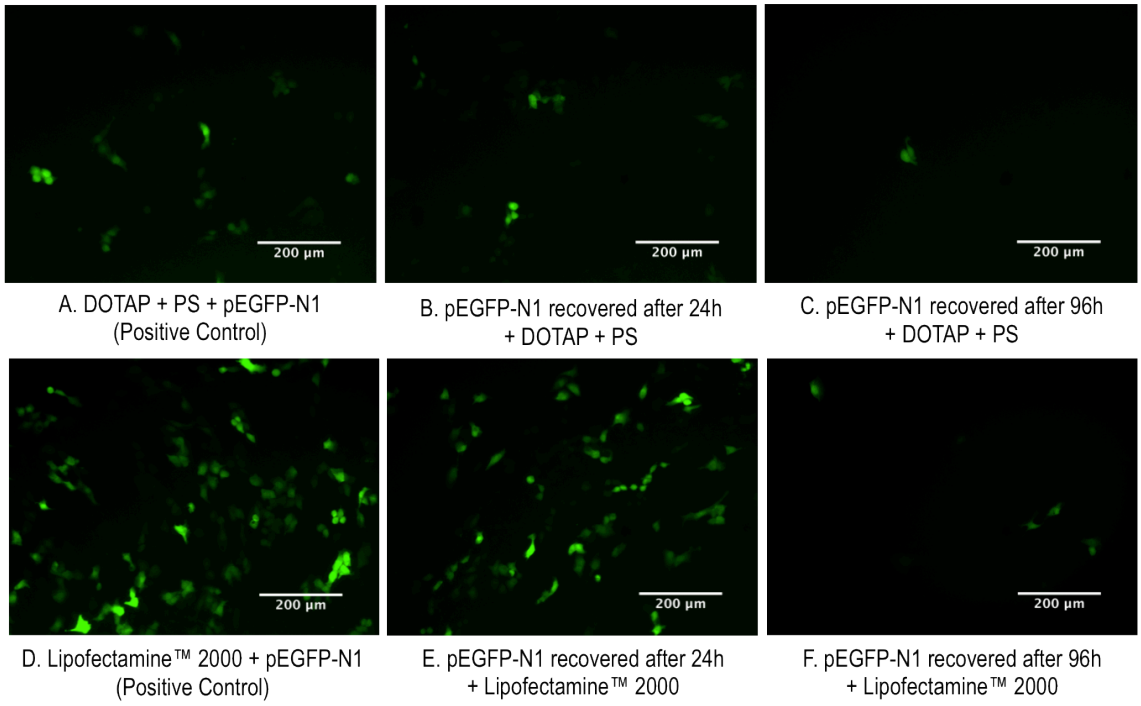

Figure 3.11: Representative fluorescence micrographs of HaCaT cells treated with DOTAP (A-C) and Lipofectamine™ 2000 (D-F) lipoplexes of pEGFP-N1 recovered from microneedle devices following 24 h and 96 h drying time (B, C, E and F). In each treatment group, pDNA mass was constant at 0.5 µg. GFP fluorescence was pseudocoloured green. (PS = Protamine sulphate)

Gene expression was greatest in lipoplexes formulated with Lipofectamine™ 2000. Compared to the positive control (26.63 ± 2.69%; n = 4), the coating and 24 h drying process reduced gene expression by 32.6% (17.95 ± 5.71%; n = 4; $p < 0.01$) whilst 96 h drying reduced gene expression by 88.8% (2.98 ± 0.77; n = 4; $p < 0.001$) in the Lipofectamine™ 2000 lipoplexes group. The mass of pDNA used for transfection was the same but functionality of the pDNA reduced with an increase in coated pDNA drying time. In the DOTAP group, the coating and 24 h drying process did not affect the

level of gene expression (7.75 ± 4.44%; n = 4) whilst 96 h drying seemed to reduce gene expression by 67.7% (2.13 ± 0.58%; n = 4) when compared to the positive control (6.60 ± 0.29%; n = 4) but the results were statistically insignificant (p>0.05).

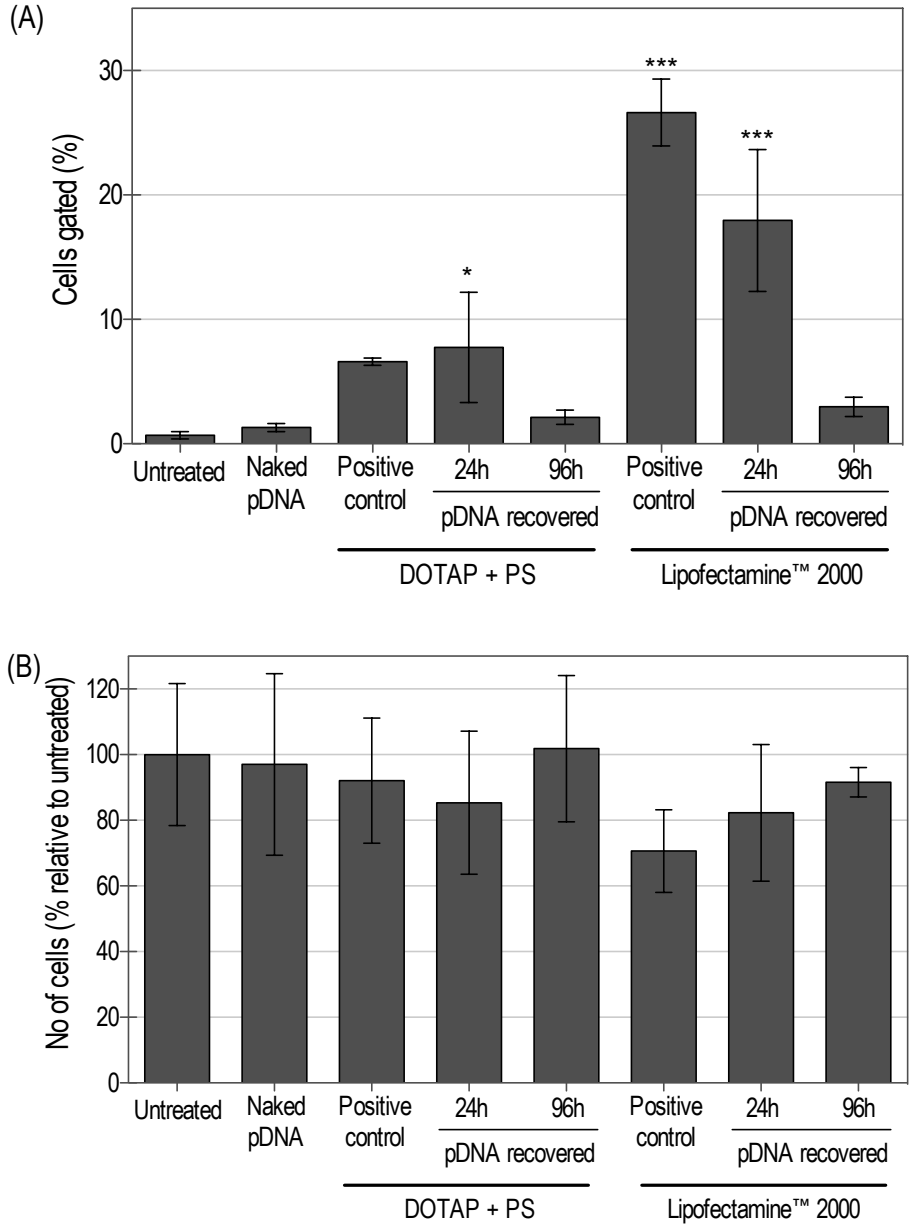

Figure 3.12: Transfection efficiency (A) and cell viability (MTT assay) (B) following treatment with pEGFP-N1 recovered from microneedle devices following 24 h and 96 h drying time and subsequently complexed with liposomes for transfection in HaCaT cells. (pDNA = 0.5 µg pEGFP-N1; PS = Protamine sulphate; n = 4; error bar = standard deviation; * = p<0.05; *** = p<0.001 compared to untreated)

Cell viability was lowest in the Lipofectamine™ 2000 positive control group (70.64 ± 12.6%; n = 4), followed by Lipofectamine™ 2000 complexed with pDNA recovered from microneedle devices following drying for 24 h (82.27 ± 20.82%; n = 4) and then DOTAP with protamine sulphate complexed with pDNA recovered from microneedle devices following drying for 24 h (85.33 ± 21.80%; n = 4). However, the differences in reduction of cell viabilities were statistically insignificant. There was some observed correlation between the apparent reduction in cell viability and increased gene expression, suggesting the small increase in cell toxicity could be related to increased expression of exogenous genetic material in the cells. When observed microscopically, most of the presumably dead cells seen to be detached from the tissue culture vessel, appeared rounded and were brightly fluorescent with GFP.

The ability to coat pDNA onto steel microneedles has previously been investigated by other members of the research laboratory (Pearton et al. 2012); data shown in Figure 3.13. Studies were performed to investigate the physical stability and biological functionality of reporter plasmid following coating for up to 7 days and recovery from the surface of electropolished steel microneedles. Microneedles were coated with pDNA using the micro-dip-coating device (Gill and Prausnitz 2007a), allowed to dry for 7 days at room temperature and recovered in a small volume of buffer. The recovered pDNA was then subjected to agarose gel electrophoresis to determine the physical stability of the tertiary supercoiled structure as well as complexed with Lipofectamine LTX reagent for delivery to HaCaT cells (Pearton et al. 2012).

The physical stability of coated pDNA, determined by the retention of supercoiled structure appears to have decreased with the relative amount of supercoiled pDNA decreasing from 80% to 50% over 7 days storage (Figure 3.13 A). However, the change in tertiary DNA structure did not appear to significantly affect the biological functionality of the coated and recovered plasmid as HaCaT cells transfection revealed similar levels of gene expression compared to positive control (Figure 3.13 B) (Pearton et al. 2012). However, it is noted that the level of transfection in this study was observably lower than found in earlier experiments using the same transfection reagent, whereby transfection efficiency of up to 17.5% (positive control and recovered pDNA) were observed in the aforementioned study compared to an average of 37% in the study presented in Figure 3.4. The authors in the study (Pearton et al. 2012) suggested that it

is possible that the cleavage of pDNA during storage occurred at a location that did not affect the mechanism of gene expression or that the dose of pDNA used in *in vitro* transfection studies was more than required and as such partial degradation in pDNA structure may result in undetectable subtle changes in biological functionality of the plasmid (Pearton et al. 2012).

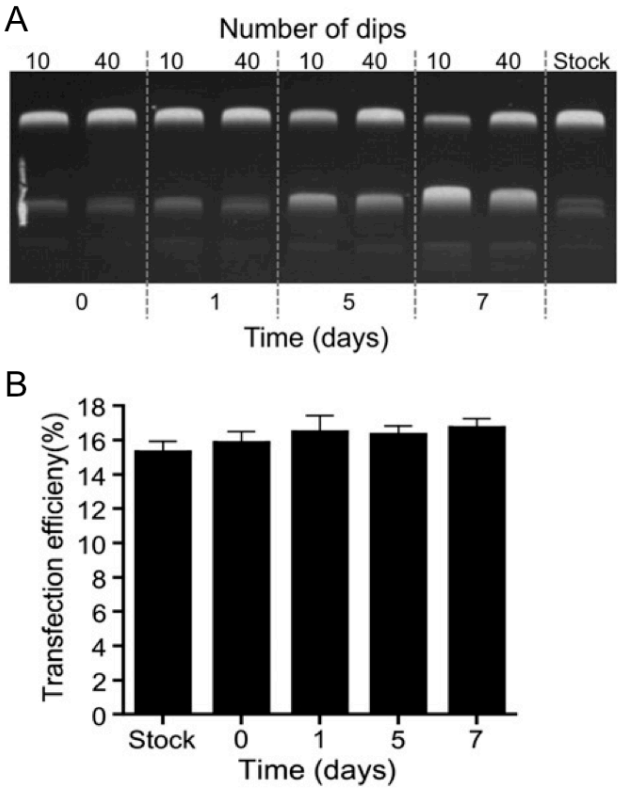

Figure 3.13: Structural stability (A) and biological functionality (B) of pDNA coated onto the surface of electro-polished steel microneedles. (A) An image of gel electrophoresis of pDNA recovered after coating for up to 7 days with either 10 or 40 dip-coats with 5 s drying time in between each immersion (dip) using a micro-dip-coating device. (B) Transfection efficiency of pEGFP-N1 recovered from the surface of microneedles following storage for up to 7 days, determined through flow cytometry analysis. pEGFP-N1 from stock and recovered from microneedles were complexed with Lipofectamine™ LTX transfection reagent. (Data presented as mean ± SD; ANOVA $p>0.05$) (taken from Pearton et al. 2012)

It was also observed that the reduction in supercoiled pDNA fraction was more prominent when a lower mass of pDNA (10 dips with approximately 2 μg compared to 40 dips with approximately 5 μg pDNA, presumably coated and recovered per

microneedle device) was coated onto the surface of microneedles (Pearton et al. 2012). The authors suggested that in samples with less materials coated, the fraction of coated nucleic acid that is in contact with either the metallic surface of microneedles or the atmosphere is higher, resulting in an increased DNA instability due to oxidation (Pearton et al. 2012). Subsequently, the physical stability of pDNA coated onto microneedles was significantly enhanced by the addition of 1.5% (w/v) disaccharide, which resulted in approximately 85% retention of the supercoiled DNA structure (Pearton et al. 2012).

Apart from the major degradative pathways of depurination and β-elimination in an aqueous solution, pDNA is also susceptible to free radical oxidation (Evans et al. 2000). The theoretical maximum mass of pDNA coated in this experiment was 3.25 μg, which is within the range used by Pearton and colleagues (approximately 1 μg for 10 dips and 5 μg for 40 dips, with 5 s drying time in between dips). However, the rough surface of unpolished microneedles increases the surface area of steel microneedles for coating. The studies in this chapter reveal the relative instability and insolubility of pDNA in TE buffer coated onto unpolished steel microneedles after prolonged storage. Pharmaceutical excipients like disaccharides could potentially be exploited in the future to help improve long-term storage stability and solubility of pDNA that are coated onto microneedles. Electropolishing the surface of steel microneedles produced locally at Cardiff University could also potentially improve dissolution of dry-coated DNA material from the surface of steel microneedles. The current and previously published studies on the stability of pDNA coated onto microneedles forms the basis for initial understanding of the limitations for nucleic acid coating onto the surface of steel microneedles.

3.3.6 Excised human skin transfection

The ability to deliver reporter pDNA to skin using a concentrated naked pDNA formulation applied to the surface of freshly excised human skin prior to skin puncture with microneedles has been previously shown in the laboratory (Birchall et al. 2005; Coulman et al. 2006b; Ng et al. 2009; Pearton et al. 2008; Pearton et al. 2012). The physical skin disruption studies detailed in this thesis serve to compare the routinely used method using microneedles with other conventional methods used to disrupt the

stratum corneum barrier to facilitate delivery of nucleic acid to excised human skin. pCMVβ reporter plasmid was the reporter plasmid of choice due to the ease of visual *en face* detection of β-galactosidase expression in the skin. The effect of delivering lipoplexes (pDNA complex with a lipid based transfection reagent) was also investigated.

In an experiment comparing (i) microneedle abrasion with (ii) tape-stripping and (iii) tape-stripping plus liquid cyanoacrylate stripping, gene expression (β-galactosidase protein expression) was observed in the microneedles abrasion method but not in other disruption methods (Figure 3.14). β-galactosidase protein expression was observed as dark blue spots *en face* after staining with X-gal solution.

As shown on the tranverse sections, β-galactosidase protein expression in the microneedle abrasion sample seems to be prominent in the viable epidermis, adjacent to skin disruptions (Figure 3.15 B). Microneedle application resulted in disruption of the stratum corneum with one of the lateral disruption sites was approximately 150 μm in depth. β-galactosidase protein expression seemed to have occurred at the basal and suprabasal layer of epidermal cells, supporting the notion that targeted delivery of nucleic acid to the appropriate cells within the epidermis is crucial for successful gene expression. It has been postulated by Pearton et al. (2012) that cellular uptake of aqueous naked pDNA formulation following microneedle administration is a transient process, whereby the shearing force of microneedle penetration temporarily disrupts cell membrane to allow pDNA entry into cells through diffusion as the cell membrane rapidly re-organise to restore integrity (Pearton et al. 2012). This hypothesis is supported by the fact that naked pDNA in the absence of a gene transfer vector does not transfect cells in a monolayer culture but is able to facilitate gene expression in viable human skin tissue.

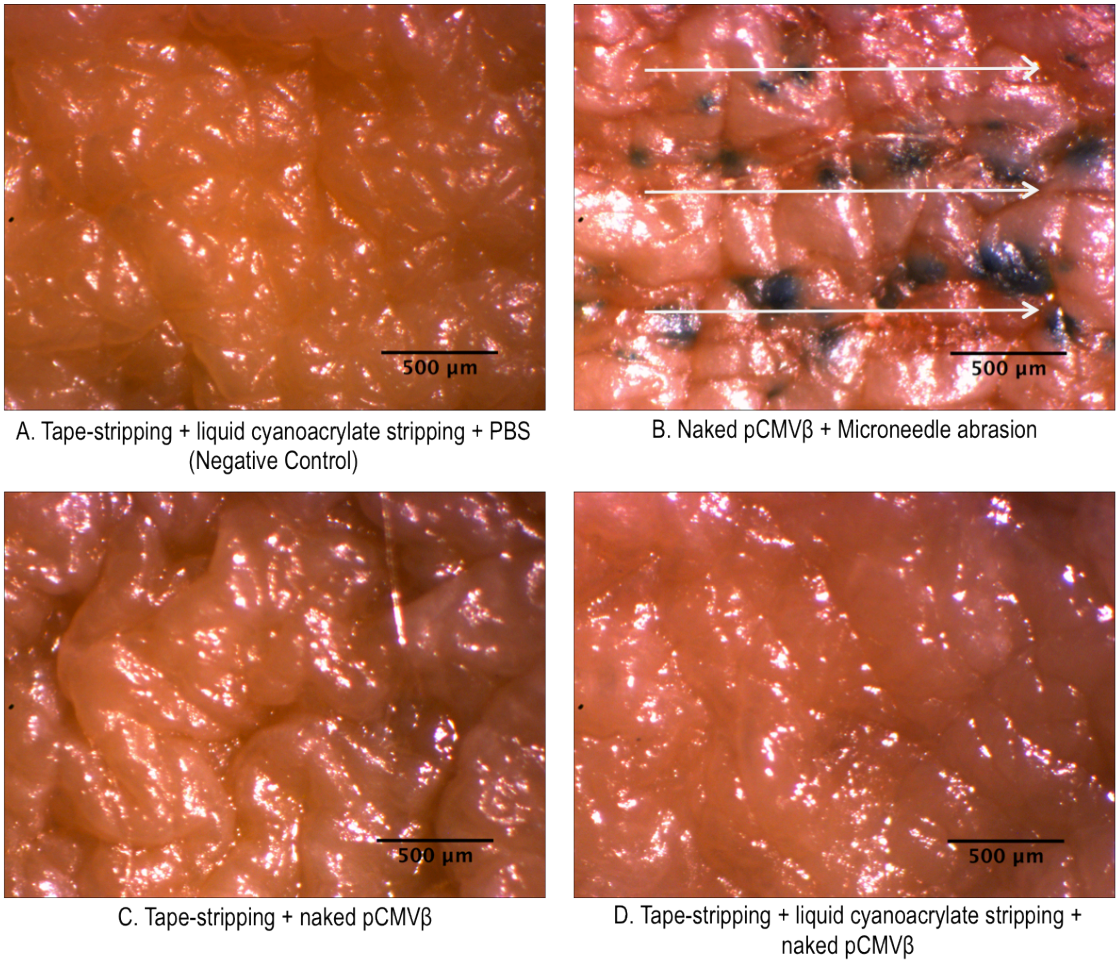

A. Tape-stripping + liquid cyanoacrylate stripping + PBS (Negative Control)

B. Naked pCMVβ + Microneedle abrasion

C. Tape-stripping + naked pCMVβ

D. Tape-stripping + liquid cyanoacrylate stripping + naked pCMVβ

Figure 3.14: ***En face*** **images of skin samples, from a 53-year-old patient that have been treated by physical disruptions and PBS only (A) or naked pCMVβ (B, C and D).** Arrows on figure B show the direction that microneedles were moved through the skin following insertion. Skin samples have been subjected to X-gal staining, which highlights the presence of β-galactosidase protein with a dark blue pigment (naked pCMVβ = 10 µL pCMVβ 6 mg mL^{-1} solution; n = 2)

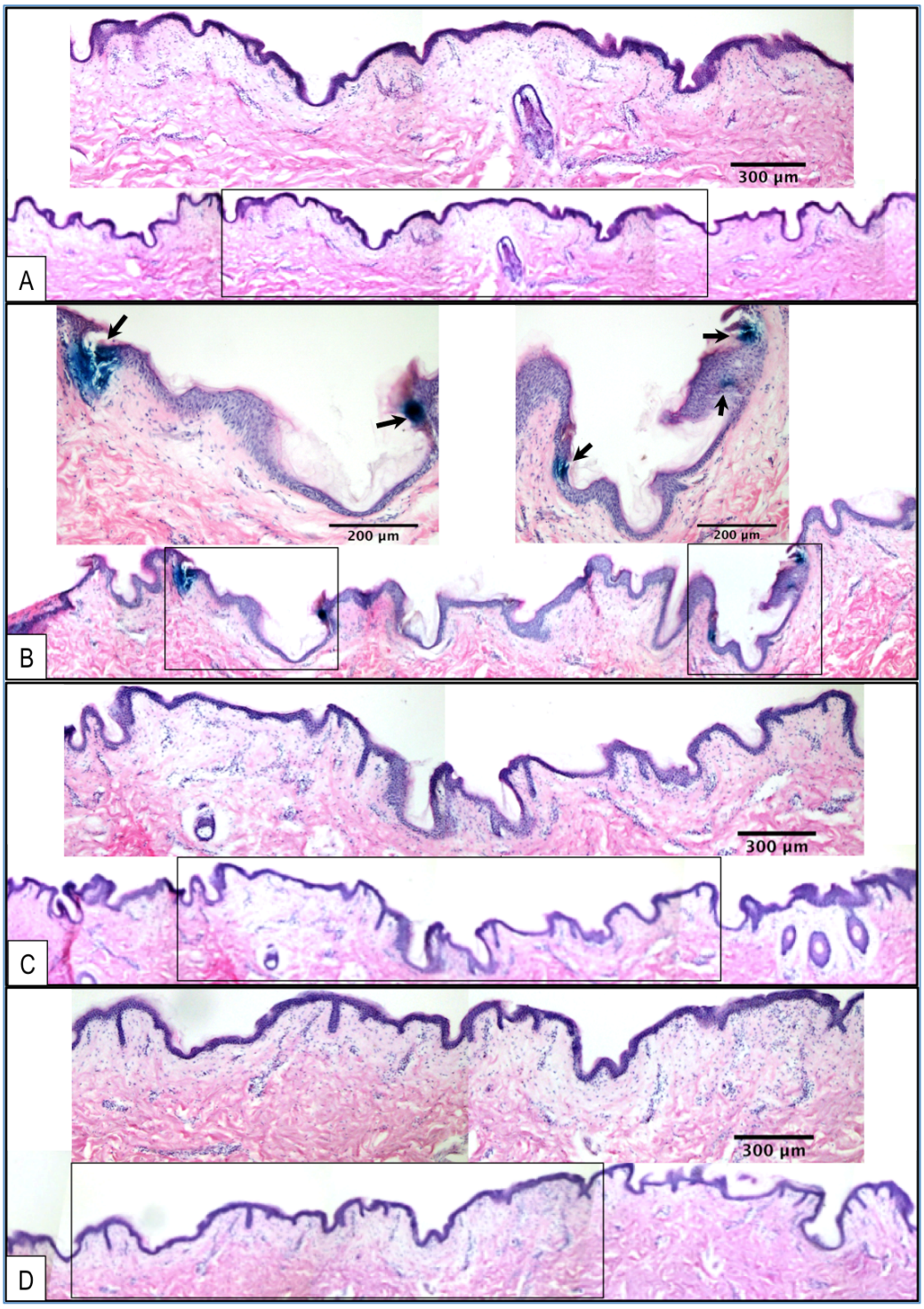

Figure 3.15: Transverse section images of a skin sample, from a 53-year-old patient, that have been treated by physical disruptions and PBS only (A) or naked pCMVβ (B-D). Skin samples (Figure 3.14) that have been subjected to X-gal staining were cryosectioned and transverse sections were H&E stained. A. Tape-stripping + liquid cyanoacrylate stripping + PBS (negative control); B. pCMVβ + microneedle abrasion; C. Tape-stripping + pCMVβ; D. Tape-stripping + liquid cyanoacrylate stripping + pCMVβ. (naked pCMVβ = 10 µL pCMVβ 6 mg mL^{-1} solution; arrow = skin area with β-galactoside expression)

Transverse sections from the tape-stripping (Figure 3.15 C) and tape-stripping plus liquid cyanoacrylate stripping (Figure 3.15 A and D) samples revealed incomplete removal of the stratum corneum. Attempts to improve on the liquid cyanoacrylate stripping method were made by repeating the cyanoacrylate applications. Methylene blue was used to determine whether the stratum corneum and/or epidermis had been removed. Methylene blue is an aqueous dye that does not penetrate skin with intact stratum corneum and could easily be wiped or washed off following application on intact skin. After 4 applications of liquid cyanoacrylate on the treatment area, methylene blue solution rapidly diffused into the dermis, indicating complete removal of the stratum corneum and epidermis (Figure 3.16 E and 3.17). From the transverse sections, the presence of stratum corneum was visible even after liquid cyanoacrylate stripping on 3 occasions. This shows the difficulty in achieving consistency in the technique, which therefore may not be ideal for widespread application. Also, forcefully removing the upper layer or the skin using liquid cyanoacrylate might cause pain and if not performed carefully or consistently, it may result in insufficient removal of the stratum corneum or complete removal of the epidermis.

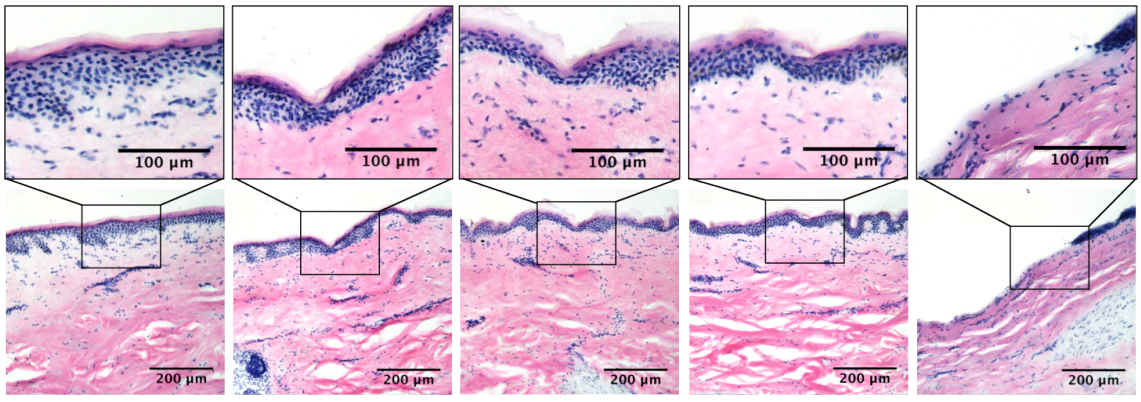

Figure 3.16: Transverse section images of defrosted skin sample, from an 83-year-old patient subjected to increasing times of liquid cyanoacrylate stripping physical disruptions. Tranverse sections were H&E stained. (LCS = liquid cyanoacrylate stripping; × 1 = applied once, × 2 = applied twice; × 3 = applied thrice and × 4 = applied 4 times)

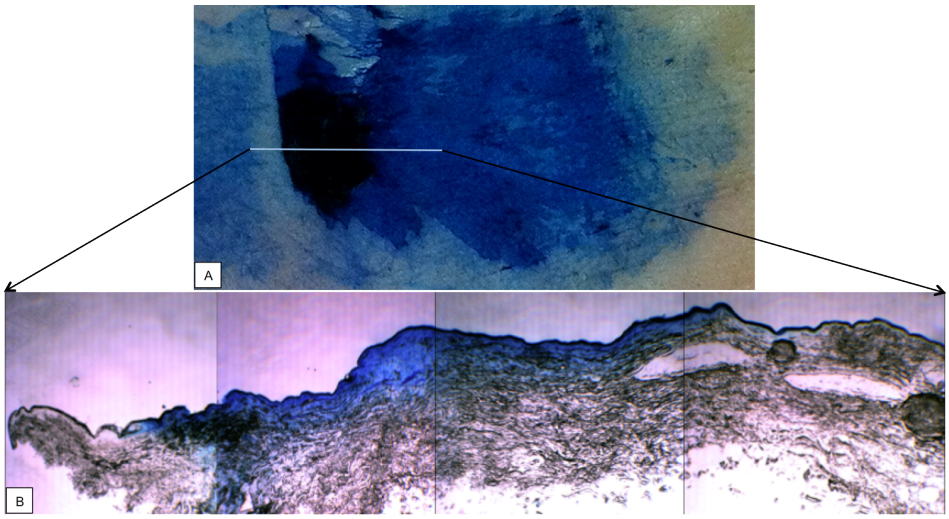

Figure 3.17: ***En face*** **image (A) and corresponding cross-section image (B) of a defrosted skin sample from an 83-year-old patient subjected to 4 repeated liquid cyanoacrylate stripping physical disruption procedures followed by staining with methylene blue.**

Nevertheless, the skin disruption experiment was repeated and liquid cyanoacrylate stripping was performed 3 times to remove the stratum corneum rather than complete removal of the epidermis, before application of pCMVβ. Gene expression was not observed when examined stereoscopically, *en face* (Figure 3.18). When the skin sample was subjected to microneedle abrasion after liquid cyanoacrylate stripping, gene expression occurred. This observation supports the hypothesis that in order for gene expression to occur following delivery of naked pDNA, skin cells have to be temporarily and minimally disrupted and nucleic acid should be targeted to the actively dividing basal epidermal cells. The action of liquid cyanoacrylate may have disrupted the upper layer of epidermis but the disruption may only be superficial. It was also noteworthy to observe that gene expression occurred subsequent to a 5 min delay in application of pDNA after microneedle abrasion, suggesting that temporary cellular membrane disruption caused by microneedle abrasion may not be as transient as previously thought.

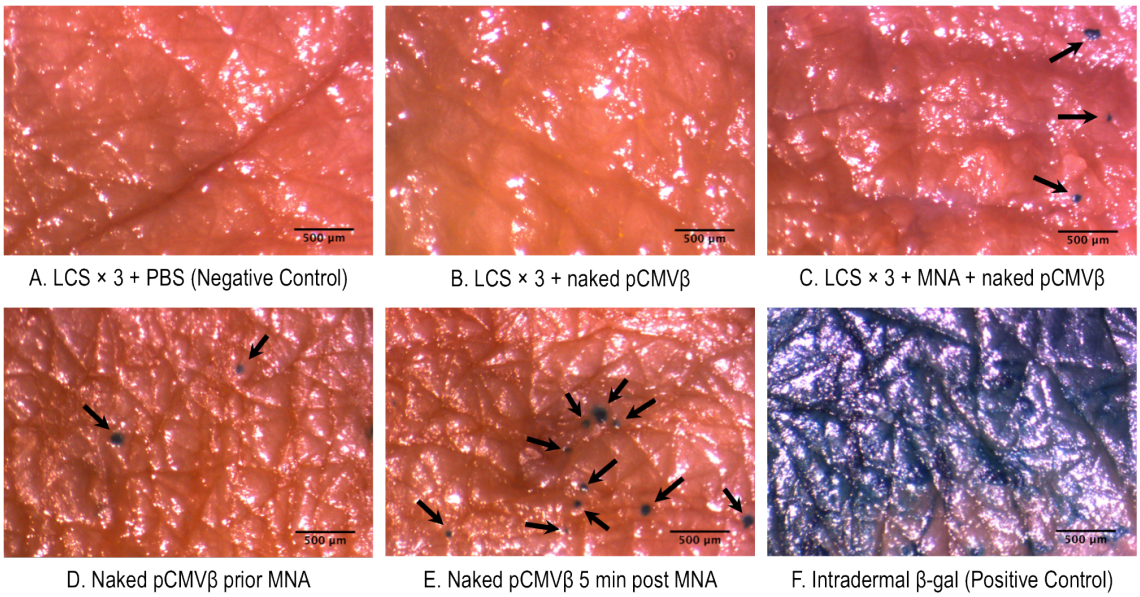

Figure 3.18: ***En face*** **images of skin samples, from a 77-year-old patient, that have been treated by physical disruptions and pCMVβ or controls.** Skin samples have been subjected to X-gal staining, which highlights the presence of β-galactosidase protein with a dark blue pigment, indicated by an arrow. (A. LCS × 3 + PBS = skin subjected to 3 times liquid cyanoacrylate stripping followed by PBS; B. LCS × 3 + naked pCMVβ = skin subjected to 3 times liquid cyanoacrylate stripping followed by naked pCMVβ; C. LCS × 3 + MNA + naked pCMVβ = skin subjected to 3 times liquid cyanoacrylate stripping and then microneedle abrasion followed by naked pCMVβ; D. Naked pCMVβ prior MNA = skin treated with naked pCMVβ prior to microneedle abrasion; E. Naked pCMVβ 5 min post MNA = skin treated with naked pCMVβ 5 min after microneedle abrasion; F. Intradermal β-gal = intradermal injection of β-galactosidase; PBS = 10 µL PBS solution; naked pCMVβ = 10 µL pCMVβ 6 mg mL^{-1} solution; n = 1)

Due to positive results from the microneedle abrasion technique, another experiment was performed to investigate the effect of applying different concentrations of naked pDNA and pDNA lipoplex on the skin using the microneedle abrasion method (Figure 3.19). Application of naked pCMVβ at concentrations of 1 mg mL^{-1} and 2.5 mg mL^{-1} resulted in reporter gene expression (Figure 3.19 B and C) and up to 6 mg mL^{-1} was effective in previous experiments (Figure 3.14 B and Figure 3.18 D). Application of pCMVβ lipoplex resulted in gene expression at concentrations higher than 2.5 mg mL^{-1} (Figure 3.19 E) but not at a concentration of 1 mg mL^{-1} (Figure 3.19 F). Previously, an attempt by another member of the research laboratory to deliver pDNA lipoplexes to *ex*

vivo human skin using the same method failed to facilitate gene expression at both lipoplex concentrations tested (Ng 2010).

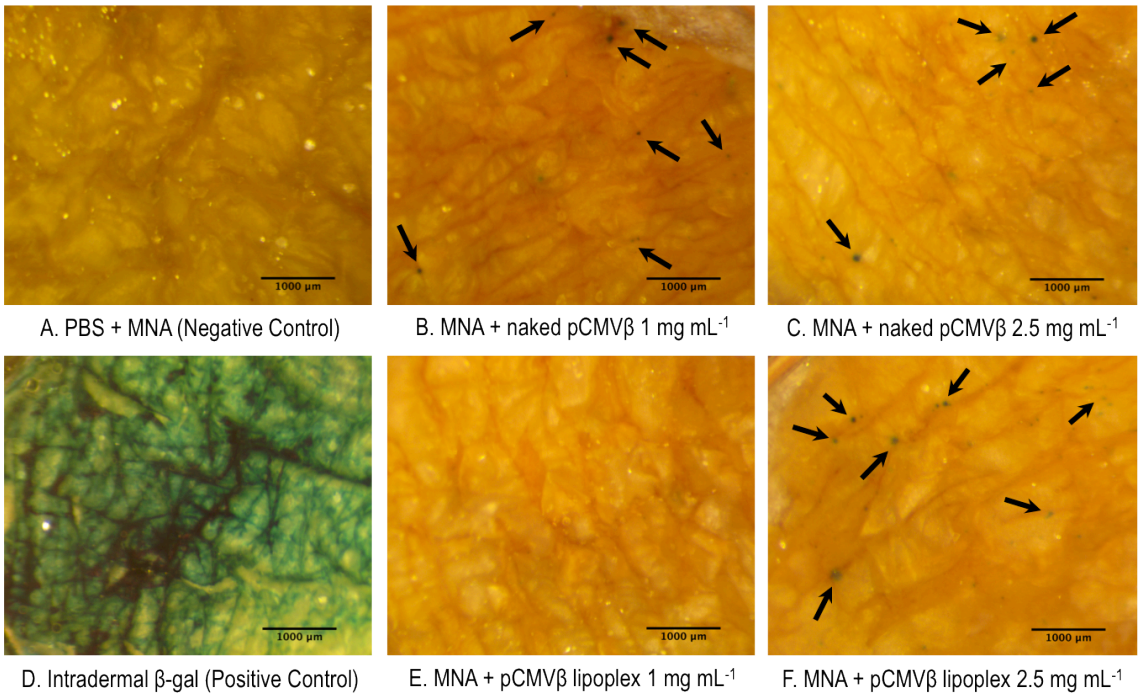

Figure 3.19: ***En face*** **images of skin samples, from a 72-year-old patient that have been treated by physical disruptions and pCMVβ or controls.** Skin samples have been subjected to X-gal staining, which highlights the presence of β-galactosidase protein with a dark blue pigment, indicated by an arrow. (MNA = microneedle abrasion; intradermal β-gal = intradermal injection of β-galactosidase; naked pCMVβ = 20 µL pCMVβ solution; pCMVβ lipoplex = pCMVβ + 50% v/v Lipofectamine™ 2000; n = 1)

However, the choice of lipid based transfection reagents between the two studies was different; Lipofectamine™ LTX was the transfection reagent used in Keng (2010) whilst Lipofectamine™ 2000 was used in this study. The compositions of these transfection reagents are proprietary to the company and hence it is unclear whether the choice of transfection reagent was the reason for the difference in results. Moreover, results from the *in vitro* studies in both HaCaT cells (Figure 3.4) and primary keratinocytes (Figure 3.9) show more efficient transfection using the Lipofectamine™ LTX transfection reagent, which was used in Keng (2010)'s study. Again, this highlights the challenges in correlating observations *in vitro* with *ex vivo* and ultimately *in vivo* settings in the complex skin structure for the delivery of nucleic acid. Furthermore, at the higher

pDNA concentration of 2.5 mg mL^{-1}, the ratio of pDNA to the transfection reagent at 50% v/v was 5:1. The ideal plasmid to lipid ratio for *in vitro* cell monolayer transfection is 1:3 and this is diluted to a final plasmid concentration of 8×10^{-4} mg mL^{-1} (0.5 μg pDNA in 600 μL transfection volume). At a higher pDNA to lipid ratio of 5:1, lipoplex formation is probably incomplete, resulting in the availability of uncomplexed naked pDNA that could have transfected the skin cells in a way similar to naked plasmid.

Moreover, if naked pDNA is efficient in human skin transfection following treatment, the value of including a lipid-based transfection reagent for nucleic acid delivery is debatable. Complexation of pDNA with lipid-based transfection reagents has been shown to be toxic, inducing acute inflammatory reactions in *in vivo* studies where animals were treated with intravenous injections (Song et al. 1997), and animal (Scheule et al. 1997) or humans (Ruiz et al. 2001) were treated with pulmonary delivery of lipoplex formulations. These studies have shown that cationic lipid and DNA were synergistic in significantly contributing to the toxicity observed (Ruiz et al. 2001; Scheule et al. 1997). The observed toxicity to keratinocyte cells *in vitro* following treatment with pDNA lipoplexes in section 3.3.3 is concerning and therefore it would be better if naked pDNA could be delivered to the skin using microneedles.

In addition to cutaneous delivery of a pDNA liquid formulation (Figures 3.14, 3.15, 3.18 and 3.19), delivery of naked pDNA from dry-coated microneedles was also investigated. However following treatment of three tissue samples with steel microneedles (5 needles per array; 700 μm in length) coated with 10 μg pCMVβ per microneedle device, β-galactosidase was only observed at one microneedle puncture site (Figure 3.20). Low transfection efficiencies with pDNA coated microneedles have previously been reported by other members of the research laboratory (Pearton et al. 2012).

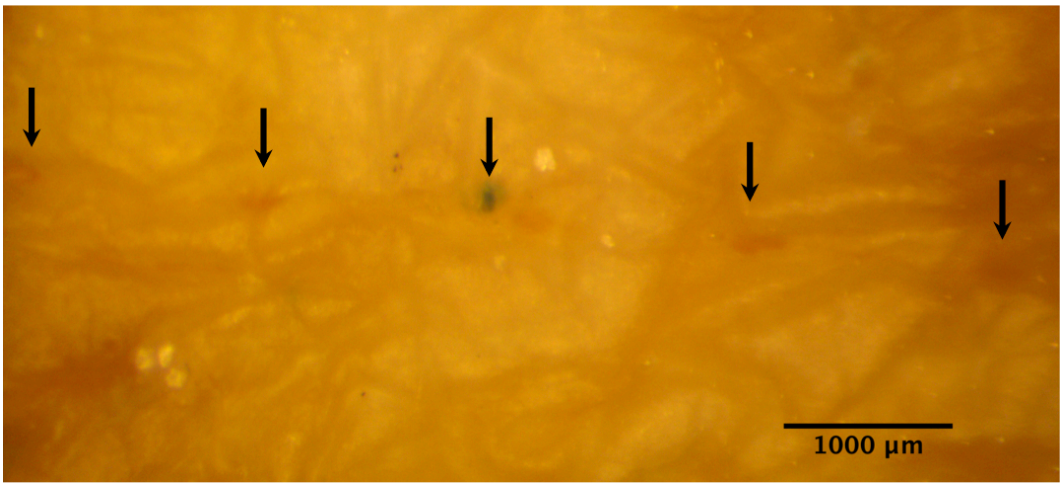

Figure 3.20: ***En face*** **images of skin samples, from a 72-year-old patient, that have been treated by naked pCMVβ coated microneedles application.** Skin samples have been subjected to X-gal staining, which highlights the presence of β-galactosidase protein with a dark blue pigment. The arrows represent visible microneedle insertion sites. (each microneedle was coated with 2 µg pCMVβ; n = 3)

This observation could be attributed to poor dissolution of dehydrated pDNA (Pearton et al. 2012). In routine laboratory use, pDNA is often dissolved to 1 mg mL^{-1}. DNA pellet obtained from plasmid extraction usually requires gentle agitation over extended period of time. For a dry-coat of pDNA on the surface of microneedles to dissolve following microneedle application, a sufficient volume of solvent in the skin environment proximal to the microneedle delivery site is required to allow rapid dissolution of pDNA from the surface of microneedles (Pearton et al. 2012). In a previous study where pDNA was recovered from the surface of microneedles after 24 h and 96 h drying time (section 3.3.5), 100 µL volume of TE buffer was used to recover a theoretical maximum loading amount of 3.25 µg dry-coat of pDNA from the surface of microneedles. The mass of pDNA recovered also decreased with time, which could be attributed to loss of material or poor solubility of the dried plasmid coat. The volume of fluid required to sufficiently dissolve solid pDNA deposited from microneedles is unlikely to be present in the skin area proximal to the microneedle insertion sites (Pearton et al. 2012).

Moreover, although a study has shown low amounts of pDNA internalisation (up to 15%) following delivery of a high concentration of pDNA (5 µg mL^{-1}) to human

keratinocyte cells *in vitro* (Basner-Tschakarjan et al. 2004), it has been estimated that in a non-dividing cell, including suprabasal keratinocytes, at least 100000 copies of pDNA has to be present in cell cytoplasm to ensure nuclear uptake and transcription of between 0.1% and 0.0001% of the plasmid (Capecchi 1980; Tseng et al. 1997). Any naked pDNA internalisation in skin cells from slow dissolution of a deposited solid pellet, after the initial phase of transient cell membrane disruption by microneedles, is probably through endocytosis and without the presence of cationic lipids, naked pDNA is not likely to escape from the endosomal membrane and is likely to be degraded in lysosomes (Lechardeur and Lukacs 2006; Lechardeur et al. 2005; Wattiaux et al. 2000).

Due to limited supply of freshly excised human skin, these human skin experiments were only performed once and if the sample size permitted, treatments would have been repeated on the same skin specimen. More studies need to be performed in the future to be able to support the observations. These results and observations are by no means conclusive but generally support what has previously been reported.

3.4 Conclusion

Preliminary studies performed in this experimental chapter demonstrated the feasibility of genetic manipulation through functional delivery of reporter pDNA in both *in vitro* and *ex vivo* human skin models. Various commercially available lipid-based transfection reagents were tested in human keratinocyte cells *in vitro*, which resulted in reporter gene expression, but transfection efficiencies were low (up to 37% gene expression) and cell toxicity was also observed in cells treated with lipoplexes, albeit insignificant. Delivery of naked pDNA to keratinocyte cells did not result in gene expression *in vitro* but topical delivery of a 1 mg mL^{-1} pDNA liquid formulation to freshly excised human skin, followed by abrasion with microneedles, resulted in reporter gene expression in the viable epidermis. Topical application of lipoplexes in liquid formulation to excised human skin treated with microneedle abrasion resulted in one occasion of reporter gene expression, at a pDNA concentration of 2.5 mg mL^{-1}. Therefore, the value of lipid-based transfection reagents in gene delivery to the skin is debatable. Overall, results from this chapter provide greater understanding of human skin models and demonstrates the functionality of the biological systems that were described in Chapter 2. This lays the foundation for siRNA delivery experiments.

CHAPTER 4

Non viral delivery of siRNA to *in vitro* human skin models

4 Non-viral delivery of siRNA to *in vitro* human skin models

4.1 Introduction

Functional delivery of reporter plasmid DNA (pDNA) and subsequent reporter gene expression in both keratinocytes in monolayer cell culture and intact excised human skin was demonstrated in the preceding chapter. The availability of a reporter gene system helps in easy identification of gene expression following gene delivery. Such reporter gene systems are also widely used for gene silencing detection following siRNA delivery in monolayer cell culture. For example, cells can be co-transfected with pDNA that expresses a reporter gene, suppression of which is attributed to the action of siRNA (Elbashir et al. 2001a). Alternatively, reporter genes may be introduced to cells to generate cell lines that stably express the reporter gene, which may then be used for subsequent siRNA mediated gene silencing experiments targeting the reporter mRNA (Hickerson et al. 2011; Kwok and Hart 2011). Unfortunately, human skin is a complex structure that does not naturally express any gene that allows easy identification through commonly used reporter gene systems. Furthermore, the use of excised human breast skin that deteriorates over time requires rapid attention and does not allow sufficient time for genetic manipulation through reporter gene introduction in this model system. Therefore, proof-of-concept siRNA delivery experiments to human skin models require selection of a suitable model gene for functional detection of siRNA mediated gene silencing. *In vitro* studies involving gene silencing detection in monolayer human keratinocyte cells were performed using lamin A/C and CD44 as model genes for RNA interference studies. These *in vitro* studies serve to optimise siRNA delivery and detection systems in a defined and controlled monolayer cell culture environment to inform and support studies in the less robust excised human skin culture system (Chapter 5).

4.1.1 Gene silencing targets

In proof-of-concept gene silencing studies, target genes are selected based on the availability of antibodies or assays required to quantitate the silencing effect (Elbashir et al. 2001a). For the same reasons, the human lamin A/C and CD44 genes were selected as model genes for functional siRNA delivery and gene silencing studies. These genes are abundant in human skin cells and the reduction of these genes in cells is not expected to affect cell viability.

4.1.1.1 Lamin A/C

The nuclear lamina is a dense protein matrix located near the inner wall of the nuclear membrane of a cell. The matrix of the nuclear lamina is composed of lamins and lamin-associated membrane proteins. During mitosis, lamin proteins are phosphorylated, resulting in reversible matrix deconstruction. The functions of the nuclear lamina include cell cycle regulation, cell differentiation, DNA replication, chromatin reorganisation, DNA replication and apoptosis (Gruenbaum et al. 2000).

The human lamins consist of two types, A (LMNA) and B (LMNB). Alternative splicing of the type A gene results in the presence of three mRNA isoforms known as Lamin A, Lamin C and Lamin Aδ10, respectively. The human lamin A/C gene (LMNA; GenBank accession number NG_008692) was selected as the gene silencing target for initial siRNA experiments involving unmodified siRNA complexed with a lipid based transfection reagent due to its abundant expression in most human cells, including keratinocyte cells.

The lamin A/C siRNA used in these studies targets all three of the human lamin A/C mRNA transcript variants: 1 (GenBank accession number NM_170707.2), 2 (GenBank accession number NM_170708.2) and 3 (GenBank accession number NM_005572.3). The human lamin A/C gene is commonly used in siRNA mediated gene silencing studies (Elbashir et al. 2001a; Elbashir et al. 2002), with a wide range of commercially available gene detection assays such as Taqman gene expression assay for detection of mRNA levels through reverse transcription quantitative polymerase chain reaction (RT-qPCR) as well as primary antibodies for detection of protein levels through Western blotting.

4.1.1.2 CD44

The human CD44 gene (GenBank accession number NG_008937.1) exists in multiple isoforms through alternative splicing. The CD44 isoforms are further modified by post-translational modifications (Screaton et al. 1992) to form a family of cell-surface glycoprotein molecules that are involved in cell-cell and cell-matrix interactions, cell adhesion and cell migration (Goodison et al. 1999; Ponta et al. 1998). The CD44 protein is the main receptor for hyaluronic acid (HA) and is also the receptor for other ligands

including osteopontin, collagens, fibronectin and laminin. It has been suggested that the expression of multiple CD44 splice variant isoforms and post-translational modification to the CD44 protein is related to tumour metastasis (Bourrguignon et al. 1995; Cichy and Pure 2003; Nagano and Saya 2004).

The predominant form of CD44 splice variant that are expressed in epidermal keratinocytes and keratinocytes in cell culture is the epican variant (Zhou et al. 1999). The CD44 siRNA used in this thesis was synthesised with a binding site that targets all CD44 isoform mRNA (Figure 4.1)(Lara et al. 2012). The location of Taqman gene expression assay probe binding sites used to determine CD44 mRNA levels through RT-qPCR and the primary antibody binding site used to determine CD44 protein levels through Western blotting are as indicated in Figure 4.1.

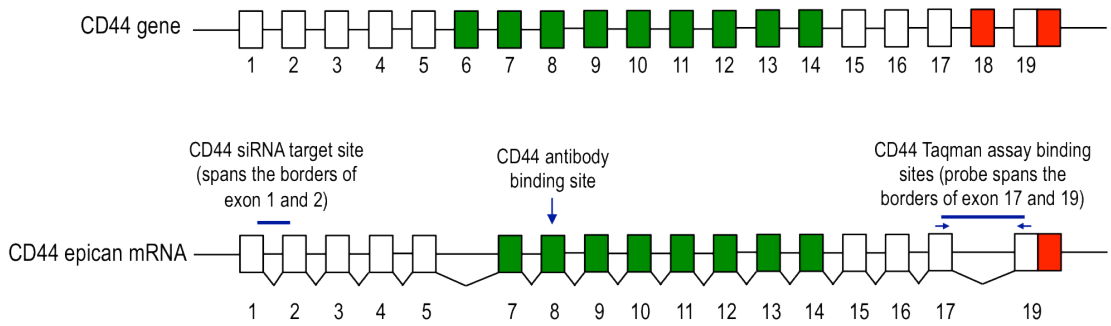

Figure 4.1: Schematic representation of CD44 gene organisation and CD44 epican mRNA structure with indication of the CD44 siRNA binding site, the probe location for the Taqman gene expression assay used for qPCR and the CD44 antibody binding epitope. The binding site of the CD44 siRNA ensures that all CD44 mRNA isoforms are targeted. Open boxes represent exons common to all known splice variants of CD44, green boxes represent the variable exons and red boxes represent alternative exons for cytoplasmic domain (adapted from Lara et al. 2012).

4.1.2 siRNA chemical modifications

siRNA are short double stranded RNA molecules vulnerable to rapid degradation by endo- and exonucleases. In human plasma, siRNA has a half-life of less than 5 min (Layzer et al. 2004). In the absence of a transfection reagent, naked siRNA is not taken up by cells (Elbashir et al. 2002). siRNA also has a relatively small size and therefore is rapidly cleared by kidney filtration after systemic administration (Soutschek et al.

2004). Transfection reagents such as cationic liposomes are often used to deliver siRNA *in vitro*, which provides protection against degradation as well as facilitating cellular delivery of siRNA. However, chemical modifications to the siRNA structure are required for increased stability against intracellular nucleases to improve gene silencing persistence without affecting the interaction of siRNA with RISC or the target. Chemical modifications are also applied to maximise siRNA potency, specificity and to reduce off-target effects. RNA therapy should also be limited to short strands of RNA molecules (shorter than 30 bp) to avoid off-target immune response, as the administration of long double stranded RNA molecules induces type 1 interferon synthesis (Manche et al. 1992; Stark et al. 1998). Nevertheless, siRNA should be routinely screened to identify and eliminate sequences that might activate an immune response.

Various proprietary chemical modifications of siRNA are now commercially available to improve nuclease stability, potency and specificity of siRNA. Most commercially available chemical modifications to siRNA serve to improve nuclease stability, however a recent siRNA modification by Dharmacon (part of ThermoFisher Scientific) allows the synthesis of "self-delivery" (sd-) siRNA that enters cells passively in the absence of a "carrier" such as liposomes. The chemical modification is propriety to the company and therefore is not known but is believed to involve steroid or lipid moieties that are covalently conjugated to the 5'-ends of the siRNAs, as previously described by a research group in Alnylam Europe AG, Germany (Lorenz et al. 2004; Soutschek et al. 2004). The addition of lipophilic moieties to negatively charged siRNA molecules may enhance siRNA uptake into cells via a receptor-mediated mechanism or by increased membrane permeability. The availability of these siRNA allows for improved targeted delivery of siRNA to a readily accessible organ such as the skin.

4.1.3 Non-viral delivery of siRNA *in vitro*

Similar to the studies using pDNA (Chapter 3), a lipid based transfection agent was selected for initial *in vitro* experiments to optimise cellular delivery of siRNA to monolayer human keratinocyte cells. Lipid based transfection reagents have also been used in numerous siRNA studies with great success (Elbashir et al. 2001a; Elbashir et al. 2002). The use of cationic liposomal transfection agent produces siRNA lipoplexes.

The efficiency of these complexes in facilitating gene silencing can be compared with that mediated by the aforementioned chemically modified sd-siRNA. The post-transcriptional gene silencing mediated by siRNA and siRNA uptake is determined using commonly used detection methods.

4.1.3.1 Detection of gene silencing

Gene silencing by siRNA occurs at the post-transcriptional level, where mRNA sequences homologous to the guide strand of siRNA are targeted, cleaved and rapidly degraded (Hammond et al. 2000; Hammond et al. 2001; Meister and Tuschl 2004). The degraded mRNA is not able to translate into protein and hence the gene is silenced when remaining protein degrades over its half-life (Wilkinson 2000). Therefore, the effect of siRNA mediated gene silencing can be detected either at the mRNA or protein level of the targeted gene.

Gene silencing at the mRNA level can be detected using reverse-transcription quantitative polymerase chain reaction (RT-qPCR). This method involves extraction of total RNA from treated cells, which is then converted to cDNA through reverse transcription (RT). Quantitative polymerase chain reaction (qPCR) is then performed to quantify levels of target genes. PCR assumes an exponential accumulation of the target gene with each replication cycle until the reaction reaches a plateau. qPCR uses fluorescent probes to quantitatively measure gene amplification, whereby the increase in fluorescent signal is proportional to the amount of DNA accumulated during each PCR cycle (Bustin 2000; Nolan et al. 2006). The level of target mRNA in each treatment group is normalised to the level of an endogenous control gene not affected by the siRNA treatment performed in parallel. The differences in mRNA levels between different treatment groups including positive and negative controls (cells treated with non-specific siRNA or untreated cell) are then compared.

A range of fluorescent detection systems has been developed and is commercially available (Bustin 2000). The two most favoured systems are the DNA-binding dye and the hydrolysis probe methods. The most commonly used dye is SYBR Green, a fluorescent dye that binds to DNA, which has been amplified using primers (Bustin 2000; Nolan et al. 2006). The hydrolysis probe or Taqman assay method uses a Taqman

probe that utilises the 5'-nuclease activity of the DNA polymerase or Taq polymerase enzyme to hydrolyse and cleave a dual-labelled hybridisation probe bound to the complementary target sequence, releasing the fluorescent dye which is then detected (Bustin 2000; Holland et al. 1991). When unbound, the fluorescent reporter dye at the 5' end is quenched by a second fluorescent dye at its 3' end and no reporter fluorescence is detected. The Taqman assay method has an improved sensitivity and specificity over other qPCR detection methods (Holland et al. 1991).

A gene is ultimately expressed in the form of protein and therefore, gene silencing can be detected by performing Western blot and/or immunofluorescence to determine protein levels. Western blotting (Towbin et al. 1992) is a widely used technique to detect specific proteins in a sample (MacPhee 2010). This technique involves (i) protein extraction from tissue or cell samples, (ii) separating extracted protein samples by molecular weight, isoelectric point and/or electric charge using gel electrophoresis, (iii) transferring separated protein from gel to nitrocellulose or polyvinylidene difluoride (PVDF) membrane, (iv) probing the membrane for specific proteins with antibodies and then (v) detecting the presence of target proteins through colorimetric, chemiluminescent, radioactive or fluorescent detection. The same amount of protein from each sample is loaded for Western blotting, usually indicated by a protein loading control, which allows meaningful comparison of protein levels of the gene targeted by the siRNA.

The immunofluorescence technique involves staining treated cells with specific antibodies, incorporating a fluorescent tag either on the primary antibody or through fluorescently labelled secondary antibodies to then detect fluorescence intensity of target protein in samples through fluorescence or confocal microscopy (Odell and Cook 2013).

4.1.3.2 Determination of siRNA uptake

In addition to gene silencing, siRNA uptake studies could provide useful information on cellular uptake kinetics and localisation of fluorescently labelled siRNA. Techniques such as flow cytometry, fluorescent microscopy, and confocal microscopy have previously been used to detect cellular uptake and/or localisation of fluorescent siRNA

(Dunne et al. 2003; Grunweller et al. 2003; Ruponen et al. 2003; Vader et al. 2010). Flow cytometry analysis of single cell suspensions of treated cells could provide useful data for quantification of siRNA uptake at various time-points. Fluorescent microscopy is a quick method to visualise if cells have taken up siRNA before further analysis with flow cytometry. Cellular localisation of siRNA could then be visualised using confocal microscopy, an imaging technique with increased optical resolution and contrast. This technique allows sequential imaging through a cellular layer, which can then be reconstructed into 3D image to provide insight of fluorescent siRNA localisation in cells, relative to counterstained nuclei.

4.1.4 Aim and objectives

The aim of this chapter was to develop functional assays to quantify detection of siRNA delivery and siRNA mediated gene silencing in *in vitro* human skin models following non-viral siRNA delivery. The objectives of the experiments were:

- To deliver functional siRNA to human keratinocyte cell monolayers and optimise gene expression detection methods.
- To perform protein extraction from cultures of human keratinocytes for quantification by Western blotting.
- To perform total RNA extraction from cultures of human keratinocytes for quantification by RT-qPCR.
- To determine the effect of siRNA treatment on cell viability.
- To observe internalisation of siRNA through delivery of fluorescently labelled siRNA to human keratinocytes.
- To determine siRNA uptake kinetics in human keratinocytes through delivery of fluorescently labelled siRNA .
- To test the ability to coat microneedles with siRNA consistently and precisely.
- To test the short term biological stability of siRNA coated onto microneedles.

4.2 Methods

Unless specified, the suppliers of all reagents and materials have previously been mentioned or were obtained from ThermoFisher Scientific, UK.

4.2.1 siRNA modification and sequences

siRNA were received either in the form of a dry pellet or pre-diluted in PBS. Dry pellets of siRNA were dissolved in a small volume of PBS to the required concentration, determined by quantification using a NanoVue or NanoDrop spectrophotometer as described in section 3.2.1.5.

4.2.1.1 Non-self-delivery siRNA

For all the experiments targeting lamin A/C mRNA, unmodified siRNA molecules were a 19+2 format, with two 3′ deoxythymidine (dT) overhangs, designed and synthesised by Eurofins MWG Operons (Ebersberg, Germany). A non-self-delivery unmodified (non-sd) lamin A/C siRNA (lamin A/C non-sd-siRNA; sequence: 5′-CUGGACUUCCAGAAGAACA) was used to target human lamin A/C mRNA. A nonspecific unmodified green fluorescent protein (GFP) siRNA (GFP non-targeting non-sd-siRNA; sequence: 5′-GGCUACGUCCAGGAGCGCACC) targeting the GFP mRNA not present in the human keratinocyte models was used as a negative control (Chong et al. 2013).

For experiments targeting the CD44 mRNA, siSTABLE modified and unmodified siRNAs (gifts from Dr. Roger Kaspar, Transderm Inc., USA) were designed and synthesised by Dharmacon Products, Thermo Fisher Scientific (Lafayette, CO, USA). siSTABLE is a proprietary modification to improve stability of siRNA by preventing degradation by nucleases. A siSTABLE modified non-self-delivery CD44 siRNA (CD44 non-sd-siRNA; siRNA sequence: 5′- GGCGCAGAUCGAUUUGAAU) was used to target human CD44 mRNA (Lara et al. 2012). A nonspecific unmodified non-self-delivery K6a_513a.12 siRNA (TD101 non-targeting non-sd-siRNA) targeting a keratin 6a mutation not present in the human keratinocyte models was used as negative control (Hickerson et al. 2011).

4.2.1.2 Self-delivery siRNA

For experiments involving self-delivery siRNA, Accell-modified siRNA (gifts from Dr. Roger Kaspar, Transderm Inc., USA) were designed and synthesised by Dharmacon Products, Thermo Fisher Scientific (Lafayette, CO, USA). Accell siRNA is a proprietary modification to produce "self-delivery" (sd-) siRNA that does not require a transfection agent to facilitate cell transfection and to improve stability of siRNA by preventing degradation by nucleases. Accell-modified self-delivery siRNA (Accell CD44 sd-siRNA; siRNA sequence: 5′- GGCGCAGAUCGAUUUGAAU) was used to target human CD44 mRNA (Lara et al. 2012). A nonspecific self-delivery K6a_513a.12 siRNA (Accell TD101 or non-targeting sd-siRNA) targeting a keratin 6a mutation not present in the human keratinocytes model was used as a negative control (Hickerson et al. 2011).

4.2.1.3 Fluorescently labelled siRNA

A BLOCK-iT™-modified Alexa 647 fluorescent siRNA (1 mg mL^{-1} in PBS) (a gift from Dr. Xavier de Mollerat du Jeu, Life Technologies, USA) was a nonspecific sequence of non-sd-siRNA with far-red Alexa Fluor® 647 fluorescent label that has an excitation maximum of 650 nm and emission maximum of 668 nm. BLOCK-iT™ is a proprietary chemical modification to enhance stability of siRNA.

An Accell-modified Red Cyclophilin B control siRNA (Accell Red sd-siRNA) was used to evaluate cellular uptake of self-delivery siRNA. A siGLO-modified Cyclophilin B control siRNA (siGLO Red non-sd-siRNA) was used as non-self-delivery control for siRNA uptake studies. siGLO has similar chemical modifications to siSTABLE for enhanced siRNA stability as well as extended fluorescence signal intensity of up to 7 days. Both Accell-modified and siGLO-modified red fluorescent siRNA are labelled with DY-547 fluorescent label with an absorbance maximum of 557 nm and emission maximum of 570 nm. Both the siRNA sequence targets the human peptidylprolyl isomerase B (PPIB), commonly referred to as cyclophilin B mRNA that is abundantly expressed in most mammalian cells. The human cyclophilin B gene is non-essential and silencing of the gene does not affect cell viability. The functional gene silencing of cyclophilin B is not a target for investigation in the siRNA uptake studies described in later sections.

4.2.2 *In vitro* gene silencing with siRNA lipoplexes in HaCaT cells

4.2.2.1 Lipofectamine™ RNAiMAX Reagent – siRNA lipoplexes

Lipofectamine™ RNAiMAX (Life Technologies, UK) transfection reagent is a proprietary formulation. Non-sd-siRNA-Lipofectamine™ RNAiMAX lipoplexes were formulated and prepared within 2 h of use. The complexation method was adapted from the supplier's recommended protocol. For each transfection sample, non-sd-siRNA was diluted with Opti-MEM® and mixed thoroughly. Lipofectamine™ RNAiMAX (Life Technologies, UK) was gently mixed before being added directly to the diluted siRNA and mixed thoroughly. The complexes were incubated for 20 min at room temperature to allow the lipoplexes to form.

4.2.2.2 Cell treatment

One day before transfection, HaCaT cells were seeded at 2.5×10^4 cells cm^{-2} in either 6-well, 12-well or 24-well plates, so that the cells were at least 50% confluent at the time of transfection and were allowed to adhere to the bottom of the plate surface overnight. Cells were seeded in 2.5 mL (per well of 6-well plate), 1 mL (per well of 12-well plate) or 0.5 mL (per well of 24-well plate) of growth medium without antibiotics.

In each well, 500 μL (per well of 6-well plate) or 200 μL (per well of 12-well plate) of the lipoplexes and controls were added to each well, respectively. The plates were gently rocked back and forth for 30 sec to ensure thorough mixing of the well contents. The cells were incubated at 37°C in a humidified atmosphere containing 5% CO_2 in air. RNA and protein extractions for gene expression analysis were performed 48 h post-transfection. Cells were treated in quadruplicate wells when necessary with triplicate samples for mRNA quantification by RT-qPCR and the remaining treatment sample for protein analysis by Western blotting.

4.2.2.3 Dose optimisation for *in vitro* siRNA lipoplex transfection

Dose optimisation of the lipoplexes was performed with lamin A/C non-sd-siRNA on HaCaT cells and the optimum transfection dose was determined by varying the concentration of lamin A/C non-sd-siRNA and Lipofectamine™ RNAiMAX complex

in a 6-well plate format to give a final transfection volume of 500 μL, as shown in Table 4.1. Cells were seeded in 2.5 mL culture medium and thus, the molar concentration of siRNA was based on a final cell culture medium volume of 3 mL post-transfection in a 6-well plate format. Protein extractions for gene expression analysis were performed 48 h post-transfection.

Table 4.1: Formulation of Lipofectamine™ RNAiMAX-siRNA complexes tested for dose optimisation (per well of 6 well plate)

No.	Description	Components			
		siRNA (50 pmol μL^{-1})		Lipofectamine™ RNAiMAX (μL)	Opti-MEM® (μL)
		GFP (μL)	Lamin A/C (μL)		
1	Untreated negative control	-	-	-	500.0
2	25 nM siGFP + 5μL RNAiMAX negative control	1.5	-	5.0	493.5
3	25 nM siLamin negative control	-	1.5	-	498.5
4	5 nM siLamin + 5μL RNAiMAX	-	0.3	5.0	494.7
5	5 nM siLamin + 7.5μL RNAiMAX	-	0.3	7.5	492.2
6	10 nM siLamin + 2.5μL RNAiMAX	-	0.6	2.5	496.9
7	10 nM siLamin + 5μL RNAiMAX	-	0.6	5.0	494.4
8	10 nM siLamin + 7.5μL RNAiMAX	-	0.6	7.5	491.9
9	25 nM siLamin + 5μL RNAiMAX	-	1.5	5.0	493.5
10	25 nM siLamin + 7.5μL RNAiMAX	-	1.5	7.5	491.0
11	50 nM siLamin + 5μL RNAiMAX	-	3.0	5.0	492.0
12	50 nM siLamin + 7.5μL RNAiMAX	-	3.0	7.5	489.5

The optimum dose for gene silencing in HaCaT cells with lamin A/C lipoplexes was determined to be 10 nM non-sd-siRNA complexed with 5 μL Lipofectamine™ RNAiMAX transfection reagent in a 6-well plate format. Further transfections with lamin A/C and non-specific control were kept at the same dose of lipoplexes and scaled-down accordingly when necessary.

Dose optimisation was also performed with CD44 non-sd-siRNA on HaCaT cells and the optimum transfection dose was determined by varying the concentration of CD44 non-sd-siRNA in a 12-well plate format to give a final transfection volume of 200 μL. Cells were seeded in 1 mL culture medium and thus, the molar concentration of siRNA

was based on a final cell culture medium volume of 1.2 mL post-transfection in a 12-well plate format. The final concentration of non-sd-siRNA tested was 1 nM, 10 nM, 20 nM and 50 nM complexed with 2 μL Lipofectamine™ RNAiMAX transfection reagent.

The optimum dose for gene silencing with CD44 lipoplexes was determined to be 10 nM non-sd-siRNA complexed with 2 μL Lipofectamine™ RNAiMAX in a 12-well plate format. Further transfections with CD44 and non-specific control were kept at the same dose of lipoplexes and scaled-down accordingly when necessary.

4.2.2.4 Duration of gene silencing from siRNA lipoplexes

HaCaT cells were treated with CD44 and lamin A/C non-sd-siRNA lipoplexes as described in section 4.2.2.2. To determine the duration of the lipoplex gene silencing effect, the treated cells were maintained in prolonged culture. In some cases, the transfection medium in wells treated with CD44 lipoplexes was replaced with growth medium without antibiotics 4 h post transfection following a washing step with growth medium without antibiotics. In other samples, the media remained unchanged. Cells were then further incubated and RNA extractions for gene expression analysis were performed 1 h, 3 h, 6 h, 24 h, 48 h and 72 h post-transfection.

4.2.3 *In vitro* gene silencing with Accell self-delivery siRNA in HaCaT cells

4.2.3.1 Preparation of Accell self-delivery siRNA

Accell sd-siRNA was prepared before use. For each transfection sample, Accell sd-siRNA was diluted to 1 μM with serum-free Accell delivery medium (Thermo Fisher Scientific, UK) and mixed thoroughly.

4.2.3.2 Cell treatment

One day before transfection, HaCaT cells were prepared as described in section 4.2.2.2. In each well, cells were treated by replacing the seeding medium with transfection mixture containing siRNA, which was prepared as described in section 4.2.3.1. The cells were incubated at 37°C in a humidified atmosphere containing 5% CO_2 in air for 24 h. After the initial incubation, the transfection medium was replaced with growth medium without antibiotics to replace serum in the medium to promote healthy cell

growth following a washing step with growth medium without antibiotics. Cells were then further incubated and RNA and protein extractions for gene expression analysis were performed 48 h or 72 h post-transfection. Cells were treated in quadruplicate wells when necessary with triplicate samples for mRNA quantification by RT-qPCR and the remaining treatment sample for protein analysis by Western blotting.

4.2.3.3 Optimisation for *in vitro* self-delivery siRNA

Dose optimisation of the lipoplexes was performed with Accell CD44 sd-siRNA on HaCaT cells and the optimum transfection dose was determined by varying the concentration of Accell CD44 sd-siRNA in a 12-well plate format to give a final transfection volume of 1000μL. The final concentration of sd-siRNA tested was 0.1 μM, 0.5 μM, 1 μM, 1.5 μM and 2 μM. Cells were seeded in 1 mL culture medium and cells were transfected by replacing the seeding medium with the transfection mixture containing siRNA. Protein extractions for gene expression analysis were performed 72 h post-transfection. The optimum dose for gene silencing with Accell sd-siRNA was determined to be 1 μM sd-siRNA. Further transfection with targeting and non-specific control was kept at the same dose of sd-siRNA.

The optimisation of transfection medium condition (with or without serum) was also performed by treating HaCaT cells with Accell CD44-sd-siRNA in (i) Accell Delivery Medium with 3% (v/v) serum, (ii) serum-free Accell Delivery Medium and (iii) serum-free Accell Delivery Medium, which was then replaced with growth medium containing serum 24 h post-transfection. Cells were incubated at 37°C in a humidified atmosphere containing 5% CO_2 in air and RNA extractions for gene expression analysis were performed 72 h post-transfection.

4.2.3.4 Duration of gene silencing effect of self-delivery siRNA

HaCaT cells were treated with Accell CD44 sd-siRNA as described in section 4.2.3.2. To determine the duration of sd-siRNA gene silencing effect, transfection medium (without serum and without antibiotics) in cells treated with Accell CD44 sd-siRNA was replaced with growth medium without antibiotics 24 h post transfection. Cells were then further incubated and RNA extractions for gene expression analysis were performed 3 h, 6 h, 24 h, 48 h and 72 h post-transfection.

4.2.4 *In vitro* fluorescent siRNA uptake

BLOCK-iT™-modified Alexa 647 fluorescent non-sd-siRNA was prepared as described in section 4.2.2.1. HaCaT cells were treated with BLOCK-iT™-modified Alexa 647 fluorescent non-sd-siRNA lipoplexes as described in section 4.2.2.2. To determine the duration of siRNA uptake of the lipoplexes, transfection medium in cells treated with the lipoplexes were (medium change) or were not (no medium change) replaced with growth medium without antibiotics 4 h post transfection before further incubation. Cells treated in triplicate wells were imaged using the Leica DM IRB epifluorescence microscope and then dissociated from the culture vessel at 1 h, 3 h, 6 h, 24 h and 48 h post-transfection for flow cytometry analysis to determine cell uptake as described in section 3.2.7.1.2.

Accell Red sd-siRNA was prepared as described in section 4.2.3.1 to a final concentration of 0.5 μM. HaCaT cells were treated with Accell Red sd-siRNA as described in section 4.2.3.2. To determine the duration of siRNA uptake of the fluorescently labelled sd-siRNA, transfection medium in treated cells were replaced with growth medium without antibiotics 24 h post transfection following two washing steps with growth medium without antibiotics and then further incubated. Following incubation, cells were imaged using the Leica DM IRB epifluorescence microscope and then dissociated from the culture vessel at 0 h, 3 h, 6 h, 24 h, 48 h and 72 h post-transfection for flow cytometry analysis to determine cell uptake as described in section 3.2.7.1.2. Cells were treated in triplicate wells.

4.2.5 *In vitro* gene silencing and siRNA uptake in primary keratinocytes

Primary keratinocytes were isolated from excised human breast skin of a 38-year-old female patient using methods described in section 2.2.4.

4.2.5.1 Gene silencing

One day before transfection, primary keratinocytes were seeded at 2×10^4 cell cm^{-2} in a 24-well or 48-well plate, so that the cells were at least 60% confluent at the time of transfection and were allowed to adhere to the bottom of the plate surface overnight.

Cells were seeded in 0.5 mL (per well of 24-well plate) or 0.25 mL (per well of 48-well plate) of keratinocyte specific culture medium without antibiotics.

Optimised dose of CD44 non-sd-siRNA-Lipofectamine™ RNAiMAX lipoplexes and Accell CD44 sd-siRNA were prepared as detailed in section 4.2.2.1 and 4.2.3.1, respectively in keratinocyte specific culture medium without antibiotics. Primary keratinocyte cells were treated with lipoplexes and sd-siRNA as described in section 4.2.2.2 and 4.2.3.2. The transfection media in all treated cells were replaced with keratinocyte specific culture medium 24 h post-transfection following a washing step with keratinocyte specific culture medium without antibiotics. RNA extractions for gene expression analysis were performed 24 h, 48 h and 72 h post-transfection.

4.2.5.2 Fluorescent siRNA uptake

One day before transfection, primary keratinocyte cells were seeded at 2×10^4 cell cm^{-2} in a 12-well or 48-well plate, so that the cells were at least 60% confluent at the time of transfection and allowed to adhere to the bottom of the plate surface overnight. Cells were seeded in 1.0 mL (per well of 12-well plate) or 0.25 mL (per well of 48-well plate) of keratinocyte specific culture medium without antibiotics.

Accell Red sd-siRNA was prepared as described in section 4.2.3.1 to a final concentration of 0.5 μM. Primary keratinocyte cells were treated with Accell Red sd-siRNA as described in section 4.2.4. To determine the duration of siRNA uptake of the fluorescently labelled sd-siRNA, transfection medium in treated cells were replaced with keratinocyte specific culture medium without antibiotics 24 h post transfection following two washing steps with keratinocyte specific culture medium without antibiotics. Cells were treated in triplicate wells in 48-well plates for fluorescent microscopy and flow cytometry. Cells were imaged using the Leica DM IRB epifluorescence microscope and then dissociated from the culture vessel at 6 h, 24 h and 48 h post-transfection for flow cytometry analysis to determine cell uptake as described in section 3.2.7.1.2. Cells were also treated in 12-well plate on glass coverslips for confocal microscopy at 6 h, 24 h and 48 h.

4.2.6 Characterisation of siRNA coating onto microneedle devices

Microneedle devices characterised in section 2.2.5 were used for studies with siRNA to determine the siRNA coating and deposition capabilities.

4.2.6.1 siRNA coating quantification

The ability to coat siRNA onto microneedles was determined using the coating, recovery and quantification method described in section 2.2.5.2 (Chong et al. 2013). To determine the efficiency and reproducibility of the coating method in coating siRNA, 3 μL of unmodified siRNA (Dharmacon Products, Thermo Fisher Scientific, Lafayette, CO, USA) (70 mg mL− 1 in PBS) was loaded into a 20 μL pipette tip as a reservoir for coating. Microneedles (set of 6 devices 5 × 700 μm Regular, Cardiff University) were coated with siRNA and were allowed to dry at 4 °C for either 1 or 20 h (3 devices for each drying time) to provide a theoretical maximum loading of 35 μg siRNA coated onto each microneedle device. The method was repeated with another 6 devices with 10 microneedles per array (10 × 700 μm Regular, Cardiff University). To determine the actual loading dose, siRNA was recovered from the microneedle devices by washing in 150 μL PBS, V for 5 min. Nucleic acid concentration, C was then quantified using the NanoDrop spectrophotometer (section 3.2.1.5) and the amount of siRNA, m recovered was then calculated using the formula below:

$$m = C \times V$$

4.2.6.2 Coated siRNA lipoplex functional stability

The functionality of non-sd-siRNA lipoplex coated onto microneedles was determined according to the schematic protocol depicted in Figure 4.2. Microneedles were coated with siRNA using the dip-coating and recovery method described in section 2.2.5.2 (Chong et al. 2013). Naked lamin A/C non-sd-siRNA coating formulation (48 pmol in 8 μL PBS) or lamin A/C non-sd-siRNA lipoplex coating formulation (48 pmol in 8 μL Lipofectamine™ RNAiMAX) was coated onto steel microneedle devices (set of 4 devices per treatment group; 5 × 700 μm Regular, Cardiff University) to provide a theoretical maximum loading dose of 12 pmol siRNA on each microneedle device. The coated microneedles were allowed to dry at 4 °C for 1 h before the naked non-sd-siRNA and lipoplexes were recovered by washing the microneedles in 50 μL PBS for 5 min.

The recovered naked non-sd-siRNA and lipoplex solutions were prepared using method as described in section 4.2.2.1 and then used to treat cells in 12-well plate format using the method as described in section 4.2.2.2.

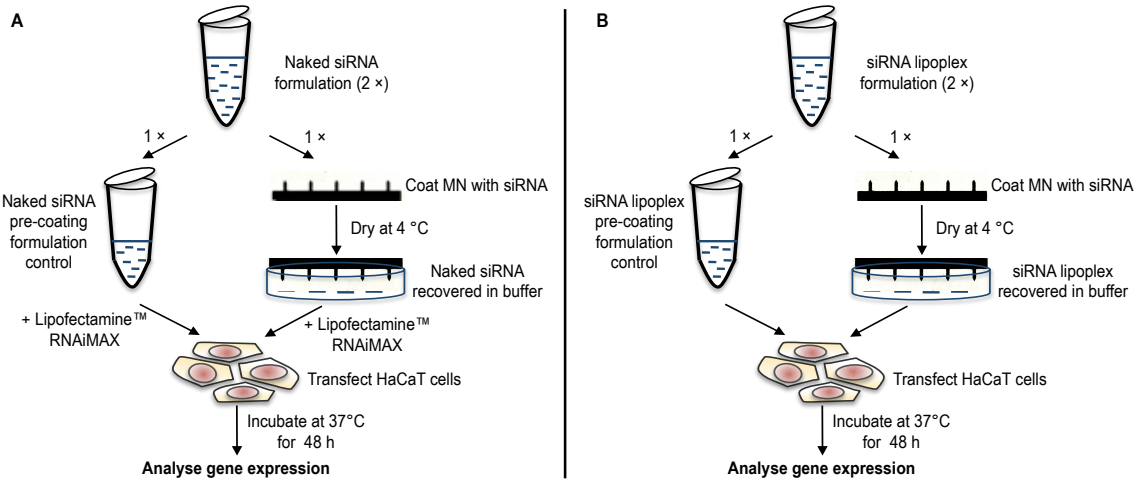

Figure 4.2: Schematic representation of protocol for testing coated naked siRNA (A) and siRNA lipoplex (B) functional stability. (MN = microneedle)

Cell populations were treated as described in table 4.2. The volume of Lipofectamine™ RNAiMAX transfection reagent in treatment groups with lipoplex was 2 µL. The final concentration of siRNA across all treatment groups with siRNA was 10 nM (12 pmol in 1200 µL transfection volume). Cells were treated in quadruplicate wells with triplicate samples for mRNA quantification by RT- qPCR and the remaining treatment sample for protein analysis by Western blotting. Treated cells were incubated at 37 °C in a humidified atmosphere containing 5% CO_2.

Table 4.2: Treatment to determine coated siRNA lipoplex functional stability

No	Description	Short form
1	GFP non-sd-siRNA 10 nM lipoplex	non-targeting control
2	naked lamin A/C non-sd-siRNA 10 nM	non-lipoplex control
3	lamin A/C non-sd-siRNA 10 nM lipoplex	positive control
4	naked lamin A/C non-sd-siRNA pre-coating formulation diluted to 10 nM formed into lipoplex	naked siRNA pre-coat + lipo
5	naked lamin A/C non-sd-siRNA recovered from microneedles and subsequently formed into lipoplex	naked siRNA recovered + lipo
6	lamin A/C non-sd-siRNA lipoplex pre- coating formulation diluted to 10 nM	siRNA lipoplex pre-coat
7	lamin A/C non-sd-siRNA lipoplex formulation recovered from microneedles	siRNA lipoplex recovered
8	Opti-MEM® solution	untreated

4.2.6.3 Coated self-delivery siRNA functional and storage stability

The functionality and stability of Accell sd-siRNA coated onto microneedles was determined by coating the microneedles using the coating and recovery method described in section 2.2.5.2 (Chong et al. 2013). A theoretical maximum loading of 1.5 nmol Accell CD44 sd-siRNA was coated onto each steel microneedle devices (5 × 700 μm Regular, Cardiff University). The coated microneedles were allowed to dry at 4°C for 10 h before the siRNA was recovered by washing the microneedles in 60 μL PBS for 5 min. The recovered siRNA solutions (20 μL of recovered siRNA solution containing approximately 500 pmol siRNA) were prepared using method as described in section 4.2.3.1 and were used to treat cells using the method as described in section 4.2.3.2.

Cell populations were treated as described in table 4.3 by replacing the seeding medium with the delivery mixture containing siRNA. Treated cells were incubated at 37°C in a humidified atmosphere containing 5% CO_2. After 24 h, the transfection medium was replaced with growth medium without antibiotics and the cells were incubated for a further 24 h. Cells were treated in triplicate wells for mRNA quantification by RT-qPCR.

The same method was used to treat cell populations with Accell CD44 sd-siRNA recovered from microneedles (5 × 700 μm, Georgia Institute of Technology, USA) after 1, 4, 7, 14 and 28 days drying time. HaCaT cells were treated with 1 μM recovered Accell CD44 sd-siRNA and the respective positive and negative controls.

Table 4.3: Treatment to determine coated sd-siRNA functional stability

No	Description	Short form
1	Accell control sd-siRNA 1 μM	Accell non-targeting control
2	siSTABLE CD44 non-sd-siRNA 1 μM	non-Accell CD44 control
3	Accell CD44 sd-siRNA 1 μM	Accell CD44 positive control
4	Accell CD44 sd-siRNA recovered from microneedles 1 μM	Accell CD44 coated

4.2.7 Analysis of gene expression

siRNA mediated gene silencing in the cells was analysed by quantifying target mRNA levels using reverse transcription quantitative polymerase chain reaction (RT-qPCR) and comparing target protein levels through the Western blotting technique.

4.2.7.1 Quantification of mRNA levels

RT-qPCR or competitive reverse transcription polymerase chain reaction (RT-PCR) was performed to quantify mRNA levels in treated cells.

4.2.7.1.1 RNA isolation from monolayer cells

Total RNA was isolated using the Ambion® PureLink™ RNA Mini Kit (Life Technologies, UK) with a protocol supplied with the kit. Briefly, culture medium was removed from the transfected adherent keratinocyte cells and washed twice with PBS. Lysis Buffer with 1% (v/v) 2-mercaptoethanol was added to lyse the cells. The lysed sample was transferred to a microcentrifuge tube and homogenised by passing 10 times through 21-gauge needle attached to a 1 mL syringe. One volume of 70% ethanol was added to each volume of cell homogenate and mixed thoroughly to disperse any visible precipitate that may form after adding ethanol. The sample was transferred to the "Spin Cartridge" with collection tube and centrifuged (Thermo Fisher Scientific, UK) at 12000 × *g* for 15 s to bind RNA to the cartridge membrane. The flow-through was discarded. The sample bound to the spin cartridge membrane was washed 3 times by centrifuging at 12000 × *g* for 15 s with wash buffers to remove impurities such a protein and DNA. The flow-through was discarded. The spin cartridge was then inserted into a recovery tube. A volume of between 30 μL to 100 μL RNase-free water was added to the centre of the spin cartridge and incubated at room temperature for 1 min. The spin cartridge was centrifuged for 2 min at 12 000 × *g* for 2 min to elute the RNA from the membrane into the recovery tube. The purified total RNA was stored at -80°C and quantified using the NanoVue spectrophotometer (section 3.2.1.5).

4.2.7.1.2 Taqman® gene expression assays

Target gene inhibition was measured using Taqman® gene expression assays specific for lamin A/C (Hs00153462_m1) or CD44 (Hs00153304_m1) and the endogenous

control GAPDH (Hs02758991_g1). All the gene expression assays span exon-exon junctions and were synthesised by Life Technologies, UK.

4.2.7.1.3 Reverse transcription

The reverse transcription (RT) step was performed to convert total RNA (0.5 to 1 μg) into first-strand cDNA using random primers with the High Capacity cDNA Reverse Transcription System (Applied Biosystems, Life Technologies, UK) using the protocol supplied with the kit. Briefly, the reverse transcription reaction master mix was prepared by combining the components as outlined in Table 4.4 in a sterile, nuclease-free microcentrifuge tube on ice and mixed gently.

Table 4.4: Formulation for reverse transcription reaction mixture (per final RT reaction volume of 20 μL)

Components	Final Volume (μL)
10× reverse transcription buffer	2.0
25× dNTP mix (100 mM)	0.8
10× random primers	2.0
MultiScribe™ Reverse Transcriptase	1.0
RNase Inhibitor	1.0
Nuclease-free Water	3.2
Total volume per reaction	**10.0**

Subsequently, a 10 μL aliquot of the reverse transcription reaction mix was added to 10 μL total RNA sample diluted to 0.1 or 0.05 μg μL^{-1} on ice for a final RT reaction volume of 20 μL per tube in 0.2 mL PCR reaction tubes. The tubes were then capped, briefly centrifuged and placed in the thermal cycler heat block and annealed by incubation at 25°C for 10 min before being extended by incubation at 37°C for 120 min. The reverse transcriptase enzyme was thermally inactivated by incubation at 85°C for 5 min. The cDNA tubes were then stored at -20 °C until further use.

4.2.7.1.4 Quantitative PCR

The quantitative PCR (qPCR) step was performed to quantitatively amplify specific regions of target genes with TaqMan® Gene Expression Assay using the ABI 7900HT

Fast Real-Time PCR system and the TaqMan® Fast Advanced Master Mix (Applied Biosystems, Life Technologies, UK) using an optimized protocol supplied with the kit. Briefly, the qPCR reaction master mix was prepared by combining the components as outlined in Table 4.5 in a sterile, nuclease-free microcentrifuge tube on ice and mixed gently.

Table 4.5: Formulation for qPCR reaction mixture (per qPCR reaction volume of 20 μL)

Components	Final Volume (μL)
2× Taqman® Fast Advanced Master Mix	10.0
20× TaqMan® Gene Expression Assay	1.0
Nuclease-free Water	7.0
Total volume per reaction	**18.0**

An 18 μL aliquot of the qPCR reaction mix was added to each well of a 96-well optical qPCR reaction plate. Then, 2 μL cDNA template or water was added to each well. The reaction plate was covered with an optical adhesive film and centrifuged briefly to spin down the contents and eliminate air bubbles. The qPCR reaction amplification was performed using the cycling program as outlined in Table 4.6 in the ABI 7900HT Fast Real-Time PCR System with the Sequence Detection System (SDS) v2.3 software (Applied Biosystems, Life Technologies, UK). After the amplification, the results were analysed using the RQ Manager software (Applied Biosystems, Life Technologies, UK). All data points reported are the mean and standard error of three separate treatments each with three replicate qPCR assays.

Table 4.6: ABI 7900HT Fast Real-Time PCR System thermal-cycling profile

Parameter	**UNG incubation**	**Polymerase activation**	**PCR (40 cycles)**	
	Hold	**Hold**	**Denature**	**Anneal/ extend**
Temperature (°C)	50	95	95	60
Time (mm:ss)	02:00	00:20	00:01	00:20

4.2.7.2 Quantification of protein levels

Western blotting was performed to semi-quantify protein levels in transfected cells using the Bio-rad Mini Protean 3 system (Bio-rad, UK).

4.2.7.2.1 Protein extraction from monolayer cells

Proteins were extracted from the treated cells by lysing the cells in lysis buffer. Lysis buffer was prepared according to the formulation outlined in Table 4.7 and cooled to 4°C. Lysis Buffer Plus was prepared by dissolving one Roche Complete Mini Protease Inhibitor Cocktail tablet (Roche, UK) in 10 mL lysis buffer. The protein extraction procedure was performed on ice. Cells were washed 3 times with chilled PBS. After the final wash, 300 μL of ice cold Lysis Buffer Plus was added into each well of different samples, respectively. The plate on ice was placed on the Stuart® Gyro-rocker (Bibby Scientific, UK) rotating at 35 rpm for 5 min. The samples were then transferred into a clean microcentrifuge tube and centrifuged at 13000 × *g* for 10 min at 4°C. The samples were stored at 4°C for use on the same day or frozen at -20°C for long-term storage.

Table 4.7: Formulation of Lysis Buffer pH 8.0 (50 mL)

Components	Final Concentration	Amount
Tris Base [tris(hydroxymethyl)aminomethane]	50 mM	0.30 g
NaCl	150 mM	0.43 g
Deionised water	-	45 mL
HCl, 3.2 M (added dropwise)	to pH 8.0	variable
Triton X-100	1%	0.50 g
Deionised water	-	to 50 mL

4.2.7.2.2 BCA protein assay

The BCA protein assay was performed to quantify the concentration of protein in extracts. The protein assay solution was prepared with 49 parts of bicinchoninic acid (BCA) and 1 part of copper sulphate solution. A 96-well plate was used to generate a concentration gradient of known quantity of 1 μg μL^{-1} bovine serum albumin (BSA) in PBS stock solution from 2 μg to 20 μg diluted in lysis buffer to a total of 20 μL in duplicate wells to obtain an average. In separate wells, a known volume from 5 to 20 μL of each protein sample extracts were added and diluted with lysis buffer to a total

volume of 20 μL in duplicates. To each well containing BSA standards and protein samples, 200 μL of the BCA protein assay solution was added. The samples were incubated at 37°C for 30 min. The samples were then allowed to cool to room temperature before an absorbance reading at 562 nm was obtained using the Titerback Sunrise™ plate reader. A calibration curve with BSA standards was generated and the linear equation was used to calculate the concentrations of the samples from the absorbance values.

4.2.7.2.3 SDS-PAGE

Sodium dodecyl sulphate polyacrylamide gel electrophoresis (SDS-PAGE) was performed to separate the protein samples according to size or molecular weight. Protein samples were prepared by diluting between 10 μg and 30 μg of protein in lysis buffer to 30 μL volume. Then, 10 μL of 4 × Laemmli protein sample buffer (Bio-rad, UK) containing 10% v/v β-mercaptoethanol (Sigma Aldrich) was added to each sample. The samples were heated in a heat block at 96°C for 5 min to denature and linearise the protein chains. The amount of protein in each sample loaded on the same gel was kept constant to allow semi-quantitative comparisons.

Mini-PROTEAN TGX Precast Gels, 10% resolving gel, 12 well (Biorad, UK) were placed in the running chamber filled with running buffer (formulation as outlined in Table 4.8). The first well on the gel was loaded with the protein molecular weight marker and the protein samples were loaded into the remaining wells, respectively. Proteins of various sizes or molecular weight in the samples were electrophoretically separated through application of electric current at 110 V for 70 min.

Table 4.8: Formulation of Running Buffer (1000 mL)

Components	Amount
Glycine	14.4 g
Tris Base	3.03 g
SDS	1 g
Deionised water	to 1000 mL

4.2.7.2.4 Protein transfer

After the electrophoresis, separated proteins were transferred from the gel to a Whatman® nitrocellulose membrane (GE Healthcare, UK). The transfer buffer with formulation as outlined in Table 4.9 was prepared fresh and chilled to 4°C before use. The gel was retrieved and washed with chilled transfer buffer. The gel was then placed in the transfer cassette, in between pre-soaked filter pads and filter papers (Sigma Aldrich, UK), next to a nitrocellulose membrane in the following order: black side of transfer cassette, filter pad, filter paper, gel, nitrocellulose membrane, filter paper, filter pad and the transparent side of the transfer cassette. The transfer cassette was assembled into the transfer chamber filled with chilled transfer buffer with an ice-cooling unit sitting in an ice-water bath. The set-up was subjected to electric current at 100 V for 100 min.

Table 4.9: Formulation of Transfer Buffer (2000 mL)

Components	Amount
Glycine	28.8 g
Tris Base	6.06 g
Methanol	400 mL
Deionised water	to 2000 mL

Alternatively, protein transfer from the gel to nitrocellulose membrane was performed using the Trans-Blot® Turbo Transfer System™ (Bio-Rad, UK) with the Trans-Blot Turbo Transfer Pack (Bio-Rad, UK). The membrane containing protein was then washed with deionised water and dehydrated at 4 °C until use.

4.2.7.2.5 Ferrozine staining

The efficiency of protein transfer was visualised by staining the nitrocellulose membranes with ferrozine. Firstly, the membrane was rehydrated with deionised water. The rehydrated membranes were then incubated in 2% v/v glacial acetic acid (Sigma Aldrich, UK) in deionised water at room temperature for 15 min. The nitrocellulose membrane was then blocked with 0.1% w/v polyvinylpyrrolidone (Sigma Aldrich, UK) in 2% v/v glacial acetic acid in deionised water. The blocked membrane was rinsed in 2% v/v glacial acetic acid in deionised water for 5 min. Ferrozine stain containing 0.75 mM ferrozine, 30 mM iron (III) chloride, 5 mM thioglycolic acid in 2% v/v glacial

acetic acid was then added to the membrane for 5 to 15 min. The stained membrane was then rinsed with 2% v/v glacial acetic acid in deionised water with 30 s agitation on a rocker. The rinsing step was repeated 5 times. The stained membrane was then imaged using the Bio-rad ChemiDoc™ XRS+ gel imaging system. The membrane was then cut into two, between the targeted protein expected band size and loading protein control. Stain was removed from the membrane using the elution solution containing 100 mM HEPES, 20 mM EDTA at pH 7.0 for 15 min.

4.2.7.2.6 Antibody blotting

The membranes were blocked and blotted with antibodies against the targeted protein and loading control. The nitrocellulose membranes were rinsed for 5 min with tris(hydroxymethyl)aminomethane (Tris) base buffer pH 7.5 (formulation as outlined in Table 4.10). Blocking buffer 5% (w/v) was prepared by adding 2.5 g Marvel milk powder (Premier Foods, UK) to 50 mL tris base buffer pH 7.5. The membranes were blocked in 25 mL blocking buffer with constant rocking at 35 rpm for 1 h at room temperature.

Table 4.10: Formulation of tris base buffer pH 7.5 (1000 mL)

Components	Amount
Tris Base	1.2 g
Deionised water	950 mL
HCl, 3.2 M (added dropwise to pH 7.5)	variable
NaCl	5.84 g
Tween 20 (Sigma Aldrich, UK)	1 mL
Deionised water	to 1000 mL

Primary mouse-anti-human and rabbit-anti-human antibodies were diluted in blocking buffer according to optimised concentration for Western blotting (Table 4.11). The nitrocellulose membranes were then incubated in respective diluted primary antibodies with constant rocking at 35 rpm for 1 hour at room temperature. Occasionally, the blocking step or the primary antibody step was performed by incubating the membranes at 4°C for 16 h.

Table 4.11: List of primary antibodies and dilution used for Western blotting

Target protein	Antibody species	Dilution	Product code	Manufacturer
α-tubulin (loading control)	Mouse-anti-human	1:3000	T9026	Sigma Aldrich, UK
Lamin A/C	Mouse-anti-human	1:500	ab8984	Abcam, UK
CD44	Rabbit-anti-human	1:1200	ab41478	Abcam, UK

After incubation with primary antibodies, the membranes were rinsed 3 times with tris base buffer pH 7.5 for at least 5 min each time with rocking at 35 rpm. Secondary HRP conjugated antibodies was diluted in blocking buffer according to optimised concentration for Western blotting (Table 4.12). The washed membranes were incubated in the diluted secondary antibody with constant rocking at 35 rpm for 1 h at room temperature. After secondary antibody incubation, the membranes were rinsed 3 times with tris base buffer pH 7.5 for at least 5 min each time with rocking at 35 rpm.

Table 4.12: List of secondary antibodies and dilution used for Western blotting

Antibody species	Dilution	Product code	Manufacturer
Goat-anti-mouse	1:5000	32430	Pierce, Thermo Fisher Scientific, UK
Goat-anti-rabbit	1:10000	7074s	Cell signalling, New England Biolabs, UK

4.2.7.2.7 Blot detection

The chemiluminescent solutions, Super Signal WestDura Stable and Lumino Enhancer solutions (Thermo Fisher Scientific) were mixed at a ratio of 1:1 in a clean microcentrifuge tube. The solutions were added to the nitrocellulose membranes for 60 s. Excess solutions were removed and the membranes were transferred into hypercassettes (GE Healthcare, UK) and transported to the dark room, where the film developer was located. In the dark room with the light switched off, Amersham Hyperfilm ECL (GE Healthcare, UK) were placed against the membranes in the hypercassettes for an appropriate amount of exposure time from 2 s to 30 min before being developed in an x-ray film developer machine. The exposure times were increased or decreased to achieve desired protein band intensity.

4.2.8 Detection of *in vitro* fluorescent siRNA uptake

4.2.8.1 Fluorescent microscopy

Fluorescent microscopy was performed to detect *in vitro* fluorescent siRNA uptake in both HaCaT cells and primary keratinocytes using Leica DM IRB epifluorescence microscope with the Openlab imaging software. The uptake of Alexa-647 and DY-547 labelled siRNA was examined under the green laser light, which excited the fluorophores at their peak excitation wavelengths of 650 nm and 557 nm, respectively.

4.2.8.2 Flow cytometry

The efficiency of siRNA uptake in cells was determined by flow cytometry using the FACSCanto II machine (BD Biosciences, UK). Cells were prepared for flow cytometry using the method described in section 3.2.7.1.2 with slight modifications. Primary keratinocyte cells were removed from the culture vessels using TrypLE™ Express instead of trypsin-EDTA. Pelleted cells were resuspended in 100 μL flow cytometry buffer containing 1% bovine serum albumin (Sigma Aldrich, UK) and 0.1% sodium azide (Sigma Aldrich, UK) in PBS and transferred into flow cytometry tubes. The cells were then fixed with 200 μL fixing buffer containing 1% paraformaldehyde and 0.1% sodium azide in PBS and analysed by flow cytometry within a week.

The flow cytometric analysis was performed as recommended by the instrument manual. The frequency of fluorescent cells in the APC or PE channel (corresponding to red fluorescence of Alexa-647 and DY-547), out of a total of at least 10^5 events analysed per sample was recorded. The data collected was analysed with the FlowJo Flow Cytometry Analysis Software for Mac Version 8.8 using method as described in section 3.2.7.1.2.

4.2.8.3 Confocal microscopy

Fluorescent siRNA uptake in treated cells was imaged using the confocal microscopy. Treated cells were prepared using methods described in section 2.2.4.6 with slight modifications. Cells were fixed with paraformaldehyde but were not permeabilised with Triton-X. Also, cells were not stained with antibodies but were counterstained with Hoechst 33342 at 5 μg mL^{-1} in PBS for 30 min at room temperature. Stained cells were

then imaged using the Leica DMI6000B confocal microscope system and analysed using the method described in section 2.2.4.6.

4.2.9 Cell viability assay

Cell transfections as described in section 4.2.2, 4.2.3 and 4.2.6.3 were scaled-down and performed in 96-well plates. MTS cell viability assay was performed using the method described in section 3.2.8.

4.2.10 Data processing and statistical analysis

Data processing and statistical analysis was performed as described in section 3.2.9.

4.3 Results and discussion

4.3.1 *In vitro* gene silencing in HaCaT cells

4.3.1.1 siRNA lipoplexes

Since the first successful introduction of siRNA into mammalian cells (Elbashir et al. 2001b), several non-viral siRNA delivery methods have been employed but the most common of these uses lipid based transfection reagent to assist cellular delivery of siRNA (Elbashir et al. 2001a; Elbashir et al. 2002; Geusens et al. 2009b; Hart 2010; Kim et al. 2009; Zhou et al. 2013). Cationic liposomal transfection formulations are commercially available and are capable of delivering nucleic acids to monolayer cell culture efficiently with minimal cell toxicity in a cost-effective manner (Hart 2010).

In an attempt to determine the optimum dose for transfection of siRNA lipoplexes in human keratinocytes, HaCaT cells were transfected with siRNA targeting the lamin A/C gene complexed with Lipofectamine™ RNAiMAX transfection reagent and protein extractions were performed 48 h post-transfection. The Western blotting technique was used to semi-quantify protein levels (Figure 4.3). The optimum dose for gene silencing in HaCaT cells based on protein levels 48 h post-transfection was determined to be 10 nM siRNA complexed with 5 μL Lipofectamine™ RNAiMAX in a 6-well plate format. Further transfections were performed with this dose of lipoplex, scaled down to the required plate format when necessary.

Dose optimisation was also performed with CD44 non-sd-siRNA lipoplex by varying the concentration of the siRNA whilst keeping the same volume of Lipofectamine™ RNAiMAX, proportionate to that used in earlier transfections with lamin A/C non-sd-siRNA lipoplex. Again, the Western blotting technique was used to semi-quantify protein levels 48 h post-transfection (Figure 4.4). CD44 protein reduction in HaCaT cells was observed with CD44 non-sd-siRNA lipoplex concentration as low as 1 nM. However, subsequent CD44 siRNA lipoplex experiments were performed with 10 nM CD44 non-sd-siRNA lipoplex concentration for consistency with the lamin A/C non-sd-siRNA dose.

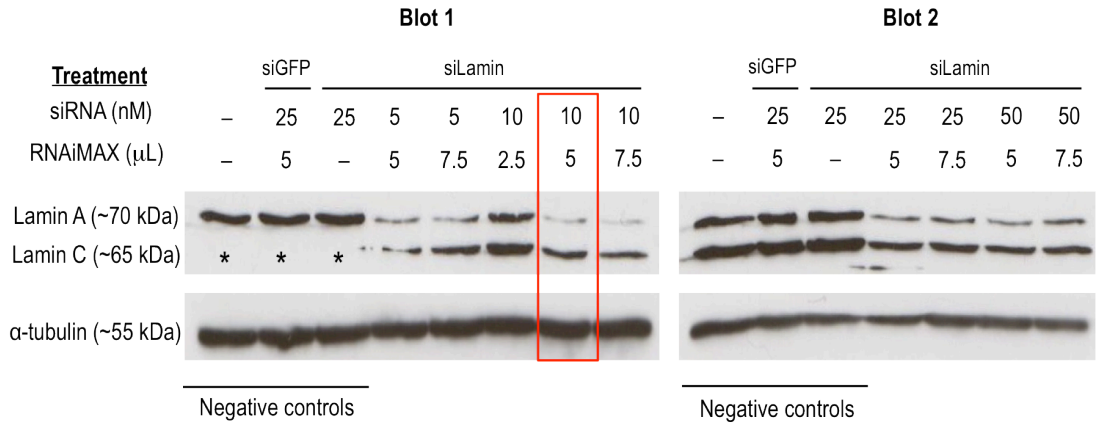

Figure 4.3: **Lamin A/C siRNA lipoplex dose optimisation.** Lamin A/C protein levels in HaCaT cells 48 h post-transfection with varying dose of non-sd-siRNA and Lipofectamine™ RNAiMAX lipoplexes. The bands were detected at approximately 70 kDa for lamin A, 65 kDa for lamin C and 55 kDa for α-tubulin. * = the lamin C band on Blot 1, lane 1, 2 and 3 was unintentionally snipped away during the process but the samples are identical to the first 3 lanes on the Blot 2 (indicated by the negative controls line) ran in a separate gel. The red open box encloses the lane with optimum siRNA lipoplex treatment dose. (siGFP = GFP non-targeting non-sd-siRNA; siLamin = lamin A/C non-sd-siRNA; RNAiMAX = Lipofectamine™ RNAiMAX; treatment volume = 3000 μL)

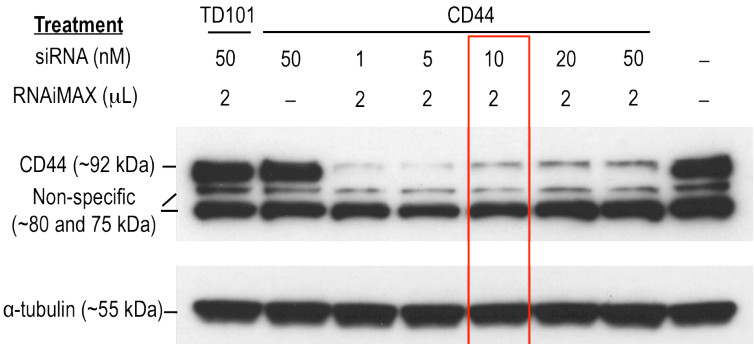

Figure 4.4: **CD44 siRNA lipoplex dose optimisation.** CD44 protein levels in HaCaT cells 48 h post-transfection with varying dose of non-sd-siRNA and Lipofectamine™ RNAiMAX lipoplexes. The bands were detected at approximately 92 kDa for CD44 and 55 kDa for α-tubulin. Non-specific bands were also detected at approximately 75 kDa and 80 kDa with the CD44 primary antibody. The red open box encloses the lane with optimum siRNA lipoplex treatment dose. (TD101 siRNA = TD101 non-targeting non-sd-siRNA; CD44 siRNA = CD44 non-sd-siRNA; RNAiMAX = Lipofectamine™ RNAiMAX; treatment volume = 1200 μL)

Several characteristic non-specific bands (Figure 4.4) were observed on the protein blot incubated with the selected CD44 primary antibody. It is unclear why these bands were detected but clear CD44 protein reductions were observed at the antibody's expected protein band size for CD44 at 92 kDa, which were visually reduced in cells treated with CD44 non-sd-siRNA lipoplexes compared to the negative controls. When mRNA is silenced by the action of siRNA, protein translation is also suppressed. Protein reduction occurs when cellular protein degrades over time depending on its half-life, which ranges from approximately 45 min to 22.5 h (Eden et al. 2011). Therefore, it is also possible that the non-specific bands are more stable forms of CD44 protein isoforms with longer half-lives and hence are still present in cells at the tested time-point.

Consistent with what has been reported in the literature, siRNA lipoplex is efficient at concentrations as low as 1 nM, which indicates that siRNA delivered through a non-viral liposomal system is a potent mediator of gene silencing (Elbashir et al. 2001a; Grunweller et al. 2003). A microarray study has suggested that delivery of siRNA at concentrations higher than 20 nM, complexed with a proprietary polymer/lipid formulation to human non-small cell lung carcinoma cells resulted in significant off target activation of immune response and non-specific gene induction (Semizarov et al. 2003). The author attributed the unwanted effects to the toxicity of siRNA in a dose-dependant manner. Therefore, it was encouraging that siRNA lipoplex used in these studies is effective at subnanomolar concentrations in human keratinocyte cells.

To determine the duration of gene silencing effect of the siRNA lipoplexes, HaCaT cells were treated with lamin A/C and CD44 non-sd-siRNA lipoplexes. Lamin A/C or CD44 mRNA levels were then detected by performing RT-qPCR analysis on mRNA extracted from the cells at 1 h, 3 h, 6 h, 24 h, 48 h and 72 h post-transfection (Figure 4.5 and 4.5). In cells treated with CD44 non-sd-siRNA, the transfection medium was replaced with growth medium 4 h post-transfection to determine whether limiting siRNA uptake to the initial 4 h affects gene silencing at later time-points (Figure 4.6).

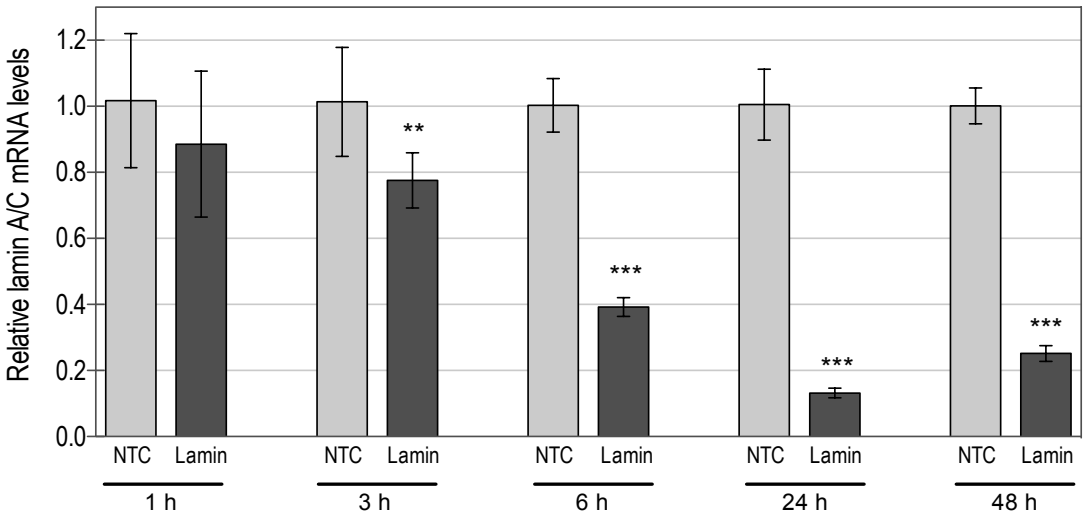

Figure 4.5: Lamin A/C mRNA levels in HaCaT cells at 1 h, 3 h, 6 h, 24 h and 48 h post-transfection with lamin A/C non-sd-siRNA lipoplex. Lamin A/C mRNA levels were relative to the non-targeting control (NTC) groups at each respective time-points and normalised to GAPDH endogenous control gene levels. (n = 3 transfection repeats, each with 3 qPCR assay replicates; error bar = standard deviation; *** = significant reduction in mRNA levels compared with non-targeting control, $p < 0.001$; ** = $p < 0.01$). (NTC = 10 nM GFP non-targeting non-sd-siRNA + Lipofectamine™ RNAiMAX; Lamin = 10 nM lamin A/C non-sd-siRNA + Lipofectamine™ RNAiMAX)

In cells treated with unmodified lamin A/C non-sd-siRNA lipoplex (Figure 4.5), a significant level of mRNA reduction (22.4%) within the first 3 h ($p < 0.01$) was observed and mRNA reduction increased with time and reached a maximum reduction of 86.8% at 24 h. mRNA reduction was significantly greater at 24 h post-transfection compared to the 6 h time-point ($p < 0.001$) but was not significantly greater than at 48 h ($p > 0.05$). An insignificant mRNA level increase at 48 h (74.8% reduction at 48 h) was observed, suggesting that unmodified non-sd-siRNA started to deteriorate past the 24 h time-point, possibly being degraded by nucleases. Cells were cultured in medium with siRNA throughout the time-points. However, nucleic acid-lipoplex formulations are usually prepared fresh before treatment, as they are known to form aggregates during storage resulting in compromised transfection efficiency. Therefore, it was hypothesised that the initial uptake of siRNA lipoplex sustained the level of mRNA silencing for up to 48 h.

To challenge the hypothesis, cells were transfected with CD44 non-sd-siRNA lipoplex where the transfection medium was replaced with growth medium in selected groups 4 h post-transfection (Figure 4.6). In contrast to the study with lamin A/C, no significant mRNA reduction was observed within the first 3 h and the first time-point with significant level of mRNA reduction was at 6 h in both the medium change (18.6% reduction) and non-medium change groups (29.0% reduction). When cells were cultured in transfection medium (non-medium change) up to the time-points, gene silencing persisted for up to 72 h (mRNA reduction of 93.5% at 72 h), the furthest time-point tested. However, when transfection medium was replaced with growth medium in cells 4 h post-transfection (medium change), mRNA reduction of up to 70.4% was observed at 24 h, which was significantly lower than the reduction of the non-medium change group at 24 h (mRNA reduction of 86.1%; $p < 0.001$). Thereafter, mRNA levels increased in the medium change group up to a reduction of 45.6% at 72 h.

It was previously thought that initial cellular siRNA lipoplex uptake causes sustained siRNA activity in cells, but this study demonstrated that siRNA lipoplex in medium may not be as unstable as reported and cellular uptake of siRNA persists for as long as siRNA lipoplexes are still present in the medium. The CD44 non-sd-siRNA used in this study is modified to increase stability against nuclease degradation, which is apparent by the sustained level of mRNA reduction of up to 72 h in the non-medium change group (Figure 4.6), compared to an observed insignificant increase in mRNA levels in cells treated with unmodified lamin A/C siRNA at 48 h under the same treatment condition (Figure 4.5). siRNA that are still complexed with transfection reagent are protected from nucleases degradation (Gershon et al. 1993; Xu et al. 1999) but siRNA lipoplex that has been internalised by cells is released from encapsulation, which renders it susceptible to degradation by intracellular nucleases. This study indicates the transient effect of siRNA lipoplex treatment and a future dosing regime would need to take into consideration the rate of drug clearance from its targeted organ and cells.

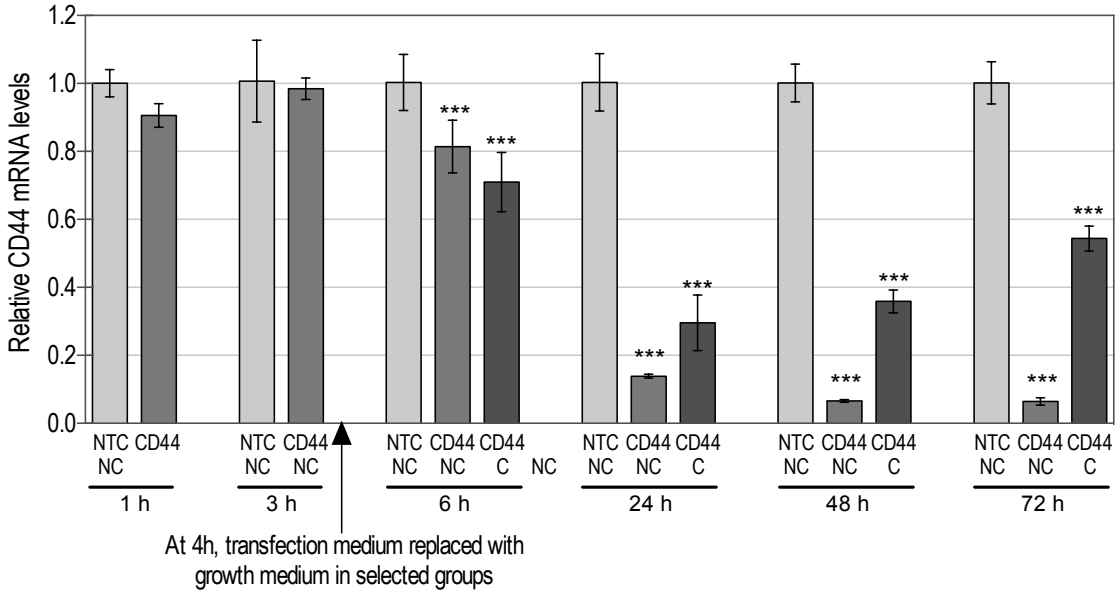

Figure 4.6: CD44 mRNA levels in HaCaT cells at 1 h, 3 h, 6 h, 24 h, 48 h and 72 h post-transfection with CD44 non-sd-siRNA lipoplex. Transfection medium was replaced with growth medium with serum 4 h post-transfection in selected treatment groups. CD44 mRNA levels were relative to the non-targeting control (NTC) groups at each respective time-point and normalised to GAPDH endogenous control gene levels. (n = 3 transfection repeats, each with 3 qPCR assay replicates; error bar = standard deviation; *** = significant reduction in mRNA levels compared with non-targeting control, $p < 0.001$). (NTC = 10 nM TD101 non-targeting non-sd-siRNA + Lipofectamine™ RNAiMAX; CD44 = 10 nM CD44 non-sd-siRNA + Lipofectamine™ RNAiMAX; NC = no change in transfection medium, C = transfection medium replaced with growth medium 4 h post-transfection)

CD44 protein levels in HaCaT cells 24 h, 48 h and 72 h post-transfection were also determined through Western blotting (Figure 4.7). CD44 protein reduction (92 kDa band) was apparent as early as the 24 h time-point. It was also obvious that protein levels in treatment groups with medium change were slightly higher than the non medium change groups at 24 h, 48 h and 72 h. Results of the protein level analysis appear to be consistent with the mRNA levels. This suggests that post-transcriptional mRNA silencing causes reduction in protein levels, which demonstrates effective gene silencing. However, mRNA reduction and subsequent protein reduction did not always have a linear relationship, as reduction in protein level is dependent on the half-life of the target protein.

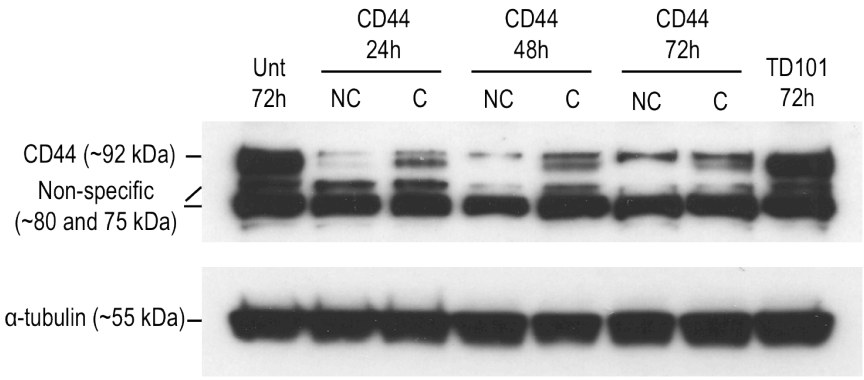

Figure 4.7: CD44 protein levels in HaCaT cells 24 h, 48 h, and 72 h post-transfection with CD44 siRNA lipoplex. Transfection medium was replaced with growth medium with serum 4 h post-transfection in selected treatment groups. The bands were detected at approximately 92 kDa for CD44 and 55 kDa for α-tubulin. Non-specific bands were also detected at approximately 75 kDa and 80 kDa with the CD44 primary antibody. (TD101 = 10 nM TD101 non-targeting non-sd-siRNA + Lipofectamine™ RNAiMAX; CD44 = 10 nM CD44 non-sd-siRNA + Lipofectamine™ RNAiMAX; NC = no change in transfection medium, C = transfection medium replaced with growth medium 4 h post-transfection)

siRNA lipoplexes were further tested for cell toxicity by performing a MTS cell toxicology assay in HaCaT cells (Figure 4.8). Results from the assay show that treatment with siRNA lipoplexes did not cause toxicity to cells as indicated by a level of cell viability similar to that of untreated cells ($p > 0.05$). This supports the use of siRNA lipoplexes as potentially effective and non-toxic transfection formulations. These results are consistent with other published studies reporting the high transfection efficiency and low toxicity associated with Lipofectamine RNAiMAX delivery to cell lines such as macrophages and human embryonic stem cells (Carralot et al. 2009; Zhao et al. 2008). However, more studies including dose-escalation toxicity studies in a few different skin cells lines like keratinocytes, melanocytes and fibroblasts with more than one type of cell viability assay like BrdU DNA synthesis assay and lactate dehydrogenase activity assay (Lappalainen et al. 1994), should be performed to ascertain the safety of siRNA lipoplexes for clinical use.

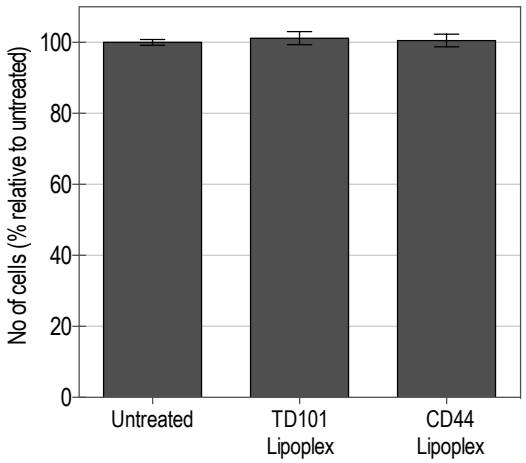

Figure 4.8: Cell viability (MTS assay) following siRNA lipoplex treatment in HaCaT cells 48 h post transfection. The percentage viability was relative to normalised untreated cells. (n = 5 transfection repeats; error bar = standard deviation; TD101 Lipoplex = 10nM TD101 non-targeting non-sd-siRNA + Lipofectamine™ RNAiMAX; CD44 Lipoplex = 10 nM CD44 non-sd-siRNA + Lipofectamine™ RNAiMAX)

4.3.1.2 Accell self-delivery siRNA

Whilst, siRNA lipoplexes were being explored as a means for delivering siRNA to human skin, the availability of Accell sd-siRNA became apparent when an siRNA delivery research group targeting the skin in Santa Cruz, USA published a paper highlighting the efficiency of the sd-siRNA delivered to transgenic reporter mouse skin (Gonzalez-Gonzalez et al. 2010b). Collaboration with the group was set up as part of the National Institutes of Health (NIH) Grand Opportunities (GO Delivery!) initiative, resulting in the availability of Accell sd-siRNA for testing in human skin models (Chapter 4 and 5) and also in the *in vivo* transgenic reporter mouse skin model (Chapter 6). The Go Delivery! grant aimed at gathering researchers with interest in skin gene delivery in a collaborative effort to jointly develop cutaneous nucleic acid delivery systems and analysis tools (Hickerson et al. 2011; Kaspar et al. 2009).

Accell sd-siRNA is modified to facilitate cellular uptake without the need for a transfection reagent. However, due to its passive cell uptake mechanism, a much higher dosage is recommended (1 μM) compared to siRNA lipoplex (10 nM). A longer duration of treatment before gene silencing detection is also suggested. The optimum dose for transfection of Accell sd-siRNA in human keratinocytes cells was determined

by treating HaCaT cells with Accell sd-siRNA targeting the CD44 gene and protein extractions were performed 72 h post-transfection for Western blotting analysis as shown in Figure 4.9.

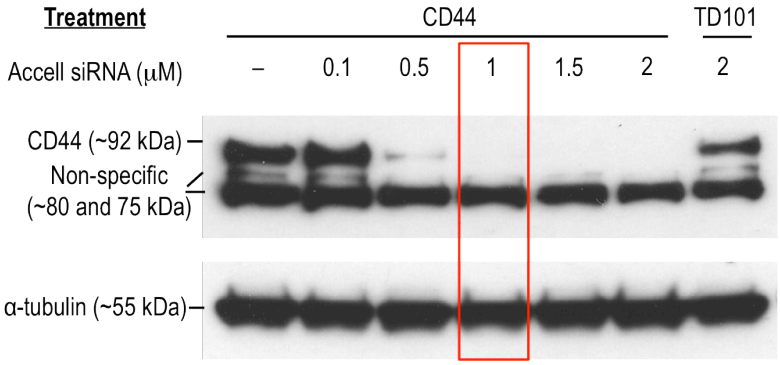

Figure 4.9: **Accell CD44 sd-siRNA dose optimisation.** CD44 protein levels in HaCaT cells 72 h post-transfection with varying dose of Accell sd-siRNA. The bands were detected at approximately 92 kDa for CD44 and 55 kDa for α-tubulin. Non-specific bands were also detected at approximately 75 kDa and 80 kDa with the CD44 primary antibody. The red open box encloses the lane with optimum Accell sd-siRNA treatment dose. (Accell TD101 siRNA = Accell TD101 non-targeting sd-siRNA; Accell CD44 siRNA = Accell CD44 sd-siRNA)

The optimum dose for gene silencing in HaCaT cells based on protein levels at 72 h post-transfection with Accell CD44 sd-siRNA was determined to be 1 μM sd-siRNA. Protein reduction was also observed with a lower dose of 0.5 μM sd-siRNA. It has been reported that siRNA lipoplex doses of more than 20 nM caused off target immune response (Semizarov et al. 2003). Microarray analysis conducted by the manufacturer of Accell sd-siRNA revealed that at 1 μM working concentration, the sd-siRNA induced minimal to no off-target effects (ThermoScientific 2011). The sd-siRNA is also claimed to be free from the toxicity and the inflammatory response associated with conventional lipid transfection reagents (Baskin et al. 2008; ThermoScientific 2011). This indicates that the off-target immune response observed with siRNA lipoplex of doses higher than 20 nM is probably due to the formulation of siRNA encapsulated in liposomes rather than the siRNA on its own. siRNA lipoplex at low doses are non-toxic to HaCaT cells, as shown by the cell viability study in section 4.3.1.1, but pDNA lipoplexes were relatively toxic to HaCaT cells (Chapter 3).

It is also recommended that Accell sd-siRNA is delivered with Accell Delivery Medium (ADM), a serum-free growth medium that has been designed specifically for optimum cellular performance of the sd-siRNA, for a minimum of 72 h. However, the growth of HaCaT cells requires serum in the growth medium. Therefore, various treatment medium conditions were tested to determine their effect on gene silencing efficiency (Figure 4.10) and cell viability (Figure 4.11). Figure 4.10 shows that mRNA reduction was higher at 72 h post-transfection when cells were kept under constant exposure to sd-siRNA. There was insignificant difference between the mRNA reduction in HaCaT cells treated in ADM with 3% serum (82.8% reduction) and serum-free ADM (83.0% reduction). When the transfection medium was replaced with growth medium with serum 24 h post-transfection, the level of mRNA reduction was significantly lower compared with the non-medium change groups (61.6% reduction). Similar to what was found with siRNA lipoplex, mRNA reduction remains higher in cells constantly exposed to siRNA in the medium.

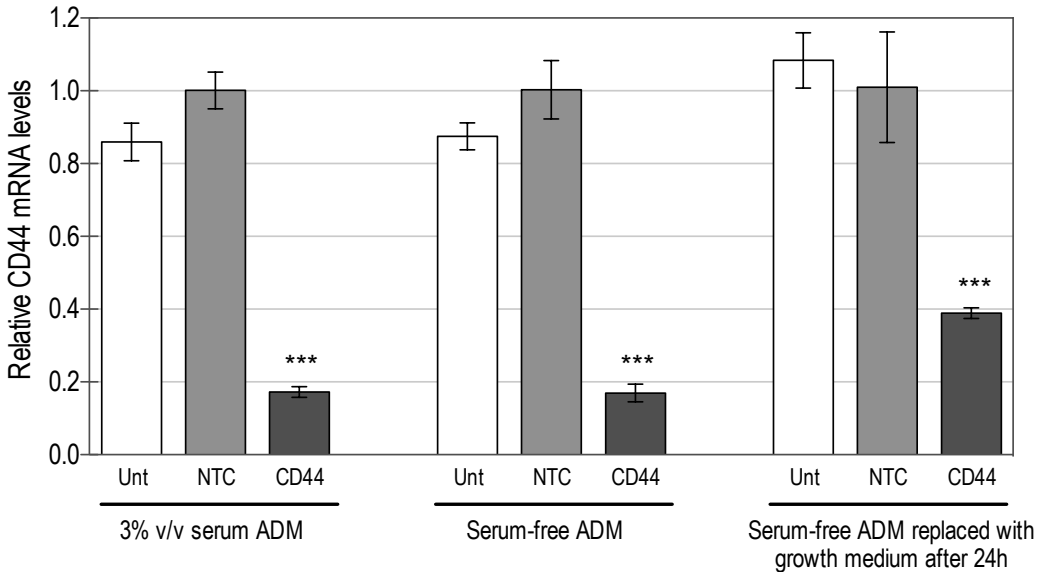

Figure 4.10: Accell sd-siRNA treatment medium condition optimisation. CD44 mRNA levels in HaCaT cells 72 h post-transfection with Accell CD44 sd-siRNA under various treatment medium conditions. CD44 mRNA levels were relative to the non-targeting control (NTC) groups at each respective time-points and normalised to GAPDH endogenous control gene levels. (n = 3 transfection repeats, each with 3 qPCR assay replicates; error bar = standard deviation; *** = significant reduction in mRNA levels compared with non-targeting control, $p < 0.001$). (NTC = 1 µM Accell TD101 non-targeting sd-siRNA; CD44 = 1 µM Accell CD44 sd-siRNA; ADM = Accell Delivery Medium)

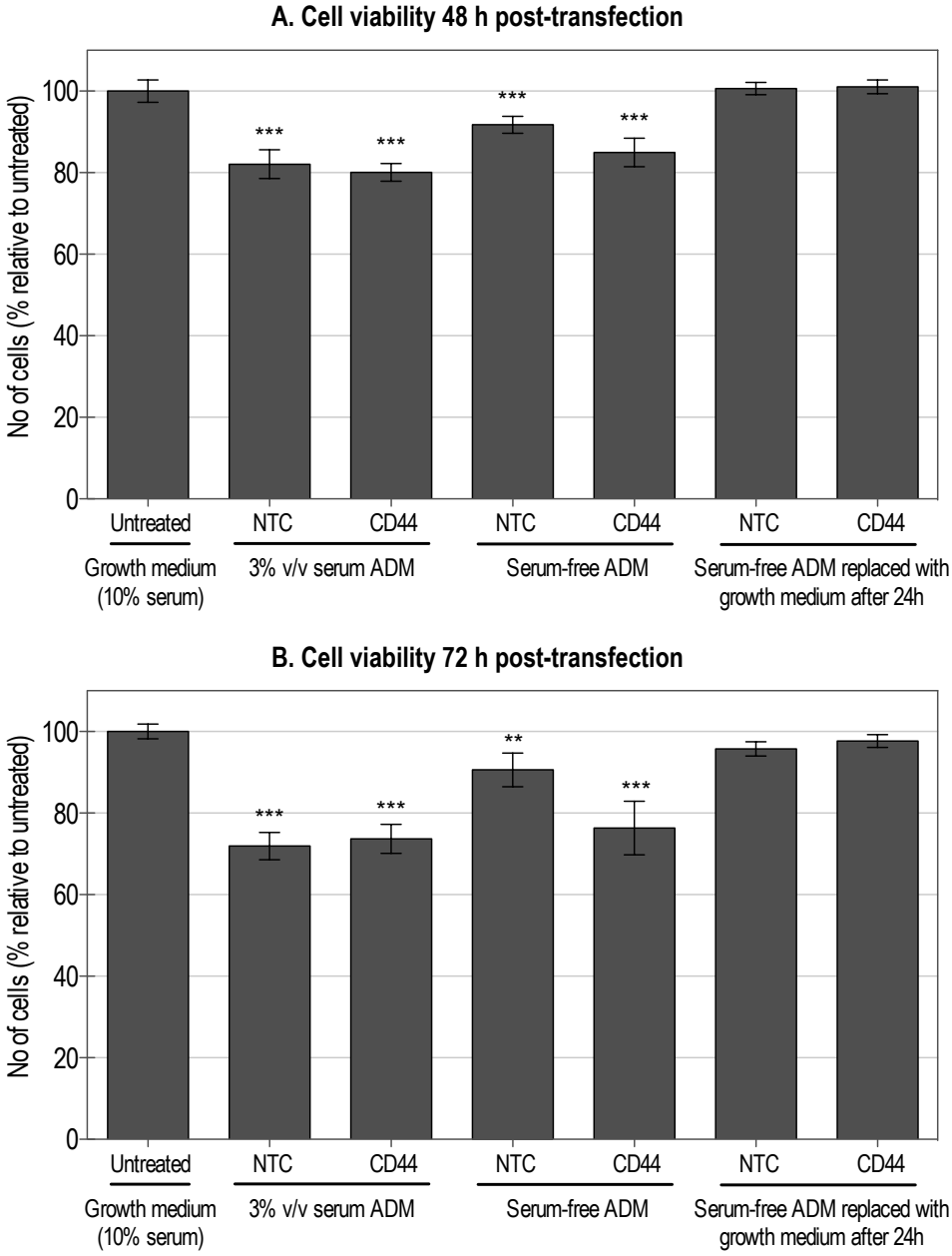

Figure 4.11: Cell viability (MTS assay) following various Accell sd-siRNA treatment medium conditions in HaCaT cells 48 h (A) and 72 h (B) post-transfection. The percentage viability was relative to normalised untreated cells. (n = 5 transfection repeats; error bar = standard deviation; *** = significant reduction in cell viability compared with untreated control, $p < 0.001$; ** = $p < 0.01$). (NTC = 1 μM Accell TD101 non-targeting sd-siRNA; CD44 = 1 μM Accell CD44 sd-siRNA; ADM = Accell Delivery Medium)

However, the cell viability studies conducted (Figure 4.11) revealed a significant reduction in cell viability of 8.3 to 20% in HaCaT cells treated with sd-siRNA in low serum (3% serum) or serum-free medium at 48 h ($p < 0.001$) and reduction of 9.4% to

28.7% at 72 h ($p < 0.01$). When observed under the microscope, the cells treated with low serum or serum free medium appeared normal but were not as confluent (more empty spaces on the culture vessels where cells have not proliferated) as untreated cells or medium change cells at their respective time points. Thus, the reduction in cell viability was probably due to slower cell growth in low serum or serum free medium rather than cell toxicity. The cell viability studies revealed the importance of serum to the healthy growth of HaCaT cells. The culture of primary keratinocytes extracted from freshly excised human breast skin does not require the presence of serum. Therefore further studies were performed on primary keratinocytes as a more representative model to human skin. These studies are described in detail in section 4.3.3.

To determine the duration of the gene silencing effect of the Accell sd-siRNA, HaCaT cells were treated with Accell CD44 sd-siRNA. CD44 mRNA levels were then detected by performing RT-qPCR analysis on mRNA extracted from the cells at 3 h, 6 h, 24 h, 48 h and 72 h post-transfection (Figure 4.12). The serum free transfection medium was replaced with growth medium with serum 24 h post-transfection in all treatment groups to promote healthy cell growth.

Accell CD44 sd-siRNA showed a significant level of mRNA reduction at 24 h (52.6% reduction) but the level of reduction is lower compared with CD44 siRNA lipoplex, where reduction was almost two-fold higher at 24 h (86.1% reduction). Nevertheless, a comparable level of CD44 mRNA reduction was achieved at 48 h with Accell sd-siRNA (78.9% reduction). As mentioned, Accell sd-siRNA enters cells passively, which explains the apparent slower rate of gene silencing. Understanding the duration of gene silencing with Accell siRNA is beneficial in informing studies with excised human skin (Chapter 5).

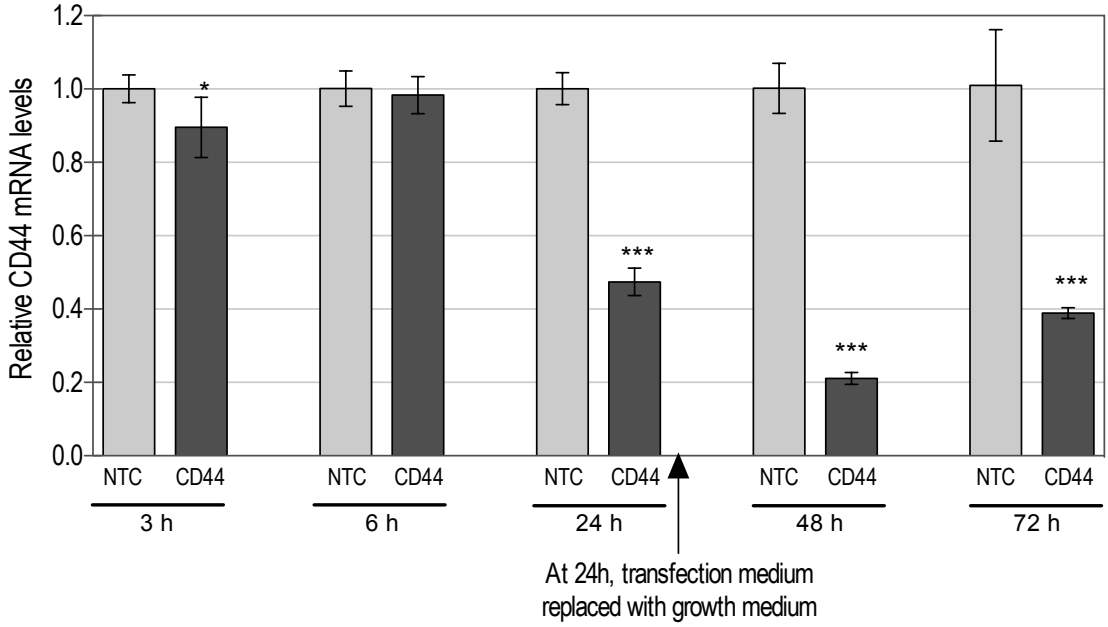

Figure 4.12: CD44 mRNA levels in HaCaT cells at 3 h, 6 h, 24 h, 48 h and 72 h post-transfection with Accell CD44 sd-siRNA. Serum free transfection medium was replaced with growth medium with serum 24 h post-transfection. CD44 mRNA levels were relative to the non-targeting control (NTC) groups at each respective time-points and normalised to GAPDH endogenous control gene levels. (n = 3 transfection repeats, each with 3 qPCR assay replicates; error bar = standard deviation; *** = significant reduction in mRNA levels compared with non-targeting control, $p < 0.001$; * = $p < 0.05$). (NTC = 1μM Accell TD101 non-targeting sd-siRNA; CD44 = 1 μM Accell CD44 sd-siRNA)

Accell sd-siRNA was again tested for toxicity under the optimised treatment conditions at 48 h post-transfection (Figure 4.13). Although delivered at a much higher dose, treatment with Accell sd-siRNA did not show any reduction in cell viability compared to untreated cells, similar to the results with siRNA lipoplex. Many studies have reported success in gene silencing following treatment of Accell sd-siRNA in *in vitro* cell culture or organotypic models (Baskin et al. 2008; Gupta et al. 2010; Hickerson et al. 2011) and *in vivo* models (Gonzalez-Gonzalez et al. 2010b; Lara et al. 2012; Nakajima et al. 2012) but none of the studies have described findings of *in vitro* cellular toxicity associated with the sd-siRNA. However, the manufacturer of the Accell sd-siRNA (Thermo Fisher Dharmacon) has stated in its product brochure (available online), the *in vitro* transfection efficiency and cell viability data in 18 cell lines, not including human keratinocyte cells (ThermoScientific 2011). The data showed

reproducible gene silencing efficiency and good cell viability. It was also stated in the brochure that Accell siRNA has been tested for efficiency in more than 70 different cell lines in peer reviewed publications including primary keratinocytes (ThermoScientific 2011).

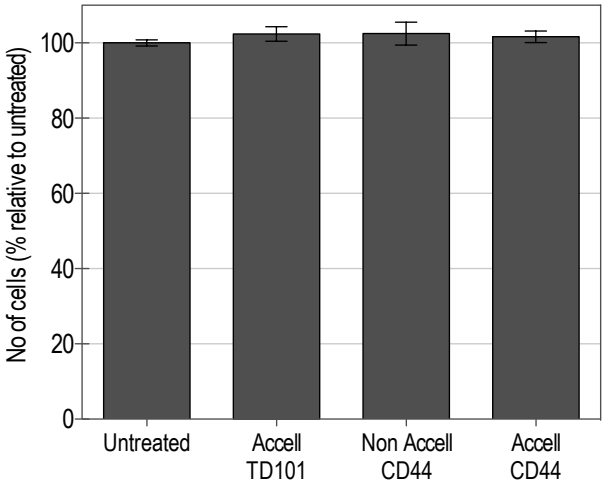

Figure 4.13: Cell viability (MTS assay) following Accell sd-siRNA treatment in HaCaT cells 48 h post-transfection. Serum free transfection medium was replaced with growth medium with serum 24 h post-transfection. The percentage viability was relative to normalised untreated cells. (n = 5 transfection repeats; error bar = standard deviation; Accell TD101 = 1 μM Accell TD101 non-targeting sd-siRNA; Non Accell CD44 = 1 μM CD44 non-sd-siRNA; Accell CD44 = 1 μM Accell CD44 sd-siRNA)

4.3.2 *In vitro* fluorescent siRNA uptake in HaCaT cells

The effect of siRNA in cells depends on efficient cellular uptake and cellular localisation of RNA to an area where RISC complex is located. siRNA uptake studies were performed to determine the ability of siRNA formulations in delivering siRNA to human keratinocyte cells.

In studies performed with 10 nM BLOCK-iT Alexa 647 fluorescently labelled non-sd-siRNA lipoplex, visualisation of treated cells under fluorescent microscope showed poor levels of fluorescent intensity. The Alexa 647 labelled siRNA used in the study emits fluorescence in the far-red spectrum and hence might not be visible by naked eye under the microscope but can be detected by the imaging system of the epifluorescent microscope. However, images capture showed poor level of fluorescence (data not

shown). Flow cytometry was also performed on treated cells at different time-points but data analysis revealed poor shifts in fluorescent signal intensity of cells treated with fluorescent siRNA lipoplex with apparent maximum siRNA uptake of 55% at 24 h post-transfection (data not shown), which is one-fold lower than the observed silencing efficiency of siRNA lipoplex shown by RT-qPCR (section 4.3.1.1).

Further investigation through visualisation of the siRNA lipoplex droplet under the fluorescent microscope revealed a decreased (tiny red fluorescent dots) fluorescence of siRNA encapsulated in the liposomal formulation (Figure 4.14). The positive control with the same concentration of naked fluorescent non-sd-siRNA showed intensely even fluorescence across the droplet. These results indicated that these methods of detecting fluorescent siRNA lipoplex uptake might not yield very meaningful results.

Figure 4.14: Fluorescent micrographs of BLOCK-iT Alexa 647 fluorescently labelled non-sd-siRNA (naked) and non-sd-siRNA lipoplex droplets. Red fluorescence was pseudocoloured red.

A similar observation has been reported in the literature with an author highlighting the quenching effects of Alexa 488 labelled siRNA formulated into lipoplex and polyplex leading to decreased mean fluorescent intensity (MFI) than that of naked siRNA (Vader et al. 2010). Flow cytometry analysis of cells transfected with different lipoplex and polyplex formulation revealed different MFI values between different formulations and cellular uptake observation by fluorescent microscopy yielded similar results (Vader et al. 2010). An alternative method where MFI was measured after cells were lysed in 1% Triton X-100 and 2% SDS in PBS to dissociates all lipoplexes and polyplexes was claimed to be a better method for quantifying siRNA uptake (Vader et al. 2010). This quenching effect has also been observed with Cy3-labelled siRNA formulated in nanoparticles (Li et al. 2008). Therefore, the uptake of siRNA lipoplex determined

using flow cytometry or fluorescent microscopy could be underestimated and should be taken into careful consideration when performing quantitative comparative studies.

Since Accell sd-siRNA enters cells in the absence of a transfection reagent, fluorescence studies with this modified sd-siRNA were more straightforward and allowed meaningful comparisons between cells treated at different time-points. HaCaT cells treated with Accell sd-siRNA were imaged using an epifluorescent microscope (Figure 4.15) at 0 h, 3 h, 6 h, 24 h, 48 h and 72 h before being processed for flow cytometry analysis (Figure 4.16). Cells were captured under the same exposure to allow meaningful comparison of fluorescent intensity at different time-points.

At the 0 h time-point, cells were treated with siRNA that was immediately removed and washed 3 times with PBS. Cells were subsequently placed on ice to minimise cellular activity, imaged and harvested for flow cytometry analysis. When visualised under the fluorescent microscope, a tinge of red fluorescence on cells treated with Accell Red sd-siRNA was observed, presumably due to the adherence of sd-siRNA to the cell membrane during the short duration of time (less than 5 s) the fluorescent siRNA was in contact with the cells. In cells treated with siGLO non-sd-siRNA at the same dose of 0.5 μM, fluorescence was not detected up to the 6 h time-point. When the cells were subjected to flow cytometry at 0 h, analysis of the data (Figure 4.16 A) showed fluorescence shift in cells treated with Accell Red sd-siRNA compared to cells treated with Accell TD101 non-fluorescent sd-siRNA control and siGLO Red non-sd-siRNA. The shift in fluorescent intensity was however significantly less than cells that have obvious cellular internalisation of Accell Red sd-siRNA at later time points (3 h, 6 h, 24 h, 48 h and 72 h). Therefore, the gate for cells with fluorescent siRNA uptake was set beyond the fluorescent shift at 0 h to consider the fluorescent shift at 0 h as siRNA adhered to the membrane but not internalised by the cells, resulting in low level of fluorescent intensity.

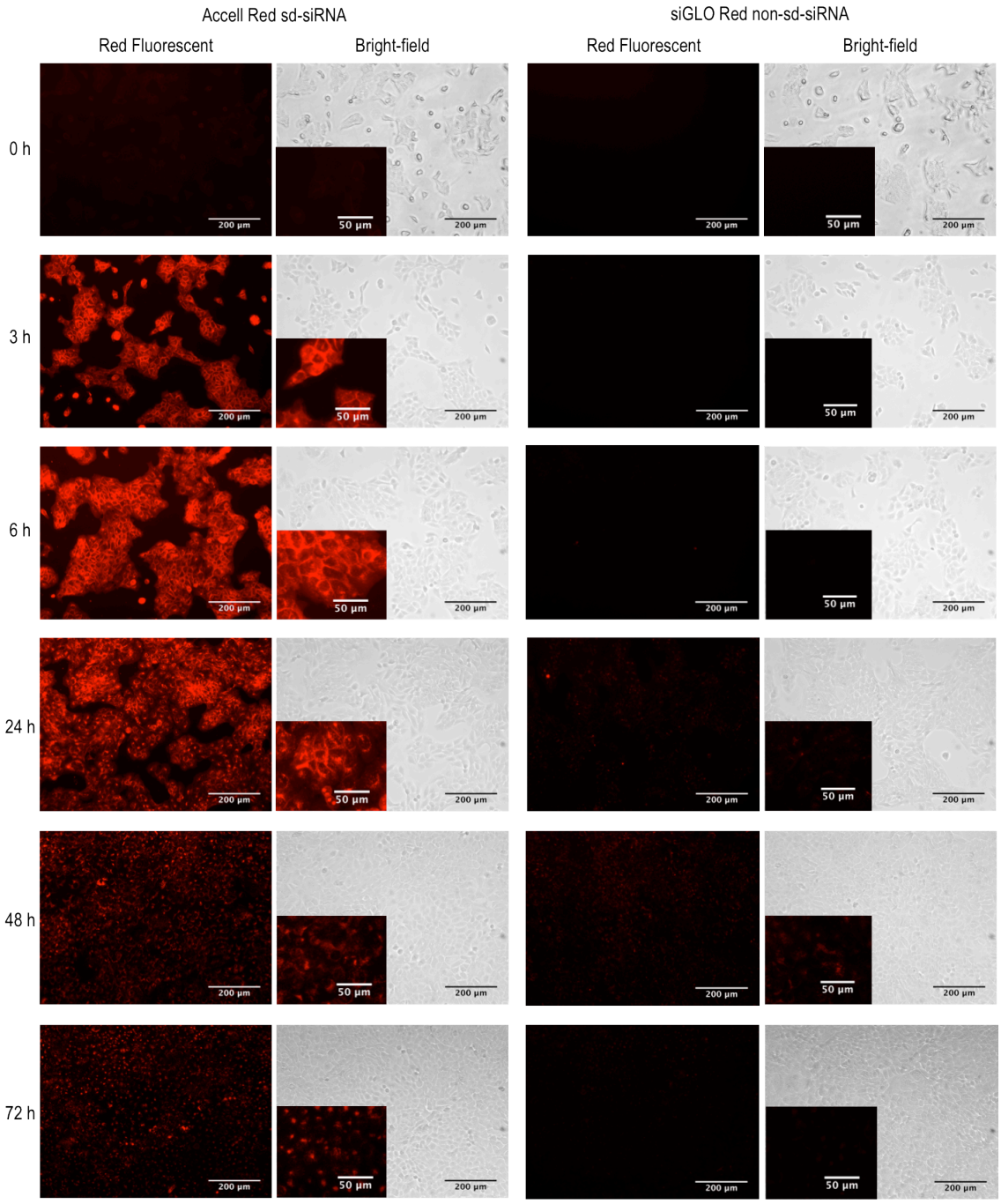

Figure 4.15: Fluorescently labelled naked Accell Red sd-siRNA and naked siGLO Red non-sd-siRNA uptake at 0 h, 3 h, 6 h, 24 h, 48 h and 72 h in HaCaT cells. Representative fluorescence and bright-field micrographs of HaCaT cells treated with 0.5 µM Accell Red sd-siRNA or 0.5 µM siGLO Red non-sd-siRNA. Serum free transfection medium was replaced with growth medium with serum 24 h post-transfection. Smaller micrographs inset of the bright-field micrographs represents enlarged fluorescent images at each respective time-point. Red fluorescence was pseudocoloured red.

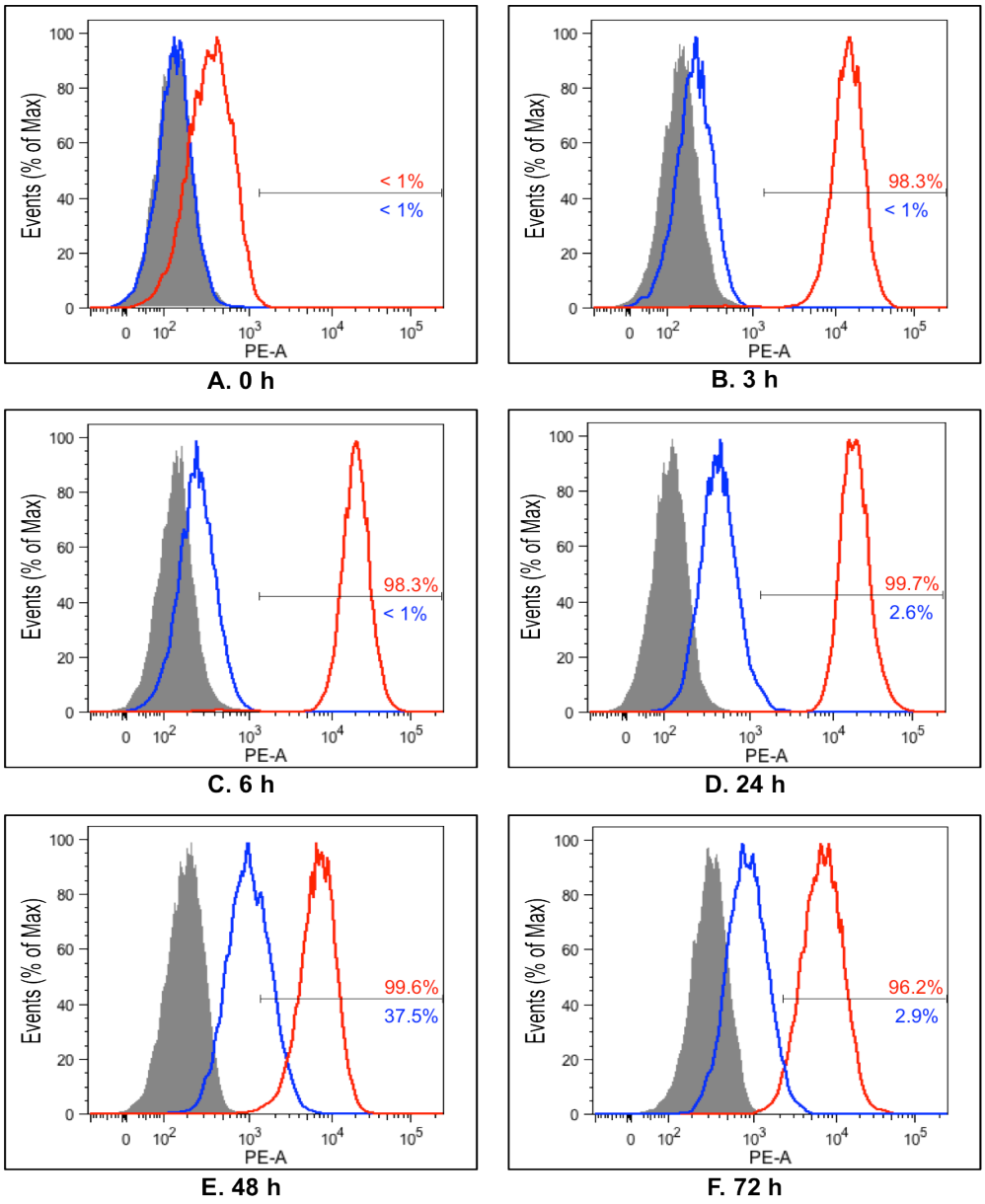

Figure 4.16: Flow cytometry histograms showing fluorescent signal intensity in HaCaT cells treated with 0.5 µM naked Accell Red sd-siRNA or naked siGLO Red non-sd-siRNA at 0 h, 3 h, 6 h, 24 h, 48 h and 72h. Serum free transfection medium was replaced with growth medium with serum 24 h post-transfection. Histograms are overlays of Accell TD101 sd-siRNA non-fluorescent control (solid grey), Accell Red sd-siRNA (red line) and siGLO Red non-sd-siRNA (blue line). Fluorescent cells were gated with reference to the shift in fluorescent signal intensity in cells treated with Accell Red sd-siRNA at 0 h (A) (considered as background fluorescence of siRNA stuck to the outermembrane of cells resulting in shift at significantly lower fluorescent intensity) to be less than 1%. The percentages of cells gated were expressed in red for Accell Red sd-siRNA and blue for siGLO Red non-sd-siRNA (average value of 3 transfection repeats).

At the 3 h time-point, flow cytometric analysis (Figure 4.16) revealed that Accell Red sd-siRNA was present in 98.3% of HaCaT cells, as demonstrated by the high level of fluorescent intensity seen in the cells on the fluorescent micrographs. Accell Red sd-siRNA continued to be present in cells in subsequent time-points, even after the serum-free transfection mediums containing siRNAs were replaced with growth medium with serum 24 h post-transfection. From the fluorescent micrographs (Figure 4.15), it was obvious that the fluorescent signal intensity of cells with Accell Red sd-siRNA reduced at 48 h and further reduced at 72 h. Flow cytometry analysis revealed that fluorescent siRNA was still present in all cells but the shifts in fluorescent signal were reduced with time after the 24 h time-point. After the 24 h time-point, cells no longer have siRNA in the medium for uptake and the siRNA that has been internalised were slowly degraded or were diluted during cell division.

Cells treated with siGLO Red non-sd-siRNA appeared to have low levels of fluorescent intensity at 24 h, peaking at 48 h and then diluted at 72 h (Figure 4.15 and 4.16). It is unclear how the cellular uptake of non-sd-siRNA occurred without a liposomal carrier but subsequent gene silencing studies with a control group of 1 μM CD44 non-sd-siRNA (Non-accell control) showed that in the absence of a transfection reagent, non-sd-siRNA at the same dose of Accell sd-siRNA do not have any gene silencing effect (section 4.3.4.3). The observed mild fluorescence in cells treated with siGLO Red siRNA could be due to fluorescence trapped between cells and the culture vessel during cell growth or due to cellular internalisation of fluorescent fragments from degraded siRNA during cell division.

The results from fluorescent sd-siRNA uptake studies support the results of the gene silencing studies, whereby the highest quantity of fluorescent siRNA was present in cells 24 h post-transfection (greatest shift in fluorescent signal intensity on the flow cytometry histogram; Figure 4.16 D) which resulted in the peak of mRNA silencing at 48 h post-transfection. The dilution of fluorescent signal intensity at the 48 h time-point indicating reduction in sd-siRNA present in cells at this point, is reflected in an increased level of mRNA at 72 h. A previously published study reported sd-siRNA delivery efficiency to T-cells of approximately 50% (Chehtane and Khaled 2010). The cellular delivery efficiency of Accell sd-siRNA is far superior in human keratinocyte

cells and knowledge of this could prove invaluable in supporting the claim for use of the modified sd-siRNA in human skin.

The fluorescent siRNA uptake studies also highlight the fact that siRNA effects in cells are transient and vulnerable to degradation and dilution as cells divide. For more sustained effect of siRNA treatment both *in vitro* and *in vivo*, a daily or every alternate day dosing regime is required for prolonged gene silencing effect. In fact, a few published studies adopt either daily or every alternate day dosing regime over a 2 to 4 weeks period for *in vivo* skin studies with Accell sd-siRNA (Gonzalez-Gonzalez et al. 2010b; Hickerson et al. 2011; Lara et al. 2012).

4.3.3 *In vitro* gene silencing and siRNA uptake in primary keratinocytes

Previously, the gene delivery and silencing efficiency of Accell sd-siRNA and non-sd-siRNA lipoplex was demonstrated in HaCaT cells. HaCaT cells are spontaneously immortalised human keratinocyte cells obtained from the distant periphery of a melanoma of a 62-year old male patient more than 25 years ago (Boukamp et al. 1988). Although many studies involving human skin models have utilised HaCaT cells as a representation of monolayer culture of human keratinocytes, the HaCaT cell lines undergoes multiple changes that correlates with transformed phenotype due to chromosomal alterations and mutations as it passages (Boukamp et al. 1997). Analysis on chromosomes of HaCaT cells in long-term culture (up to passage 225) revealed increased incidence of chromosomal translocations and deletions. However, investigation of chromosomal balance through comparative genomic hybridisation showed that most individual chromosomes remain unchanged, an indication of chromosomal balance in HaCaT cells that is stable for long-term culture (Boukamp et al. 1997).

In order to ensure that the siRNA designed is as efficient in HaCaT cells as in human epidermal keratinocyte cells that will be used in subsequent *ex vivo* skin culture studies (Chapter 5), gene silencing (Figure 4.17 and 4.18) and siRNA uptake (Figure 4.20 and 4.21) studies were performed in primary human keratinocytes extracted from freshly excised human breast skin of a 38-year old female. Experiments were performed at a smaller scale with reduced number of time-points due the limited number of primary

cells available. Transfection medium was replaced with keratinocyte specific growth medium 24 h post-transfection with siRNA lipoplex and Accell sd-siRNA to allow meaningful comparison of data.

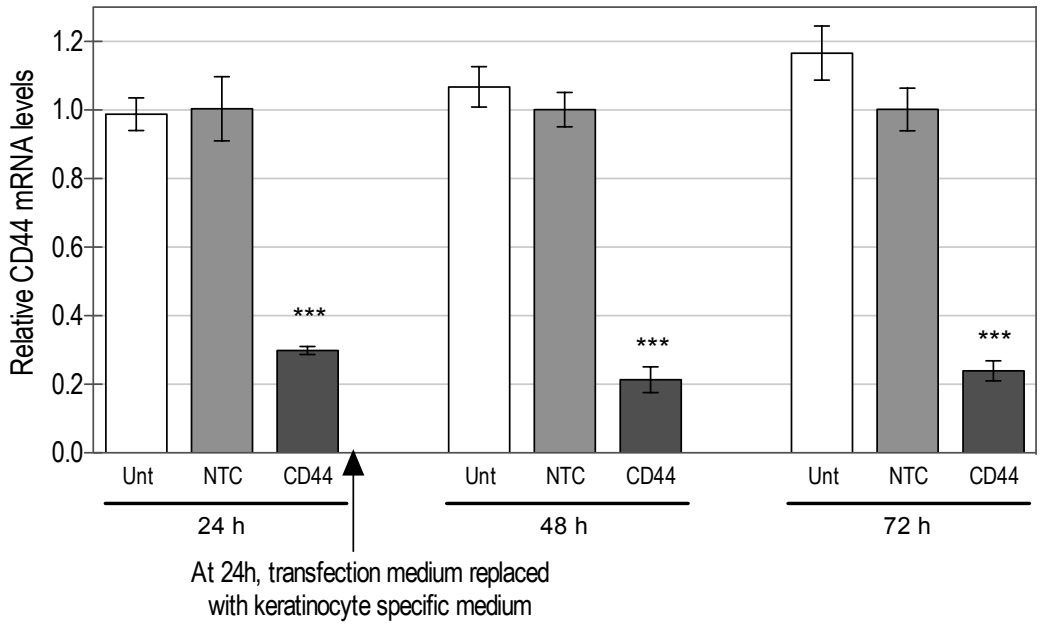

Figure 4.17: CD44 mRNA levels in primary keratinocyte cells at 24 h, 48 h and 72 h post-transfection with CD44 siRNA lipoplex. Transfection medium was replaced with keratinocyte specific growth medium 24 h post-transfection. CD44 mRNA levels were relative to the non-targeting control (NTC) groups at each respective time-points and normalised to GAPDH endogenous control gene levels. (n = 3 transfection repeats, each with 3 qPCR assay replicates; error bar = standard deviation; *** = significant reduction in mRNA levels compared with non-targeting control, $p < 0.001$). (Unt = untreated; NTC = 10nM TD101 non-targeting non-sd-siRNA + Lipofectamine™ RNAiMAX; CD44 = 10 nM CD44 non-sd-siRNA + Lipofectamine™ RNAiMAX).

The gene silencing results with both the CD44 non-sd-siRNA lipoplex (Figure 4.17) and Accell CD44 sd-siRNA (Figure 4.18) were comparable with that of HaCaT cells with some minor deviation. CD44 mRNA levels were lowest in cells treated with siRNA lipoplex at 48 h (21.37 ± 0.038%). In HaCaT cells, CD44 mRNA levels were considerably lower at 24 h, 48 h and 72h (between 6% and 14%) when the transfection medium was not changed. The transfection medium was replaced with growth medium 24 h post-transfection in primary keratinocytes but the levels of mRNA silencing

seemed to have sustained for up to 72 h with no significant level of mRNA increase between the 48 h and 72 h time-points ($p > 0.05$). The longer duration of time that primary keratinocytes had to internalise siRNA lipoplex (24 h incubation with transfection medium) could have resulted in increased level of siRNA lipoplex, which prolonged the gene silencing effect of siRNA.

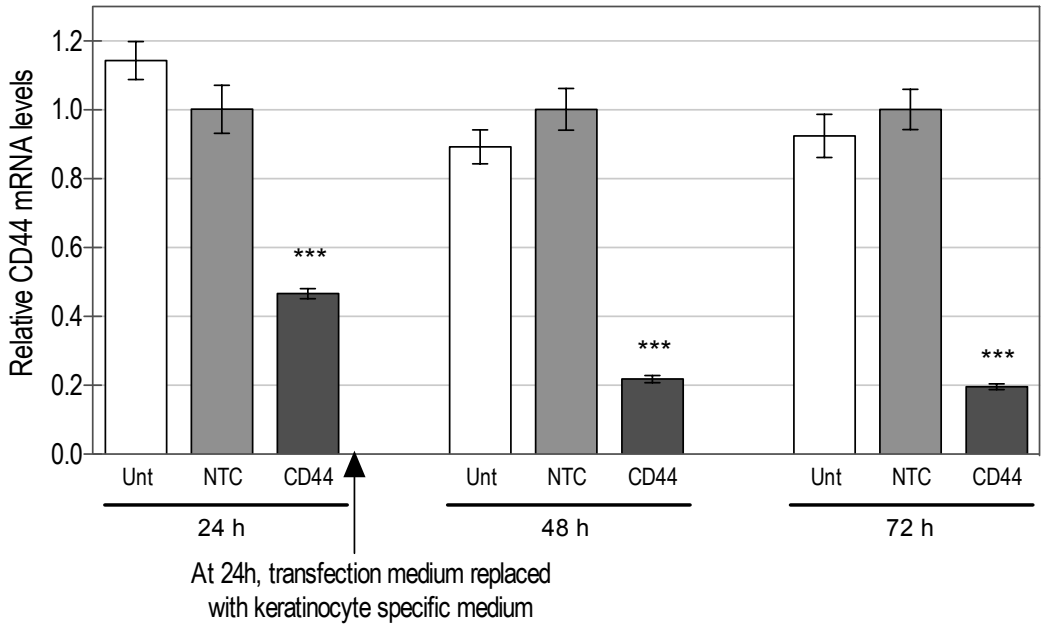

Figure 4.18: CD44 mRNA levels in primary keratinocyte cells at 24 h, 48 h and 72 h post-transfection with Accell CD44 sd-siRNA. Transfection medium was replaced with keratinocyte specific growth medium 24 h post-transfection. CD44 mRNA levels were relative to the non-targeting control (NTC) groups at each respective time-points and normalised to GAPDH endogenous control gene levels. (n = 3 transfection repeats, each with 3 qPCR assay replicates; error bar = standard deviation; *** = significant reduction in mRNA levels compared with non-targeting control, $p < 0.001$). (Unt = untreated; NTC = 1 μM Accell TD101 non-targeting sd-siRNA; CD44 = 1 μM Accell CD44 sd-siRNA)

The primary keratinocyte cells were treated with Accell CD44 sd-siRNA in the same treatment condition as HaCaT cells (Figure 4.18). The level of CD44 mRNA reduction in primary keratinocytes at 24 h and 48 h post-transfection (Figure 4.18) was identical to that with HaCaT cells (Figure 4.12). At the 72 h time-point, there was a significant

level of mRNA increase in HaCaT cells (17.8% increase; $p < 0.001$) but not in primary keratinocytes. At 72 h, CD44 mRNA reduction in primary keratinocytes was 80.4%, which is an insignificant further 2.1% reduction compared to the level of mRNA reduction at 48 h (78.3% reduction; $p > 0.05$). The gene silencing effect of Accell sd-siRNA in primary keratinocytes appeared to be more sustained than in HaCaT cells. This could possibly be because of a lower rate of cell growth in primary cells, which reduces the effect of siRNA dilution due to cell division.

Apart from differences in cell growth rate, primary keratinocytes were treated and cultured in different media. Primary keratinocytes were treated and cultured in serum-free keratinocyte specific medium. HaCaT cells were treated with serum-free transfection medium and then cultured in growth medium with serum 24 h post-transfection. Unmodified siRNA are vulnerable to degradation by nucleases present in serum (Hickerson et al. 2008). Even though Accell sd-siRNA has been modified for increased nuclease stability, the presence of serum affects the functional stability of Accell siRNA, as the manufacturer recommends siRNA treatment in serum-free ADM. It is unclear whether subsequent culture (24 h post transfection) in growth medium with serum in HaCaT cells could have affected the intracellular stability of Accell sd-siRNA and hence affecting its gene silencing stability at the later time-points.

Both the siRNA lipoplex and Accell sd-siRNA was tested for toxicity in primary keratinocytes 24 h, 48 h and 72 h post-transfection (Figure 4.19). There were insignificant differences in cell viability compared to untreated cells at all the tested time-points. This shows that the treatment with siRNA lipoplex and Accell sd-siRNA do not cause cell toxicity in primary keratinocytes, consistent with the safety profile in HaCaT cells.

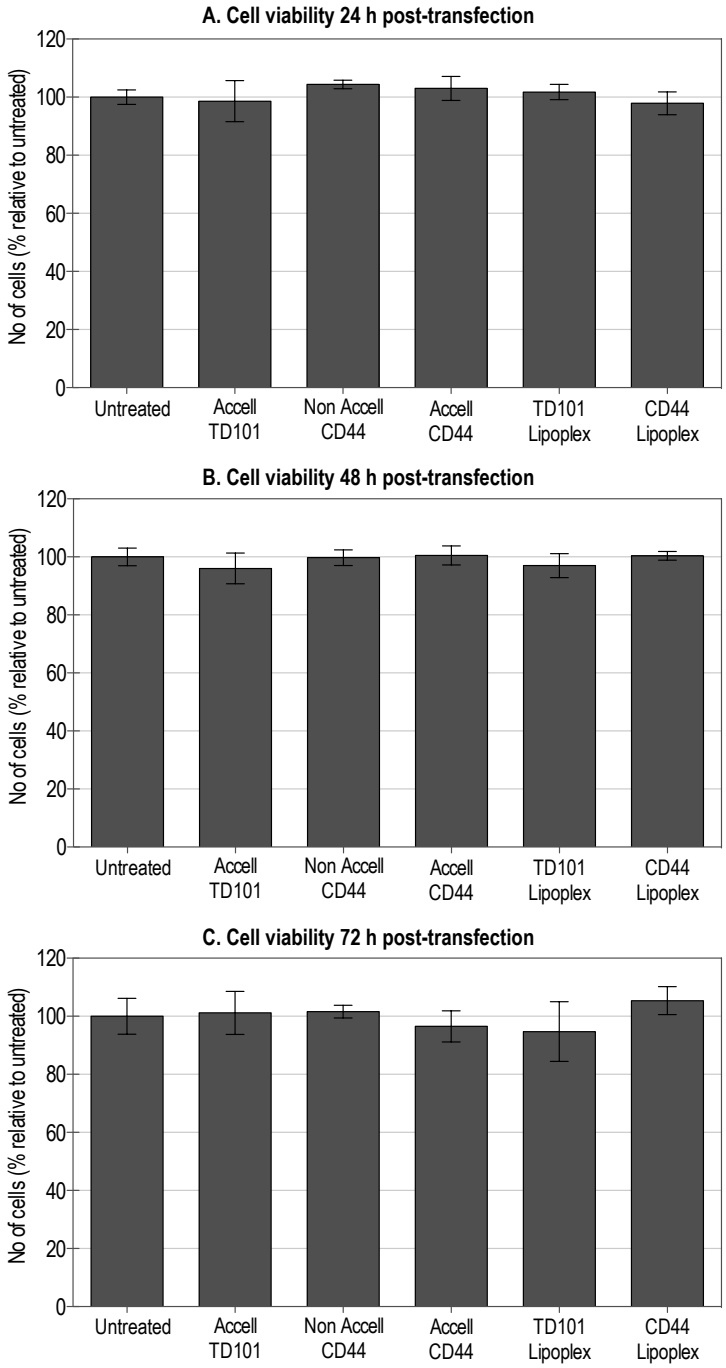

Figure 4.19: Cell viability (MTS assay) following siRNA lipoplex and Accell sd-siRNA treatment in primary keratinocyte cells 24 h (A), 48 h (B) and 72 h (C) post-transfection. Transfection medium was replaced with keratinocyte specific growth medium 24 h post-transfection. The percentage viability was relative to normalised untreated cells. (n = 5 transfection repeats; error bar = standard deviation; Accell TD101 = 1 μM Accell TD101 non-targeting sd-siRNA; Non Accell CD44 = 1 μM CD44 non-sd-siRNA; Accell CD44 = 1 μM Accell CD44 sd-siRNA; TD101 Lipoplex = 10 nM TD101 non-targeting non-sd-siRNA + Lipofectamine™ RNAiMAX; CD44 Lipoplex = 10 nM CD44 non-sd-siRNA + Lipofectamine™ RNAiMAX)

The cellular uptake and localisation of fluorescently labelled Accell sd-siRNA at 6 h, 24 h and 48 h post-transfection was investigated using fluorescent microscopy, flow cytometry and confocal microscopy. Cells treated with Accell Red sd-siRNA, siGLO Red non-sd-siRNA (non-sd-siRNA control) and Accell non-specific non-fluorescent sd-siRNA (non targeting negative control) were observed under the epifluorescent microscopy (Figure 4.20), before being processed for flow cytometry analysis (Figure 4.21). No fluorescence was observed with the negative control siRNA (images not shown). Cellular uptake of Accell Red sd-siRNA was complete at 6 h, as shown by a significant shift in fluorescent signal intensity on the flow cytometry histogram (Figure 4.21) as well as brightly fluorescent cells with obvious fluorescent siRNA intracellular accumulation observed under the epifluorescent microscope (Figure 4.20). This is consistent with what was found in HaCaT cells (section 4.3.2).

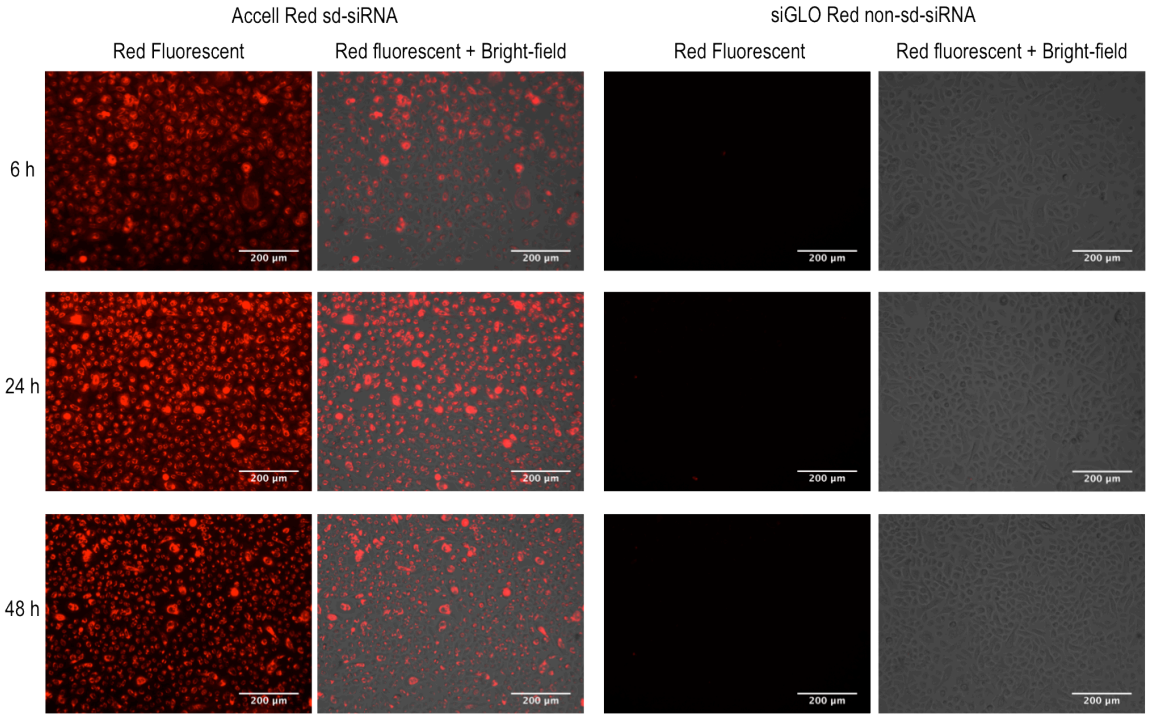

Figure 4.20: Fluorescently labelled naked Accell Red sd-siRNA and naked siGLO Red non-sd-siRNA uptake at 6 h, 24 h and 48 h in primary keratinocyte cells. Representative fluorescence micrographs of HaCaT cells treated with 0.5 µM Accell Red sd-siRNA or 0.5 µM siGLO Red non-sd-siRNA. Transfection medium was replaced with keratinocyte specific growth medium 24 h post transfection. Red fluorescence was pseudocoloured red.

The fluorescent intensity was visualised to be the highest at 24 h post-transfection and did not appear to have decreased significantly at 48 h (Figure 4.19). This was in contrast with the observation in HaCaT cells, whereby the fluorescent signal intensity appeared to be diluted at 48 h and further at 72 h (Figure 4.14). This supports the gene silencing study results, whereby sustained level of gene silencing was observed in primary keratinocytes up to 72 h post-transfection and supports the hypothesis that sd-siRNA remains longer in cells due a lower rate of cell growth and cell division. There is also a possibility that Accell sd-siRNA is simply more stable intracelullarly in primary keratinocytes and hence is degraded less than in HaCaT cells resulting in a more sustained duration of action. Primary keratinocytes did not show any cellular uptake or membrane binding of siGLO Red non-sd-siRNA, which were prominent in HaCaT cells at 24 h, 48 h and 72 h (Figure 4.14 and 4.15). Again, this is possibly due to the lower rate of cell division in primary cells.

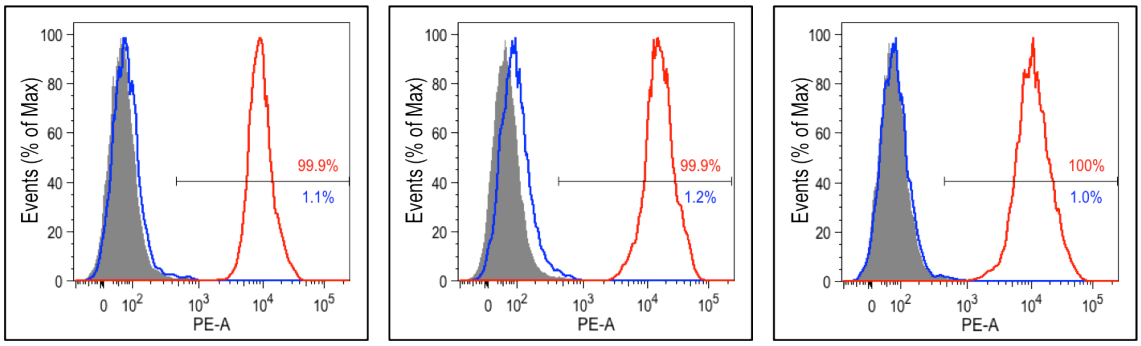

Figure 4.21: Flow cytometry histograms showing fluorescent signal intensity in primary keratinocyte cells treated with 0.5 µM naked Accell Red sd-siRNA or naked siGLO Red non-sd-siRNA at 6 h, 24 h and 48 h. Transfection medium was replaced with keratinocyte specific growth medium 24 h post transfection. Histograms are overlays of Accell TD101 sd-siRNA non-fluorescent control (solid grey), Accell Red sd-siRNA (red line) and siGLO Red non-sd-siRNA (blue line). Fluorescent cells were gated with reference to untreated cells considered as background fluorescence to be less than 1%. The percentages of cells gated were expressed in red for Accell Red sd-siRNA and blue for siGLO Red non-sd-siRNA (average value of 3 transfection repeats).

Primary keratinocytes were also grown and treated on coverslips before processing for confocal microscopy. Images were captured at every 0.6 µm from the top to the bottom

of the cells attached to coverslips over cell thickness of approximately 12 to 15 µm (Figure 4.22). The resulting 20 to 25 image frames were then stacked to provide projected 3D structures of the treated cells to allow visualisation of fluorescent siRNA localisation in cells, relative to the nuclei counterstained with Hoechst 33342. Analysis of images obtained using confocal microscopy revealed presence of Accell sd-siRNA in primary keratinocyte cells at all the tested time-points. Cells treated with siGLO Red non-sd-siRNA did not take up the fluorescent siRNA, with the exception of a few, presumably dead cells captured at 24 h with fluorescent siRNA in its nucleus. It was clear from the confocal images that Accell Red sd-siRNA taken up by cells were localised at the perinuclear region of the cells, close to the nuclear membrane but not in the nucleus.

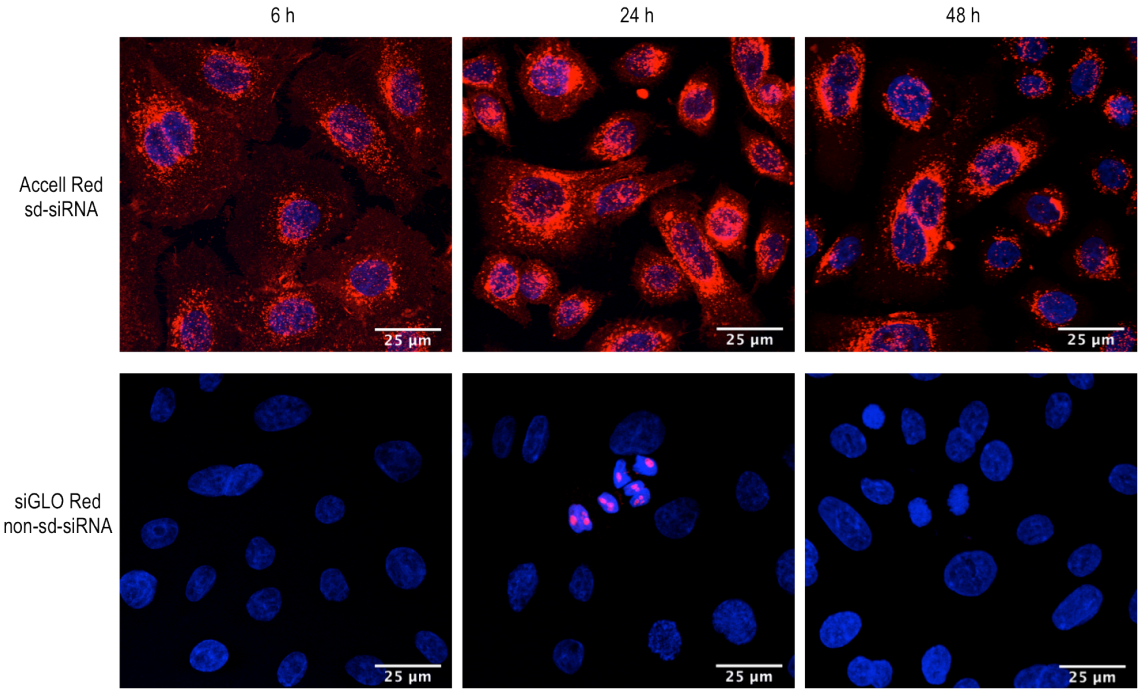

Figure 4.22: Confocal micrographs of fluorescently labelled naked Accell sd-siRNA and naked siGLO non-sd-siRNA uptake at 6 h, 24 h and 48 h in primary keratinocyte cells. HaCaT cells were treated with 0.5 µM Accell Red sd-siRNA or 0.5 µM siGLO Red non-sd-siRNA. Transfection medium was replaced with keratinocyte specific growth medium 24 h post transfection. Nuclei were counterstained with Hoechst 33342 and pseudocoloured blue. Red fluorescence was pseudocoloured red. Each image is a z-stacked projection of approximately 20 slices of images taken over a cell layer thickness of approximately 12 µm.

It has been said in a review of the RNAi machinery that the action where Dicer aids loading of siRNA into the RISC complex prevents free diffusion of siRNAs in the cytoplasm (Siomi and Siomi 2009). This would explain the accumulated presence of fluorescently labelled siRNA near the nucleus (Figure 4.22), where the RISC complexes are located. An earlier study, conducted with Cy3-labelled siRNA complexed to Lipofectamine 2000 (siRNA lipoplex), reported similar perinuclear localisation of fluorescent siRNA with accumulation around the nucleus (Grunweller et al. 2003). However, the image quality was poor and there was little indication on the transfection efficiency with the siRNA lipoplex (Grunweller et al. 2003). As previously mentioned, encapsulation of siRNA in liposomes following siRNA complexation with a transfection reagent resulted in fluorescence quenching (Vader et al. 2010). Fluorescence from the siRNA could be visualised under a fluorescent microscope when siRNA has escaped from the complexes. However, results with siRNA lipoplex should not be considered quantitatively. An *in vivo* study has also reported the delivery of Accell Green sd-siRNA to a rat brain through a single intracerebraventricular injection that resulted in convincing cellular uptake of the FAM-labelled sd-siRNA in different cell types of the adult rat brain, which also correlated to functional gene silencing in the respective brain regions (Nakajima et al. 2012).

Taken together, the gene silencing and siRNA uptake studies in primary keratinocytes gave strong implication of the potential usefulness of the Accell sd-siRNA in an *ex vivo* human skin model (Chapter 5). Non-sd-siRNA lipoplexes may also be useful as they are effective at 100-times lower dose than the Accell sd-siRNA and studies in the following section (section 4.3.4) will further reveal the skin gene delivery potential of both siRNA formulations in a coated steel microneedle system.

4.3.4 Characterisation of siRNA coating onto microneedle devices

Microneedles are capable of penetrating the stratum corneum of human skin to allow effective delivery of nucleic acid (Birchall et al. 2005; Birchall et al. 2000; Chabri et al. 2004; Coulman et al. 2006b; Gonzalez-Gonzalez et al. 2011; Ng et al. 2009; Pearton et al. 2008; Pearton et al. 2012) in a minimally invasive manner (Birchall 2006; Coulman et al. 2011; Haq et al. 2009). The ability of steel microneedles to deliver dry coated small molecules, macromolecules and vaccines to the skin is well established (Gill and

Prausnitz 2007a; Gonzalez-Gonzalez et al. 2011; Kim et al. 2012b; Kim et al. 2010; Pearton et al. 2012). However, the coated steel microneedle system has not previously been examined for the delivery of siRNA to the skin (Chong et al. 2013). Firstly, in order to utilise the coated steel microneedle system for the delivery of siRNA to the skin, the functional stability of siRNA following coating onto the surface of microneedles is characterised with the following *in vitro* functional activity studies.

4.3.4.1 siRNA coating quantification

In the preceding chapter with pDNA (Chapter 3), it has been discussed that pDNA coated onto steel microneedles did not readily dissolve when deposited in the skin, resulting in inconsistent observation of usually poor gene expression compared to the delivery of a liquid formulation of pDNA. This has been attributed to the relatively poor liquid solubility of pDNA (up to 6 mg mL^{-1}) and insufficient fluid in the skin adjacent to the microneedle penetration area to dissolve coated pDNA payload (Pearton et al. 2012). In contrast, siRNA is highly soluble with solubility of up to 200 mg mL^{-1} (Lara et al. 2012). The following study was performed to determine the ability to coat siRNA onto steel microneedles and then recover the full quantity of coated siRNA in a small volume of buffer in 5 min.

The optimised pipette dip-coating method described in section 2.2.5.2 was used to coat steel microneedles with siRNA. Microneedle devices that were of identical needle dimensions (700 μm Regular; Cardiff University, UK) but with different densities of microneedles per array (5 or 10 microneedles) were respectively coated with the same theoretical maximum loading dose of siRNA. As shown in Figure 4.23, the method developed for coating steel microneedles resulted in a reproducible mass of siRNA coated onto and then recovered from each microneedle array. The microneedles were coated with a theoretical maximum loading mass of 35 μg siRNA and an average of 35 μg siRNA was recovered from each microneedle array. The ability to recover siRNA was not affected by prolonged drying of the coated microneedles of up to 20 h. The error bar represents standard deviation, which shows reproducibility of the coating method for coating siRNA.

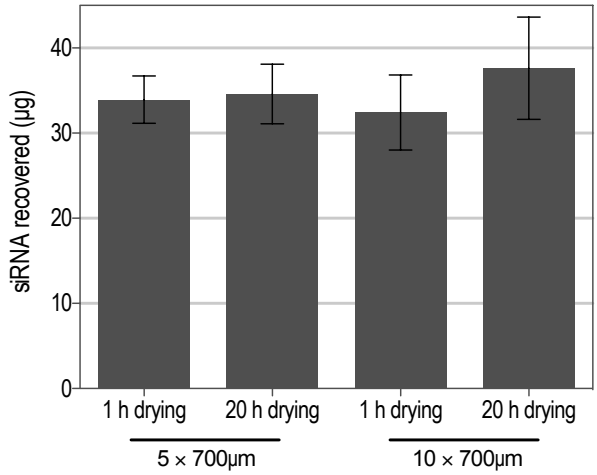

Figure 4.23: siRNA coating onto steel microneedles. A theoretical maximum mass of 35 µg of siRNA per microneedle device was loaded onto two sets of microneedle devices with different densities of microneedles per array (6 with 5 microneedles per array and 6 with 10 microneedles per array). siRNA from 3 devices was recovered from each set of microneedle devices at the drying time-points. (h = hour; n = 3; error bar = standard deviation).

4.3.4.2 Coated siRNA lipoplex functional stability

siRNA lipoplexes require more complex preparation but they are more cost-effective since lower doses of freshly prepared siRNA is required for efficient transfection in monolayer cell culture. To determine whether the siRNA lipoplex remains biologically functional following coating and recovery from the surface of microneedles, lamin A/C non-sd-siRNA lipoplex and naked lamin A/C non-sd-siRNA were coated onto microneedles (5 × 700 µm Regular; Cardiff University, UK), allowed to dry and then recovered in a small volume of buffer. Naked lamin A/C non-sd-siRNA was then complexed with Lipofectamine™ RNAiMAX and then both the recovered non-sd-siRNA lipoplex (siRNA lipoplex recovered) and naked non-sd-siRNA subsequently complexed to a transfection reagent (naked siRNA recovered + lipo) were delivered to HaCaT cells (Figure 4.2). Gene silencing was then determined at both the mRNA (Figure 4.24 A) and protein level (Figure 4.24 B) (Chong et al. 2013).

Lamin A/C mRNA levels were significantly reduced in HaCaT cells treated with non-sd-siRNA that were previously coated onto microneedles, recovered and subsequently complexed with a transfection reagent (naked siRNA recovered + lipo) before cell treatment ($p < 0.001$). The level of mRNA reduction of 85.4% was comparable to that

achieved with the positive control (non coated lamin A/C siRNA 10 nM + Lipofectamine™ RNAiMAX; 85.2% reduction). However, there was no reduction of lamin A/C mRNA when cells were treated with lamin A/C siRNA pre-complexed with transfection reagent prior to coating and recovery from microneedles (siRNA lipoplex recovered). Lamin A/C protein expression determined by Western blotting (Figure 4.24 B) agreed with the reduction in mRNA levels determined by RT-qPCR (Figure 4.24 A).

Non-sd-siRNA lipoplex formulations when freshly prepared have proven to be very effective in HaCaT cells and in primary keratinocytes at a dose as low as 1 nM in HaCaT cells. However, the microneedle coating, drying and recovery process diminished biological functionality of the siRNA that has been pre-complexed with a transfection reagent. This is possibly due to alteration in structural conformation of the cationic liposomal complex and/or the instability of the lipid-based reagent following the coating and drying processes (Chong et al. 2013). It has been suggested that nucleic acid-liposome complexes should be prepared immediately before use as they are prone to forming aggregates upon storage in liquid formulation, resulting in reduced transfection efficiency (Seville et al. 2002). However, some studies have demonstrated that in the presence of sugars as lyoprotectants, nucleic acid-liposome complexes can be freeze-dried, freeze-thawed or spray dried with minimal effect on the biological functionality of the lipoplex (Seville et al. 2002; Yadava et al. 2008). The presence of carbohydrate in a coating formulation has also been shown to improve the physical stability of pDNA following coating onto microneedle (Kim et al. 2010; Pearton et al. 2012). Future studies could investigate the potential of stability-enhancing formulations for coating of siRNA lipoplex onto steel microneedles (Chong et al. 2013).

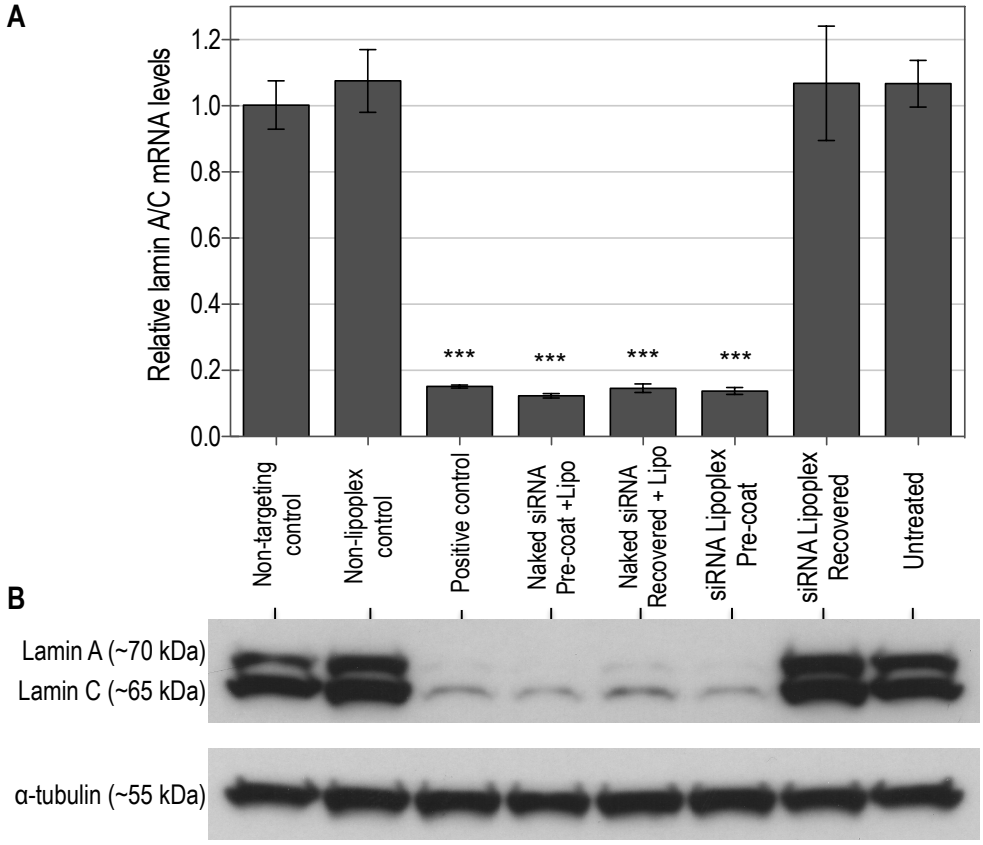

Figure 4.24: Biological functionality of siRNA following microneedle coating. Lamin A/C mRNA (A) and protein (B) levels in HaCaT cells 48 h post-transfection with non-sd-siRNA. (A) Lamin A/C mRNA expressions were relative to the non-targeting negative control group and normalised to GAPDH endogenous control gene levels. (n = 3 transfection repeats, each with 3 qPCR assay replicates; error bar = standard deviation; ***significant reduction in mRNA expression compared with negative control, $p < 0.001$). (B) Lamin A/C protein expression with α-tubulin as the protein loading control. Lamin A/C siRNA recovered from microneedle devices (naked siRNA recovered) was subsequently complexed with Lipofectamine™ RNAiMAX for transfection in HaCaT cells. The same amount of siRNA (10 nM) was used across all the treatment groups. (Non-targeting control = GFP non-sd-siRNA 10 nM + Lipofectamine™ RNAiMAX; non- lipoplex control = lamin A/C non-sd-siRNA 10 nM; positive control = lamin A/C non-sd-siRNA 10 nM + Lipofectamine™ RNAiMAX; naked siRNA pre-coat + lipo = lamin A/C non-sd-siRNA pre-coating formulation diluted to 10 nM + Lipofectamine™ RNAiMAX; siRNA lipoplex pre-coat = lamin A/C non-sd-siRNA lipoplex pre-coating formulation diluted to 10 nM; siRNA lipoplex recovered = lamin A/C siRNA lipoplex formulation (10 nM siRNA + Lipofectamine™ RNAiMAX) recovered after coating onto microneedles).

4.3.4.3 Coated self-delivery siRNA functional and storage stability

Coating microneedles with siRNA lipoplex appears to have compromised the biological functionality of siRNA *in vitro*, which will probably translate to limited gene silencing efficiency *in vivo*. Naked siRNA was however still functional following coating and recovery from the surface of steel microneedles. This is encouraging due to the availability of Accell sd-siRNA, which can enter cells passively in the absence of a transfection reagent. Using the same coating method, microneedles were coated with Accell CD44 sd-siRNA and allowed to dry before recovery in a small volume of buffer. The recovered sd-siRNA was then delivered to HaCaT cells and gene expression 48 h post-tranfection was determined by performing RT-qPCR to analyse the CD44 mRNA levels (Figure 4.25). There was significant reduction in CD44 mRNA levels in cells treated with both the recovered sd-siRNA previously coated onto microneedles (Accell CD44 coated; 67.4% reduction) and the positive control with Accell CD44 sd-siRNA 1 μM (74.5% reduction). Naked CD44 non-sd-siRNA (non-Accell CD44 control) at a dose as high as 1 μM did not reduce mRNA levels when exposed to cells without a transfection reagent.

It has previously been noted that fluorescently labeled non-sd-siRNA when delivered to HaCaT cells at a dose of 0.5 μM resulted in the presence of fluorescent siRNA presumably in cells at 24 h, 48 h and 72 h post-transfection, with a level of intensity much lower than Accell sd-siRNA (section 4.3.2). The observed cellular fluorescence with non-sd-siRNA delivered at a dose of 0.5 μM (Figure 4.15 and 4.16) did not translate to gene silencing as shown in this study, where CD44 non-sd-siRNA delivered at a dose of 1 μM did not result in reduction in mRNA level (Figure 4.25). The intracellular target site of siRNA is the cytoplasm near the nuclear membrane, where the RISC complex is located, one barrier less than pDNA. However, in order for gene silencing effect to be significant, a sufficiently high concentration of siRNA needs to be present for sustained gene silencing efficiency (Carralot et al. 2009). It has been said with pDNA that without the presence of cationic lipids, cellular endosomal escape of naked pDNA internalised through endocytosis is inefficient and therefore is likely degraded in the lysosomes, which could also hold true for siRNA (Lechardeur and Lukacs 2006; Lechardeur et al. 2005; Wattiaux et al. 2000).

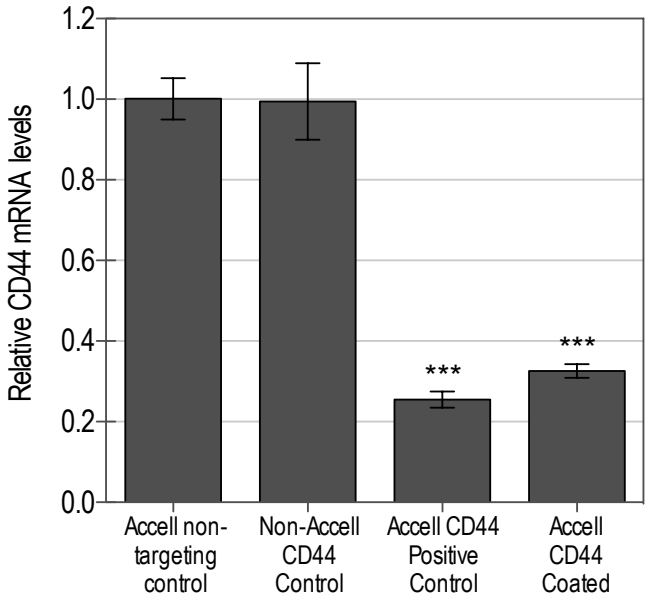

Figure 4.25: Biological functionality of Accell sd-siRNA following microneedle coating. CD44 mRNA levels were determined in HaCaT cells 48 h post-treatment with siRNA. Serum free transfection medium was replaced with growth medium with serum 24 h post-transfection. CD44 mRNA expressions were relative to the Accell non-targeting negative control group and normalised to GAPDH endogenous control gene levels. (n = 3 transfection repeats, each with 3 qPCR assay replicates; error bar = standard deviation; ***significant reduction in mRNA expression compared with Accell non-targeting control, $p < 0.001$). (Accell non-targeting control = Accell control sd-siRNA 1 μM; non-Accell CD44 control = CD44 non-sd- siRNA 1 μM; Accell CD44 positive control=Accell CD44 sd-siRNA 1 μM; Accell CD44 coated = Accell CD44 sd-siRNA recovered after coating onto microneedles, 1 μM).

Having established the functional stability of Accell sd-siRNA coated and recovered from microneedles, the short-term stability of the coated sd-siRNA was tested. Analysis of the CD44 mRNA levels in HaCaT cells treated with recovered Accell CD44 sd-siRNA that has previously been coated onto steel microneedles, allowed to dry and stored at 4°C revealed that Accell sd-siRNA remains biologically functional after 28-days storage (Figure 4.26); prolonged storage did not result in any reduction of cell viability (Figure 4.27).

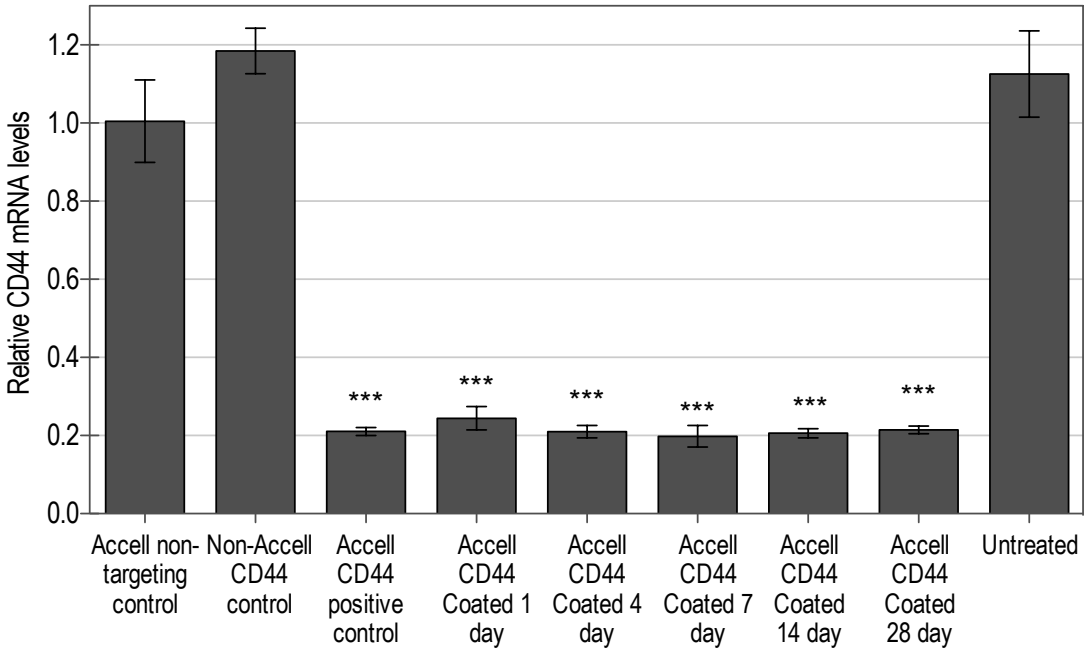

Figure 4.26: Stability of Accell sd-siRNA coated onto steel microneedles. CD44 mRNA levels in HaCaT cells 48 h post-transfection with recovered Accell CD44 sd-siRNA previously coated onto steel microneedles for up to 28 days. Serum free transfection medium was replaced with growth medium with serum 24 h post-transfection. CD44 mRNA levels were relative to the non-targeting control (NTC) groups at each respective time-points and normalised to GAPDH endogenous control gene levels. (n = 3 transfection repeats, each with 3 qPCR assay replicates; error bar = standard deviation; *** = significant reduction in mRNA levels compared with non-targeting control, $p < 0.001$). (Accell non-targeting control = Accell control sd-siRNA 1 μM; non-Accell CD44 control = CD44 non-sd- siRNA 1 μM; Accell CD44 positive control = Accell CD44 sd-siRNA 1 μM; Accell CD44 coated = Accell CD44 sd-siRNA recovered after coating onto microneedles, 1 μM).

A published study has indicated that unmodified siRNA is stable when stored in various conditions including multiple freeze/thaw cycles (up to 10 cycles), extended incubation (over 1 year at room temperature) and high temperatures (up to 95°C) for a short period of time (Hickerson et al. 2008). The integrity of siRNA was not affected under the aforementioned storage conditions as determined by polyacrylamide gel electrophoresis and functional biological assay. siRNA in contact with hair and skin at 37°C was also stable. However, the physical stability and biological functionality of siRNA was compromised following exposure to fetal bovine or human sera at 37°C for up to 48 h (Hickerson et al. 2008). The authors also reported that partial physical degradation of

siRNA, as observed by a change in electrophoretic mobility did not consistently result in loss of biological functionality, suggesting that siRNA retains biologically functionality despite partial degradation (Hickerson et al. 2008). Furthermore, siRNA lipoplexes (also used in the study mentioned) were found to be active at concentrations as low as 1 nM (section 4.3.1.1), which means that the amounts of siRNA lipoplex used in most formulations is in excess. It is possible therefore that full biological activity can be retained even if the siRNA is partially degraded.

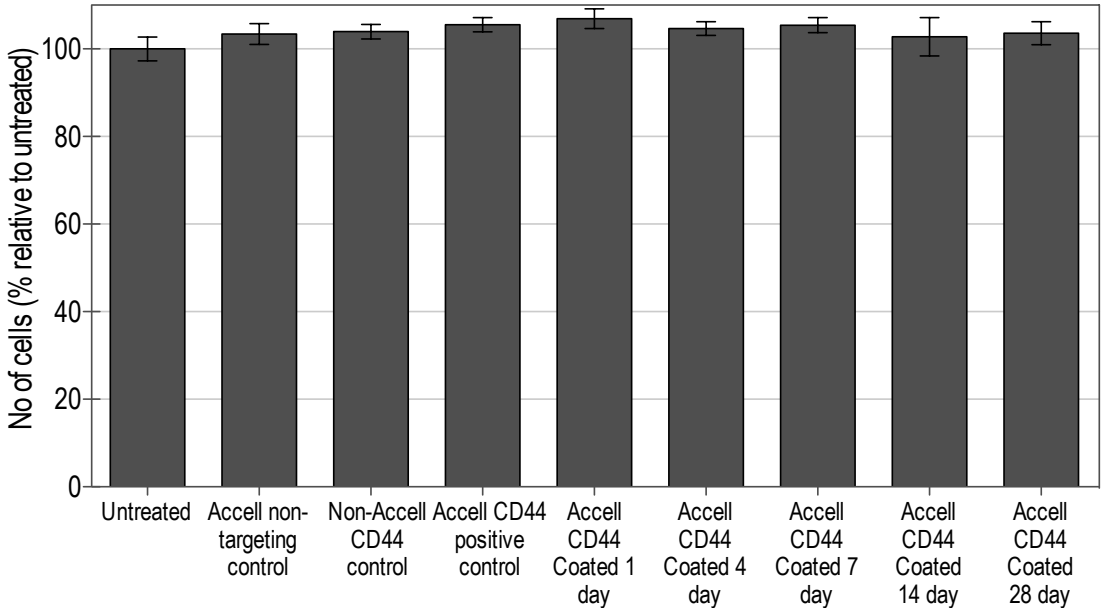

Figure 4.27: Cell viability (MTS assay) in HaCaT cells 48 h post-transfection with recovered Accell sd-siRNA previously coated onto steel microneedles. Serum free transfection medium was replaced with growth medium with serum 24 h post-transfection. The percentage viability was relative to normalised untreated cells. (n = 5 transfection repeats; error bar = standard deviation; Accell TD101 = 1 μM Accell TD101 non-targeting sd-siRNA; Non Accell CD44 = 1 μM CD44 non-sd-siRNA; Accell CD44 = 1 μM Accell CD44 sd-siRNA; Accell CD44 coated = Accell CD44 sd-siRNA recovered after coating onto microneedles, 1 μM)

4.4 Conclusion

The *in vitro* studies in this chapter demonstrate the gene silencing ability of siRNA lipoplex and Accell sd-siRNA in monolayer human keratinocyte cells. siRNA lipoplex resulted in higher level of gene silencing at earlier time-points compared to Accell sd-siRNA. At later time-points, both siRNA formulations resulted in similarly significant levels of gene expression reduction. Reduction in mRNA levels generally resulted in reduction of protein levels. Cellular uptake studies performed with fluorescently labelled Accell sd-siRNA revealed complete siRNA internalisation within 3 h in HaCaT cells and the presence of fluorescent siRNA up to 72 h, the furthest time-point tested. siRNA was localised to the perinuclear region of the cells and was concentrated to an area close to the cell nucleus. Both the siRNA lipoplex and Accell sd-siRNA were equally as efficient in terms of gene silencing but siRNA lipoplex is more cost-effective as it mediated gene silencing at a dose 100 times lower than Accell sd-siRNA.

Studies on the biological stability of siRNA lipoplex and Accell sd-siRNA coated onto microneedles revealed functional stability of recovered naked siRNA following coating onto the surface of steel microneedles. However, siRNA pre-formulated into lipoplex was not functional following coating and recovery from microneedles rendering the lipoplex formulation invalid for further *ex vivo* or *in vivo* studies. On the other hand, Accell sd-siRNA was stable following coating onto steel microneedles and storage at 4°C for up to 28 days. The biological stability of Accell sd-siRNA coated onto the surface of steel microneedles taken together with the reported stability of unmodified siRNA when stored in various conditions provides strong support for the use of Accell modified sd-siRNA in the coated steel microneedle system (Chong et al. 2013; Hickerson et al. 2008). In all the published studies reviewed so far, studies with Accell sd-siRNA generally reported positive findings both *in vitro* and *in vivo*, which renders this formulation of naked modified sd-siRNA an exciting prospect for gene delivery to excised human skin, cultured in an *ex vivo* environment (Chapter 5).

CHAPTER 5

Delivery of siRNA to *ex vivo* human skin

5 Non-viral delivery of siRNA to *ex vivo* human skin

5.1 Introduction

The human skin is an attractive organ for delivery of nucleic acid as it is easily accessible and is the largest, outermost organ of the human body. Cutaneous siRNA delivery allows strategic modulation of local gene expression whilst avoiding systemic side effects. Theoretically, RNAi has a broad therapeutic potential due to the possibility of sequence-specific suppression of any disease-associated genes (Geusens et al. 2009b). Published studies to date have reported the use of animal models or human skin equivalents as pre-clinical models for the delivery of siRNA to the skin. *Ex vivo* human skin represents a model with the closest physiological resemblance to *in vivo* human skin (Godin and Touitou 2007; Ng et al. 2009), avoiding the structural diversity of skin between species and the use of human skin equivalents, which have been shown to have less developed barrier functions than *in vivo* human skin (El Maghraby et al. 2008; Netzlaff et al. 2005). Previous chapters described the optimisation of *ex vivo* human skin culture (Chapter 2), characterisation of microneedles as a physical skin disruption method to penetrate the stratum corneum (Chapter 2 and 3) and the optimisation of siRNA delivery to monolayer *in vitro* human skin models (Chapter 4). This chapter describes microneedle penetration through *in vivo* human skin visualised using the optical coherence tomography (OCT) imaging system and the delivery of Accell sd-siRNA via coated steel microneedles to freshly excised human breast skin in an *ex vivo* skin culture environment.

5.1.1 Human skin imaging techniques

In order for microneedles to target certain cell populations in the skin, it is imperative to have a basic knowledge of skin thickness for efficient delivery of therapeutic molecules to the target site. Skin thickness is measured using invasive and non-invasive techniques. Invasive techniques require acquisition of biopsy samples from post-mortem or living human volunteers for further histological processing to visualise skin sections through light microscopy or electron microscopy (Therkildsen et al. 1998). Whilst microscopy methods can achieve images of high resolution and precision, skin biopsy samples are subjected to significant processing such as formalin fixation and cryosectioning (Lee and Hwang 2002; Sandby-Moller et al. 2003), which alters skin structure and may induce artefacts (Coulman et al. 2011; Huzaira et al. 2001). The

conventional formalin-paraffin processing distorts the anatomy of the stratum corneum making the stratum corneum measurements using this technique unreliable (Pfeiffer et al. 2000; Therkildsen et al. 1998).

More recently, non-invasive techniques, such as *in vivo* confocal laser scanning microscopy are increasingly being used as they do not require tissue processing and can be performed in live skin, *in situ* (Huzaira et al. 2001; Sauermann et al. 2002). The concept of *in vivo* reflectance confocal laser scanning microscopy involves detection of photons back-scattering from living tissue that has been illuminated with a laser. This is a high resolution and high contrast imaging technique capable of scanning skin up to a limited depth of 250 to 300 μm, which is sufficient for epidermal measurements as it includes the epidermis and superficial dermis (Huzaira et al. 2001).

With regards to non-invasive *in vivo*, *in situ* imaging of microneedle insertion into human skin, optical coherence tomography (OCT) have been used to visualise skin structure up to a depth of 2 mm from the surface of the skin (Coulman et al. 2011; Enfield et al. 2010; Huang et al. 1991). The principle of OCT is based on local optical backscatter, the technique being similar to ultrasound with light replacing sound. OCT technology is becoming routine in opthamology and is increasingly being developed for use in dermatology as better light source and detection system is becoming available as technology progresses. This leads to availability of improved OCT systems capable of imaging skin with increased speed, resolution, contrast and penetration depth (Alex et al. 2010; Coulman et al. 2011).

5.1.2 Recent advances in siRNA delivery to human skin

The first human skin clinical trial involving successful targeted delivery of functional siRNA to the skin of a patient with pachyonychia congenita was reported in 2009 (Leachman et al. 2009). However, intradermal injection of the therapeutic siRNA caused considerable pain, prompting investigation of less invasive methods for the delivery of siRNA to sensitive skin (Lara et al. 2012; Leachman et al. 2009). Other skin conditions caused by aberrant gene expression with potential for siRNA treatment include allergic skin diseases (Inoue et al. 2007; Ishimoto et al. 2008; Ritprajak et al. 2008), alopecia (Nakamura et al. 2008), hyperpigmentation (Kim et al. 2012a), psoriasis

(Funding et al. 2006; Jakobsen et al. 2009; Johansen et al. 2006), skin cancer (Hoeflich et al. 2006; Matsumoto et al. 2006; Nakai et al. 2010; Nakai et al. 2007; Sharma et al. 2005; Tao et al. 2005; Tran et al. 2008) and wound healing (Thanik et al. 2007).

Most *in vivo* siRNA delivery studies reported were performed on laboratory generated or animal skin through electroporation, low-frequency ultrasound delivery or subcutaneous injection of naked or liposomal siRNA (Gonzalez-Gonzalez et al. 2009; Inoue et al. 2007; Nakai et al. 2010; Nakamura et al. 2008; Sharma et al. 2005; Tran et al. 2008). siRNA delivery based on topical application of cream formulations (Ritprajak et al. 2008; Takanashi et al. 2009; Thanik et al. 2007) and peptide enhancer (Hsu and Mitragotri 2011) has also been reported.

Microneedles have been reported as a minimally invasive skin disruption method to penetrate the skin's stratum corneum barrier for local cutaneous delivery of siRNA (Chong et al. 2013; Gonzalez-Gonzalez et al. 2010b; Lara et al. 2012). Studies on siRNA delivery to the skin using microneedle devices so far has been limited to delivery of siRNA to *in vivo* mouse skin (Chong et al. 2013; Gonzalez-Gonzalez et al. 2010b) and *in vivo* human skin equivalents grafted onto immunocompromised mice (Lara et al. 2012). There are considerable interspecies skin architecture differences between human and mouse skin and therefore the effect of siRNA delivery to mouse skin may not be directly translated to human skin (Godin and Touitou 2007). Commercially cultured human skin equivalent grafted onto immunocompromised mice represents a promising *in vivo* human skin model but developing a siRNA delivery and detection method in *ex vivo* culture of freshly excised human skin could prove to be a simple and exciting prospect for pre-clinical testing of therapeutic siRNA.

5.1.3 Aim and objectives

The aim of this chapter was to develop an optimised method for delivery of siRNA and detection of gene silencing in *ex vivo* human skin following siRNA delivery *via* coated steel microneedles. The objective of the experiments were:

- To characterise human skin in terms of skin thickness across different sites of a healthy human volunteer as imaged using an optical coherence tomography (OCT) system.

- To visualise the physical skin disruptions caused by application of steel microneedles on healthy human volunteers using OCT.
- To test the ability of siRNA-coated steel microneedles to deposit siRNA into excised human skin.
- To quantify fluorescent siRNA uptake by epidermal cells following coated microneedle administration using flow cytometry on single cell suspensions of *ex vivo* human skin cells.
- To quantify gene expression in *ex vivo* human skin following functional siRNA delivery by microneedles using RT-qPCR on RNA extracted from treated skin epidermis.

5.2 Methods

Unless specified, the suppliers of all reagents and materials have previously been mentioned or were obtained from Thermo Fisher Scientific, UK.

5.2.1 Human skin imaging using optical coherence tomography (OCT)

5.2.1.1 OCT imaging of human skin

Various sites of the human skin including the forearm, palm, arm, breast, upper abdomen, lower abdomen, dorsal gluteal and thigh on a healthy 27 year old female volunteer was imaged using the VivoSight OCT system (Michelson Diagnostics, UK) following written consent and full ethical approval from Cardiff School of Pharmacy and Pharmaceutical Sciences School Ethics Committee (reference 123-28). OCT imaging was performed as previously described (Coulman et al. 2011). Briefly, a hand-held probe was placed on the skin of the subject and a real-time preview was performed to view cross-section of the skin on a computer screen with software connected to the OCT probe to optimise parameters to ensure the sampling area was sufficiently covered. Images were then captured where each transverse sections was an area of 6 mm in length across the sampling area and 2 mm in depth into the skin and were separated by a 4 μm gap between each transverse sections capturing 500 transverse sections across each sampling area forming a 6 mm (length) × 2mm (depth) × 2mm (height) 3-dimensional skin block.

5.2.1.2 OCT imaging of microneedle insertion into human skin

Steel microneedles of various needle densities were tested on healthy 34 year old and 41 year old male subjects following written consent and full ethical approval from Cardiff School of Pharmacy and Pharmaceutical Sciences School Ethics Committee (reference 123-28). The treatment area was imaged before, during and after microneedle insertion. A proposed treatment area of 2 × 5 cm in the left hand of the volunteer sterilised with 70% isopropyl alcohol swab (University Hospital Supplies Ltd, UK) before imaging with a hand-held probe as described in section 5.2.1.1. After the initial pre-treatment images were captured, the selected treatment area was swabbed prior to the application of microneedles. Microneedles were inserted manually into the skin at a pressure sufficient for skin penetration, held in place for 5 s and then retracted. The treated area

was imaged as described in section 5.2.1.1 and the edge of the imaging area was marked so that imaging of the treatment area could be repeated. Some steel microneedles were also imaged *in situ*, by tilting the array following insertion and subsequently capturing images over the microneedle treated area with the hand-held probe as previously described. Images over the microneedle treated area were also captured 1 h and 4 h post-treatment.

5.2.1.3 Data processing and analysis of OCT images

After acquisition, the image data saved was exported to a dicom format and analysed using ImageJ (National Institute of Health, USA). Using ImageJ, the 3D image stack was resliced to obtain *en face* view of the tissue imaged.

5.2.2 siRNA modification and sequences

Accell sd-siRNAs utilised in this chapter are as described in section 4.2.1.2 (Accell CD44 sd-siRNA and Accell TD101 non-targeting sd-siRNA) and section 4.2.1.3 (Accell Red sd-siRNA).

5.2.3 *Ex vivo* siRNA uptake in excised human breast skin

5.2.3.1 Coating of fluorescent siRNA onto steel microneedle devices

Electropolished steel microneedle devices (5 × 700μm; Georgia Institute of Technology, USA) were coated with fluorescently labelled Accell Red sd-siRNA using the pipette tip dip-coating method as described in section 2.2.5.2 to provide a theoretical maximum loading of 2 μg siRNA coated onto each microneedle device. The coated steel microneedles were imaged using the Leica DM IRB epifluorescence microscope and imaging system before and after insertion into freshly excised human breast skin as described in section 5.2.3.2.

5.2.3.2 siRNA coated microneedles application to excised human skin

Human breast skin samples were acquired and prepared as described in section 2.2.3.2 and were surface dapped-dry with sterile lens tissue paper. The excised skin was stretched and pinned using 1 cm push pins on a planar corkboard with the epidermal side facing up. Further grease moisture was minimised by applying 70% isopropyl

alcohol swab on the surface of the skin. Microneedles coated as described in section 5.2.3.1 were inserted manually into the skin surface at a pressure sufficient for skin penetration and left in place for 10 min before being removed. On a skin area of 8 mm x 8 mm dimension, 4 arrays of microneedle devices were administered in an evenly spaced manner to cover the area with 20 microneedle penetration sites as illustrated in Figure 5.1. The stretch of the treated skin pinned to the corkboard was then minimally loosened before being cut using an 8 mm diameter biopsy punch (Figure 5.2). The treated skin samples were then incubated in a hanging insert organ culture setup as described in section 2.2.3.3 for 0 h, 3 h, 6 h, 24 h and/or 48 h. After incubation, treated skin samples were subjected to vigorous rinsing in PBS for 5 min and then wiped with isopropyl alcohol swabs to remove fluorescent material from the surface of the skin. The samples were then either (i) embedded in OCT medium and frozen on dry ice for cryosectioning (section 5.2.3.3) or (ii) subjected to epidermal sheet separation for imaging (section 5.2.3.3) or further processing for flow cytometry (section 5.2.3.4).

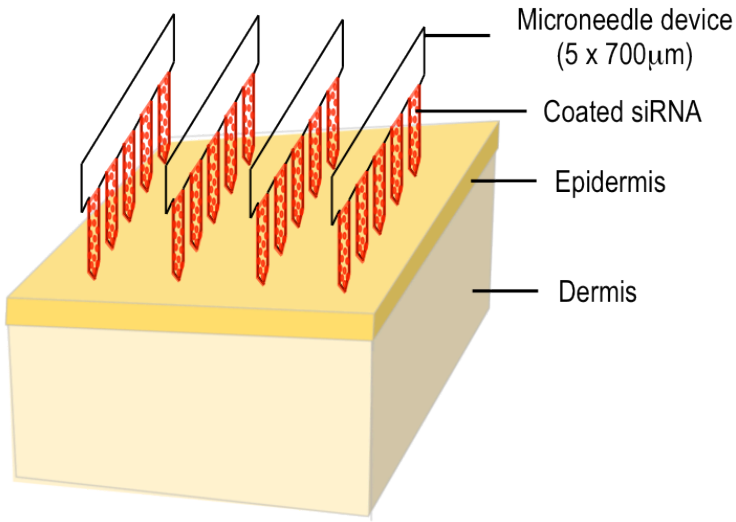

Figure 5.1: A schematic diagram of the orientation of steel microneedle devices coated with Accell siRNA inserted into an area of freshly excised human breast skin of approximately 1 cm x 1 cm surface area.

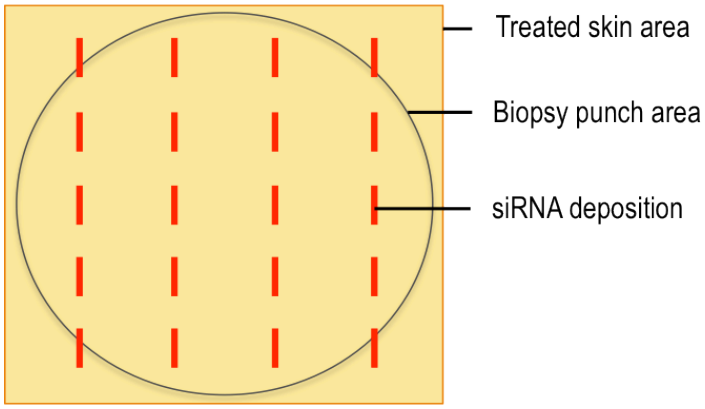

Figure 5.2: A schematic diagram of the skin area treated with coated microneedles and the area cut by 8 mm biopsy punch for subsequent culture.

5.2.3.3 Visualisation of fluorescent siRNA delivery to human skin

Treated skin samples were incubated for 24 h, subjected to vigorous rinsing in PBS and then embedded in OCT, frozen on dry ice and then cryosectioned as described in section 2.2.4.7. Skin sections captured onto microscope slides were kept frozen at -80°C until visualisation. Frozen skin sections were defrosted for 5 min before being mounted with VECTASHIELD® Mounting Medium containing 1.5 μg mL^{-1} 4,6-diamidino-2-phenylindole (DAPI; Vector Laboratories Ltd., UK) for nuclear staining. siRNA deposition was then visualised under the Leica DM IRB epifluorescence microscope and imaging system.

Alternatively, treated skin samples incubated for 0 h, 3 h, 6 h, 24 h and 48 h were subjected to vigorous rinsing in PBS before epidermal sheet separation with 3.8% w/v ammonium thiocyanate in PBS as described in section 2.2.4.2. Separated epidermal sheets were fixed in 4% (w/v) paraformaldehyde in PBS for up to 24 h at 4°C. The fixed epidermal sheets were rinsed 4 times in PBS for 5 min each time and stained with 5 μg mL^{-1} Hoechst 33342 in PBS for 60 min at room temperature. The epidermal sheets were then rinsed 4 times in PBS for 5 min each time and mounted on microscope slides with Dako fluorescence mounting medium. The mounted epidermal sheets were visualised under the Leica DM IRB epifluorescence microscope and imaging system.

5.2.3.4 Quantification of siRNA uptake in human epidermal cells

Fluorescent siRNA treated skin samples incubated for 24 h were subjected to vigorous rinsing in PBS before epidermal sheet separation with an enzyme cocktail solution containing 2 caseinolytic units mL^{-1} solution of Dispase II, 197 units mL^{-1} solution of Collagenase D and 20 units mL^{-1} solution of DNase I from bovine pancreas in RPMI medium as described in section 2.2.4.2. A single cell suspension of epidermal cells were then extracted from the epidermal sheets using the method described in section 2.2.4.3 with slight modification. Following trypsin activity and the addition of soybean trypsin inhibitor, cells were centrifuged at 400 × *g* for 5 min at room temperature. The cell pellet was gently resuspended in 0.025% v/v DNase 1 with 10% v/v FCS in PBS and incubated at 37°C for 1 h. Cells were then filtered through a 70 μm cell strainer and centrifuged at 400 × *g* for 5 min. Cell pellets were rinsed once by resuspending the pellet in PBS.

Cells were then centrifuged and re-suspended in PBS containing near-infrared (IR) LIVE/DEAD® Fixable Dead Cell Stain (Life Technologies, UK) and prepared according to the manufacturer's recommendation. Cells were incubated in the live dead stain for 30 min at 4°C and then centrifuged and resuspended in 100 μL flow cytometry buffer containing 1% bovine serum albumin (Sigma Aldrich, UK) and 0.1% sodium azide (Sigma Aldrich, UK) in PBS. Cells were rinsed in flow cytometry buffer twice before being resuspended in 100 μL flow cytometry buffer containing 1% bovine serum albumin (Sigma Aldrich, UK) and 0.1% sodium azide (Sigma Aldrich, UK) in PBS and transferred into flow cytometry tubes. The cells were fixed with 200 μL fixing buffer containing 1% paraformaldehyde and 0.1% sodium azide in PBS and analysed by flow cytometry within a week.

The flow cytometric analysis was performed as recommended by the instrument manual. The frequency of fluorescent cells in the APC-Cy7 and PE channel (corresponding to fluorescence of near-IR live dead stain and Accell Red DY-547 fluorescence), out of a total of at least 10^6 events analysed per sample was recorded. The data collected was analysed with the FlowJo Flow Cytometry Analysis Software for Mac Version 8.8 using method as described in section 3.2.7.1.2. A viable cell population was selected from cells that had not taken up the live dead marker.

Following flow cytometry, the single cell suspension of epidermal cells remaining was centrifuged, resuspended in PBS and counterstained with 5 μg mL^{-1} Hoechst 33342 in PBS for 30 min at room temperature. Cells were centrifuged and rinsed 3 times in PBS. Cell pellets were then resuspended in a small volume of PBS (up to 50 μL) and 5 μL of cell suspension was transferred to a microscope slide, allowed to dry and mounted in Dako fluorescent mounting medium with coverslip. Cells were then imaged using the Leica DMI6000B confocal microscope system and analysed using the method described in section 2.2.4.6.

5.2.4 *Ex vivo* gene silencing in excised human breast skin

5.2.4.1 Coating siRNA onto steel microneedle devices

Electropolished steel microneedle devices (5 × 700μm; Georgia Institute of Technology, USA) were coated with Accell CD44 sd-siRNA using the pipette tip dip-coating method as described in section 2.2.5.2 to provide a theoretical maximum loading of 20 μg siRNA coated onto each microneedle device.

5.2.4.2 siRNA coated microneedles application on excised human skin

Human breast skin samples, acquired and prepared as described in section 2.2.3.2, were surface dapped-dry with sterile lens tissue paper. The excised skin was then processed as described in section 5.2.3.2 and then treated with steel microneedles coated with Accell CD44 sd-siRNA as described in section 5.2.4.1. The treated skin samples were then incubated in a hanging insert organ culture setup as described in section 2.2.3.3 for 48 h. After incubation, treated skin samples were subjected to epidermal sheet separation with 3.8% w/v ammonium thiocyanate in PBS as described in section 2.2.4.2 and stored in RNAlater® solution (Life Technologies, UK) at -20°C. For each treatment group, 2 biopsy punch samples that were treated similarly were pooled to allow sufficient tissue sample for RNA extraction.

5.2.4.3 siRNA delivery dose quantification

Steel microneedles were coated with Accell CD44 sd-siRNA as described in section 5.2.4.1. For each skin sample specimen, 12 microneedle devices were coated with a theoretical maximum loading of 20 μg siRNA per device. Skin specimens were treated

with 8 siRNA-coated microneedle devices for two punch biopsies (Figure 5.2) from each treatment group and the remaining 4 siRNA-coated microneedle devices were retained. All 12 used and unused siRNA coated microneedle devices were then washed in a small volume of buffer (50 μL) with agitation for 5 min to recover siRNA from the surface of the microneedles. The concentration of the recovered siRNA was measured using the NanoVue spectrophotometer as described in section 3.2.1.5 and the mass of siRNA recovered was calculated as described in section 3.2.5.1. The mass of siRNA deposited on the skin was calculated by deducting the average mass of siRNA remaining on the microneedles that have been used to treat the skin sample from the unused coated microneedles.

5.2.4.4 Visualisation of skin disruption by siRNA coated microneedles

Physical skin disruption on excised human breast skin caused by siRNA coated steel microneedles was assessed using the OCT system, as described in section 5.2.1.

5.2.4.5 Quantification of gene silencing in human epidermis

Cardiff University Central Biotechnology Services (CBS) performed RNA extractions from human epidermal skin samples. Epidermal sheets stored in RNAlater® solution at -20°C were transported on ice to the CBS for RNA extraction. Briefly, the tissue samples were homogenised in lysis buffer from the Qiagen RNeasy Mini kit (Qiagen, UK) using IKA T10 Basic Ultra-Turrax Disperser (Cole-Parmer Instrument Co. Ltd, UK). RNA was then extracted according to the instructions of the Qiagen RNeasy Mini kit and eluted in 30μL nuclease free water. The quality and purity of extracted RNA was tested using the Agilent 2100 Bioanalyzer (Agilent Technologies, UK).

CD44 gene expression in the RNA samples were analysed by quantifying CD44 mRNA levels using RT-qPCR as described in section 4.2.7.1.3 and section 4.2.7.1.4. All data points reported are the mean and standard error of three replicate qPCR assays.

5.2.5 Data processing and statistical analysis

Data processing and statistical analysis was performed as described in section 3.2.9.

5.3 Results and discussion

5.3.1 Human skin imaging using optical coherence tomography (OCT)

There are various factors such as body site, gender, age and skin type, that affect the thickness of healthy human skin epidermis (Sandby-Moller et al. 2003). Conventionally, human skin epidermis thickness is measured using invasive techniques that require acquisition of biopsy samples from human volunteers for further histological processing to visualise skin sections through light microscopy (Therkildsen et al. 1998). The availability of non-invasive imaging systems allows analysis of *in vivo* epidermal skin thickness that prevents alteration of skin structure and artefacts cause by the invasive techniques (Coulman et al. 2011; Huzaira et al. 2001).

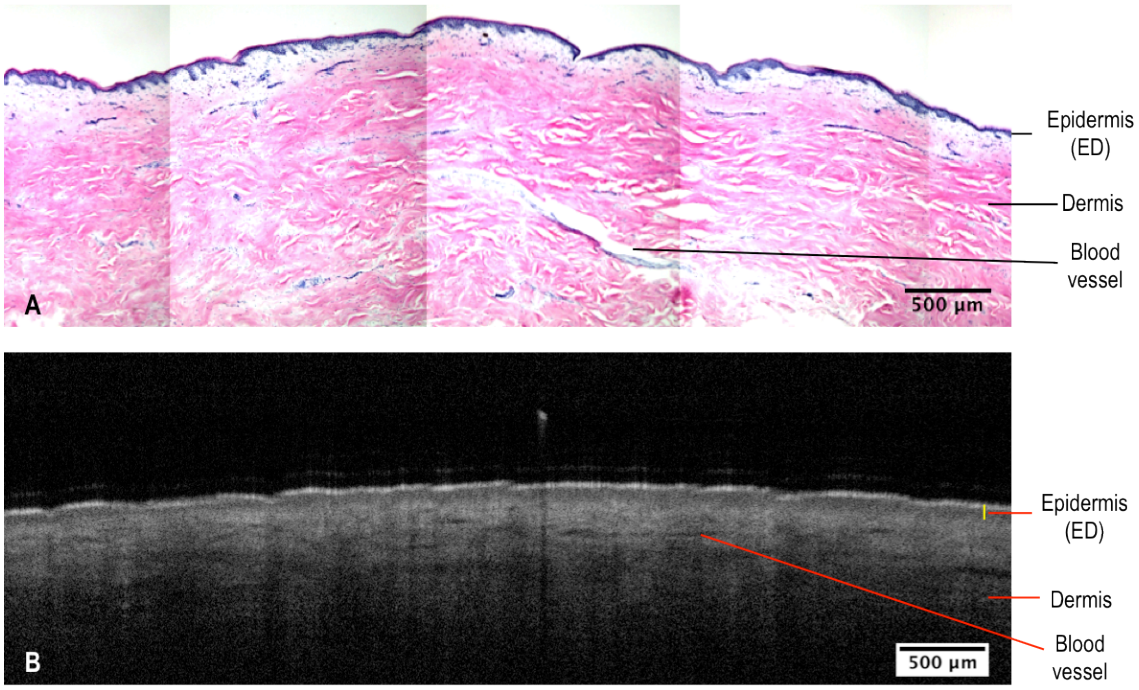

Figure 5.3: A comparison of human breast skin transverse sections obtained through (A) light microscopy of cryosectioned unfixed skin biopsy sample from a 83-year-old female subject and subsequently subjected to H&E staining and (B) *in vivo* OCT imaging of skin from a 27-year-old subject. (Yellow line = thickness of the epidermis)

Figure 5.3 compares transverse sections of human breast skin obtained through light microscopy of haematoxylin and eosin (H&E) stained cryosection of unfixed skin biopsy from a 83-year-old female subject and *in vivo* OCT imaging of skin from a 27-year-old subject. From the images, it was obvious that light microscopy of H&E stained

transverse section produced an image of higher resolution than OCT imaging. The objective of the light microscope could be increased to further magnify the image for precise measurement of the skin epidermis and stratum corneum thickness, which is not achievable with current technology of the OCT imaging system (Figure 5.4). However, excised human skin loses its natural elasticity, resulting in alteration of the tension in skin structure. The process of H&E staining and subsequent alcohol dehydration for mounting onto microscopy slides also affects skin structure leading to false measurement of skin thickness.

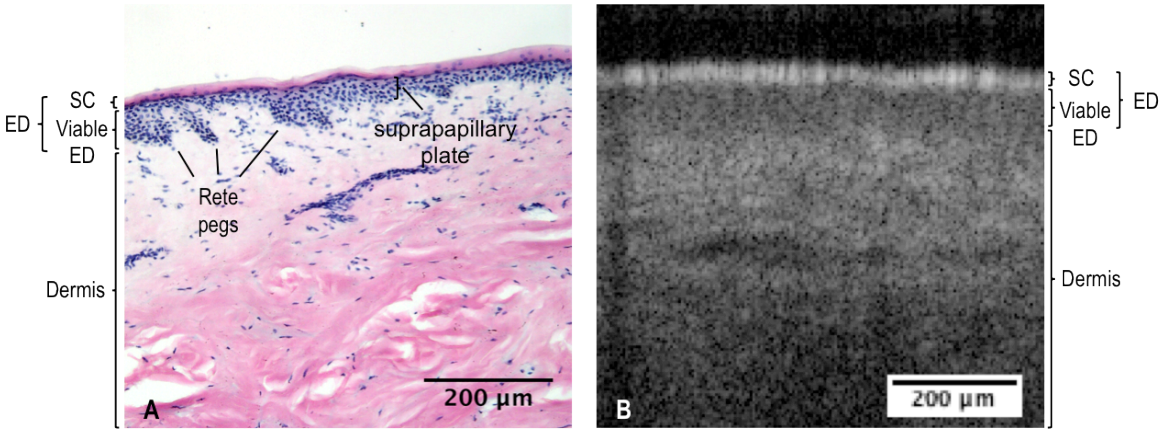

Figure 5.4: A comparison of human breast skin of magnified transverse sections obtained through (A) light microscopy of cryosectioned unfixed skin biopsy sample from a 83-year-old female subject and subsequently subjected to H&E staining and (B) *in vivo* OCT imaging of skin from a 27-year-old subject.

Overall, OCT imaging is able to distinguish epidermis from dermis to allow measurement of epidermis thickness at its natural *in vivo* state. It is more difficult to separate the thickness of the stratum corneum (SC) and viable epidermis due to low resolution of the images (Figures 5.5 and 5.6), with the exception of the palm. The epidermis represents the upper layer of skin including the stratum corneum and the viable epidermis. Human palmar skin has a characteristic thickened stratum corneum that is easily distinguishable from the transverse section shown in Figure 5.5. The stratum corneum is defined by the region of consistent dark grey band, approximately 145 µm in thickness with the presence of eccrine sweat glands that have distinctive spiralling structures. A thin, distinctively darker contour separates the stratum corneum from the viable epidermis, which was approximately 160 µm in thickness.

Transverse sections of skin in other regions of the body revealed surface skin structure that differs significantly from the thicker skin on the palm (Figure 5.5 and 5.6). The stratum corneum in other body sites was almost indistinguishable by OCT imaging but appeared as the thin bright region that was approximately 10 to 20 μm in thickness. A region of consistent dark grey band approximately 70 μm to 100 μm in thickness defines the viable epidermis. The dermal layer is defined by a light grey region below the viable epidermis with identifiable blood vessels that appeared as horizontal elongated and darkened areas. *En face* projection of skin surfaces showed variation in the characteristic pavement pattern of the skin folds with hairs protruding from the surface of the skin. These observations were consistent with a previously published study using a similar OCT technique reporting the structure of palm and upper arm skin (Coulman et al. 2011).

A study performed using invasive technique on skin biopsies of 71 healthy volunteers in different sites of the body including the forearm dorsal, shoulder and buttocks has reported average thickness of between 11.0 μm and 18.3 μm for stratum corneum and between 56.6 μm and 81.5 μm for viable epidermis (Sandby-Moller et al. 2003). The study also revealed that variation in epidermal thickness is mainly explained by body site, but there is significant individual variation. There was direct correlation between stratum corneum thickness and pigmentation but inverse correlation between stratum corneum thickness and the number of smoking years. Thickness of the cellular epidermis had positive correlation with blood content, which was greater in males than in females. Age and skin type was found to have no correlation with epidermal thickness (Sandby-Moller et al. 2003). Another invasive study performed on 452 biopsies on 28 different regions of healthy skin including palm, sole and eyelid on Korean men and women revealed a range of epidermal thickness of 31 μm to 637 μm (Lee and Hwang 2002).

Another study performed using a non-invasive technique with near-IR reflectance confocal microscopy of 10 healthy volunteers in different skin sites including the forehead, cheek, inner and outer forearm, lower back and leg revealed *in vivo* skin thickness of between 8.08 μm and 13.66 μm for stratum corneum, between 50.83 μm to 65.44 μm for the suprapapillary plate of the viable epidermis and between 101.58 μm to 134.55 μm for the depth of rete pegs (Huzaira et al. 2001). The epidermis thickness of

skin from different sites of a 27-year-old female subject as measured using OCT imaging system generally agreed with what was observed in other published studies (Coulman et al. 2011; Huzaira et al. 2001; Lee and Hwang 2002; Sandby-Moller et al. 2003)

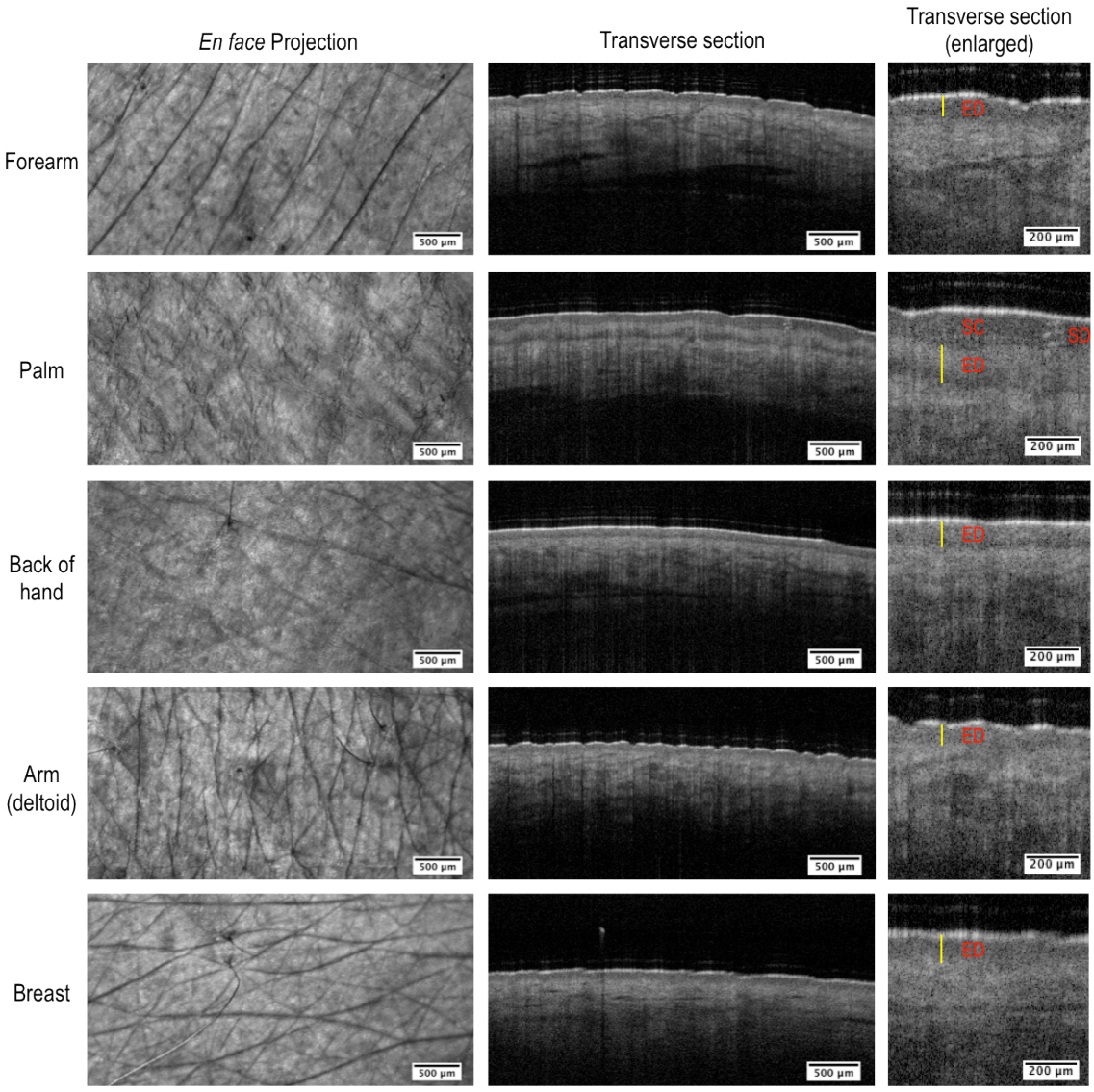

Figure 5.5: ***En face*** **and transverse sections of skin at different upper body sites of a 27-year-old female subject obtained through** ***in vivo*** **OCT imaging.** Transverse sections were from the middle regions of the *en face* images. (Yellow line = thickness of the epidermis; ED = epidermis; SC = stratum corneum; SD = sweat duct)

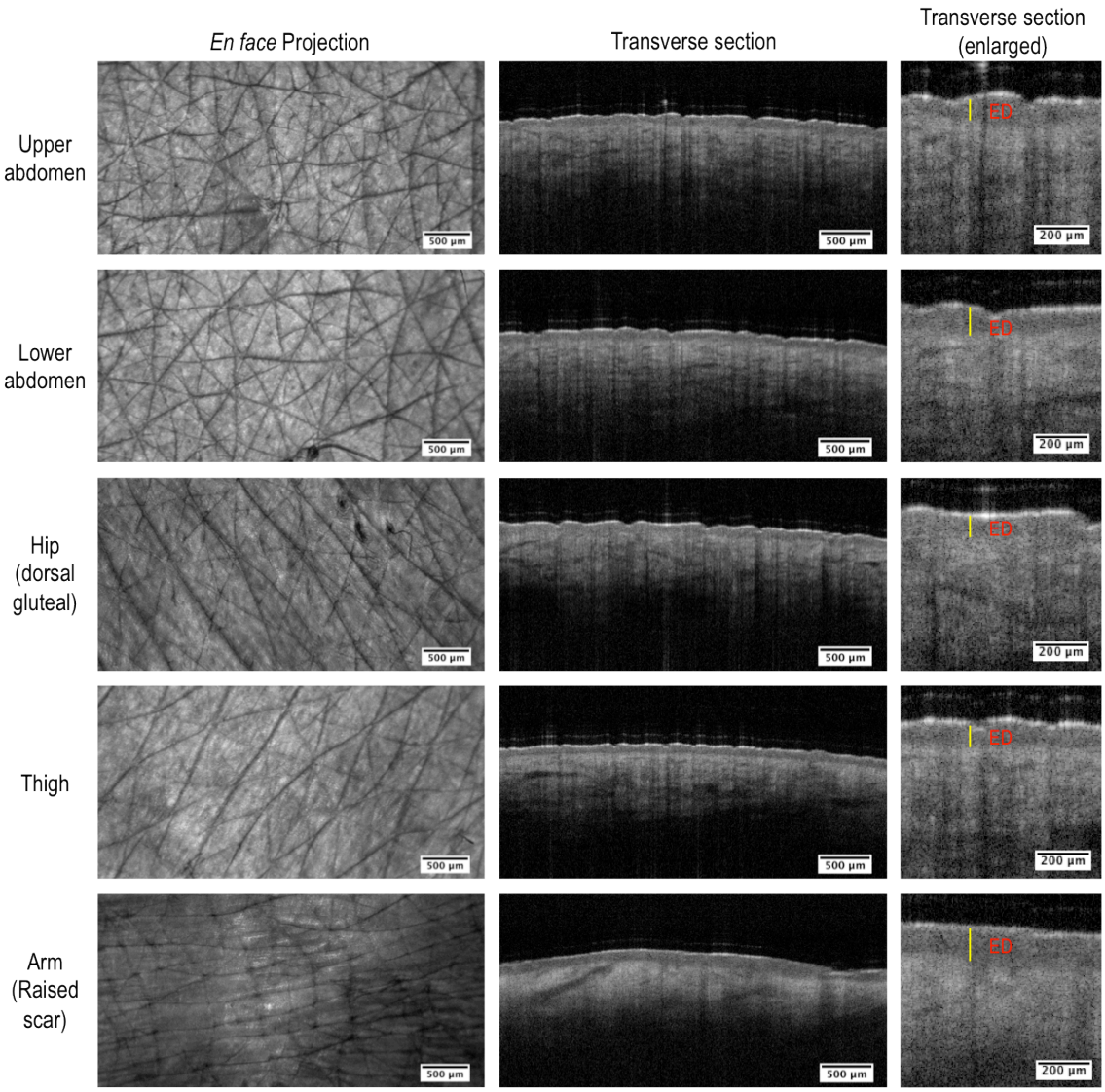

Figure 5.6: ***En face*** **and transverse sections of skin at different lower body sites of a 27-year-old female subject obtained through** ***in vivo*** **OCT imaging.** Transverse sections were from the middle regions of the *en face* images. (Yellow line = thickness of the epidermis; ED = epidermis)

The study of skin thickness at different sites using the OCT imaging system highlights that it is not a high resolution technique for precise measurement of skin thickness but is a quick non-invasive technique to image healthy or diseased human skin *in vivo* prior to treatment with microneedles. Pre-determining skin thickness could assist the selection of microneedle length and size ideal for delivery of therapeutic molecules to its target site of the epidermis, dermis or both. One of the advantages of steel microneedles is that the manufacturing process allows mass production of microneedles of any length, shape and size at low cost per unit to suit various skin thickness across different body sites.

Furthermore, a non-invasive method is ideal when surgical incision or skin biopsy on diseased skin may exacerbate the condition or potentiate pain.

5.3.2 OCT imaging of microneedle insertion into human skin

Conventional microneedle delivery studies often characterise the depth and morphology of channels created by microneedle insertion through histological methods, which involve skin biopsy and sectioning. These studies are not usually conducted on *in vivo* human skin but rather on *ex vivo* excised human skin or animal models. Human skin that has been excised from the body suffers from considerable changes to the biomechanical properties of the tissue, which should be taken into consideration when interpreting the result of microneedle penetration. The principal of OCT imaging uses local optical backscatter. Therefore, the technique is capable of reflecting light from steel microneedle devices to allow *in vivo*, *in situ* imaging of microneedle penetration into skin of human volunteers (Coulman et al. 2011). *In situ* microneedle penetration on the back of the hand and palm of human volunteers with healthy skin was captured using the OCT imaging system (Figure 5.7).

From the *en face* projection and transverse section of the *in situ* microneedle insertion OCT images (Figure 5.7), visible skin deformation upon microneedle insertion was observed, indicating skin compression below the point of individual needle insertion (Coulman et al. 2011). Skin folds around the microneedle penetration site were more prominent in the *en face* projection of the surface of the palm skin compared to the surface of the back of hand skin, possibly related to the thickness of the stratum corneum, which is thicker and more resistant to penetration on the palm. Both sets of *in situ* microneedle insertion experiments in different skin sites show incomplete microneedle insertion or microneedle retraction due to the skin's elasticity. Nevertheless, light reflectance from the tip of microneedles was seen in transverse sections with a depth of up to 300 μm from the surface of both the palm and back of hand skin, which is approximately 40% the length of a 700 μm microneedle.

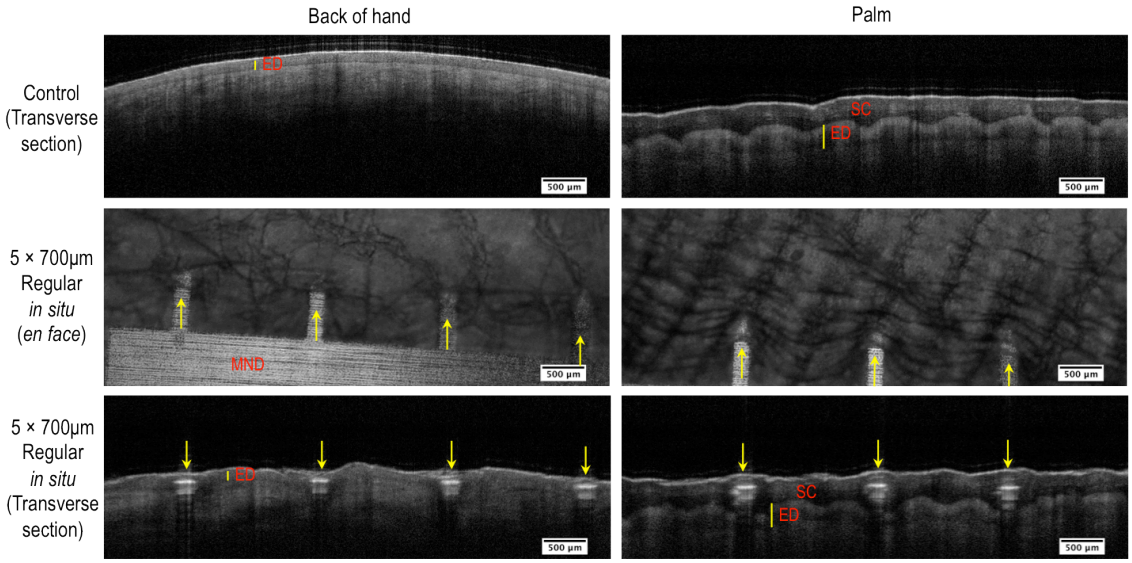

Figure 5.7: ***En face*** **and transverse sections of** ***in situ*** **blank steel microneedle (5 × 700µm Regular, Cardiff University) insertion into the skin at the back of the hand of a 34-year-old male subject and palm of a 41-year-old male subject obtained through** ***in vivo*** **OCT imaging.** Transverse sections were from the middle regions of the control *en face* images or resliced across the microneedle penetration sites of the treated *en face* images. (Yellow line = thickness of the epidermis; Yellow arrow = microneedle penetration site; ED = epidermis; SC = stratum corneum; MND = microneedle device)

Following the removal of microneedle device from the back of the hand, *en face* projection of OCT images (Figure 5.8) revealed distinct darkened spots corresponding to the spacing of microneedles in the microneedle device (5 × 700µm Regular, Cardiff University). Transverse sections across the length of the penetration sites distinguished by the appearance of darkened spots on the *en face* image revealed upper skin punctures in the epidermis of up to approximately 100 µm in depth from the surface and 90 µm in width. Underneath the skin punctures, trails of vertical discrete darkened areas were observed, which was the artefact from the channels created above as optical light travels through the punctured skin epidermis with delayed backscattering, leaving a trail of shadow in the dermis. The microchannels created by microneedle insertion appeared primarily in the upper layer of the epidermis and not the dermis, possibly due to the presence of elastic connective tissue that quickly tighten deformed skin in the dermis.

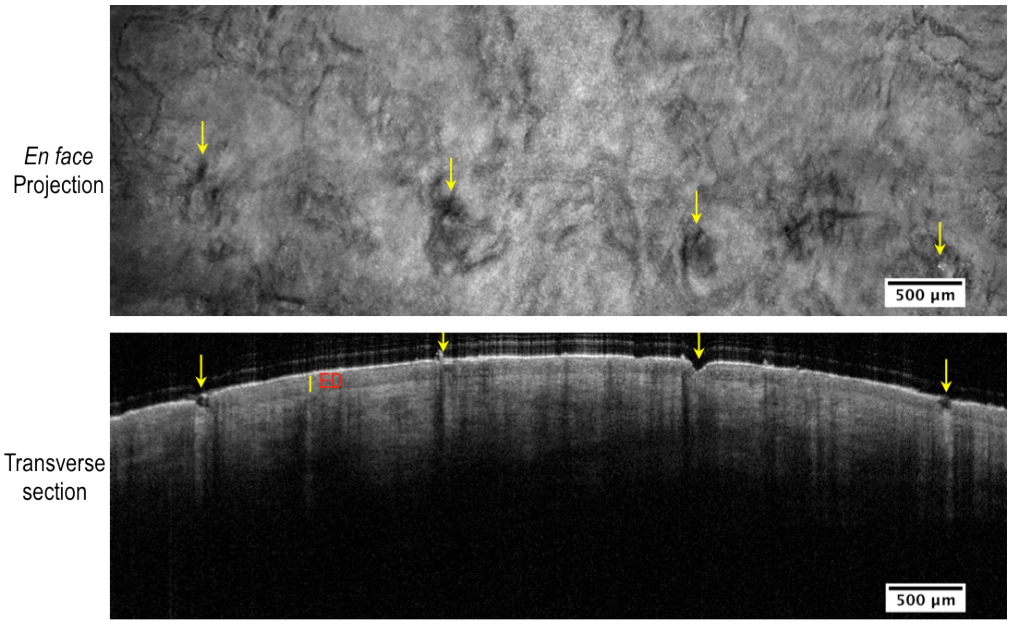

Figure 5.8: ***En face*** **and transverse sections of blank steel microneedle (5 × 700µm Regular, Cardiff University) penetration site on the skin at the back of the hand of a 34-year-old male subject obtained through** ***in vivo*** **OCT imaging.** These microneedle penetration sites correspond to skin disruption caused by microneedle insertion in Figure 5.7. Transverse section were resliced across the microneedle penetration sites of the treated *en face* image. (Yellow line = thickness of the epidermis; Yellow arrow = microneedle penetration site; ED = epidermis)

A short-term time-scale study was also performed to determine the effect of steel microneedle penetration over 4 hours on the forearm skin of two male volunteers with healthy normal skin (Figure 5.9 and 5.10). *En face* projection of the OCT images showed distinct darkened spots created by microneedle penetration, similar to that found in the back of hand skin (Figure 5.8). The darkened spots appear to be most prominent at 0 h time-point and appear less contrasting at later time-points. Transverse sections across the microneedle penetration sites of the *en face* images showed obvious vertical trails of darkened area, up to 100 µm in width, representing artefact from the micron-scale channel in the broken epidermis above that appeared less obvious at 1 h and 4 h time-points. These observations indicate that the microchannels created slowly fade as microwounds created by microneedle insertion heal with time. When microneedles are withdrawn, skin's elastic properties rebound the skin back to its original conformation and the wound healing process of inflammation, re-

epitheliasation and remodelling takes place resulting in pore closure to maintain the integrity of the skin barrier (Barrientos et al. 2008; Menon et al. 1992).

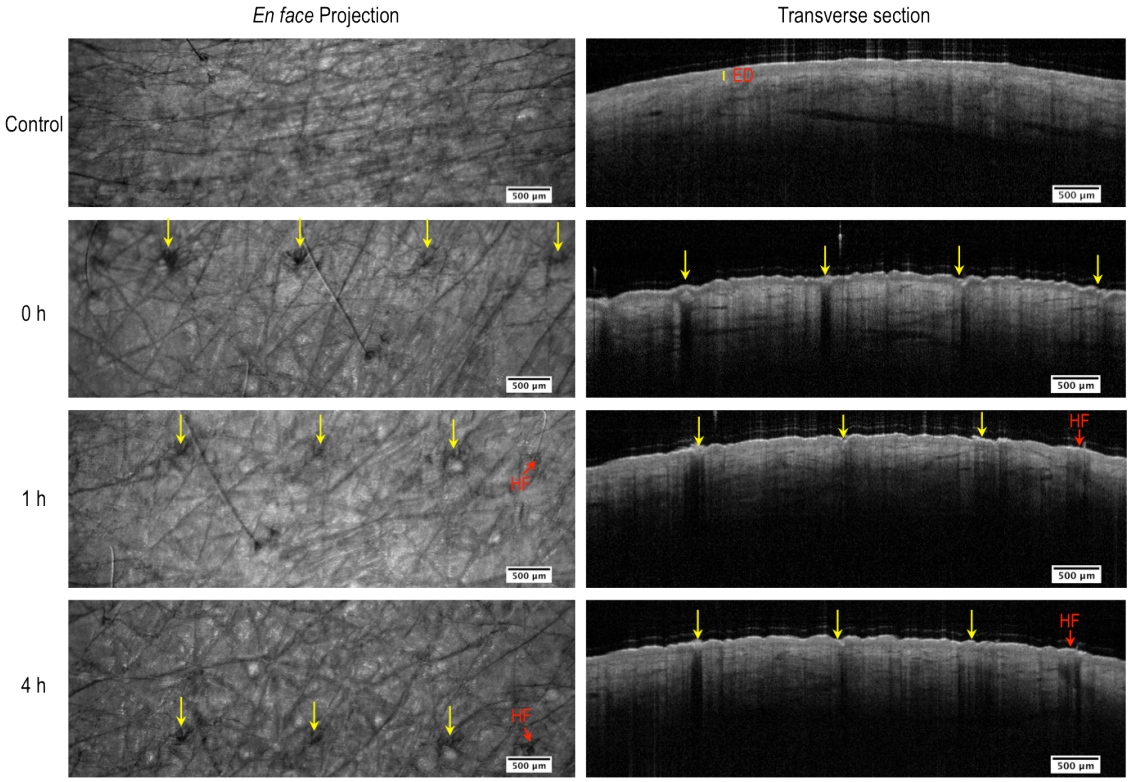

Figure 5.9: ***En face*** **and transverse sections of blank microneedle (5 × 700µm Regular, Cardiff University) penetration sites on the forearm skin of a 34-year-old male subject at 0 h, 1 h and 4 h after microneedle insertion obtained through** ***in vivo*** **OCT imaging.** Transverse sections were from the middle regions of the control *en face* images or resliced across the microneedle penetration sites of the treated *en face* images. (Yellow line = thickness of the epidermis; Yellow arrow = microneedle penetration site; ED = epidermis; HF = hair follicle)

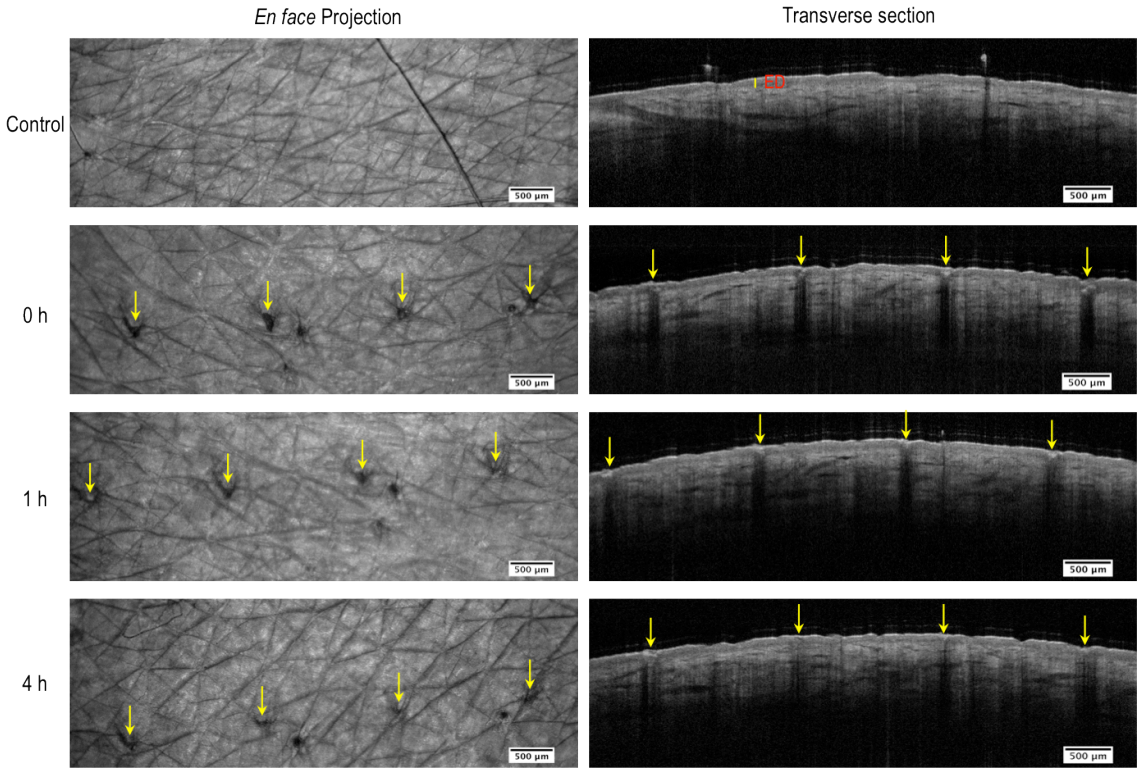

Figure 5.10: ***En face*** **and transverse sections of blank microneedle (5 × 700µm Regular, Cardiff University) penetration sites on the forearm skin of a 41-year-old male subject at 0 h, 1 h and 4 h after microneedle insertion obtained through** ***in vivo*** **OCT imaging.** Transverse sections were from the middle regions of the control *en face* images or resliced across the microneedle penetration sites of the treated *en face* images. (Yellow line = thickness of the epidermis; Yellow arrow = microneedle penetration site; ED = epidermis)

A study investigating the kinetics of pore resealing after steel microneedle insertion using electrical impedance measurements in human subjects showed that in the absence of occlusion, pores formed by microneedles recovered their barrier properties within 2 hours regardless of microneedle geometry (Gupta et al. 2011). In the presence of occlusion, the skin resealing time varies from 3 h to 40 h depending on the geometry of microneedles used (Gupta et al. 2011; Wermeling et al. 2008). The skin resealing kinetics is affected by factors such as microneedle length, density and the cross-sectional size a microneedle (Gupta et al. 2011). The authors hypothesised that skin occlusion provides an artificial barrier that reduces transepidermal water loss, preventing the formation of a water gradient that is required for initiation of cellular response to repair the disrupted stratum corneum barrier (Gupta et al. 2011; Menon et al. 1992). The observations reported in the skin resealing study provided insight towards

the safety and efficacy of microneedle-based drug delivery approaches (Gupta et al. 2011). The ability to prolong the presence of microchannels after microneedle application is useful for delivery of drug-loaded patches for sustained drug delivery into the skin. Upon patch removal, the skin rapidly reseals resulting in termination of the delivery, which is an inherent safety feature (Gupta et al. 2011; Wermeling et al. 2008). The quick resealing of microchannels under non-occlusive conditions reduces the risk of infection following microneedle treatment (Gupta et al. 2011). This provides a good indication of the safety of non-occlusive drug-coated microneedle systems, which is used for the delivery of siRNA to the skin in this thesis.

Denser microneedle arrays, with more closely spaced microneedles in the device (10 × 700μm Regular, Cardiff University) were also tested on the forearm skin of both the healthy male volunteers (Figure 5.11). From the *en face* projections and transverse sections across the microneedle penetration sites of the *en face* images, denser microneedles appear to have created microchannels that are less prominent than the regular devices (5 × 700μm Regular, Cardiff University). The skin is composed of nonlinear viscoelastic layers, which are easily deformed upon microneedle application to its surface (Crichton et al. 2011; Groves et al. 2012). Upon insertion into the skin, microneedles that are more closely spaced are bound to encounter more resistance from the natural elasticity of *in vivo* human skin, resulting in less penetration, compared to microneedle devices with less dense spacing. A study has shown that microneedles with longer length (≥600 μm *vs.* <600 μm) and lower microneedle density (2000 needles per cm^2 *vs.* 5625 needles per cm^2) were more easily inserted into the skin as they overcome skin deformation (Yan et al. 2010). This highlights the importance in determining the ideal microneedle length and spacing when designing microneedle arrays to minimise skin resistance whilst covering the treatment area sufficiently.

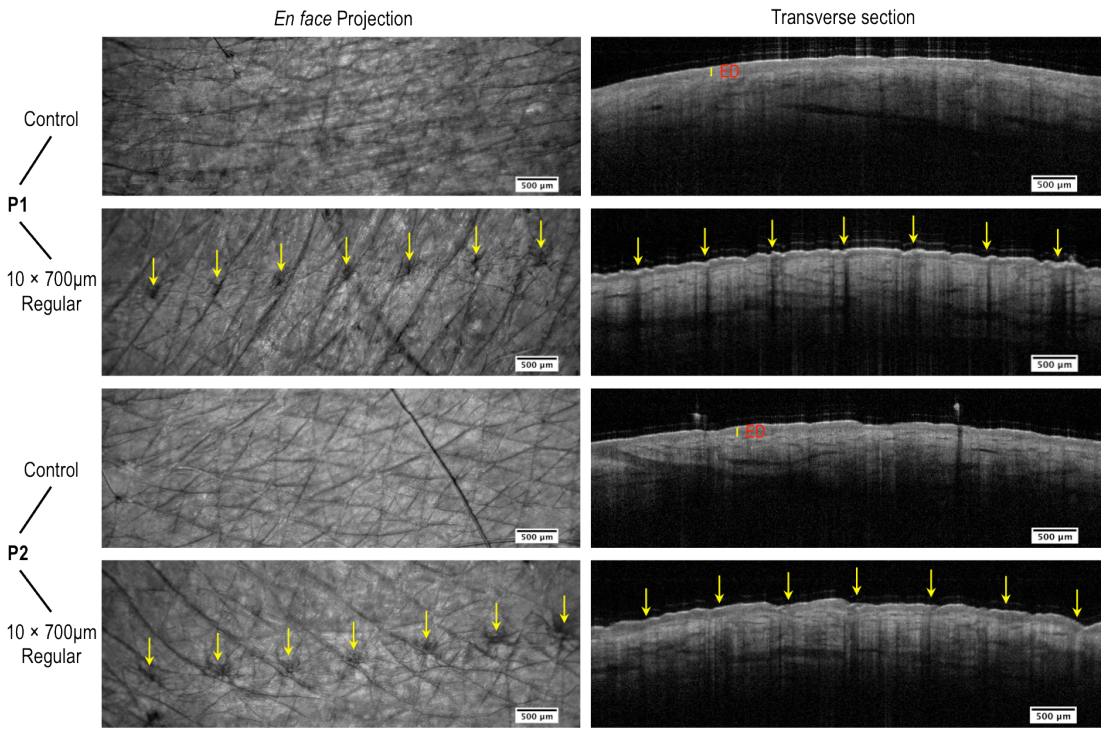

Figure 5.11: *En face* and transverse sections of blank microneedle (10 × 700µm Regular, Cardiff University) penetration sites on the forearm skin of a 34-year-old (P1) and 41-year-old (P2) male subjects at 0 h after microneedle insertion obtained through *in vivo* OCT imaging. Transverse sections were from the middle regions of the control *en face* images or resliced across the microneedle penetration sites of the treated *en face* images. (Yellow line = thickness of the epidermis; Yellow arrow = microneedle penetration site; ED = epidermis)

5.3.3 *Ex vivo* siRNA uptake in excised human breast skin

After establishing the ability of steel microneedles in penetrating the stratum corneum barrier layer of skin *in vivo*, the ability to deposit siRNA in human skin was determined using excised human breast skin in an *ex vivo* skin culture system. In the preceeding chapter (Chapter 4), Accell modified sd-siRNA was found to be suitable for coating onto steel microneedles with maintained siRNA functionality for up to 28 days. Accell sd-siRNA was also efficient and non-toxic *in vitro*. Therefore, the following studies with *ex vivo* human skin investigated the delivery of Accell sd-siRNA to excised human skin *via* coated steel microneedles.

Firstly, the ability to evenly coat the surface of steel microneedles with Accell sd-siRNA using the pipette tip dip-coating method was determined by imaging a series of

microneedle devices coated with fluorescently labelled Accell Red sd-siRNA. For each skin specimen treated (n = 3), a set of 10 microneedle devices (5 × 700μm, Georgia Institute of Technology) was coated. Out of the 10 microneedle devices that were coated, 3 devices were randomly selected for inspection under the fluorescent microscope.

The image of an individual coated microneedle shown in Figure 5.12 A, which shows even distribution of fluorescent siRNA coated on the surface of steel microneedle was representative of other microneedles inspected. The microneedles were then imaged again following insertion into excised human breast skin. Figure 5.12 B represents the microneedle shown in Figure 5.12 A after insertion into human skin for 10 min before retraction. This particular microneedle penetrated the skin to a depth of approximately 650 μm, as shown by removal of siRNA from the surface of microneedles when placed in the the skin. The depth of microneedle penetration differs between devices and position of microneedles in the array but skin penetration depth of at least 50% the microneedle length was achieved with all microneedles in the array, with an average of approximately 70% the length of the microneedles (Figure 5.13 A).

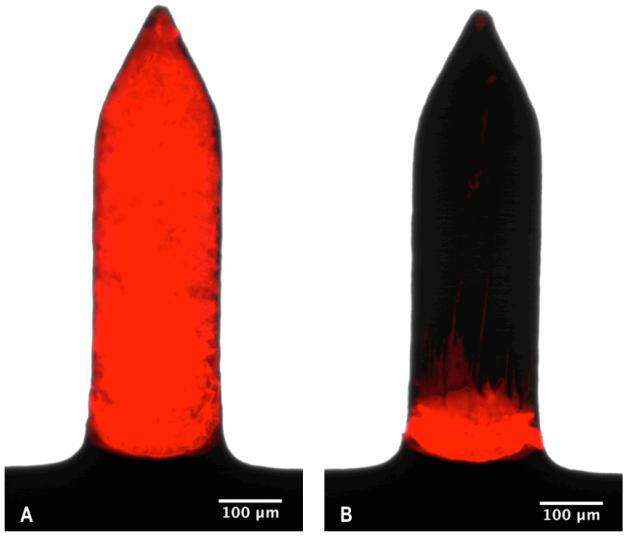

Figure 5.12: Fluorescence and bright-field overlay images of an electropolished microneedle (from an array of 5 × 700μm, Georgia Institute of Technology) coated with approximately 0.4 μg fluorescent Accell Red sd-siRNA pre- (A) and post- (B) insertion into excised human breast skin. The images shown are representative of other microneedles analysed in the array and devices used**.** Red fluorescent from the sd-siRNA was pseudocoloured red.

It was also important to determine whether the siRNA recovery method by washing a microneedle device in a small volume of buffer provides complete removal of material from the surface of microneedles. Fluorescent siRNA coated microneedles that had been inserted into excised human skin were imaged before and after washing in a small volume of buffer with agitation for 5 min (Figure 5.13). As shown in Figure 5.13 B, near complete removal of siRNA from the surface of steel microneedles was achieved with the recovery method used, providing confidence in the efficiency of the method, even in microneedles that have been inserted into human skin.

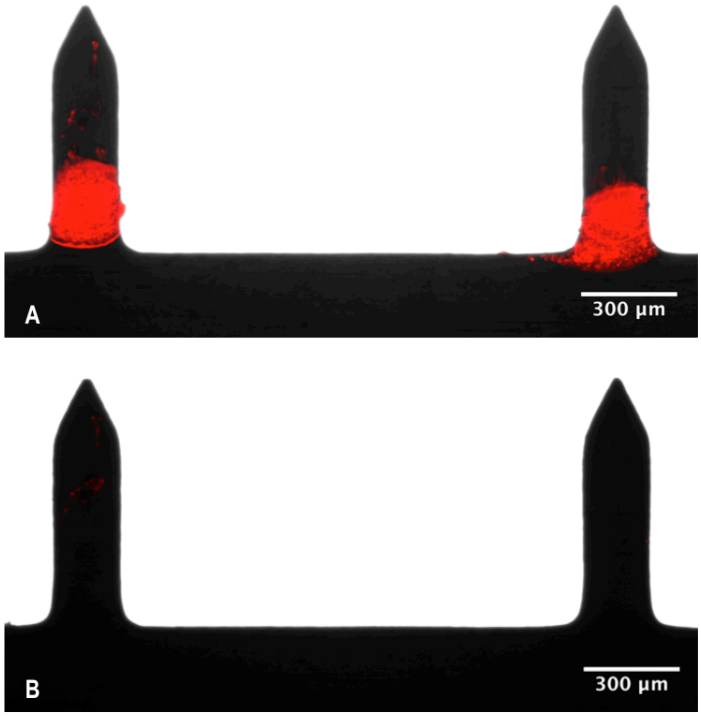

Figure 5.13: Fluorescence and bright-field overlay images of a set of two electropolished microneedles (from an array of 5 × 700µm, Georgia Institute of Technology) coated with approximately 0.4 µg fluorescent Accell Red sd-siRNA per microneedle post-insertion (A) into excised human breast skin and then post-recovery (B) in a small volume of buffer. The images shown are representative of other microneedles analysed in the array and devices used**.** Red fluorescent from the sd-siRNA was pseudocoloured red.

Figure 5.14 A shows digital images of excised human breast skin, stretched and pinned to foiled corkboard with steel microneedles inserted in the skin in an orientation illustrated in Figure 5.1 for each biopsy sample. Figure 5.14 B and C show digital *en*

face images of areas of skin samples from two different skin specimens with obvious fluorescent siRNA deposition in the penetration sites following microneedle retraction. Figure 5.14 D shows a digital image of a treated skin biopsy supported at air liquid interface in a hanging insert organ culture setup for incubation until analysis. These digital images clearly show microneedle penetration and siRNA depositions that were appropriately spaced over a biopsy sample area for consistent data analysis. In-plane microneedle devices are easier to manipulate in laboratory settings but future clinical application of microneedles is likely to involve design of evenly spaced microneedles in multiple arrays in a device to cover a sufficient treatment area.

The deposition of fluorescently labelled Accell Red sd-siRNA was determined using a histological method where unfixed treated skin samples were frozen for cryosectioning and then observed under the fluorescent microscope, before (Figure 5.15) and after (Figure 5.16) mounting in fluorescent mounting medium containing the nuclei counterstain, DAPI. As depicted in Figure 5.15, microneedle insertion resulted in penetration of the stratum corneum, epidermis and dermis, with visible channels, areas without skin autofluorescence, observed up to a depth of approximately 550 μm from the surface. Figure 5.16 depicts microneedle penetration site 2 that clearly shows a layer of skin epidermis with a high number of closely arranged nucleated cells stained by DAPI. Fluorescent sd-siRNA deposition appeared to concentrate in the upper layer of the epidermis and diffused in the dermis around the site of penetration.

Depending on its target site, microneedle geometry, length and density can be manipulated to allow targeted delivery to the desired skin layer (Al-Qallaf and Das 2009). For more uniform penetration, mechanical insertion devices may be used to prevent variation in application force and depth induced by manual microneedle insertion (Singh et al. 2011; Verbaan et al. 2008). In the experimental setup of the excised human breast skin, removal of skin from its natural *in vivo* environment would have resulted in considerable biomechanical changes to the tissue, which resulted in deeper microneedle penetration with less effort. Nevertheless, the dermal layer of the skin is still present in the excised human skin setup, stretched and pinned to foiled corkboard, providing considerable similarity to the elasticity of *in vivo* skin environment. Therefore, microneedle penetration is often not the full length of the microneedles but between 50 to 90% the length of the microneedles.

Figure 5.14: ***En face*** **digital images of excised human breast skin with (A)** ***in situ*** **microneedles penetration, (B) a microneedle array post-insertion into the skin with fluorescent Accell Red sd-siRNA deposition sites following coated microneedle insertion, (C) enlarged equivalent of image B, and (D) a punch biopsy of treated skin in a hanging insert organ culture setup.** (Microneedle device used = 5 × 700μm, Georgia Institute of Technology; each microneedle coated with approximately 0.4 μg fluorescent Accell Red sd-siRNA)

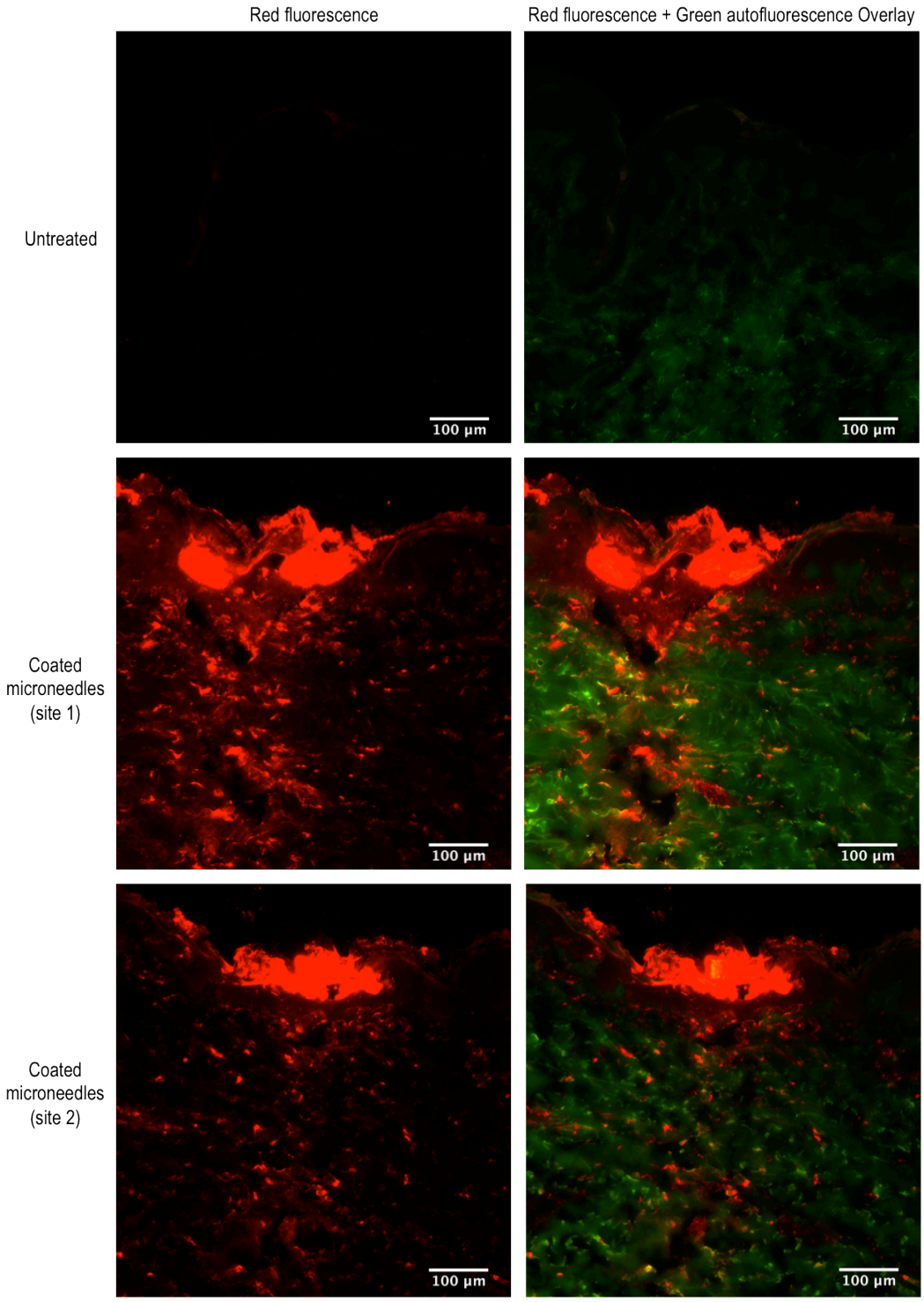

Figure 5.15: Fluorescent transverse section images of excised human breast skin of a 49-year-old female subject treated with Accell Red sd-siRNA-coated microneedles at 24 h post-delivery. Skin section autofluorescence was pseudocoloured green and red fluorescent from the sd-siRNA was pseudocoloured red (Microneedle device used = 5 × 700µm, Georgia Institute of Technology; each microneedle coated with approximately 0.4 µg fluorescent Accell Red sd-siRNA)

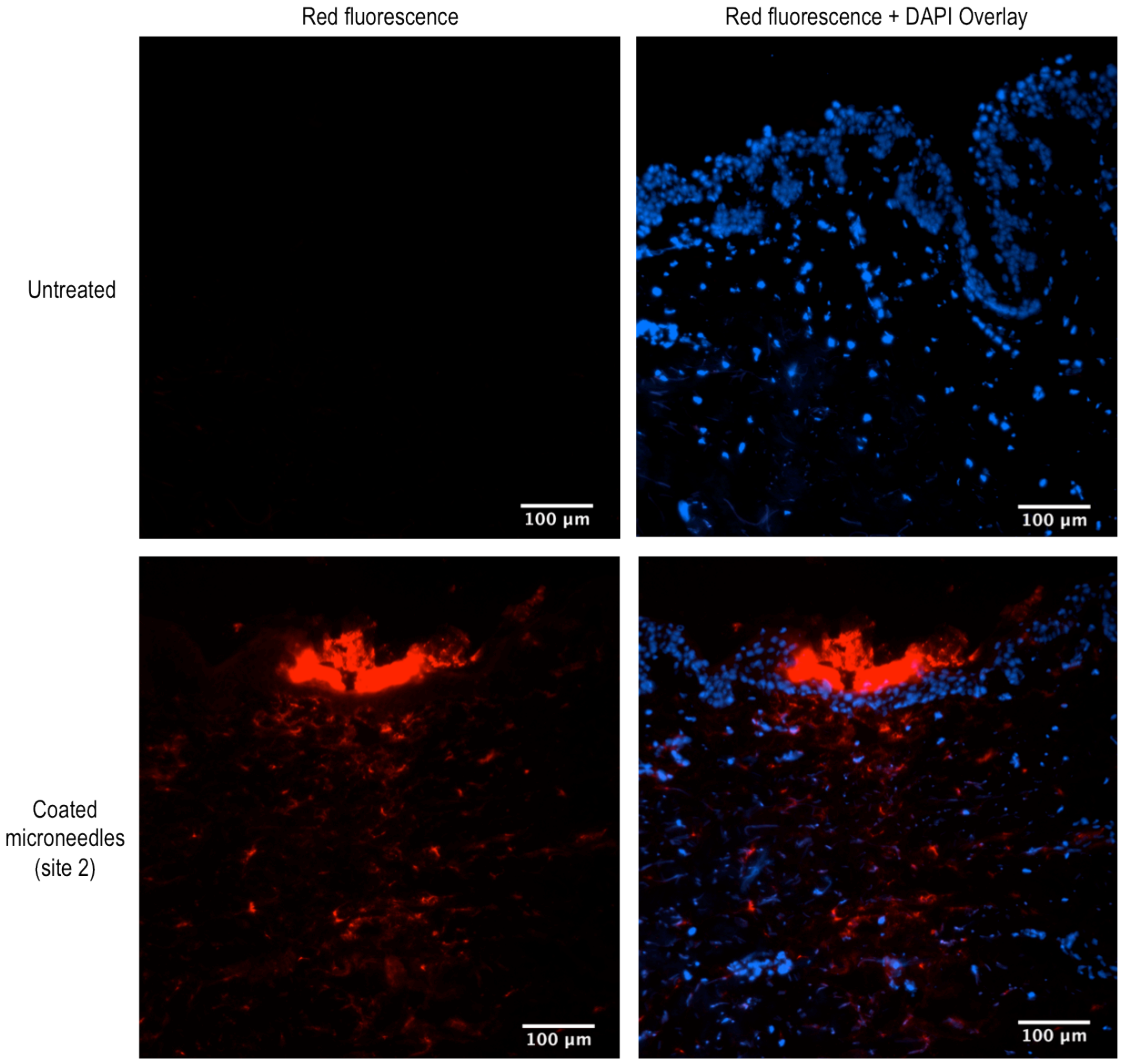

Figure 5.16: Fluorescent transverse section images of excised human breast skin of a 49-year-old female patient treated with Accell Red sd-siRNA-coated microneedles at 24 h post-delivery. Red fluorescent from the sd-siRNA was pseudocoloured red and Hoechst 33342 nuclei counterstain was pseudocoloured blue. (Microneedle device used = 5 × 700µm, Georgia Institute of Technology; each microneedle coated with approximately 0.4 µg fluorescent Accell Red sd-siRNA)

If therapeutic siRNA is delivered to the deeper layer of the dermis where blood vessels are present, the effect of systemic siRNA absorption needs to be taken into consideration. Unmodified siRNA is vulnerable to rapid degradation by nucleases present in serum, therefore siRNA is probably degraded following clearance from the skin into the blood stream or tissues with higher nuclease activity (Hickerson et al. 2008; Layzer et al. 2004). Unmodified siRNA also has a rapid renal clearance with a reported elimination half-life of 6 min (Soutschek et al. 2004). On the other hand,

modified siRNA conjugated with cholesterol resulted in significantly increased stability *in vivo* with elimination half-life up to 95 min (De Paula et al. 2007; Soutschek et al. 2004). This raises safety concerns of local cutaneous siRNA delivery with regards to systemic side effects. Some skin conditions are dominant-negative genetic skin disorders with gene mutation that only occurs within a particular cell population in the skin (Leachman et al. 2008). Properly designed siRNA targeting mRNA specific to the local genetic mutation coupled with prior testing to establish minimal off target effects and nonspecific gene silencing could address this safety concerns as systemically absorbed siRNA will have no target to cause side-effects.

The epidermal distribution and uptake effect of fluorescently labelled Accell Red sd-siRNA over 48 h post-delivery with coated microneedles was investigated by fluorescent microscopy of epidermal sheets separated chemically using ammonium thiocyanate (Figure 5.17). For samples at 0 h, the skin sample was treated by coated microneedle insertion for 10 min before microneedle withdrawal. The sample was then immediately incubated in ammonium thiocyanate for 30 min for epidermal sheet separation before epidermal sheet fixing in paraformaldehyde. Therefore, the treated skin epidermis sample at 0 h has in fact been exposed to siRNA for 10 min before epidermal sheet separation and 40 min before epidermal sheet fixation.

From Figure 5.17, fluorescent sd-siRNA was present in cells proximal (within approximately 50 μm) to the penetration site at 0 h. siRNA deposition appeared more diffused (approximately 100 μm) at 3 h, with brighter sd-siRNA fluorescence in cells proximal (approximately 50 μm) to the delivery site. At 6 h, the area of siRNA diffusion was similar to 3 h but the area of brighter sd-siRNA fluorescence in cells proximal to the delivery site reduced to approximately 30 μm. Fluorescent signal intensity appeared to be reduced at 24 h and further reduced at 48 h with an approximate siRNA diffusion area of 70 μm at 24 h and 40 μm at 48 h. Brighter sd-siRNA fluorescence in cells proximal to the delivery site reduced to approximately 20 μm at 24 h and to almost non-existence at 48 h. The rate of fluorescent siRNA signal reduction seems to be consistent with that observed in monolayer cell culture of human keratinocyte cells (Chapter 4), whereby siRNA fluorescent intensity was highest at 3 h and fluorescent intensity visibly reduced after 24 h.

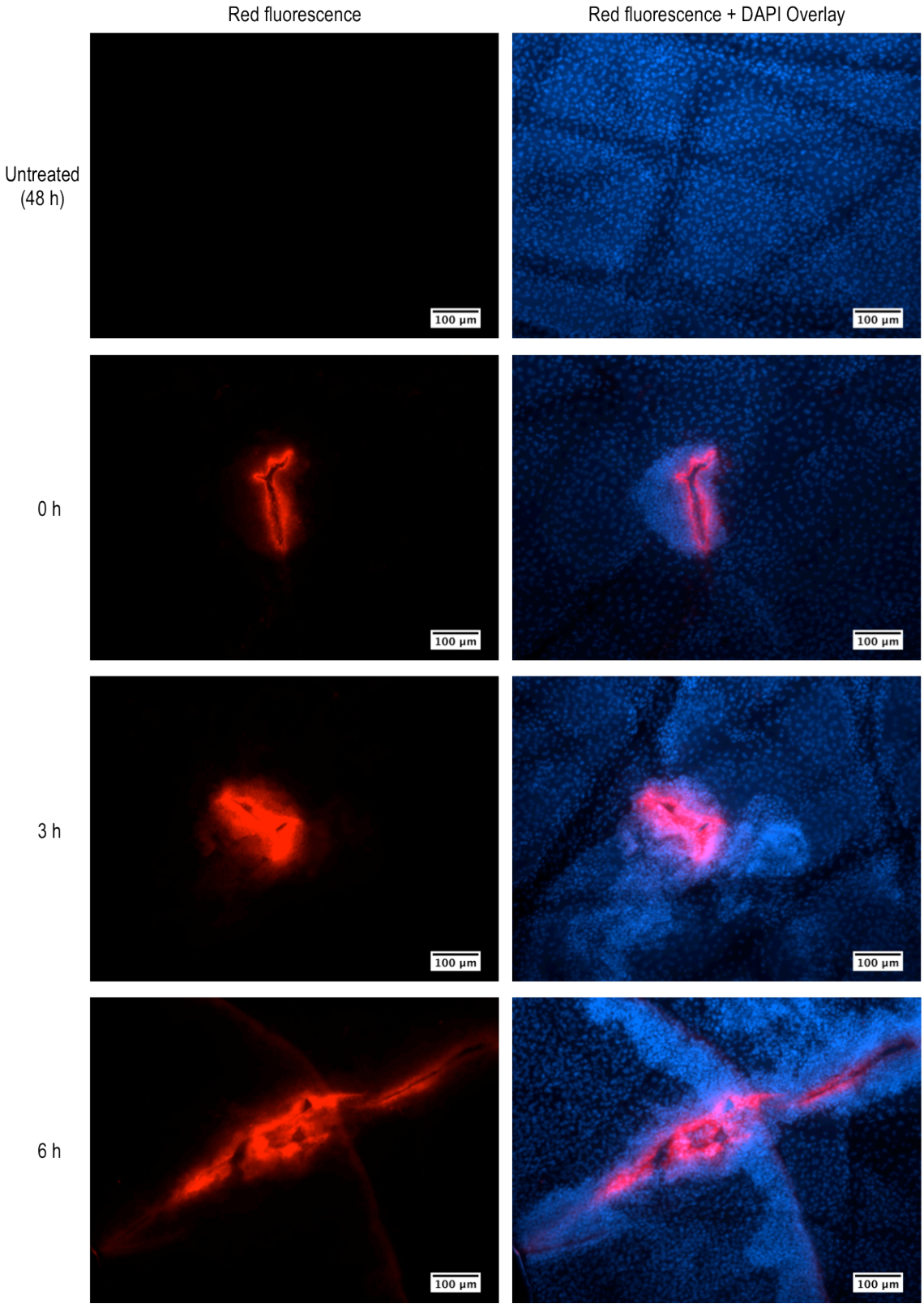
Red fluorescence
Red fluorescence + DAPI Overlay
Untreated (48 h)
0 h
3 h
6 h
100 µm

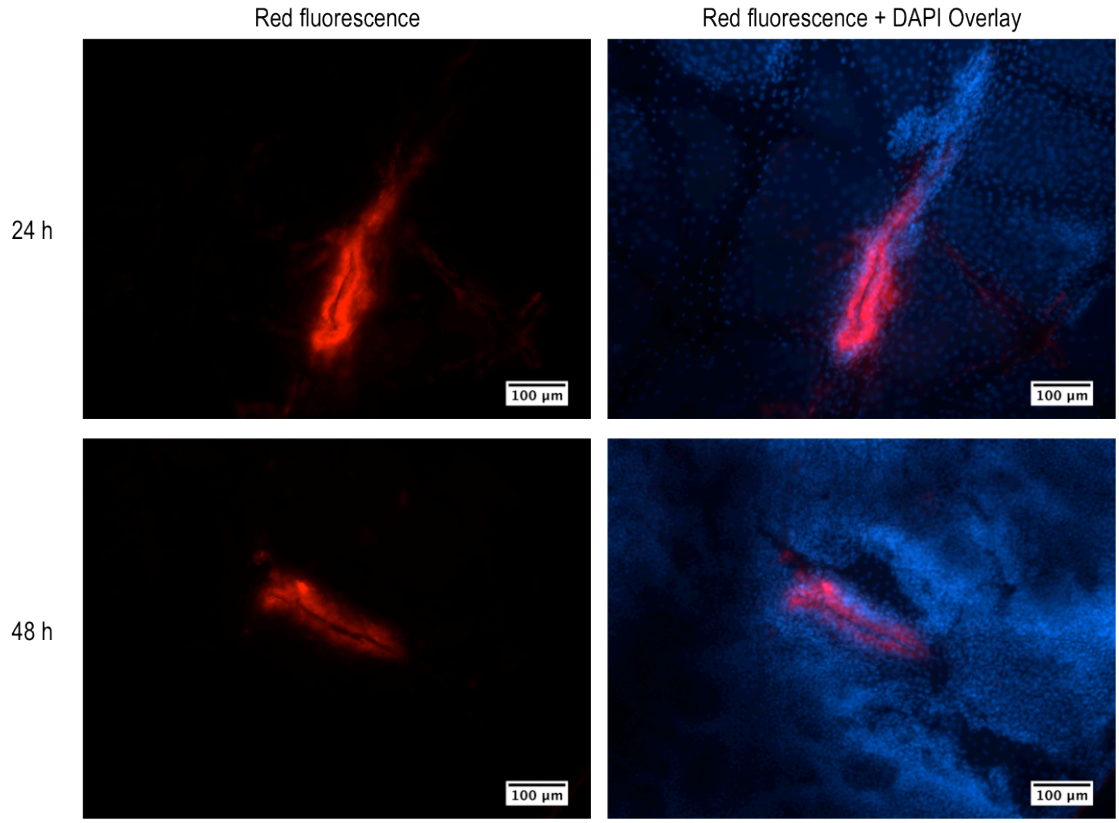

Figure 5.17: Fluorescent images of the excised human breast skin epidermis of a 51-year-old female patient treated Accell Red sd-siRNA-coated microneedles at 0 h, 3 h, 6 h, 24 h and 48 h post-delivery. Red fluorescence from the sd-siRNA was pseudocoloured red and Hoechst 33342 nuclei counterstain was pseudocoloured blue. (Microneedle device used = 5 × 700µm, Georgia Institute of Technology; each microneedle coated with approximately 0.4 µg fluorescent Accell Red sd-siRNA)

Flow cytometry was performed on epidermal cells extracted from 3 human skin specimens that had been microneedle treated with coated Accell Red sd-siRNA 24 h previously. Flow cytometric analysis revealed siRNA uptake of between 10.1% and 30.6% in epidermal cells of 3 excised human skin specimens treated with fluorescently labelled Accell Red sd-siRNA (Figure 5.18).

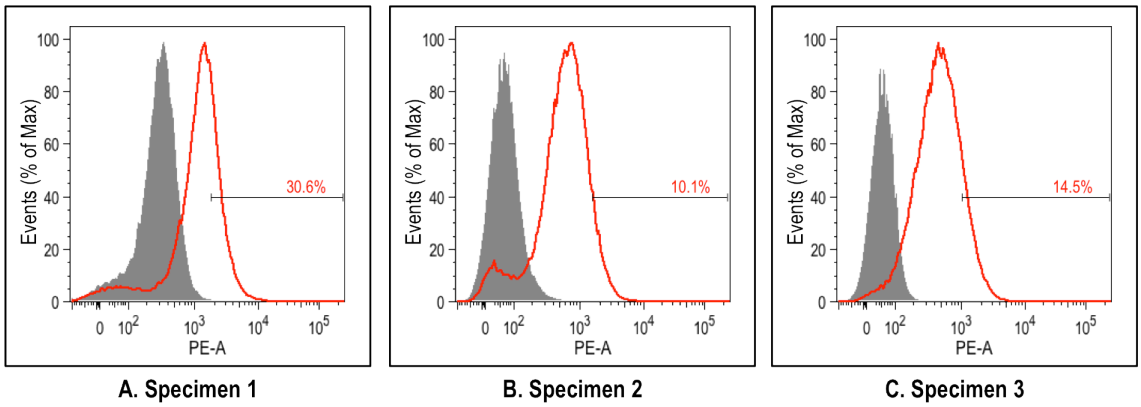

Figure 5.18: Flow cytometry histograms showing fluorescent signal intensity in epidermal cells extracted from excised human breast skin of (A) 49-year-old, (B) 78-year-old and (C) 38-year-old female patients treated with Accell Red sd-siRNA-coated microneedles at 24 h post-delivery. Histograms are overlays of untreated (solid grey) and Accell Red sd-siRNA (red line). Fluorescent cells were gated with reference to the shift in fluorescent signal intensity in HaCaT cells treated with Accell Red sd-siRNA at 24 h (considered as fluorescence due to siRNA uptake, fluorescence intensity below that considered as fluorescence of siRNA stuck to the outermembrane of cells). The percentages of cells gated were expressed in red for Accell Red sd-siRNA. (Microneedle device used = 5 × 700μm, Georgia Institute of Technology; each microneedle coated with approximately 0.4 μg fluorescent Accell Red sd-siRNA; each treatment group (epidermis from two 8 mm diameter punch biopsies) treated with approximately 10 μg Accell sd-siRNA)

In skin samples treated with Accell Red sd-siRNA, a shift of fluorescence intensity above the untreated baseline was observed in almost all cells in the sample. Cell extraction was a 3 h process involving enzymatic separation of epidermis from the dermis, cell dissociation with trypsin and then DNase incubation with multiple centrifugation steps. During the cell extraction steps, cells were kept viable and it is possible that cell activity would have resulted in fluorescent siRNA diffusion from cell to cell, resulting in a shift in fluorescent signal above baseline fluorescence in a proportion of cells that were not proximal to the siRNA delivery site. Cells were gated so that cells that have obviously taken up siRNA and not cells with siRNA stuck to the outermembrane were selected. As a positive control, HaCaT cells that were treated with the same fluorescent sd-siRNA for 24 h or flow cytometry compensation beads labelled with a similar fluorophore were processed together with all skin specimens and a

narrow gate that was representative of the positive control population was used to define epidermal cells that have taken up siRNA. Even with the cautious fluorescent shift gating, it was difficult to establish the validity of the flow cytometry data without further optimisation. Development of a more robust technique to measure fluorescent siRNA uptake in the skin is required and could be exploited in the future.

Epidermal cells from two of the same patient samples were further subjected to confocal microscopy in the absence (Figure 5.19) and presence (Figure 5.20) of nuclei counterstain with Hoechst 33342. Confocal images from the human skin specimens (Figure 5.19) showed low levels of fluorescence in most cells with high levels of fluorescence in a few cells. The 3 h long cell extraction process mentioned involves many incubation steps with high volumes of reagents that could have diluted any freely diffusing fluorescent sd-siRNA present in the reagents several fold. Therefore, it is unlikely that cells that have not taken up siRNA during the skin incubation period of 24 h would have taken up sufficient siRNA for intense fluorescence over the 3 h tissue processing time. It was therefore encouraging to be able to detect cells with intense red fluorescence using confocal microscopy.

Specimen 2 was also imaged with fluorescent channels for the near-IR live dead marker (performed prior to cell fixation) and also the Hoechst 33342 nuclei counterstain (performed after flow cytometry) (Figure 5.20). Dead cells that have taken up the near-IR live dead marker (pseudocoloured green) displayed low level of red autofluorescence in the same channel as the fluorescently labelled Accell Red sd-siRNA. This can be seen from the image of the control cells whereby red fluorescence was not present in any live cells (live cells are not stained by the live dead marker). In treated cells, all cells had a low level of red fluorescent signal including the live cells and higher levels of red fluorescent signal were found in some live cells, which clearly indicates siRNA uptake in those cells. The results from confocal microscopy support the flow cytometry studies, providing evidence that epidermal cells, presumably proximal to the microneedle penetration site, are able to take up Accell sd-siRNA delivered via coated microneedles.

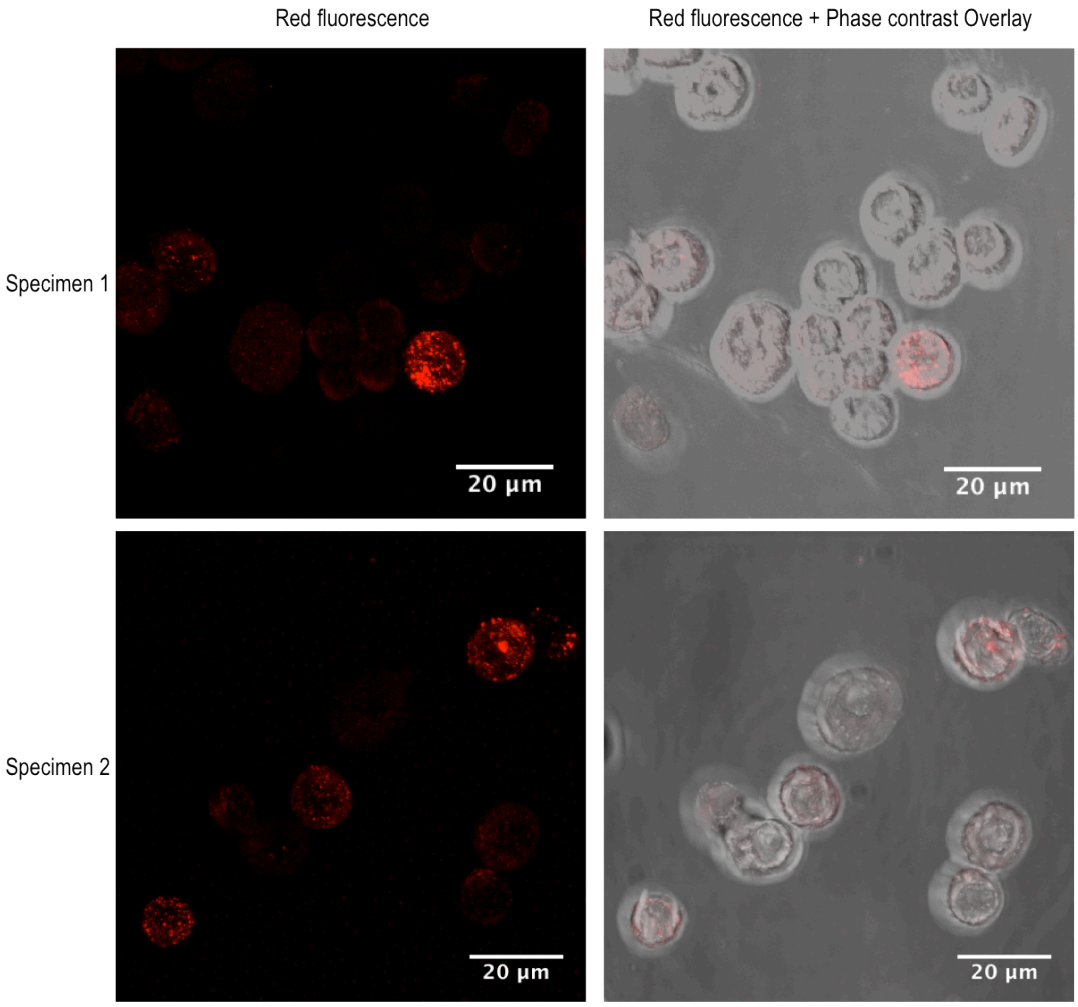

Figure 5.19: Fluorescent (left column) and fluorescent and phase contrast overlay (right column) confocal images of epidermal cells extracted from excised human breast skin epidermis of 49-year-old (Specimen 1) and 78-year-old (Specimen 2) female patients treated with Accell Red sd-siRNA-coated microneedles at 24 h post-delivery. Red fluorescent from the sd-siRNA was pseudocoloured red. Each image is a z-stacked projection of approximately 30 slices of images taken over a cell layer thickness of approximately 20 µm. (Microneedle device used = 5 × 700µm, Georgia Institute of Technology; each microneedle coated with approximately 0.4 µg fluorescent Accell Red sd-siRNA; each treatment group (epidermis from two 8 mm diameter punch biopsies) treated with approximately 10 µg Accell sd-siRNA)

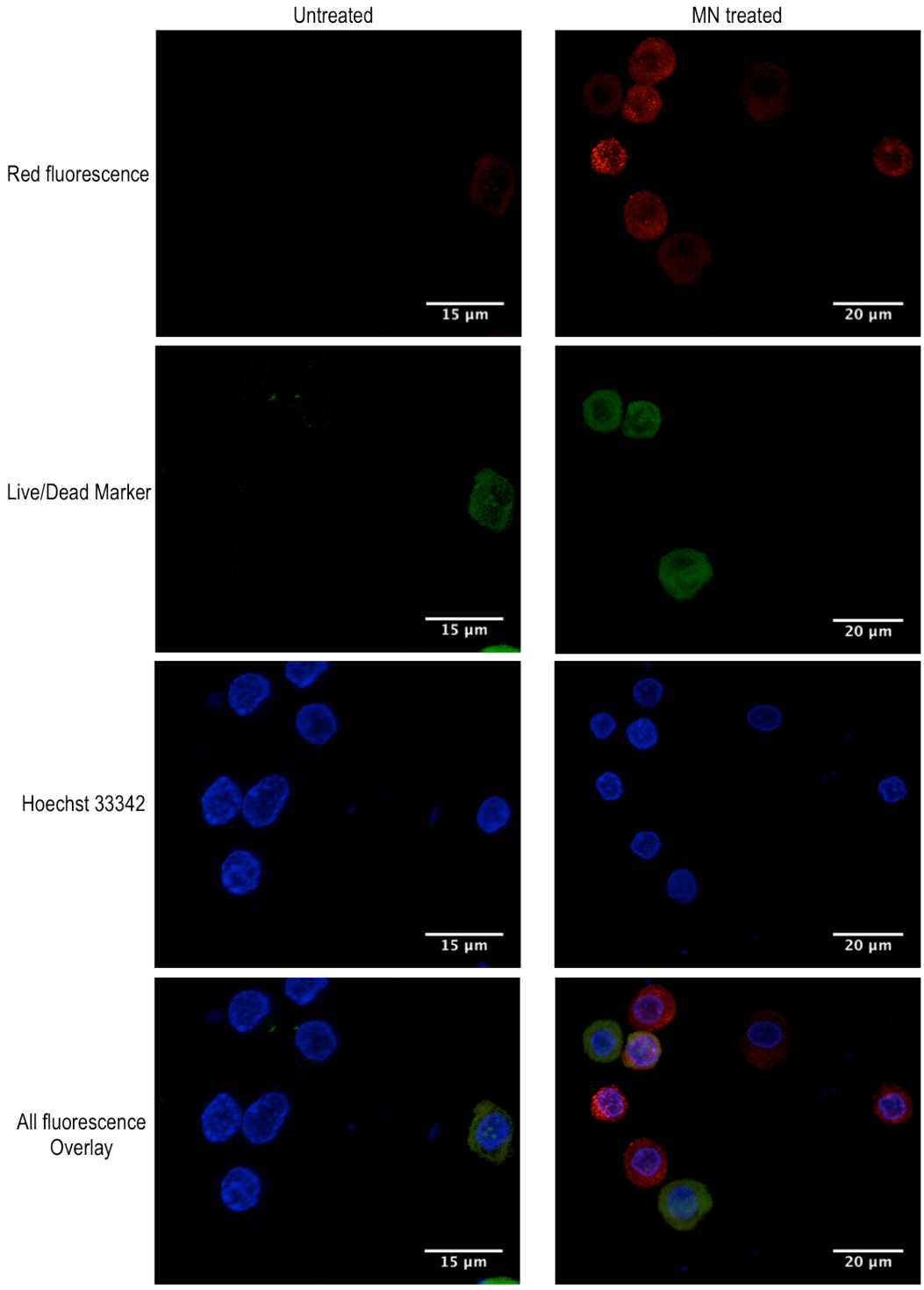

Figure 5.20: Fluorescent confocal images of epidermal cells extracted from excised human breast skin epidermis of a 78-year-old (Specimen 2) female patient treated with Accell Red sd-siRNA-coated microneedles at 24 h post-delivery. Red fluorescent from the sd-siRNA was pseudocoloured red, near infrared fluorescent from live dead marker pseudocoloured green and Hoechst 33342 nuclei counterstain was pseudocoloured blue. Each image is a z-stacked projection of approximately 30 slices of images taken over a cell layer thickness of approximately 20 µm. (Same sample as Figure 5.19 specimen 2)

Several published *in vivo* studies with animal models have reported successful delivery and cellular uptake of fluorescently labelled Accell sd-siRNA to adult rat brain (Nakajima et al. 2012) and mouse footpad skin (Gonzalez-Gonzalez et al. 2010b). In the study with mouse footpad skin, siGLO Red non-sd-siRNA was directly compared with Accell Red sd-siRNA following soluble protrusion array device (PAD) delivery. PAD is essentially a soluble microneedle device made of polyvinyl alcohol (PVA) polymer. siGLO Red non-sd-siRNA was found to moderately distribute in the epidermis near the deposited "plug" with no clear evidence of cellular uptake. In contrast, Accell Red sd-siRNA appeared more widely distributed throughout the epidermis of mouse paw with red fluorescence signal that localised mainly in the perinuclear region of epidermal cells, suggesting cellular uptake and localisation in the cytoplasm (Gonzalez-Gonzalez et al. 2010b).

Fluorescent sd-siRNA distribution in human skin epidermis seems to be localised to the microneedle penetration site (Figure 5.17). Accell Red sd-siRNA in the human skin study was delivered to skin surface that had been swapped with 70% isopropyl alcohol, which could have dehydrated the surface of the skin. The thicker coat of siRNA deposited at the microneedle penetration site resulted in intense fluorescence overexposure at the deposition sites (Figure 5.16 and 5.17), which could have led to a false negative visualisation of siRNA uptake in cells further away from the deposition sites. In the mouse skin study, PAD microneedles are more closely spaced (1 mm spacing) (Gonzalez-Gonzalez et al. 2010b) than in-plane steel microneedles (1.5 mm spacing). The difference in observed Accell Red sd-siRNA distribution in *in vivo* mouse skin and *ex vivo* human skin could also be attributed to interspecies variability in skin architecture (Godin and Touitou 2007). Also, siRNA delivered to *in vivo* mouse footpad skin, where the treated mouse is allowed to regain consciousness following anaesthetic effect and roam around the cage, might have aided siRNA distribution throughout the footpad skin layers.

Nevertheless, Accell sd-siRNA is shown to be readily taken up by keratinocyte cells in monolayer cell culture, including primary keratinocyte cells extracted from freshly excised human breast skin, as demonstrated in the preceding chapter (Chapter 4). Keratinocytes are the main cell population in human skin epidermis and taken together these results provide confidence that if Accell sd-siRNA is deposited in the viable layer

of the epidermis with minimally invasive microneedle devices, it should be taken up at least by cells proximal to the deposition area. For more widespread distribution of Accell sd-siRNA in human skin epidermis, siRNA can be delivered using more closely spaced microneedles in an array or multiple devices can be delivered to the same treatment area to maximise skin deposition area.

5.3.4 *Ex vivo* gene silencing in excised human breast skin

Subsequent studies were performed in an attempt to detect functional gene silencing in excised human breast skin following Accell CD44 sd-siRNA delivery *via* coated steel microneedles. Steel microneedles were coated with either Accell CD44 sd-siRNA or Accell TD101 non-targeting control sd-siRNA and then delivered to 6 freshly excised human skin specimens (Table 5.1). CD44 gene expression was then analysed 48 h post-delivery by RT-qPCR to determine the levels of siRNA mediated gene silencing.

Table 5.1: List of human breast skin specimens with their respective age that were treated with functional Accell sd-siRNA-coated microneedles.

Human Skin Specimen No.	Age (-year-old)	Gender
1	unknown	Female
2	54	Female
3	54	Female
4	70	Female
5	69	Female
6	50	Female

The ability to coat steel microneedles with siRNA of high concentration (siRNA solubility of up to 200 mg mL^{-1}) allows the loading of high doses of siRNA onto steel microneedles (up to 40 μg). Coating using the pipette tip coating method provides accurate estimation of *theoretical maximum* siRNA loading onto the surface of steel microneedles based on known siRNA concentration and predetermined coating reservoir volume. siRNA coated onto steel microneedles can then be recovered by washing in a small volume of buffer, the concentration of nucleic acid of which can be quantified using high sensitivity UV spectrophotometer to establish the efficiency of the coating technique by quantifying the actual amount of siRNA loaded onto the microneedle devices (Chong et al. 2013). The optimised microneedle coating and

siRNA recovery techniques lead to the ability to accurately quantify siRNA deposition payload in the skin after microneedle delivery.

For each human skin specimen, 12 microneedle devices were coated, 4 of which were randomly selected for siRNA recovery for quantification to determine the average siRNA coating dose (pre) and the remaining 8 devices were delivered to the excised human breast skin. The amount of siRNA left on the microneedle devices after (post) delivery to human skin was then recovered and quantified (Figure 5.21).

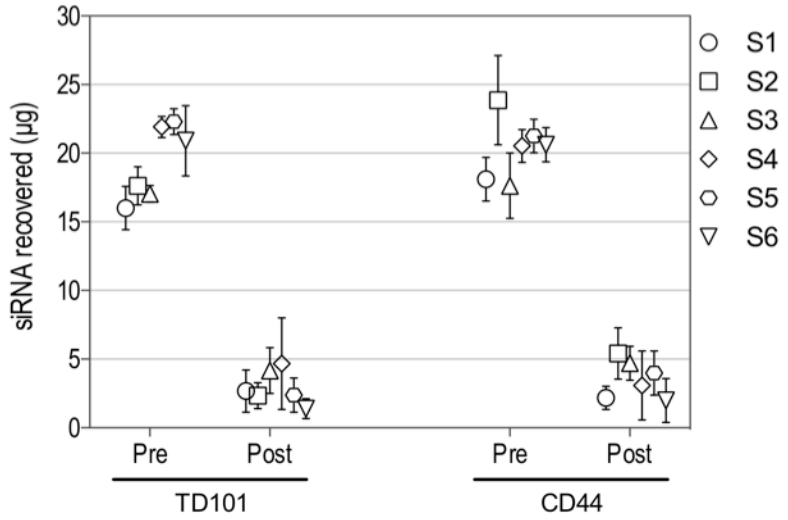

Figure 5.21: Accell sd-siRNA coating recovered from the surface of steel microneedles pre- and post-insertion into excised human breast skin. A theoretical maximum loading mass of 20 µg of sd-siRNA per device was loaded (pre). (Microneedle device used = 5 × 700µm, Georgia Institute of Technology; TD101 = Accell TD101 non-targeting control sd-siRNA; CD44 = Accell CD44 sd-siRNA; n = 4 for pre; n = 8 for post; error bar = standard deviation; S1 to S6 = human skin specimens with age specified in Table 5.1)

As depicted in Figure 5.21, for a theoretical maximum loading dose of 20 µg, between 16.0 ± 1.58 µg and 23.9 ± 3.26 µg Accell sd-siRNA was coated onto the microneedle device. Between 73.3 ± 7.02 % and 93.3 ± 3.48 % siRNA was then deposited into excised human breast skin (Figure 5.22), leaving between 1.4 ± 0.73 µg and 5.4 ± 1.87 µg siRNA on the microneedles post-insertion into human skin (Figure 5.21). The ability to accurately determine theoretical maximum nucleic acid loading and then quantify delivery dose *via* coated steel microneedles is a novel achievement (Chong et al. 2013)

as previously reported microneedle delivery dose was based on rough estimates of drug loading and presumed delivery dose estimated from average depth of coated microneedle penetration (Gill and Prausnitz 2007a; Gill et al. 2010; Gonzalez-Gonzalez et al. 2011) or estimation based on observed microneedle tip dissolution in the case of soluble microneedle devices (Gonzalez-Gonzalez et al. 2011; Lara et al. 2012).

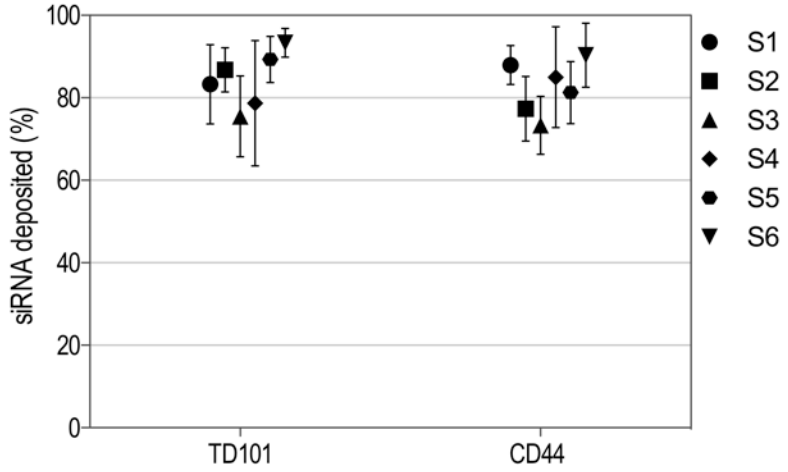

Figure 5.22: Percentage of Accell sd-siRNA deposited into excised human breast skin specimens as calculated from Figure 5.21. (Microneedle device used = 5 × 700μm, Georgia Institute of Technology; TD101 = Accell TD101 non-targeting control sd-siRNA; CD44 = Accell CD44 sd-siRNA; n = 8; error bar = standard deviation; S1 to S6 = human skin specimens with age specified in Table 5.1)

Skin penetration after blank and coated steel microneedle insertion on freshly excised human breast skin was compared using the OCT imaging system (Figure 5.23). The *en face* projection showed contrasting darkened spots that represent the microneedle penetration sites following blank microneedle insertion. The distinct penetration marks appeared to be more obvious than the penetration marks left by *in vivo* blank microneedles insertion in the back of hand and forearm skin of male volunteers (Figure 5.8, 5.9 and 5.10). Transverse sections across the microneedle penetration sites revealed distinct microchannels on the skin epidermis and neighbouring superficial dermis as a result of blank microneedle insertion (Figure 5.23). In contrast, the appearance of microneedle penetration marks left by siRNA-coated microneedles was less contrasting with the natural skin tone of the *en face* projection. It is possible that whilst blank steel microneedles created what seemed like empty micron-scale channels, coated steel

microneedles may have deposited the siRNA payload into the microchannel, leaving a less obvious conduit. Transverse sections across the microneedle penetration sites revealed distinct microchannels that were not as wide or deep as those left by blank microneedles. This indicates that siRNA might have been deposited in the channels. However, this is an isolated observation, which needs to be repeated in more samples but is a nevertheless an encouraging observation.

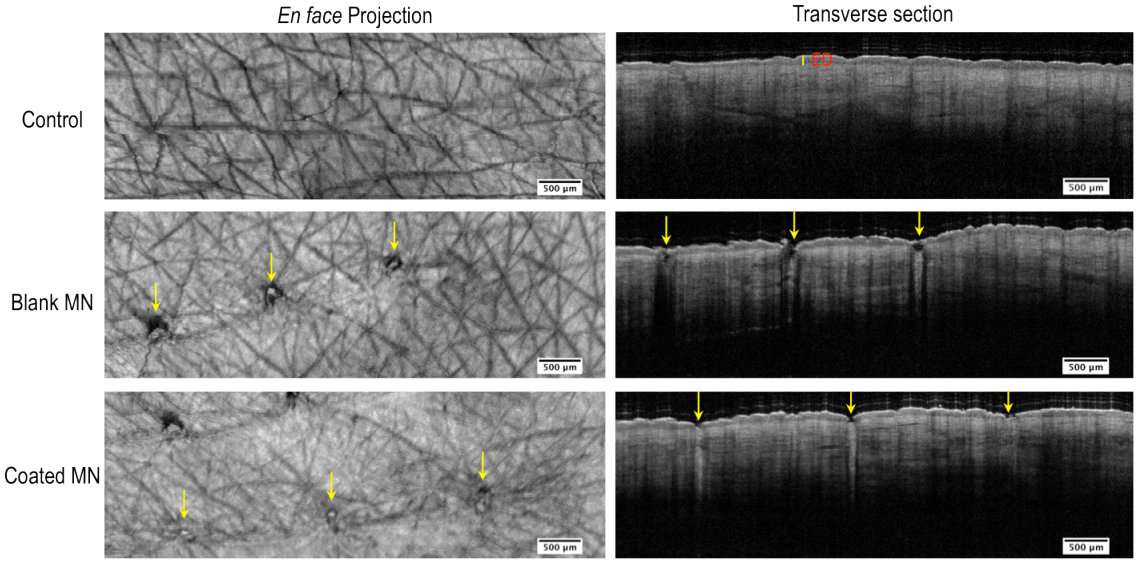

Figure 5.23: ***En face*** **and transverse sections of blank microneedle and siRNA coated microneedle (both devices 5 x 700µm, Georgia Insititute of Technology) penetration sites on excised human breast skin of a 38-year-old female patient at 0 h after microneedle insertion obtained through** ***in vivo*** **O.C.T. imaging.** Transverse sections were from the middle regions of the control *en face* images or reslices across the microneedle penetration sites of the treated *en face* images. (Each coated microneedle coated with approximately 4 µg Accell CD44 sd-siRNA; Yellow line = thickness of the epidermis; Yellow arrow = microneedle penetration site; ED = epidermis)

Finally, siRNA mediated gene silencing *ex vivo* was determined by quantifying mRNA levels of target gene (CD44) in excised human breast skin specimens that were treated with Accell CD44 sd-siRNA or Accell TD101 non-targeting control coated microneedles. Steel microneedles were inserted in the same orientation depicted in Figure 5.1, left in place for 10 min to allow sufficient time for the siRNA payload to dissolve before microneedle withdrawal. The treated skin area was then biopsied as shown in Figure 5.2. It was previously estimated that approximately 16.7 µg siRNA was

deposited from each microneedle device (Figure 5.21 and 5.22). Each treatment area was treated with 20 microneedles from 4 devices and approximately 16 microneedle puncture sites were in each 8 mm punch biopsy that was subsequently cultured for 48 h in a hanging insert organ culture setup before epidermal separation for RNA extraction and RT-qPCR quantification of the CD44 mRNA levels (Figure 5.24). Each treatment group (each bar on Figure 5.24), for which total RNA was extracted from two 8 mm diameter punch biopsies, was treated with approximately 53.4 μg siRNA.

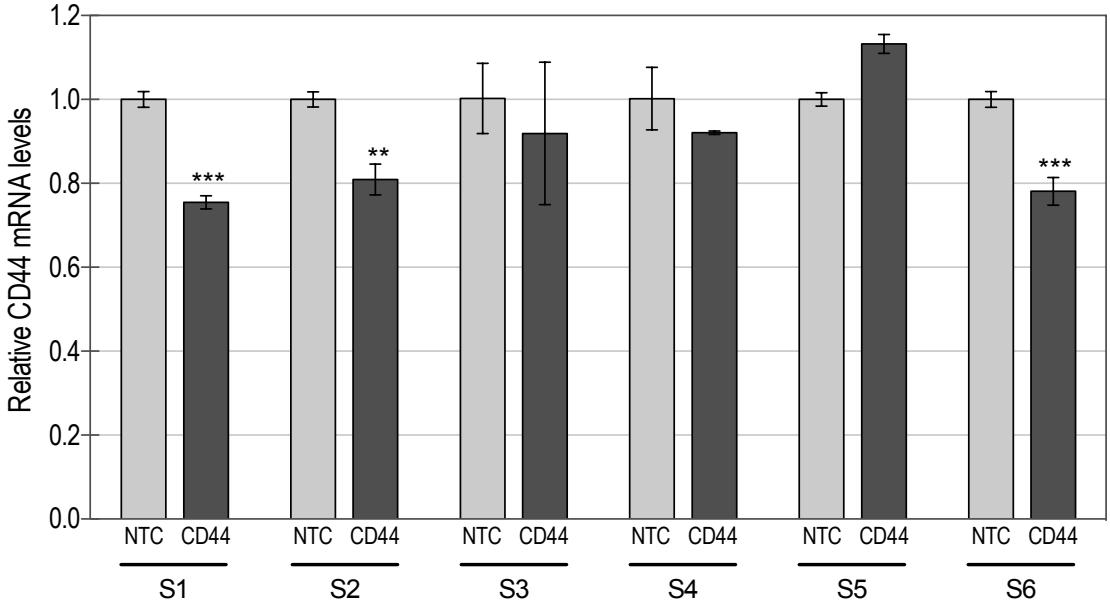

Figure 5.24: CD44 mRNA levels in epidermal cells of human skin specimens treated with Accell CD44 sd-siRNA-coated microneedles at 48 h post-transfection. CD44 mRNA levels were relative to the non-targeting control (NTC) groups at each respective time-points and normalised to GAPDH endogenous control gene levels. (Microneedle device used = 5 × 700μm, Georgia Institute of Technology; NTC = Accell TD101 non-targeting sd-siRNA; CD44 = Accell CD44 sd-siRNA; n = 3 qPCR assay replicates; error bar = standard deviation; unpaired two-tailed t-test *** = significant reduction in mRNA levels compared with non-targeting control, $p < 0.0001$; ** = $p < 0.001$)

Significant CD44 mRNA reduction of 19.1 to 24.5% was found in 3 out of 6 treated skin specimens (specimen 1, 2 and 6). Insignificant CD44 mRNA reduction was found in another 2 skin specimens (specimen 3 and 4) and an increase in CD44 mRNA (specimen 5) was found in the remaining skin specimen. Consistent targeted mRNA reduction in skin tissue proved to be challenging, as the human skin is arguably the

most complex organ of the human body (Coulman et al. 2006a; Menon 2002). The human skin epidermis is formed from dividing basal keratinocytes that progressively differentiate and mature to form multiple skin layers in the viable epidermis over approximately 14 days. Cell differentiation and maturation terminates in the stratum corneum with the formation of anucleated keratin-filled corneocyte cell layer anchored in a lipophilic matrix to form densely cross-linked protein structure (Bouwstra and Honeywell-Nguyen 2002; Menon and Elias 2001).

With constant cell differentiation in the viable layer of the skin epidermis and shedding of the stratum corneum, it is difficult to observe changes in mRNA levels mediated by siRNA following a single dose administration of siRNA. Most *in vivo* studies involving siRNA delivery to the skin have daily or every alternate day dosing regime over a 2 to 4 week period (Gonzalez-Gonzalez et al. 2010b; Hickerson et al. 2011; Lara et al. 2012). It is technically impossible to apply a multiple dosing regime on excised human breast skin cultured in an *ex vivo* environment as skin removed from its *in vivo* environment deteriorates rapidly over time (Ng et al. 2009). Furthermore, physiological variability may exist between different skin donors that may affect treatment outcome and rate of skin deterioration during culture. From the point of surgery, excised human skin is stored and collected in organ culture medium at 4°C until the experiments were performed. The time lapse between human skin excision and skin treatment may have affected the freshness or viability of some of the excised skin samples. Moreover, the spacing and orientation of steel microneedles applied in these studies seem to deliver siRNA to cells proximal to the penetration site with localised siRNA diffusion, leaving the large surface area on the skin sample inaccessible to deposited siRNA.

A recently published study (by a collaborating research group who provided the functional Accell sd-siRNA) demonstrated convincing CD44 gene silencing following Accell CD44 sd-siRNA delivery *via* soluble PAD microneedles on human skin equivalent grafted on immunocompromised mice (Lara et al. 2012). On each mouse, human skin graft of approximately 2×2 cm^2 was microneedle treated with an estimated (base on observed average needle erosion) daily dose of 15 μg siRNA per mouse for 10 days. For each treatment day, three consecutive arrays of 5×5 microneedle arrays with 2 mm spacing between each microneedle was applied over the same treatment area. CD44 inhibition of 45±6% was observed after CD44 sd-siRNA (n = 5) treatment of the skin

xenografts compared with non-specific sd-siRNA (n = 3). The observed reduction in CD44 mRNA levels was also supported by immunofluorescence of CD44 protein levels in histology sections of the skin samples (Lara et al. 2012). It appears that future clinical dosing of cutaneous siRNA delivery should involve frequent dosing with multiple applications of microneedle devices over the same treatment area to maximise surface area of siRNA deposition.

5.4 Conclusion

The studies performed in this chapter provided strong evidence for the use of steel microneedles as a minimally invasive skin disruption method to deliver siRNA to the skin. Steel microneedles have been shown to penetrate the skin stratum corneum to deposit its coated siRNA payload in the viable epidermis as well as the dermis along the length of microneedle penetration. *In vivo* and *ex vivo* OCT skin imaging following microneedle penetration highlights the difference between the biomechanical properties of the skin in its natural *in vivo* environment and excised skin used in laboratory settings. Nevertheless, excised human skin represents a pre-clinical skin model with the closest skin architecture resemblance to *in vivo* human skin.

Overall, the series of *ex vivo* skin experiments performed in this chapter highlights the difficulty in designing robust siRNA delivery and gene silencing detection studies in excised human skin. Fluorescent siRNA delivery studies provided information on siRNA deposition in excised human skin following microneedle administration and the diffusion characteristics of siRNA from the deposition sites. Quantification of cellular siRNA uptake with flow cytometric analysis was inconclusive but was confirmed by confocal microscopy whereby cells with visible cytoplasmic siRNA presence were observed. Gene silencing detection results were not consistent, as target mRNA reduction was significant in only 3 out of 6 human skin specimens. Given the single dosing regime applied in the study as well as the short duration of excised skin viability, it was remarkable to be able to detect gene silencing in an organ as structurally complex as the human skin.

The techniques and knowledge acquired from these studies provides useful insight towards future development of clinical gene delivery strategies targeting the human skin. The positive results published on *in vivo* delivery of Accell sd-siRNA (Chong et al. 2013; Gonzalez-Gonzalez et al. 2010b; Lara et al. 2012) coupled with the efficiency of Accell sd-siRNA in monolayer *in vitro* culture of keratinocyte cells (Chapter 4) further supports the use of the modified sd-siRNA for local delivery of siRNA to the skin for the treatment of skin conditions caused by aberrant gene expression.

CHAPTER 6

Delivery of nucleic acids to *in vivo* skin models

6 Delivery of nucleic acids to *in vivo* skin models

6.1 Introduction

It has previously been mentioned that the laboratory model with closest structural resemblance to *in vivo* human skin is excised human skin, cultured in an *ex vivo* environment. In the preceding chapter (Chapter 5), despite evidence of cellular uptake of fluorescent siRNA in *ex vivo* human skin, consistent detection of siRNA mediated gene silencing at the cellular level was not achieved. There were inherent difficulties in maintaining viability of long-term culture of excised human skin to accommodate the need for multiple siRNA dosing over a period of 7 to 14 days, as excised human skin deteriorates rapidly after 72 h in culture (Ng et al. 2009).

Although *in vivo* mouse skin models are not representative of human skin, they have widely been used in laboratory testing of nucleic acid delivery to the skin (Gonzalez-Gonzalez et al. 2011; Gonzalez-Gonzalez et al. 2009; Gonzalez-Gonzalez et al. 2010b; Hengge et al. 1996; Hsu and Mitragotri 2011; Inoue et al. 2007; Meykadeh et al. 2005; Nakai et al. 2010; Nakai et al. 2007). The skin barrier layer, the stratum corneum is also present in mouse skin, which can be tested for disruption by microneedle devices (Chong et al. 2013; Gonzalez-Gonzalez et al. 2011; Gonzalez-Gonzalez et al. 2010b). As part of the NIH "GO Delivery!" grant collaboration, a visit was made to laboratories in Stanford University and Transderm Inc. in the USA to share the coated steel microneedles gene delivery system, to take advantage of the sophisticated animal models and analysis tools available in collaborators' facilities and to exchange gene delivery expertise between laboratories. This collaboration resulted in the investigation of delivery of nucleic acid such as pDNA and siRNA to mouse paw skin and transgenic mouse paw skin, respectively.

6.1.1 *In vivo* skin models for nucleic acid delivery

This thesis takes advantage of the availability of freshly excised human skin, which is the most relevant membrane for skin studies. However, the availability of fresh human skin is limited and therefore, animal skin, which includes primates, porcine, mouse, rat and guinea pig is frequently used by other research groups (Godin and Touitou 2007; Kim et al. 2012b; Wang et al. 2007). These animal skin models are more readily

available than human skin and are important in basic proof-of-concept research to improve the understanding of drug delivery across the skin barrier.

In the case of nucleic acid delivery, mouse, pig skin and human skin or human skin equivalents xenografted onto immunocompromised mice are commonly used as *in vivo* models for gene expression or silencing (Gonzalez-Gonzalez et al. 2011; Gonzalez-Gonzalez et al. 2009; Hengge et al. 1996; Hsu and Mitragotri 2011; Lara et al. 2012). Porcine skin has been shown to bear the closest structural resemblance to human skin with comparable skin permeability results (Godin and Touitou 2007) and epidermal gene expression patterns following intradermal delivery of naked pDNA (Hengge et al. 1995; Hengge et al. 1996). In porcine ear skin, the thickness of stratum corneum is approximately 17 to 28 μm and thickness of viable epidermis is approximately 60 to 85 μm (Jacobi et al. 2007), which is comparable to human skin (Huzaira et al. 2001; Lee and Hwang 2002; Sandby-Moller et al. 2003). Porcine skin is used in some *in vivo* gene delivery studies but it is used mainly as freshly excised skin, in an *ex vivo* culture environment similar to excised human skin (Hengge et al. 1996; Vogel 1999).

Rodent skins are most commonly used in *in vivo* studies due to their availability, small size, uncomplicated handling and relatively low cost. However, a study comparing gene expression in the human, porcine and mouse epidermis following intradermal pDNA injection found that mouse skin expressed the reporter gene in the epidermis, dermis and underlying fat and muscle layers whilst gene expression was found predominantly in the viable layer of the human and porcine skin epidermis (Hengge et al. 1996). The mouse skin is thin with epidermis thickness of approximately 10 μm (Hansen et al. 1984). As a consequence, it was more difficult to inject and resulted in significantly lower quantitative expression compared to human and porcine skin (Hengge et al. 1996). The reason for differences in pattern and level of gene expression in mouse skin was unclear but it is thought to be related to structural difference between mice and human or pig skin (Hengge et al. 1996).

6.1.2 Delivery of nucleic acid to mouse paw skin

The studies in this chapter describe gene delivery to mouse paw skin. The mouse paw skin is considerably thicker than other parts of the mouse body with stratum corneum

thickness of approximately 50 μm and viable epidermis thickness of approximately 100 μm (Gonzalez-Gonzalez et al. 2009). The mouse paw skin was selected for gene delivery studies due to its thickness and similarity in terms of upper skin layer composition to human skin. The collaborating group was also particularly interested in a monogenic skin disorder, pachyonychia congenita, which manifests mainly in human foot sole (Leachman et al. 2008; Leachman et al. 2009).

6.1.2.1 pUbc-luc2/eGFP reporter plasmid DNA

The pUbc-luc2/eGFP is a dual-mode reporter plasmid that co-expresses a variant of the bioluminescent firefly luciferase enzyme (luc2) fused to enhanced green fluorescent protein (eGFP) to enable localisation of regions of gene transfer and characterisation of the transfected cells within the skin. The plasmid utilises the human ubiquitin C (Ubc) promoter, which improves the uniformity of gene expression throughout the epidermal layers (Gonzalez-Gonzalez et al. 2011). The commonly utilised plasmid promoter, the human cytomegalovirus (CMV) promoter causes confined reporter gene expression in the upper layer (granular and stratum corneum) of the epidermis (Gonzalez-Gonzalez et al. 2010a; Sawamura et al. 2002).

A previously published study has reported that pUbc-luc2/eGFP pDNA coated onto steel microneedles was capable of delivering higher amounts of nucleic acid that resulted in significantly sustained and prolonged expression of reporter gene compared to soluble biodegradable protrusion array device (PAD) (Gonzalez-Gonzalez et al. 2011). In this collaborative study, the effect of increasing the amount of pDNA deposited using steel microneedle devices with different shapes (regular, serrated and concave), needle length (750μm and 500μm) and spatial density between one needle tip and another (1.6 mm and 0.8 mm) on reporter transgene expression was investigated.

6.1.2.2 Tg CBL/hMGFP mouse

The Tg CBL/hMGFP mouse that co-expresses click beetle luciferase (CBL) and humanised monster green fluorescent protein (hMGFP) genes in the skin was generated through cross-breeding of a silenced dual-reporter mouse (CBL and hMGFP) with a mouse expressing Cre recombinase driven by a keratin 14 (K14) promoter that was specific to keratinocytes (Gonzalez-Gonzalez et al. 2009). Gene expressions in the

resultant transgenic reporter mouse are driven by a synthetic "chick" β-actin (CAG) promoter, which is a hybrid of the human CMV immediate early enhancer element and β-actin promoter. The hybrid promoter results in localised gene expression in the epidermis, mainly as aggregates in the granular layer and uniformly throughout the stratum corneum. Expression of hMGFP mRNA is also confined to the upper epidermal layers (Gonzalez-Gonzalez et al. 2009). In previous studies, delivery of functional naked CBL3 non-sd-siRNA through intradermal injection (Gonzalez-Gonzalez et al. 2009) and functional Accell CBL3 sd-siRNA through PAD (Gonzalez-Gonzalez et al. 2010b) resulted in reporter gene silencing in the transgenic mouse model. The CBL3 siRNA targets the CBL coding region of the CBL/hMGFP gene.

The drug-coated steel microneedle system is a simple and cost-effective method for cutaneous delivery of sufficient doses of therapeutic nucleic acids with high reproducibility, biocompatibility and reliable skin puncture, giving the coated steel microneedle system prospective clinical advantages over alternative microneedle and other systems (Gonzalez-Gonzalez et al. 2011; Pearton et al. 2012). The ability to demonstrate gene silencing *in vivo* in a transgenic mouse model following functional delivery of Accell sd-siRNA through coated steel microneedles would further support the utility of the coated steel microneedle system for the delivery of nucleic acid to the skin.

6.1.3 Aim and objectives

The aim of this chapter was to determine the ability of steel microneedle devices in facilitating the delivery of nucleic acid to *in vivo* animal skin models and subsequently influence gene expression. The objective of the experiments were:

- To deliver reporter pDNA to mouse paw skin using the coated steel microneedle system for gene expression
- To investigate the effect of needle shapes, length and spatial density on pDNA delivery and expression
- To deliver functional siRNA to transgenic mouse paw skin using the coated steel microneedle system for silencing of reporter gene
- To quantify gene expression reduction by intravital imaging, RT-qPCR and fluorescence imaging

6.2 Methods

Unless specified, the suppliers of all reagents and materials have previously been mentioned or were obtained from Thermo Fisher Scientific, UK.

6.2.1 pUbc-luc2/eGFP plasmid DNA delivery to mouse paw

These experiments were performed at either Transderm Inc., Santa Cruz, USA under the supervision of Dr. Roger Kaspar or Stanford University, Stanford, California, USA under the supervision of Dr. Christopher Contag with the help of Dr. Emilio Gonzalez-Gonzalez and Dr. Maria Fernanda Lara. All materials except the steel microneedle devices were gifts from Dr. Roger Kaspar and Dr. Christopher Contag and were used as provided unless stated otherwise.

6.2.1.1 pUbc-luc2/eGFP plasmid DNA

The pUbc-luc2/eGFP pDNA is a 3.7 Kb construct generated by ligation of the Ubc promoter and the luc2/eGFP coding region of pFULG60 into the backbone of pCMV-hMGFP/CBL with the aid of enzyme digestions (Gonzalez-Gonzalez et al. 2011). Ready prepared pDNA solutions of 4.6 mg mL^{-1} and 9.2 mg mL^{-1} concentrations were used.

6.2.1.2 Animal models

CD1 mice (Charles River, USA) were used according to procedures approved in animal protocol number 21627 by the Administrative Panel for Laboratory Animal Care at Stanford University, using the guidelines set by the Institutional Animal Care and Use Committees of the National Institutes of Health and Stanford University.

6.2.1.3 Microneedle coating and delivery of pUbc-luc2/eGFP

6.2.1.3.1 Coating pUbc-luc2/eGFP onto microneedle devices

Steel microneedle devices (Cardiff University, UK) were coated with pUbc-luc2/eGFP pDNA using the pipette tip dip-coating method as described in section 2.2.5.2. Two sets of experiments (Experiment 1 and Experiment 2) were performed on two sets of mice with different loading doses of pDNA.

Experiment 1: For a set of 3 microneedle devices of the same dimension and design, 3 μL of pUbc-luc2/eGFP pDNA 4.6 mg mL^{-1} in TE buffer was used to coat the microneedle devices (5 × 700μm Regular, 5 × 700μm Serrated and 5 × 700μm Concave) to provide a theoretical maximum loading of 4.6 μg plasmid DNA per microneedle device. The coated microneedle devices were then allowed to dry at 4°C for 18 h.

Experiment 2: For a set of 6 microneedle devices of the same dimension and design, 4.5 μL pUbc-luc2/eGFP plasmid DNA 9.2 μg μL^{-1} in TE buffer was used to coat the microneedles (5 × 700μm Regular, 10 × 700μm Regular, 5 × 700μm Serrated, 5 × 700μm Concave, 5 × 500μm Regular and 10 × 500μm Regular) to provide a theoretical maximum loading of 6.9 μg pDNA per microneedle device. The coated microneedle devices were then allowed to dry at 4°C for 32 h.

6.2.1.3.2 Liquid loading pUbc-luc2/eGFP onto microneedle devices

Experiment 1: The pUbc-luc2/eGFP pDNA was liquid loaded onto steel microneedle devices (5 × 500μm Pocketed; Cardiff University, UK) by pipetting 1 μL pUbc-luc2/eGFP pDNA 4.6 μg μL^{-1} onto the microneedles immediately before use to provide a theoretical maximum loading of 4.6 μg pDNA per microneedle device.

6.2.1.3.3 Delivery of dry-coated pUbc-luc2/eGFP to mouse paw

Mice were anaesthetised with 2-3% isoflurane during microneedles insertion.

Experiment 1: Two cohorts of mice (3 mice per group) were treated with the solid-coated or liquid loaded steel microneedles. The first cohort of mice were treated with 5 × 700μm Regular coated microneedle devices on the left paws and 5 × 500μm Pocketed liquid-loaded microneedle devices on the right paws. The second cohort of mice were treated with 5 × 700μm Serrated coated microneedle devices on the left paws and 5 × 700μm Concave coated microneedle devices on the right paws. The coated and liquid-loaded microneedle devices were held tightly with a pair of forceps and manually inserted into the middle region of mouse paw (in between the footpads) and held in place for 5 min. The microneedle devices were then left seated on the skin for an

additional 15 min (total insertion time 20 min) before being removed. Transgene expressions on the treated paws were analysed 24 h post treatment by *in vivo* bioluminescence imaging as detailed in section 6.2.1.4.2.

Experiment 2: Three cohorts of mice (3 mice per group) were treated with the solid-coated steel microneedles. The first cohort of mice were treated with 5 × 700μm Regular microneedle devices on the left paws and 10 × 700μm Regular microneedle devices on the right paws. The second cohort of mice were treated with 5 × 700μm Serrated microneedle devices on the left paws and 5 × 700μm Concave microneedle devices on the right paws. The third cohort of mice were treated with 5 × 500μm Regular microneedle devices on the left paws and 10 × 500μm Regular microneedle devices on the right paws. The coated microneedle devices were applied as described in Experiment 1. Transgene expression on the treated paws were analysed 24 h (Day 1) and 120 h (Day 5) post treatment by *in vivo* bioluminescence imaging as detailed in section 6.2.1.4.2.

6.2.1.4 Analysis of pUbc-luc2/eGFP delivery and transgene expression

6.2.1.4.1 Quantification of pUbc-luc2/eGFP deposition

Prior to application, the mass of pDNA loaded onto each microneedle device was estimated from the mass of pDNA in the known volume of coating formulation that was used to coat the microneedles. Following application, the microneedle devices were rinsed with a small volume of buffer (100–150 μL) with agitation for 10 min to recover pDNA from the surface of the microneedles. The concentration of the recovered siRNA was measured using the NanoDrop spectrophotometer as described in section 3.2.1.5 and the mass of plasmid DNA recovered was calculated as described in section 3.2.5.1. The mass of pDNA deposited on the paw skin was calculated by deducting the average mass of pDNA remaining on the microneedles after treatment from the theoretical maximum loading dose. Microneedle devices were then cleaned for re-use using the method described in section 3.2.5.2.

6.2.1.4.2 *In vivo* bioluminescent imaging of gene expression

Mice were imaged at the indicated time points following microneedle application using the IVIS Spectrum Imaging System (Perkin Elmer, USA) (Contag and Bachmann 2002; Gonzalez-Gonzalez et al. 2011). Mice were anaesthetised with isoflurane and D-luciferin (Biosynth International, Inc., USA) was injected (100 mL of a 30 mg mL^{-1} solution; 150 mg kg^{-1} body weight) into the peritoneal cavity of the mice. After 10 min, the anaesthetised mice were imaged *in vivo* using the IVIS system. The resulting light emission was quantified using the Living Image software version 3.1 (Perkin Elmer, USA).

6.2.2 siRNA delivery to the paws of transgenic mouse

These experiments, except the skin sectioning and immunofluorescence imaging experiments were performed at either Transderm Inc., Santa Cruz, USA under the supervision of Dr. Roger Kaspar or Stanford University, Stanford, California, USA under the supervision of Dr. Christopher Contag with the help of Dr. Emilio Gonzalez-Gonzalez, Dr. Maria Fernanda Lara and Dr. Tycho Speaker. All materials except the steel microneedle devices were gifts from Dr. Roger Kaspar and Dr. Christopher Contag and were used as provided unless otherwise stated.

6.2.2.1 siRNA sequences

Accell modified sd-siRNA (Accell CBL3 sd-siRNA; siRNA sequence: 5′-UAACGAUCCACGACGUAAA) was used to target the CBL3 coding region of transgenic hMGFP/CBL mouse mRNA. A nonspecific self-delivery K6a_513a.12 siRNA (Accell TD101 non-targeting sd-siRNA) targeting a keratin 6a mutation not present in the mouse model was used as a negative control (Hickerson et al. 2011).

6.2.2.2 Animal models

Transgenic (Tg) CBL/hMGFP mice (Gonzalez-Gonzalez et al. 2009), were obtained from the breeding colonies at Stanford University, Stanford, California, USA. Transgenic hairless (Tg-h) CBL/hMGFP mice (Chong et al. 2013) were bred by Dr. Emilio Gonzalez-gonzalez by crossbreeding Tg CBL/hMGFP mice, with skh1 hairless mice, purchased from Charles River (Wilmington, MA, USA). All mice were treated

according to the guidelines of both the National Institutes of Health and Stanford University.

6.2.2.3 Microneedle coating and delivery of siRNA

6.2.2.3.1 Coating siRNA onto microneedle devices

The Accell CBL3 siRNA (Dharmacon, Thermo Fisher Scientific, USA) 70 μg μL^{-1} and Accell TD101 siRNA (Dharmacon, Thermo Fisher Scientific, USA) 80 μg μL^{-1} in PBS were coated onto steel microneedle devices (10 × 700μm Regular, 5 × 500μm Regular; Cardiff University, UK) using the dip-coating method described in section 2.2.5.2. Two μL of the siRNA coating solutions were loaded into pipette tips as reservoirs for coating. Then, steel microneedle devices (4 devices per treatment group) were coated with siRNA to provide a theoretical maximum loading of 35 μg Accell CBL3 and 40 μg Accell control sd-siRNA onto microneedle devices, respectively. The coated microneedle devices were then allowed to dry at 4°C for up to 18 h.

6.2.2.3.2 Delivery of siRNA to the paws of transgenic mice

Two cohorts of transgenic mice (4 mice per group) were treated with the siRNA-coated microneedles. The first cohort of hairless transgenic mice (Group 1) were treated with 5 × 700 μm Regular solid-coated microneedle devices loaded with Accell CBL3 siRNA on the right paws. On the counterpart left paws, Accell TD101 non-targeting control siRNA were administered. The second cohort of transgenic mice (Group 2) were treated with 10 × 500 μm Regular solid-coated microneedle devices loaded with Accell CBL3 siRNA on the right paws. On the counterpart left paws, Accell TD101 non-targeting control siRNA was administered.

Mice were anaesthetised with 2-3% isoflurane prior to microneedle administration. The coated microneedle devices were applied as described in section 6.2.1.3.3. The mice were treated at the same location daily for 10 days, except day 2. At day 10, the mice were sacrificed by CO_2 asphyxiation and the treated paw skin was removed by surgical dissection. Analysis of gene silencing was then performed using the methods detailed in section 6.2.2.4.

6.2.2.4 Analysis of siRNA delivery and gene silencing

6.2.2.4.1 Quantification of siRNA deposition

Prior to application, the mass of siRNA loaded onto each microneedle device was estimated from the mass of siRNA in the known volume of coating formulation that was used to coat the microneedles. Following application, the mass of siRNA deposited was quantified as described in section 6.2.1.4.1, substituting plasmid DNA with siRNA. The mass of siRNA deposited on the paw skin was calculated by deducting the average mass of siRNA remaining on the microneedles after treatment from the theoretical maximum loading dose.

6.2.2.4.2 Quantification of protein expression

Prior to initial treatment (Day 0), mice were anaesthetised with 2-3% isoflurane and imaged intravitally using the Maestro Optical imaging system (Perkin Elmer, USA) (Gonzalez-Gonzalez et al. 2010b; Hickerson et al. 2008). Imaging was repeated every alternate day, on days 2, 4, 6, 8 and 10 of the treatment regimen. An excitation filter of 445–490 nm and a long-pass emission filter (515 nm) were used. Filter sets were set to capture images with 10 nm windows automatically from 500 to 850 nm using the Maestro software, with an automatically calculated exposure time. The resulting TIFF cube image was spectrally unmixed using a user-defined hMGFP protocol. Each spectrum was set by unmixing autofluorescence from a negative non-hMGFP expressing mouse analysed in parallel with a Tg CBL/hMGFP positive mouse to select appropriate regions. In the case of Tg-h mice, each spectrum was set by unmixing autofluorescence from a hairless skh1 negative non-hMGFP expressing mouse analysed in parallel with a Tg-h CBL/hMGFP positive mouse to select appropriate regions. The conditions and subject positioning for image acquisition were standardized to facilitate meaningful data comparison.

Quantitative analysis was performed using ImageJ software by selecting the treatment area (avoiding the brighter footpads of each paw) and calculating the average signal (counts s^{-1} mm^{-1}) at the various imaging time-points. The ratio of average signal in the right (CBL3 treatment) versus left (TD101 non-targeting control) paws was determined for each mouse, normalised with respect to the pre-treatment (Day 0) levels.

6.2.2.4.3 Quantification of gene expression

At the end of 10-day treatment, skin tissues from three mice per cohort were immediately frozen in dry ice. Tissue from each sample was lysed by Dr. Maria Fernanda Lara using the Qiazol lysing reagent (Qiagen, UK) and homogenised for 120 s at 6 m s^{-1} in a FastPrep-24 'bead beater' instrument (MP Biomedicals, USA) using D matrix to mechanically lyse the cells. Total RNA was isolated using the Qiagen RNeasy Mini Kit (Qiagen, UK) according to the manufacturer's instructions. Total RNA isolated was quantified using the NanoDrop spectrophotometer, as described in section 3.2.1.5.

Reverse transcription on the isolated RNA was performed by Dr. Maria Fernanda Lara, using the Superscript III First Strand Synthesis system (Invitrogen Life Technologies, USA) with 1 to 2 μg of total RNA and random hexamer primers. The RT enzyme was heat denatured at 85°C for 5 min. The qPCR reactions were prepared by combining 1 μL Taqman 20× gene expression assay, 10 μL Taqman 2× PCR mix and 9 μL of diluted cDNA samples in a 96-well plate. The qPCR reactions were run using the ABI 7500 Fast Sequence Detection system (Applied Biosystems, USA). Taqman gene expression assays, specifically designed for hMGFP (hMGFP-F: 50-CCCCAAGGACATCCCTGACT; hMGFP-R: TGCTTCGCTCCCACGAGTA and probe: 6FAM-TCAAGCAGACCTTCCCCGA-MGBN FQ; Applied Biosystem, USA) was used for the target gene and specific for CD44 (Hs00153304_m1) was used as the endogenous gene control. All data points reported are the mean of three replicate assays and the standard error is reported.

6.2.2.4.4 Skin sectioning and immunofluorescence

Skin tissue from the region between the footpads of one mouse per cohort was excised, embedded in OCT and frozen on dry ice. The samples embedded in OCT blocks were cryosectioned using the Leica CM3050S Cryostat. Skin sections of 10 μm thickness were captured onto microscope slides and then mounted with VECTASHIELD® Mounting Medium containing 1.5 μg mL^{-1} 4,6-diamidino-2-phenylindole (DAPI; Vector Laboratories Ltd., UK) for nuclear staining. Transgene fluorescence was visualised using the Leica DM IRB epifluorescence microscope and imaging system.

6.2.3 Data processing and statistical analysis

Data processing and statistical analysis was performed as described in section 3.2.9.

6.3 Results and discussion

6.3.1 *In vivo* pUbc-luc2/eGFP delivery and expression in mouse paw

To evaluate the effect of microneedle shape, length and spatial density on the effect of pDNA deposition and subsequent gene expression, microneedles of various dimensions and spatial densities were coated with pUbc-luc2/eGFP pDNA and delivered to mouse paw skin. Using the nucleic acid recovery method as previously described, the dose of plasmid DNA deposited on the skin was determined (Figure 6.1).

The theoretical maximum loading doses of pDNA coated per microneedle device were 4.6 μg for experiment 1 and 6.9 μg for experiment 2. The mass of pDNA deposited on mouse paw was determined by assuming that the difference in mass between the theoretical maximum loading dose and that of nucleic acid recovered from the coated microneedles after insertion into mouse paw was due to deposition within skin. In experiment 1 (Figure 6.1A), average doses of nucleic acid deposited per solid-coated microneedle device were between 2.076 ± 1.14 μg (5 × 700μm Regular; Cardiff University, UK) and 3.707 ± 1.79 μg (5 × 700μm Concave; Cardiff University, UK), which were statistically insignificant ($p > 0.05$). Liquid-loaded pDNA deposition was not quantified as visible liquid formulation of pDNA was deposited on top of the skin surface rather than within the skin, which would lead to inaccurate estimation of delivered dose.

In experiment 2 (Figure 6.1B), the average doses of pDNA deposited per solid-coated microneedle device were between 0.811 ± 1.009 μg (10 × 500μm Regular; Cardiff University, UK) and 3.526 ± 0.5357 μg (5 × 700μm Regular; Cardiff University, UK). The differences in nucleic acid deposition between the treatment groups with top two highest depositions (5 × 700μm Regular and 5 × 700μm Concave; Cardiff University, UK) and top two lowest depositions (10 × 500μm Regular and 5 × 500μm Regular; Cardiff University, UK) were statistically significant ($p < 0.05$).

The results show that microneedles of longer needle length (700μm) deposited higher doses of nucleic acid than microneedles of shorter needle length (500μm). Several studies have suggested that the length, tip sharpness, spatial density and hardness of

microneedles influence the skin penetration ability of microneedle devices (Verbaan et al. 2007; Yan et al. 2010). A study reported that manual application of steel microneedles fabricated from the tip of 30G hypodermic needles of 300 μm in length on human skin that has been dermatomed to a thickness of 300 to 400 μm was unsuccessful in piercing the skin through the stratum corneum (Verbaan et al. 2007). Microneedles of 550 μm length or longer were successful in piercing the skin. The authors postulated that microneedles have to be long enough to overcome the skin's elasticity in order for skin rupture and puncture to occur following microneedle application (Verbaan et al. 2007).

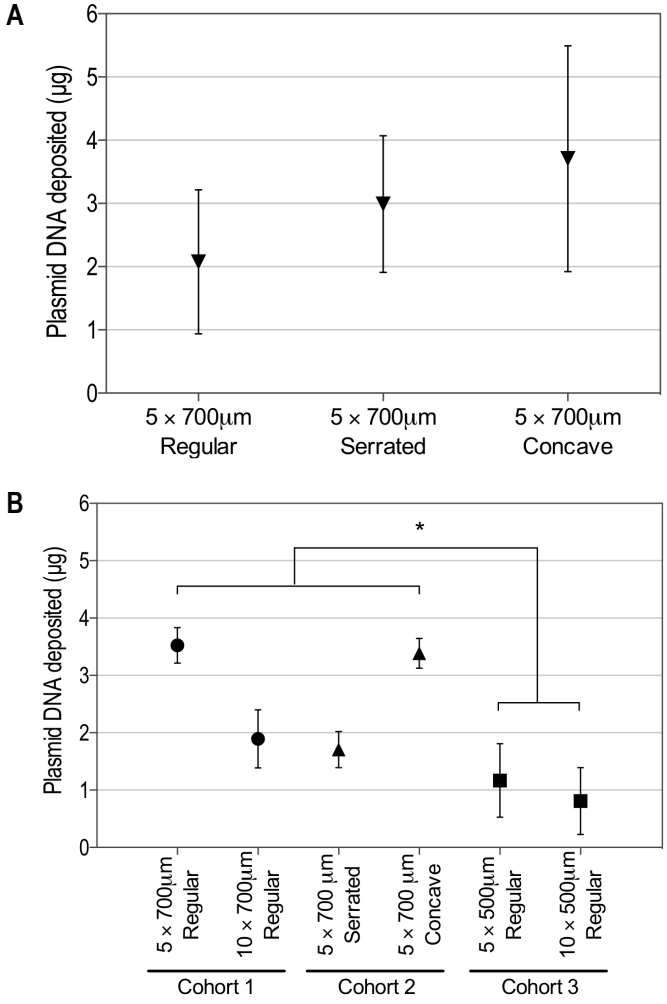

Figure 6.1: pUbc-luc2/eGFP plasmid DNA deposited into mouse paws in experiment 1 (A) where a theoretical maximum loading of 4.6 μg pDNA was coated per microneedle device and experiment 2 (B) where a theoretical maximum loading of 6.9 μg pDNA was coated per microneedle device. (n = 3; * = significant difference in plasmid DNA deposition between indicated groups, $p < 0.05$)

Another study investigating solid silicon needle length of 100 to 1100 μm and needle densities of 400 to 11900 needles cm^{-1} on heat separated human epidermal membrane reported significantly increased drug flux across epidermal membrane when microneedles of 600 μm and longer with needle densities of 2000 needles cm^{-1} or lower were used (Yan et al. 2010). Similar to the aforementioned study, the authors attributed the lower microneedle penetration ability with microneedles of shorter length to the skin's elastic properties, allowing the skin to fold around the microneedles during insertion, leading to ineffective puncture, which is overcomed by microneedles of longer length (Yan et al. 2010). Furthermore, skin penetration improved with microneedles of the same length of 400 μm but with lower needle density of 2000 needles cm^{-1} compared to 5625 needles cm^{-1}. This phenomenon can be explained by the "bed of nails" effect, whereby the pressure required by each needle tip to rupture and penetrate the skin is insufficient due to distribution of microneedle application force over a higher density of microneedles (Yan et al. 2010).

From experience, studies using steel microneedles of 250 μm (5 × 500μm Regular; Cardiff University, UK) resulted in varying degree of success in *in vivo* human skin, *in vivo* mouse skin and *ex vivo* human skin (data not shown). More force was required when applying the microneedles of shorter length and inconsistent penetration was achieved. In addition, the depth of microneedle penetration on the skin is usually less than the actual length of the microneedles as shown in previous chapters and by other studies (Kim et al. 2010; Verbaan et al. 2007), thus resulting in lower doses of nucleic acid deposited from microneedles of shorter length when the same loading dose of nucleic acid is coated. From Figure 6.1B, plasmid DNA deposition from in-plane microneedle devices of higher needle spatial densities (10 needles per device) appeared lower than their lower needle density counterparts (5 needles per device) but the differences were statistically insignificant ($p > 0.05$).

Transgene expressions following pUbc-luc2/eGFP delivery via solid-coated and liquid-loaded steel microneedles were detected as bioluminescent signals that were standardised to the same exposure between all the cohorts. Localised region of interests of the same dimension were drawn on the treated paws to allow meaningful comparison of relative luminescence (Figure 6.2).

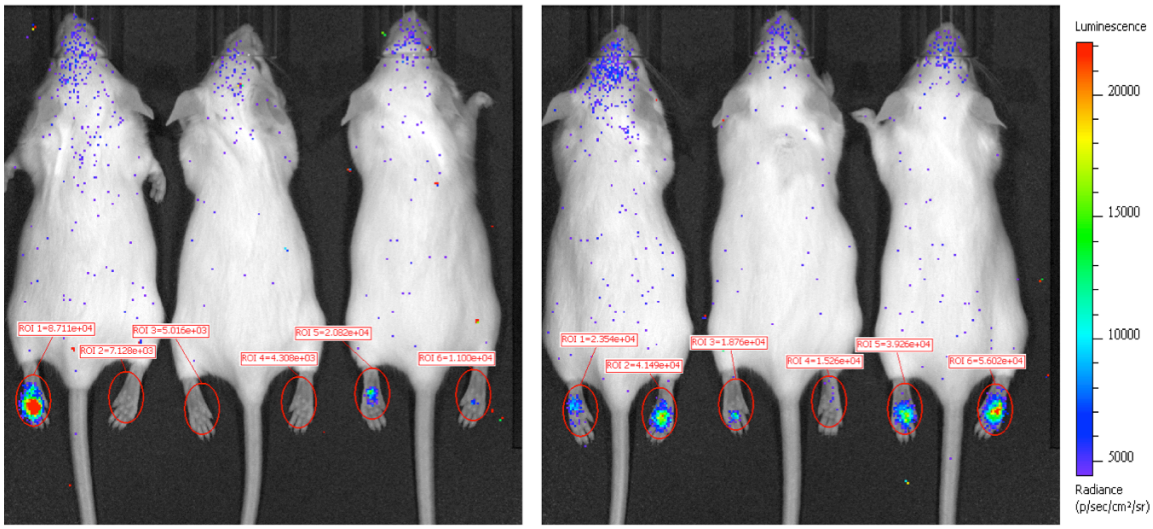

Figure 6.2: In vivo bioluminescent imaging of pUbc-luc2/eGFP expression in mouse paws 24 h post-treatment with pDNA solid-coated and liquid loaded onto microneedle devices (Experiment 1). Cohort 1 mice were treated with 5 × 700µm Regular solid-coated microneedle devices on the left paws and 5 × 500µm Pocketed liquid loaded microneedle devices on the right paws. Cohort 2 mice were treated with 5 × 700µm Serrated solid-coated microneedle devices on the left paws and 5 × 500µm Concave solid-coated microneedle devices on the right paws. Luminescence signals expressed within the region of interest (ROI; marked with red circles) were quantified using the IVIS software (numbers in red text boxes). (All microneedles were from Cardiff University, UK)

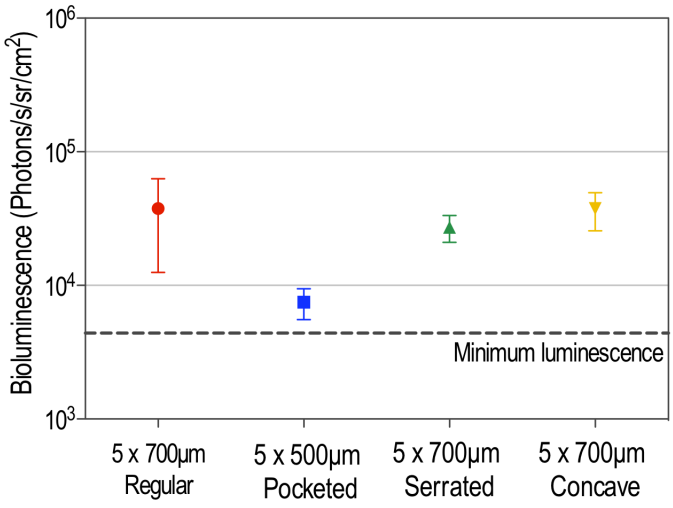

Figure 6.3: Bioluminescence quantification of pUbc-luc2/eGFP expression in mouse paws 24 h post-treatment with pDNA solid-coated and liquid loaded onto microneedle devices (Experiment 1). (n = 3)

From experiment 1, reporter gene expression was detected following delivery of pUbc-luc2/eGFP solid-coated onto microneedle devices (Figure 6.3). Bioluminescence values were comparable between all the solid-coated microneedles treatment groups ($p > 0.05$). Delivery of liquid-loaded pDNA did not result in transgene expression and therefore, was not pursued further in experiment 2. The pocketed microneedles were 500 μm in length with a cavity (pocket) in between each needle opening to a larger cavity in the middle of the microneedle device (Figure 6.4). The presence of the cavity greatly reduced the strength of the microneedles with several needles from each device breaking upon application on the mouse paws. Attempts to strengthen the microneedles by attaching the device to a metal piece proved futile as liquid-loaded delivery using the repaired microneedles failed to result in significant gene expression possibly due to the inability of these weak microneedles to penetrate the tough skin of mouse paws. Even if penetration was achieved by some of the pocketed microneedles, it is likely that liquid formulation of pDNA was deposited on the surface of the skin rather than into the skin.

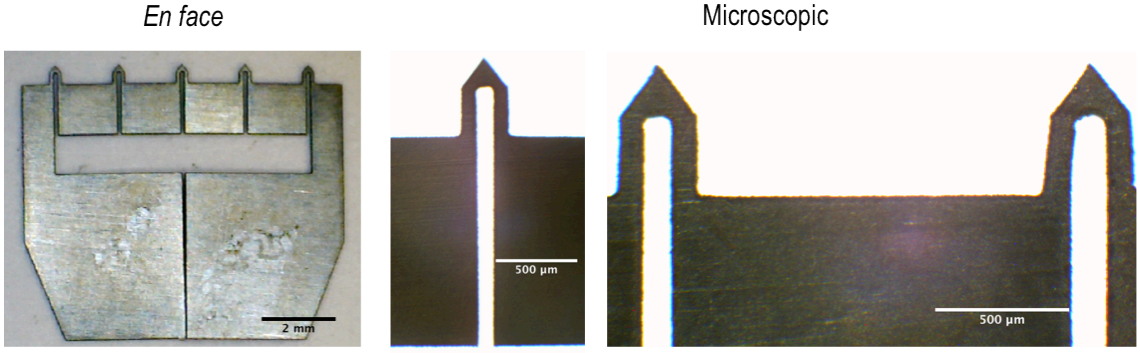

Figure 6.4: ***En face*** **and microscopic images of the 5 × 500μm Pocketed microneedle device (Cardiff University, UK).**

In experiment 2, mice were imaged for bioluminescence transgene expression at day 1 and day 5 post-delivery (Figure 6.5). Overall, bioluminescence signals at day 1 were similar across all treatment groups ($p > 0.05$) (Figure 6.6). At day 5, bioluminescence signals for both the treatment groups in cohort 1 were significantly higher than the rest of the treatment groups in cohort 2 and 3 ($p < 0.05$; $n = 3$). Comparison between other treatment groups at day 5 did not reveal any significant differences ($p > 0.05$; $n = 3$).

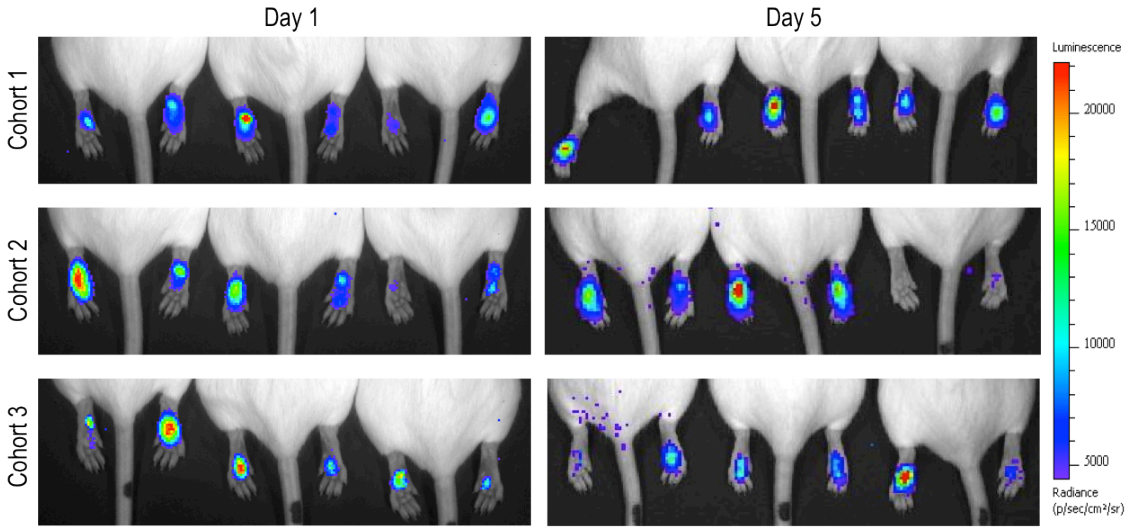

Figure 6.5: ***In vivo*** **bioluminescent imaging of pUbc-luc2/eGFP expression in mouse paws day 1 and day 5 post-treatment with pDNA solid-coated onto microneedle devices (Experiment 2).** Cohort 1 mice were treated with 5 × 700µm Regular solid-coated microneedle devices on the left paws and 10 × 700µm Regular solid-coated microneedle devices on the right paws. Cohort 2 mice were treated with 5 × 700µm Serrated solid-coated microneedle devices on the left paws and 5 × 700µm Concave solid-coated microneedle devices on the right paws. Cohort 3 mice were treated with 5 × 500µm Regular solid-coated microneedle devices on the left paws and 10 × 500µm Regular solid-coated microneedle devices on the right paws.

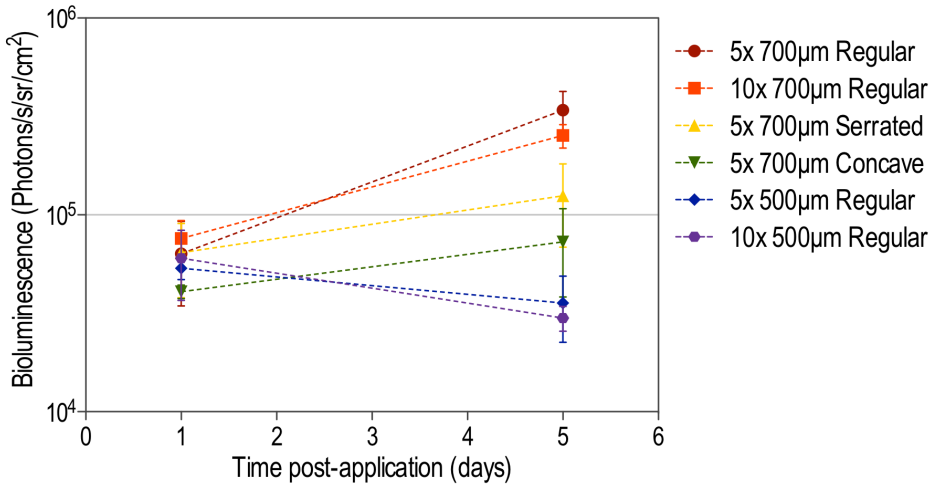

Figure 6.6: **Bioluminescence quantification of pUbc-luc2/eGFP expression in mouse paws day 1 and day 5 post-treatment with pDNA solid-coated onto microneedle devices (Experiment 2).** (n = 3)

When comparing between day 1 and day 5, bioluminescence signals increased for cohort 1 and 2 whilst signals decreased in cohort 3. The parameter that was different in cohort 3 was the microneedle length, whereby in cohort 3 shorter microneedles (500 μm length) were used compared to cohort 1 and 2 (700 μm length). Cohort 3 also deposited the least amount of pDNA (Figure 6.1B) due to the needle length. However, there was no clear correlation between the amount of pDNA deposited (Figure 6.1) and the resulting transgene expression (Figure 6.6), suggesting microneedle length may play a crucial role in determining the depth of nucleic acid deposition, which consequently affects transgene expression in mouse paws.

Previous work has shown that intradermal delivery of large doses of naked pDNA (20 μg) resulted in one to two orders of magnitude higher intensity signal than the use of either coated steel microneedles or PAD, as measured by *in vivo* bioluminescent imaging at 24 h (Gonzalez-Gonzalez et al. 2011). Subsequent attempts to increase pDNA delivery using microneedle devices did not result in significant improvement and this was again demonstrated in this study. Up to 3.7 μg pDNA was delivered using microneedle devices of different needle shapes, length and spatial densities but an improvement in gene expression compared to previous studies with intradermal injection was not observed.

It has previously been reported that an increasing volume of intradermal injection increases reporter plasmid expression, suggesting that naked nucleic acid uptake into skin cells following intradermal injections is driven by hydrodynamic pressure (Gonzalez-Gonzalez et al. 2010a). Such hydrodynamic pressure is not present in the delivery of pDNA solid-coated onto microneedle devices, which could explain the observed lower magnitude of reporter gene expression using microneedles. Furthermore, there is a limit to the coating capacity of the microneedles and therefore, a lower dose of therapeutic material could be delivered using microneedle devices compared to intradermal injections (Gill and Prausnitz 2007b).

The mechanism of DNA uptake in epidermal cells following microneedle application is still unclear but has been postulated to involve transient cell membrane disruption during microneedle penetration. However, previous unpublished work by collaborators noted that delivery of unmodified siRNA using soluble microneedle devices did not

result in detectable functional gene silencing in mouse skin despite siRNA being a significantly smaller and shorter nucleic acid sequence. These results imply that cellular uptake mechanism in the complex multilayer structure of skin varies between nucleic acids types and sizes as well as the species of skin model tested.

It was also interesting to observe that with the coated steel microneedles, prolonged and sustained gene expression occurred for more than 30 days post treatment that was an order of magnitude higher than with the PADs (Gonzalez-Gonzalez et al. 2011). Apart from the higher dose of DNA delivered by the steel microneedle devices, the thin mouse skin and greater strength of solid steel microneedles may have resulted in deeper skin penetration of up to 700 μm (Kim et al. 2010). Therefore, pDNA delivered to the mouse skin using steel microneedles was probably deposited deep in the dermis or muscles of the mouse paw to allow sustained gene delivery and expression. In this study, where shorter (500 μm) steel microneedles were used, significantly less nucleic acid was deposited. Due to the reduced length of the needle, nucleic acid delivery could be more superficial as with the PAD compared to the use of regular length (700μm) steel microneedle devices. This observation could not be translated to human skin as the human skin has thicker dermis and subcutaneous layer than the mouse paw skin (Hengge et al. 1996).

In chapter 3, delivery of reporter pDNA coated onto steel microneedles resulted in rare, inconsistent, irregular reporter gene expression in excised human skin. The same observation has also been reported in a publication, suggesting insufficient hydration in human skin to dissolved deposited pDNA payload (Pearton et al. 2012). In excised human skin, steel microneedles penetrate up to the superficial dermis whilst in mouse paws, penetration could be much deeper than the dermis. Furthermore, the movement of mouse in the cage could potentially aid in the dissolution of pDNA plug deposited in the paw. This warrants an investigation in future human skin delivery studies via coated steel microneedles. The human skin could be hydrated with cream or lotion before treatment with coated microneedles to improve drug dissolution in the skin.

6.3.2 *In vivo* siRNA delivery and silencing in transgenic mouse paw

The potential of modified Accell sd-siRNA-coated stainless steel microneedles to mediate gene silencing *in vivo* was examined in a well-established transgenic mouse model (Gonzalez-Gonzalez et al. 2009; Gonzalez-Gonzalez et al. 2010b). Accell CBL3 sd-siRNA has been designed to target the CBL coding region of the hMGFP/CBL mRNA. Steel microneedles (10 × 700μm Regular and 5 × 500μm Regular; Cardiff University, UK) were coated with Accell CBL3 and Accell non-targeting control sd-siRNAs with theoretical maximum loading doses of 35 μg (Accell CBL3 sd-siRNA) and 40 μg (Accell non-targeting sd-siRNA) per microneedle device. The solid-coated microneedles were inserted into the central region of the Tg or Tg-h CBL/hMGFP mouse paws (Figure 6.7) and the doses of siRNA deposited in the skin were then quantified (Figure 6.8). The treatment was administered daily, except on day 2, for 10 days.

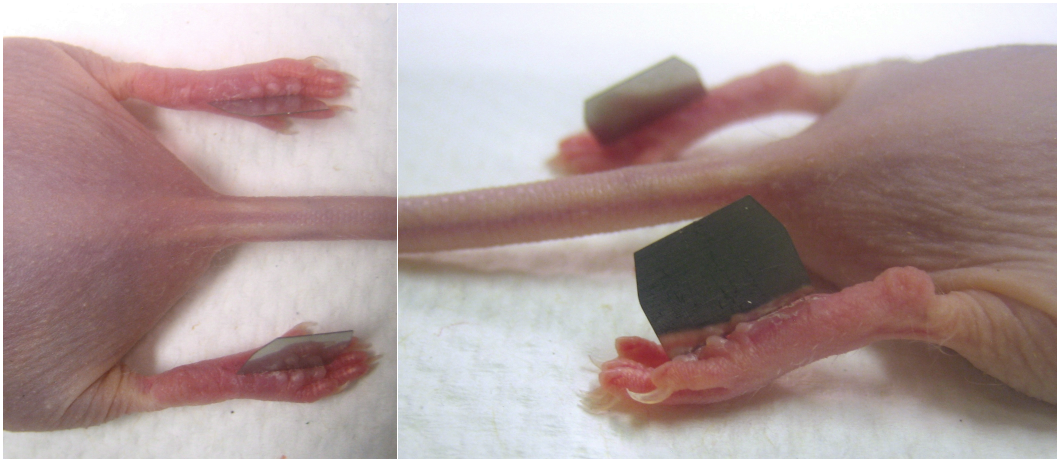

Figure 6.7: Digital images of the Tg-h CBL/hMGFP mouse paws treated with Accell siRNA solid-coated onto steel microneedle devices.

On day 1, the dose of siRNA deposited into the skin was relatively low (less than 15 μg) (Figure 6.8). The reduced deposition was probably due to inexperience in microneedle application to the mouse paw skin model resulting in inadequate skin insertion (Chong et al. 2013). Drug delivery efficiency from coated microneedles is influenced by factors such as coating formulation, coating uniformity, depth of microneedle penetration and the skin hydration (Pearton et al. 2012). In this case, the limiting factor was probably the microneedle penetration depth, as inserting an in-plane microneedle array into the contoured area of mouse footpad for the first time was technically challenging (Chong

et al. 2013). Moreover, as the microneedles were coated using a manual coating procedure, some of the materials would inevitably be coated on the base of the microneedle device, which would not be deposited on the mouse paw but would be accounted for when quantifying post-insertion (Chong et al. 2013). Thereafter, techniques improved with deposition of approximately 54% to 82% (19 μg to 33 μg) of loaded siRNA from the 10 × 700μm Regular microneedle devices and approximately 27% to 67% (11 μg to 24 μg) of loaded siRNA from the 5 × 500μm Regular microneedle devices during each treatment. As expected, microneedles of shorter length (500 μm) deposited on average lower doses of siRNA.

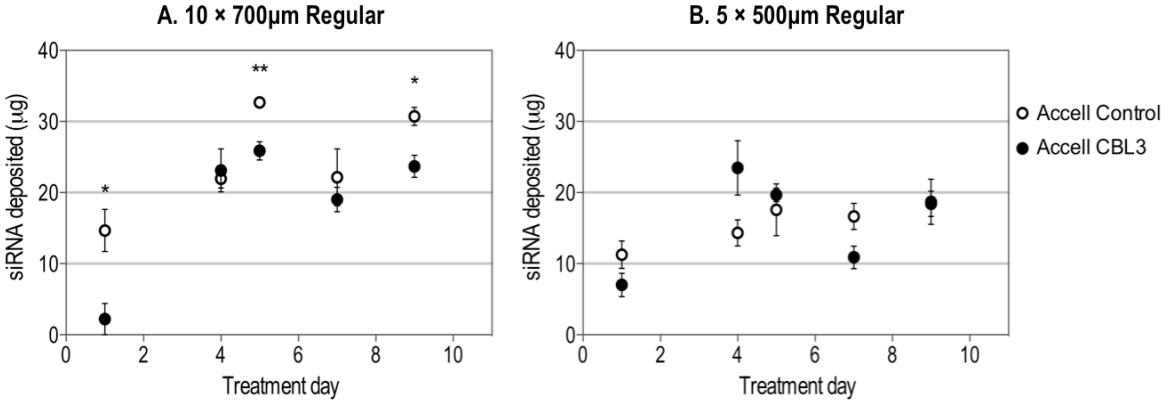

Figure 6.8: siRNA deposition dose in mouse paws treated with Accell CBL3 or control sd-siRNA-coated microneedles (A. 10 × 700μm Regular; B. 5 × 500μm Regular) on treatment days 1, 4, 5, 7 and 9 of the 10 day-regime. (n = 4; * = significant difference in siRNA deposition between the control and CBL3 groups, $p < 0.05$; unpaired two-tailed t-test for each treatment time-point)

At certain time-points, the average doses of siRNA deposited were significantly different between treatment groups but were not noteworthy as they were variable between time-points with no apparent trend. In the cohort of mice treated with 10 × 700 μm Regular microneedle devices, the deposition dose of control sd-siRNA on day 1, 5 and 9 was significantly ($p < 0.05$) higher than that of CBL3 sd-siRNA and the delivery dose of non-targeting control sd-siRNA was never significantly lower than the CBL3 sd-siRNA (Figure 6.8A). The difference between siRNA doses deposited in the cohort of mice treated with 5 × 500μm Regular microneedle devices was statistically insignificant (Figure 6.8B). It is sufficient to note that on average, significant doses of siRNA were deposited on the treatment area from both the steel microneedle devices at

all the dose quantification time-points. Previous study has delivered an estimate of 120 ng siRNA (10% of the coated dose) per treatment using three PAD arrays (4 × 5 needle array; 2 mm spacing between needles) every 48 hours (Gonzalez-Gonzalez et al. 2010b). Steel microneedles have the capacity to load and deliver higher doses of siRNA, resulting in less wastage, which has important cost and clinical efficacy implications for the delivery of expensive biotherapeutics to the skin (Chong et al. 2013).

At the end of treatment at day 10, mice were sacrificed and tissue from the treated skin area was harvested from three mice per cohort for gene expression analysis (Figure 6.9). In the cohort of mice treated with 10 × 700μm Regular microneedle devices, hMGFP mRNA reduction was found in two out of three mice. Mouse 2 and mouse 3 showed an average relative mRNA reduction of 49% and 38%, respectively. In the cohort of mice treated with 5 × 500μm Regular microneedle devices, hMGFP mRNA reduction was found in one out of three mice. Mouse 2 had an average relative mRNA reduction of 50%. Gene silencing at the mRNA level was undetectable in other mice in the cohorts.

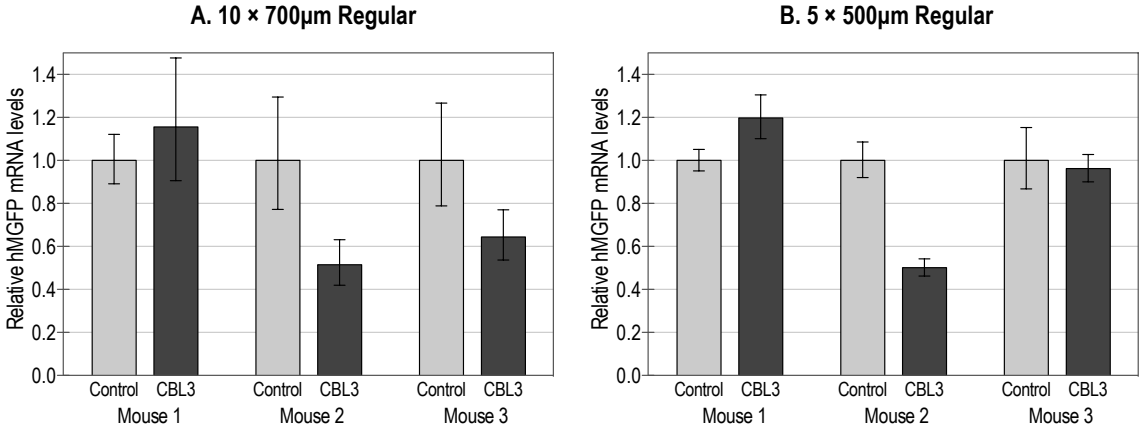

Figure 6.9: hMGFP mRNA levels in transgenic CBL/hMGFP mouse paws treated with Accell CBL3 or control sd-siRNA-coated microneedles (A. 10 × 700μm Regular; B. 5 × 500μm Regular) over a 10-day treatment regime. hMGFP mRNA levels from the CBL3 treated paw were quantified relative to the non-targeting control treated paw and normalised to CD44 endogenous gene control. Each column corresponds to the mean of three qPCR replicates and the error bars indicate 95% confidence interval.

Overall, the qPCR data showed poor technical reproducibility but due to limited time and sample quantities, the studies could not be repeated. Nevertheless, there are several factors that could have contributed to the equivocal RT-qPCR results. This study was conducted with an aggressive daily treatment regime whilst the study with the PADs was conducted with a less aggressive treatment regime of every 48 h to allow time for recovery following treatment. A recovery time in between treatment could prove crucial, as application of more rigid steel microneedle devices would have resulted in deeper needle penetration than the PADs. At least 1 mouse per cohort bled on at least one foot during each treatment with the steel microneedle devices and visible skin surface (stratum corneum) peeling caused by steel microneedle application was observed in all the mice treated with the coated steel microneedle devices. Despite the apparent physical aggressiveness of steel microneedles treatment, the mobility of treated mice was not affected throughout the daily treatment regime for 10 days.

It is likely that tissue injury could have affected the expression of endogenous CD44 gene control used for qPCR normalisation. CD44 is a major receptor for hyaluronic acid, which is involved in tissue repair and wound healing (Chen and Abatangelo 1999; Zhao et al. 2013). Hyaluronic acid is elevated transiently in granulation tissue during the wound healing process and the increased presence of hyaluronic acid stimulates increased generation of CD44 receptors (Chen and Abatangelo 1999; Zhao et al. 2013). CD44 is perhaps not the ideal endogenous gene control for evaluation of mRNA levels in the skin that has been treated with an invasive therapy. Throughout the 10 days treatment duration, any injured mouse skin may be in a different stage of wound healing to the other leading to variation in endogenous gene control levels.

CD44 was also the target gene in *ex vivo* human skin studies in the preceding chapter (Chapter 5). Different individuals have different wound healing capacity, which may lead to variation between endogenous gene levels. However, within the same human skin specimens, treatment conditions were standardised whereby the non-targeting control and CD44 treatment group were treated similarly with siRNA-coated microneedle once and then cultured for the same duration of 48 h. Since CD44 mRNA was targeted, similar levels of CD44 mRNA increase induced by microneedle treatment in both the control and CD44 treatment group would ideally lead to a wider gene silencing effect of CD44 siRNA in the skin, which is ideal for proof of concept gene

silencing studies. Results are affected if CD44 mRNA levels rise significantly higher in one treatment group than the other, which may lead to false positive or false negative interpretation of results, as seen by statistically insignificant gene silencing in 3 out of 6 humans skin specimens. Nevertheless, measures had been taken to ensure procedure standardisation and with the efficiency of Accell sd-siRNA *in vitro* (Chapter 4), it could be assumed that if sd-siRNA delivered through microneedle devices has been deposited in the viable epidermis, it should be taken up by skin cells proximal to the microneedle penetration site.

Prior to using CD44 as the endogenous control gene, K14 was used but hMGFP mRNA reduction was not detectable in any treated mice. K14 is a keratinocyte-specific protein and K14 mRNA and protein is expressed in the basal layer of healthy mouse skin epidermis (Gonzalez-Gonzalez et al. 2009). In response to epidermal injury, migration of basal keratinocytes that express K5 and K14 to the wound occurs to help restore skin integrity (Patel et al. 2006). It is probable that in the process of wound re-epithelialisation in some mouse paw injured by microneedle insertion, K14 gene expression is altered (Patel et al. 2006; Usui et al. 2005).

Regular size steel microneedle devices are considered minimally invasive in human skin but when applied to mouse skin would be considered highly invasive due to the difference in skin structure of both human and mouse skin and the sheer difference in size of both species. These equivocal mRNA results highlight the degree of challenge in studying gene silencing in *in vivo* and *ex vivo* skin models. Gene silencing detection *in vitro* can easily be performed following direct exposure of cells to relevant doses of siRNA in a controlled monolayer environment. It is a far greater challenge to deliver and evaluate gene silencing at the sub cellular level within the complex skin structure with accuracy and reproducibility (Chong et al. 2013).

Ideally, qPCR should have been repeated using a different endogenous control gene but due to limitations in the amount of total RNA isolated from small tissue samples, repetition of qPCR quantification was not performed. If qPCR was to be repeated, careful selection and validation of endogenous control gene that is stably expressed at different stages of wound healing have to be performed. A published study has reported the identification of endogenous control gene stable at hourly-defined stages of wounds

in mouse skin model (Turabelidze et al. 2010) but with a daily treatment regime, it would have been impossible to identify the stages of wound repair the mouse paws were undergoing. Therefore, siRNA mediated gene silencing at the mRNA level may not be the best indication of treatment outcome if an aggressive treatment regime was employed as in the mouse paws or an acute minimally invasive treatment was administered as in excised human skin, which by its own right is wounded at the edges when biopsied.

Nevertheless, the transgenic mouse model expresses GFP in the upper layers of the epidermis (granular layer and stratum corneum). This enabled assessment of the effect of siRNA delivery on protein expression through non-invasive intravital imaging (Gonzalez-Gonzalez et al. 2009). The effect of Accell sd-siRNA delivery through coated steel microneedles on hMGFP protein expression during treatment was evaluated using an intravital fluorescence imaging system pre-treatment and every other day throughout the treatment regime (Figure 6.10).

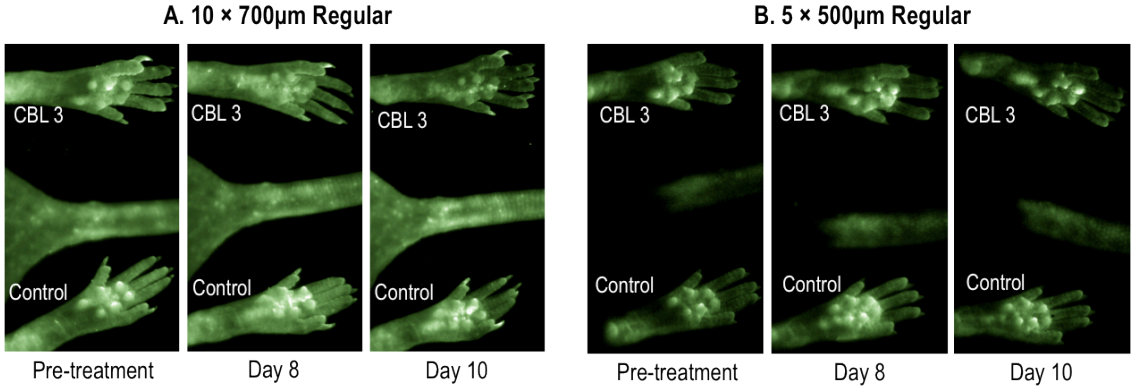

Figure 6.10: Intravital fluorescence imaging of hMGFP protein expression in the paws of (mouse 2 of both cohorts as a representative example) transgenic CBL/hMGFP mouse treated with Accell CBL3 or control sd-siRNA-coated microneedles (A. 10 × 700µm Regular; B. 5 × 500µm Regular) at pre-treatment, day 8 and day 10 of a 10-day treatment regime. hMGFP fluorescence images was captured through the Maestro imaging system and fluorescence was pseudocoloured green.

In both cohorts, quantification of fluorescence signal intensity at the treatment sites of mouse paws treated with Accell CBL3 sd-siRNA revealed reduction in hMGFP protein expression after 8 and 10 days relative to the non-targeting control paws (Figure 6.11).

At the end of treatment, at day 10, the reduction in signal intensities ranged from 33% to 51% (average 39.2%; n = 4) in the cohort of mice treated with 10 × 700μm Regular microneedle devices and 32% to 63% (average 38.9%; n = 4) in the cohort of mice treated with 5 × 500 μm Regular microneedle devices. These results indicated that delivery of siRNA through coated steel microneedles mediated a reduction in hMGFP protein expression at the treatment area of both cohorts of mice.

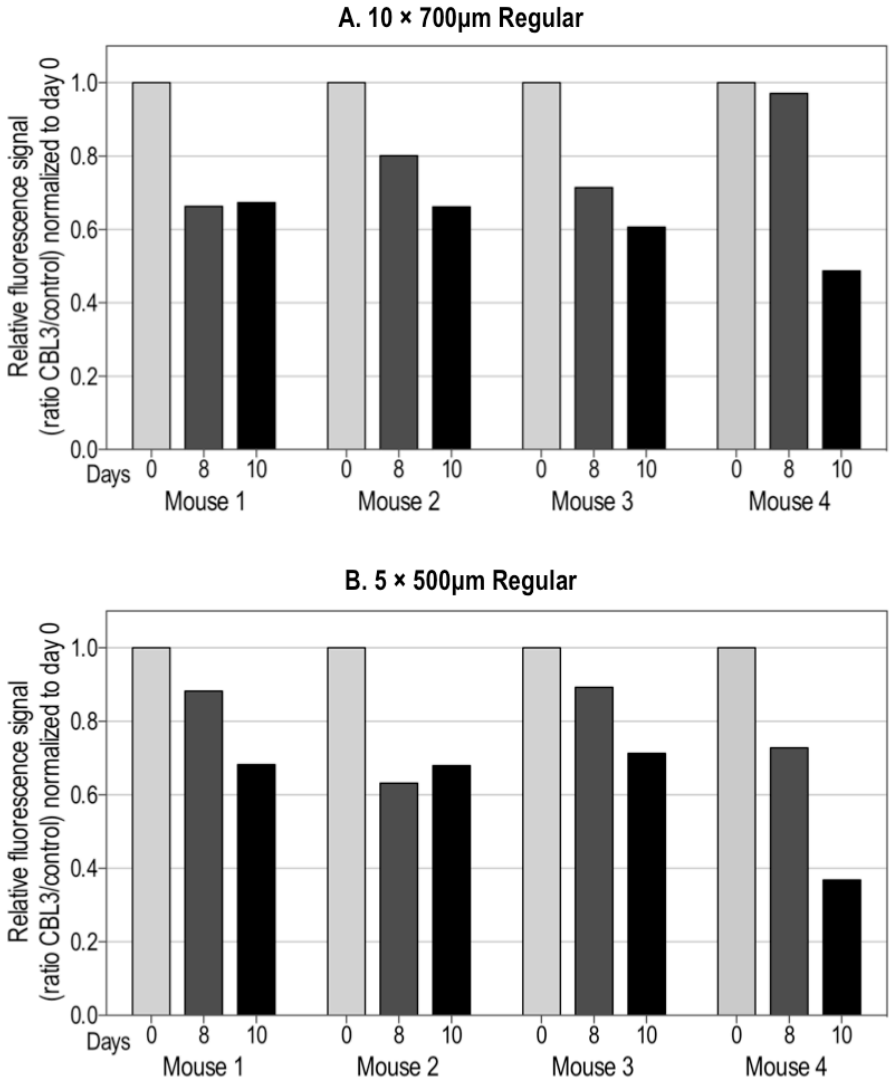

Figure 6.11: Quantification of hMGFP protein expression in transgenic CBL/hMGFP mouse paws treated with Accell CBL3 or control sd-siRNA-coated microneedles (A. 10 × 700μm Regular; B. 5 × 500μm Regular) at pre-treatment, day 8 and day 10 of a 10-day treatment regime. Intravital images captured using the Maestro imaging system were processed through ImageJ and quantified. The ratio of the signal intensity of the CBL3 treated area was relative to the non-targeting control treated area and normalised to day 0 (pre-treatment).

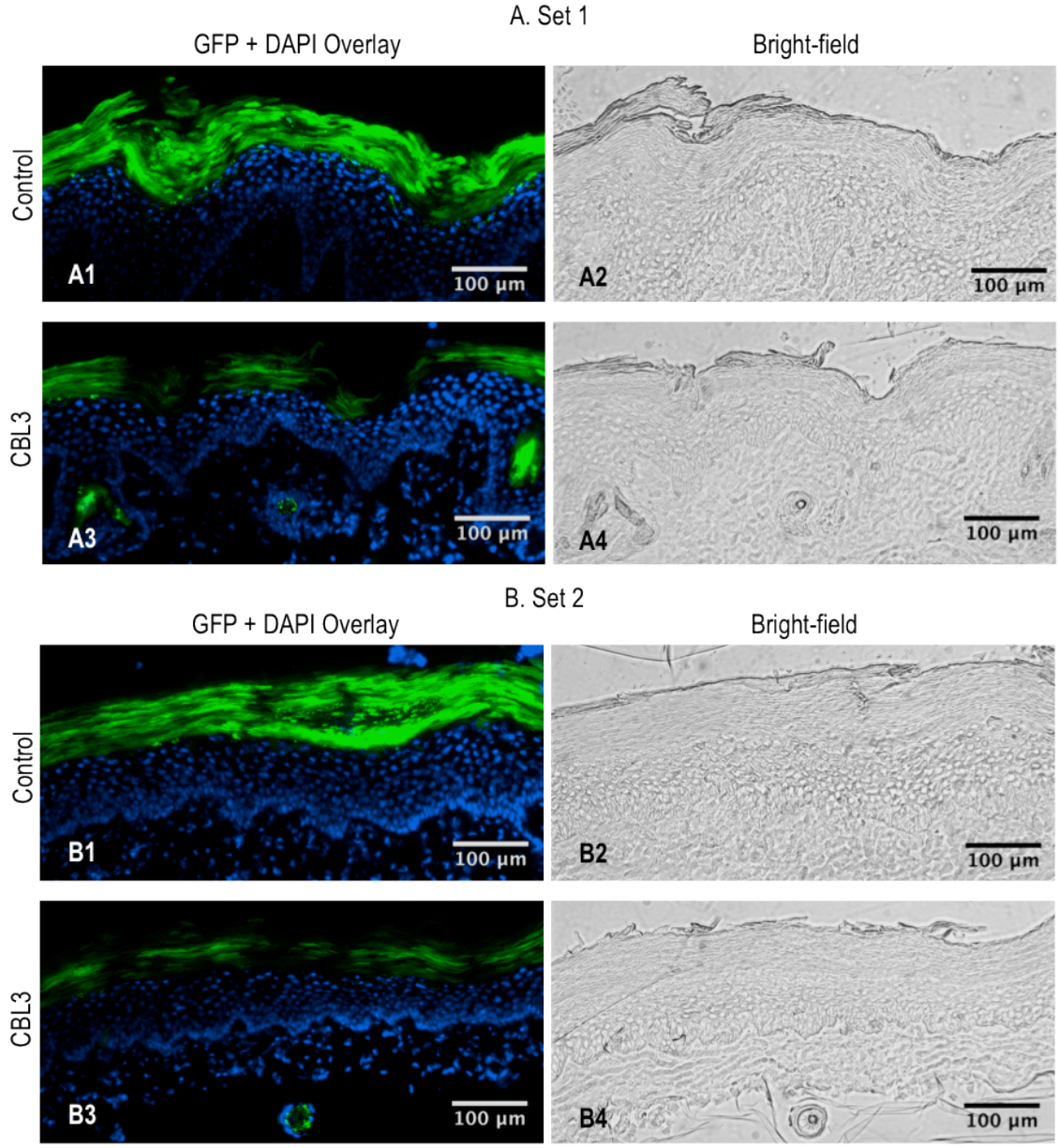

Figure 6.12: Fluorescence microscopy of transverse sections (10 µm) of transgenic CBL/hMGFP mouse paws following 10 days of treatment with Accell CBL3 or control sd-siRNA-coated steel microneedles (10 × 700µm Regular). Two sets of representative images (A and B) are shown from different areas of the skin samples. In each set, hMGFP protein expression (and lack thereof) was visualised from mouse paws treated with Accell non-targeting control (top panel of each set; A1 and A2; B1 and B2) or Accell CBL3 (bottom panel of each set; A3 and A4; B3 and B4) sd-siRNA. The left panel shows the fluorescence overlay and the right panel shows the corresponding bright-field images. hMGFP fluorescence is pseudocoloured green. Nuclei were counterstained with DAPI and pseudocoloured blue.

hMGFP expression in the paw skin from the remaining mouse in each cohort was analysed at the skin structure level using established histology methods. Unfortunately, the placement of paw skin tissue in OCT medium from the mouse treated with Accell CBL3 sd-siRNA coated onto 5 × 500μm Regular microneedle devices was misinterpreted during the skin sectioning process, resulting in sectioning perpendicular to transverse sections, rendering results from the skin sections void. Nonetheless, paw skin tissues from the mouse treated with Accell sd-siRNA coated onto 10 × 700 μm Regular microneedle devices was successfully processed and fluorescence microscopy of the skin sections confirmed reduction in hMGFP protein expression (Figure 6.12).

Skin sections from the sample treated with the non-targeting control sd-siRNA (Figure 6.12 A1 and A2; B1 and B2) show intense GFP signal from the expression of hMGFP gene in the upper layers of the epidermis (Gonzalez-Gonzalez et al. 2009), which is clearly reduced in the CBL3 treated paw (Figure 6.12 A3 and A4; B3 and B4). The images in Figure 6.12 were taken from two separate areas within the treated region and are representative of all the sections over the treated area of the samples. The bright-field images (right panel in Figure 6.12) show that the stratum corneum is intact in all the sections, including the regions of low fluorescence, confirming that the reduced fluorescence in the CBL3 treated paw was due to a reduction in protein expression rather than an artefact as a result of physical disruption in the skin caused by microneedle treatment (Chong et al. 2013).

In any microneedle delivery system, dosing capacity is one of the major limiting factors. A previous study have demonstrated that delivery of Accell sd-siRNA using PAD microneedles induced reporter gene silencing in the Tg CBL/hMGFP reporter mouse (Gonzalez-Gonzalez et al. 2010b). However, partial mRNA reduction of up to 50% (n = 3) was achieved (Gonzalez-Gonzalez et al. 2010b) and it was thought to be related to limited dose loading capacity of the PAD microneedles. Therefore, steel microneedle devices were explored as an alternative for enhanced drug loading capacity with the aim of improving gene silencing efficiency (Chong et al. 2013; Gonzalez-Gonzalez et al. 2011; Pearton et al. 2012). The enhanced loading capacity of steel microneedles (up to 40 μg) did not result in increased gene silencing efficiency at the mRNA level compared to previous study whereby an estimated 120 ng of siRNA was administered through PAD microneedles per treatment (Gonzalez-Gonzalez et al. 2010b). However,

the method of siRNA administration with the PAD microneedles was different. With regards to PAD delivery, siRNA was coated onto three separate arrays of 4 × 5 PAD microneedles (60 in total) to deliver the coated dose over a wider area (Gonzalez-Gonzalez et al. 2010b). In contrast, an in-plane array of steel microneedles (5 or 10 needles per device) was used to deliver the coated dose over a narrow skin region (Chong et al. 2013). It is a possibility from previous experience (Chapter 5) that fewer microneedle penetration sites may have restricted the number of cells exposed to the siRNA treatment, thus compromising the efficiency of gene silencing. It is also evident from publications describing cutaneous delivery of functional siRNAs that gene silencing at the mRNA level in excess of 50% is rarely observed, regardless of siRNA dose or method of delivery (Gonzalez-Gonzalez et al. 2009; Gonzalez-Gonzalez et al. 2010b; Hsu and Mitragotri 2011; Lara et al. 2012). Therefore, even at a greater dose with well-validated qPCR endogenous control, detection of a further reduction in gene expression at the mRNA level may not be possible.

From these results, higher loading capacity was achieved with steel microneedles but did not result in obvious biological advantage over the use of PAD microneedles in mouse skin. However, the drug-coated steel microneedle system is a simple delivery method capable of loading high doses of biotherapeutics and may potentially be beneficial in *in vivo* human skin tissue for the treatment of conditions that requires larger dose of therapeutic nucleic acid (Chong et al. 2013). Overall, this study demonstrated for the first time, functional siRNA delivery using the coated steel microneedle system to mediate reporter protein silencing *in vivo*.

6.4 Conclusion

The specialised gene detection systems and techniques developed in collaboration and exploited in the *in vivo* studies detailed in this chapter greatly informed the research project. Despite the obvious differences in mouse models compared to human skin, their availability makes them widely used tools in gene manipulation studies. The study on reporter pDNA delivery to mouse paws showed that naked pDNA dry-coated onto steel microneedles of various dimensions and densities resulted in significant levels of gene expression, which previously failed to manifest convincingly in the *ex vivo* excised human skin model. Successful *in vivo* gene expression from deposition of dry-coated pDNA via steel microneedles confirms the value of the coated steel microneedle system in delivery of nucleic acid to the skin.

The *in vivo* siRNA mediated gene silencing study in the transgenic mouse model demonstrated for the first time the utility of the simple coated steel microneedle delivery system for delivery of functional siRNA to the skin. The study also demonstrated great siRNA loading and dosing capacity, deposition of siRNA within the skin and siRNA functionality as shown by reduction in protein expressions *in vivo*. The results from the *in vivo* study also highlights the complexity in detecting functional gene silencing at the mRNA level in a complex multilayer organ such as the skin, especially when treatment results in tissue injury. Nevertheless, the excellent gene silencing efficiency of Accell sd-siRNA *in vitro*, strong evidence of siRNA uptake *in vitro*, indication of siRNA deposition and uptake *ex vivo* in excised human skin as well as evident gene silencing of hMGFP gene *in vivo* gives impetus for clinical use of the coated steel microneedle system for the delivery of therapeutic siRNA to human skin.

CHAPTER 7

General discussion

7 General discussion

7.1 Overview

In the majority of pre-clinical and clinical studies performed to date, nucleic acid is delivered to the skin through intradermal injection. However, intradermal injection causes significant pain, which may be potentiated in certain skin conditions (Leachman et al. 2009). Therefore, less invasive physical skin disruption methods are actively pursued for targeted delivery of nucleic acid to the skin. While the ability of microneedle devices to penetrate the stratum corneum barrier in a minimally invasive and pain-free manner (Gill et al. 2008; Haq et al. 2009; Widera et al. 2006) for delivery of a range of therapeutic substances (extensively reviewed by Kim et al. 2012b) and nucleic acid, particularly pDNA (Coulman et al. 2006b; Gonzalez-Gonzalez et al. 2011; Ng et al. 2009; Pearton et al. 2012) has previously been demonstrated, the potential of such systems for the delivery of siRNA had not been shown at the start of the PhD (Geusens et al. 2009b). siRNA mediated RNA interference is an exciting therapeutic prospect as skin conditions caused by aberrant gene expression can potentially be treated by supressing the overexpressing gene through targeting and disrupting mRNA with complementary base sequences. This thesis aims to understand gene expression and gene silencing in *in vitro*, *ex vivo* and *in vivo* skin models employing various gene detection systems to realise the potential of targeted nucleic acid delivery to the skin using microneedles.

Firstly, *in vitro* and *ex vivo* human skin culture models were developed (Chapter 2). The relative ease of growth and maintenance of the immortalised HaCaT cell line helped in preliminary and optimisation experiments while primary keratinocytes cultured in a controlled monolayer environment bore closer biological proximity to keratinocyte cells in the corresponding excised human skin. *Ex vivo* human skin culture was employed as a relevant pre-clinical model for gene delivery and expression studies.

Steel microneedles of various shapes and dimensions were then characterised. Previously, steel microneedles were coated with drug formulations using a reusable dip-coating station that has a dead volume, resulting in poor estimation of coating dose, material wastage and possible contamination with residual materials from previous coating process. A new technique for dip-coating microneedles was developed (Chapter

2) using single use pipette tips as a reservoir for coating, which allows precise estimation of the coated material and quantification of nucleic acid deposition following skin treatment (Chapter 5 and 6). It was also found that electropolishing the surface of steel microneedles might result in improved drug removal from its surface following skin treatment but this did not affect highly soluble molecules such as siRNA.

Genetic manipulation in human skin models through delivery of pDNA to human skin models was demonstrated in Chapter 3. Reporter gene expression was found in *in vitro* human keratinocytes following delivery of pDNA lipoplex and in the viable epidermal layer within human skin culture following delivery of aqueous formulation of naked pDNA by microneedle abrasion. Although *in vitro* pDNA delivery with non-viral vectors were moderately effective (37% efficiency) compared to a viral vector (90% efficiency) (Chen et al. 2003), the level of gene expressions was comparable with the highest found to date with commercially available lipid-based vectors in comparable human keratinocytes models (Ng 2010; Yamano et al. 2010).

In human skin studies, naked pDNA was more efficient than a lipoplex formulation and therefore the value of lipid-based transfection reagents in gene delivery to human skin is ambiguous. Furthermore, pDNA lipoplexes were relatively toxic *in vitro* with observed reduction in cell viability following transfection. Therefore, it is ideal that the use of lipid-based vectors in the skin can be avoided. Human skin studies were conducted in only a small number of samples, but the observations were not isolated incidents, as previous studies have reported similar findings (Ng 2010; Ng et al. 2009; Pearton et al. 2012). Microneedles were capable of penetrating the stratum corneum and assist the delivery of naked pDNA across the skin barrier into keratinocytes in the epidermis for subsequent transgene expression. However, reporter gene expression in the skin following pDNA delivery through microneedle abrasion was not found in every cell within the treatment area, rather in scarcely spaced populations of cells along the microneedle abrasion sites. Even though gene expression in excised human skin was not better than previous findings (Coulman et al. 2006b; Ng et al. 2009; Pearton et al. 2012) and might represent a significant challenge for skin conditions that require gene correction in a large population of skin cells, these results reiterated the great potential of microneedle-assisted pDNA delivery for applications such as DNA vaccination. Skin vaccination with pDNA only requires protein antigen expression from a few cells within

the epidermis for epidermal Langerhans cells to acquire the antigen and stimulate an immune response (Larregina and Falo 2005). The ability to achieve similar findings to previous studies was encouraging as studies with pDNA served to provide the basis and foundation of understanding genetic manipulation in human skin models using pre-validated protocols for further investigation of nucleic acid delivery to human skin.

Nucleic acid delivery to human skin models progressed with the delivery of siRNA to *in vitro* keratinocytes as the first step to developing and optimising methods for siRNA mediated gene silencing in human skin. Cationic lipids are commonly used as non-viral vectors to facilitate cellular uptake and release of siRNA from endosomal membranes following endocytosis. The siRNA lipoplex was highly efficient in mediating gene silencing of lamin A/C and CD44 model genes in *in vitro* human skin cells and visibly reduced target protein levels at a concentration as low as 1 nM, with no evidence of cellular toxicity at a concentration of 10 nM (Chapter 4). These initial studies demonstrated the high potency of siRNA as a mediator of gene silencing in human skin cells.

Microneedle delivery of siRNA in the form of dry-coat on the surface of microneedles is advantageous because storage of siRNA in a solid state could improve its stability and coated solid microneedles are strong enough to penetrate the skin together with the coated payload to deposit coated drug in the skin. The suitability of siRNA lipoplex, delivered in its dry form through the coated steel microneedle system was investigated and it was found that the siRNA lipoplex lost its biological functionality following the siRNA coating and recovery process. If the siRNA lipoplex was functional following coating onto steel microneedles, it would have been ideal as siRNA lipoplex were highly efficient at low doses. Nevertheless, naked siRNA recovered following coating onto steel microneedles remained biologically functional, which is the first indication of the stability of siRNA coated onto the surface of steel microneedles.

As part of the NIH funded “GO Delivery!” initiative, an international collaboration with Stanford University and Transderm Inc. (California, USA) was instigated. This resulted in the availability of proprietary Accell modified “self-delivery” siRNA that enters cell passively without the need of a carrier for testing in human skin models (Chapter 4 and 5) as well as in an *in vivo* transgenic reporter mouse skin model (Chapter 6). Due to the

passive cellular entry mechanism of Accell sd-siRNA, *in vitro* gene silencing required approximately 100 times higher doses of siRNA than the siRNA lipoplex formulation. Accell CD44 sd-siRNA was efficient (up to 80% mRNA reduction at 48 h) in mediating gene silencing at concentration of at least 0.5 μM in human keratinocyte cells *in vitro*, with no evidence of cellular toxicity at a concentration of 1 μM. Cellular uptake studies provided sound evidence of sd-siRNA internalisation in both HaCaT and primary keratinocytes with presence of fluorescently labelled sd-siRNA in all cells within 3 h of treatment. Internalised siRNAs were localised in the perinuclear region of the keratinocyte cell cytoplasm, near the nuclear membrane where the RISC complexes are located. This series of *in vitro* studies demonstrated that siRNA-mediated gene silencing with naked sd-siRNA is efficient and non-toxic in human epidermal keratinocytes. This led to the hypothesis that if microneedles are used to overcome the skin's physical barrier, Accell sd-siRNA deposited within the skin could effectively silence genes in cells proximal to the microneedle insertion site. The use of Accell sd-siRNA in a coated steel microneedle system was supported by its stability in storage (at 4°C) of up to 28 days.

Animal models are widely accepted as pre-clinical *in vivo* models to investigate nucleic acid delivery to the skin. However, mouse skin models are not a good representation of human skin due to interspecies variability that results in a different pattern of reporter gene expression following intradermal delivery of pDNA (Hengge et al. 1996). Therefore, developing a siRNA delivery and gene detection method in *ex vivo* culture of freshly excised human skin would provide a more suitable pre-clinical model to test therapeutic siRNA. siRNA coated steel microneedles penetrated the skin's stratum corneum barrier and deposited siRNA in the viable epidermis as well as the dermis (Chapter 5). However, determination of siRNA uptake and gene silencing in the excised skin epidermis was challenging due to the short-term viability (up to 72 h) of the culture system. Confocal microscopy demonstrated the presence of isolated epidermal cells with siRNA uptake but attempts to detect gene silencing at the molecular level following a single administration of siRNA-coated microneedles gave equivocal results. This is probably because the viability of skin deteriorates with time and is likely to differ between different skin specimens, which are dependant on a surgery schedule and have limited availability throughout the year. Whilst administration of a single application of liquid pDNA following microneedle abrasion may be sufficient for gene

expression, multiple doses of siRNA delivered over a period of 7 to 10 days may be required to observe significant level of gene silencing within the structurally complex and self-renewing layers of the skin. Furthermore, several published studies in animal models have reported the *in vivo* gene silencing efficiency of Accell modified siRNA (Gonzalez-Gonzalez et al. 2010b; Nakajima et al. 2012). When a suitable human skin model becomes available, for example full thickness human skin xenografted onto immunocompromised mouse, the skills and insight gained with respect to siRNA delivery to the skin would be invaluable in designing future studies.

The delivery of nucleic acids via coated steel microneedles was also investigated in mouse skin models to determine *in vivo* biological functionality (Chapter 6). pDNA was coated onto in-plane steel microneedle devices of different needle length, spatial densities and dimensions. pDNA liquid-loaded onto pocketed microneedle devices did not result in reporter gene expression in treated mouse paws as it was observed during microneedle administration that liquid loaded pDNA formulation deposited on the surface of the skin rather than into the viable layers of skin. Delivery of pDNA dry-coated onto steel microneedles resulted in gene expression (observed via an intravital imaging system) in treated mouse paws. Longer (700 μm) microneedles deposited a greater dose of pDNA in the mouse paws but initial (24 h) reporter gene expression was similar across all treatment groups. After 5 days, reporter gene expression increased in mouse paws treated with longer microneedles but appeared to have decreased in mouse paws treated with shorter (500 μm) microneedles.

The positive result achieved in this *in vivo* mouse skin study with pDNA coated steel microneedles was in contrast to that achieved with excised human skin (Chapter 3). Delivery of pDNA dry-coated onto steel microneedles resulted in inconsistent gene expression, presumably due to insufficient hydration in skin proximal to pDNA deposition to dissolve deposited pDNA or instability of the pDNA coated on the surface of steel microneedles. However, the mouse skin study has shown that pDNA remains biologically functional following coating onto the surface of steel microneedles. There are differences in skin structure and thickness between mouse paw skin and human skin, and therefore it is possible that longer microneedles deposited pDNA in the muscles of the mouse paws, which provided better hydration for the dissolution of the deposited pDNA and resulted in sustained release of pDNA over several days. The steel

microneedles are designed for use in human skin, to penetrate the stratum corneum in a minimally invasive manner, but when used in mouse skin it is possible that they deliver nucleic acids to deeper tissues. This study highlighted the inter-species differences in skin anatomy that should always be considered when designing and interpreting results from *in vivo* experiments using animal models.

The functionality of siRNA delivered via coated steel microneedles was investigated in a transgenic reporter mouse model that expresses reporter gene in the upper layers of its epidermis, which can be silenced with specific Accell sd-siRNA (Chapter 6). Following microneedle delivery of siRNA, reporter mRNA level (in the paw skin tissue) was reduced in 2 out of the 3 mice studied. It is postulated that the equivocal change in gene expression at the mRNA level is due to lack of a suitable endogenous control gene for qPCR normalisation, which is stably expressed in skin that has been injured following daily microneedle application. As mentioned, the length and dimension of steel microneedles were designed for use in human skin and when applied to mouse paw this may be considered more invasive. Nevertheless, quantification of reporter gene expression and visualisation of fluorescent protein intensity in skin sections confirmed gene silencing at the protein level. This study demonstrated for the first time, functional siRNA delivery and reporter protein reduction in a transgenic mouse model using the coated steel microneedle system.

Although a previous study has also shown functional siRNA delivery to mouse skin models through coated biodegradable PAD microneedles (Gonzalez-Gonzalez et al. 2010b) with comparable gene silencing, at the protein level, steel microneedles are capable of loading significantly higher doses of nucleic acids to enable a greater dose to be deposited in the skin. siRNA loading onto an in-plane array of steel microneedles (5 needles per array) of up to 40 μg (8 μg per needle) was demonstrated in this thesis and a higher dose of siRNA could potentially be coated. Coated steel microneedles are also capable of delivering up to 90% of their coated dose as shown by studies in Chapter 5 and other published studies (Gill and Prausnitz 2007a; Gonzalez-Gonzalez et al. 2011; Kim et al. 2010). In contrast, PAD microneedles are capable of coating up to 2 μg siRNA per needle and only deposit approximately 15% of their coated dose. The higher coating capacity and deposition of coated dose from steel microneedles is advantageous

as sufficient doses of therapeutic materials can be delivered using this delivery system with minimal wastage of expensive biotherapeutics.

Furthermore, the coated steel microneedle system could potentially be developed to produce pre-coated dose of biotherapeutics as a one step delivery device that could be prescribed to patients for self-administration. This would be particularly useful in improving patient compliance with the treatment of cutaneous skin disorders that will probably require life-long genetic correction, due to the self-renewing nature of the skin. The production of steel microneedles can also be easily adapted to create needles of different shapes and sizes to suit various applications to different sites of the body.

7.2 Current limitations and future studies

Local manufacture of steel microneedle devices of various dimensions, needle length and spatial density was attempted for the first time. This resulted in production of microneedle devices that were unpolished with a rough surface, compared to electropolished microneedles obtained from other sources. It was not apparent at the time of manufacture that the surface properties of the microneedles would influence dissolution of less soluble drug formulations, which has been demonstrated in preliminary studies in this thesis. Future design of steel microneedle devices should consider polishing the surface of the microneedles. Various drug dissolution profiles from both polished and unpolished microneedles could be compared to ascertain how the surface of steel microneedles may affect drug deposition in the skin.

A novel, simple and precise microneedle dip-coating method was developed for the purpose of small-scale studies in this thesis. However, this method of manual microneedle coating is time-consuming and would be inefficient in large-scale coating of steel microneedles for clinical applications. The dose of drug that can be coated onto microneedles is often limited by drug solubility in the aqueous coating formulation and coating microneedles has the advantage of being able to layer on drug coats following a short period of drying time (30 s). An automated microneedle coating process that is capable of coating precise and sufficiently high doses drug formulation onto microneedles in a good manufacturing practice (GMP) environment has to be developed for future clinical applications.

Both siRNA lipoplex and modified self-delivery siRNA formulations are highly efficient in delivering siRNA to human keratinocytes. However, it was apparent from the *in vivo* mouse model and *ex vivo* human skin studies that the major limitation to gene silencing detection at the mRNA level in skin treated with physically invasive method is the selection of suitable endogenous control gene for qPCR normalisation. In response to tissue injury, certain endogenous genes may be over or under expressed, leading to inaccurate analysis of qPCR quantification. Identification and validation of endogenous control genes stable at all stages of skin treatment with microneedle-based therapies represents a significant challenge that could be undertaken in future studies in order to improve the accuracy of gene silencing detection at the mRNA level.

Otherwise, gene silencing detection at the protein level should always be performed alongside detection of mRNA levels. In a transgenic reporter mouse model, visualisation of target protein expression was possible but in the case of excised human skin, the short-term viability of the skin in culture poses significant challenges to quantifying protein expression.

Comparison of results from the siRNA delivery studies in excised human skin with cutaneous siRNA studies reported in the literature suggests that multiple siRNA doses over a period of 7 to 10 days are required to observe significant levels of gene silencing within the complex skin strata (Gonzalez-Gonzalez et al. 2010b; Lara et al. 2012). Although there is evidence suggesting that incorporation of siRNA into the RISC complex improves intracellular stability of siRNA (Hoerter et al. 2011), the effect of siRNA is transient in comparison with stable genomic integration achievable with some viral vectors. Whilst the use of excised human skin as a representative model for pre-clinical testing of cutaneous siRNA therapy has limitations due to restricted viability of the *ex vivo* skin culture systems, a recently published study by our collaborators demonstrates the suitability of full thickness human skin xenografted onto the back of immunocompromised mice as a pre-clinical model for siRNA testing (Lara et al. 2012). The potential of the coated steel microneedles for cutaneous delivery of nucleic acid could therefore be further tested using this skin model.

Although sd-siRNA and siRNA lipoplex formulations were not toxic *in vitro*, there are significant concerns about the unwanted off target effects and immune response that may be induced by *in vivo* siRNA treatment. These concerns need to be addressed in suitable pre-clinical models before the potential of siRNA therapeutics can be realised in clinical practice (Vicentini et al. 2013). These studies were beyond the scope of this PhD thesis but it is important that future development of cutaneous siRNA treatment should involve detailed microarray and toxicology studies to determine if the therapeutic siRNA affects the expression of non-target genes within tissue. The systemic side effects of cutaneous siRNA delivery should also be investigated in suitable models to ensure clinical safety of localised siRNA delivery to human skin.

7.3 Concluding remarks

Overall, the studies in this thesis provide new insight and improved understanding of nucleic acid delivery and gene detection in the skin. Excised human skin studies involving pDNA provided evidence of the ability to deliver nucleic acid to the *ex vivo* skin culture model for transgene expression within epidermal cells. The potential of siRNA-based therapeutics in various skin models was shown in a series of *in vitro*, *ex vivo* and *in vivo* studies. Although it was not always possible to clearly demonstrate effective gene silencing at the mRNA level in skin tissues, *in vitro* and *in vivo* studies serve to confirm the potential of siRNA as a powerful class of gene inhibitors that has great potential in cutaneous disorders.

The availability of modified sd-siRNA coupled with the skin delivery capability of microneedle devices shows promise for the simple, pain-free and potentially self-administrable treatment of skin disorders cause by aberrant gene expression.

References

A Fomani, A. and Mansour, R. R. 2011. Fabrication and characterization of the flexible neural microprobes with improved structural design. *Sensors and Actuators A: Physical* 168(2), pp. 233-241.

Aasen, T. and Izpisua Belmonte, J. C. 2010. Isolation and cultivation of human keratinocytes from skin or plucked hair for the generation of induced pluripotent stem cells. *Nat Protoc* 5(2), pp. 371-382.

Aguiar, J. C. et al. 2001. Enhancement of the immune response in rabbits to a malaria DNA vaccine by immunization with a needle-free jet device. *Vaccine* 20(1-2), pp. 275-280.

Al-Qallaf, B. and Das, D. B. 2009. Optimizing microneedle arrays to increase skin permeability for transdermal drug delivery. *Ann N Y Acad Sci* 1161, pp. 83-94.

Alarcon, J. B. et al. 2007. Preclinical evaluation of microneedle technology for intradermal delivery of influenza vaccines. *Clin Vaccine Immunol* 14(4), pp. 375-381.

Alex, A. et al. 2010. Multispectral in vivo three-dimensional optical coherence tomography of human skin. *J Biomed Opt* 15(2), p. 026025.

Almofti, M. R. et al. 2003. Cationic liposome-mediated gene delivery: biophysical study and mechanism of internalization. *Arch Biochem Biophys* 410(2), pp. 246-253.

Alonso, L. and Fuchs, E. 2003. Stem cells of the skin epithelium. *Proc Natl Acad Sci U S A* 100 Suppl 1, pp. 11830-11835.

Arendt-Nielsen, L. et al. 2006. Pain following controlled cutaneous insertion of needles with different diameters. *Somatosens Mot Res* 23(1-2), pp. 37-43.

Arora, A. et al. 2008. Micro-scale devices for transdermal drug delivery. *Int J Pharm* 364(2), pp. 227-236.

Babiuk, S. et al. 2000. Cutaneous vaccination: the skin as an immunologically active tissue and the challenge of antigen delivery. *J Control Release* 66(2-3), pp. 199-214.

Badran, M. M. et al. 2009. Skin penetration enhancement by a microneedle device (Dermaroller) in vitro: dependency on needle size and applied formulation. *Eur J Pharm Sci* 36(4-5), pp. 511-523.

Bains, B. K. et al. 2010. In vitro reporter gene transfection via plasmid DNA delivered by metered dose inhaler. *J Pharm Sci* 99(7), pp. 3089-3099.

Balicki, D. and Beutler, E. 1997. Histone H2A significantly enhances in vitro DNA transfection. *Mol Med* 3(11), pp. 782-787.

Balicki, D. et al. 2002. Structure and function correlation in histone H2A peptide-mediated gene transfer. *Proc Natl Acad Sci U S A* 99(11), pp. 7467-7471.

Bariya, S. H. et al. 2012. Microneedles: an emerging transdermal drug delivery system. *J Pharm Pharmacol* 64(1), pp. 11-29.

Barrandon, Y. and Green, H. 1985. Cell size as a determinant of the clone-forming ability of human keratinocytes. *Proceedings of the National Academy of Sciences of the United States of America* 82(16), p. 5390.

Barrandon, Y. and Green, H. 1987. Three clonal types of keratinocyte with different capacities for multiplication. *Proceedings of the National Academy of Sciences of the United States of America* 84(8), p. 2302.

Barrientos, S. et al. 2008. Growth factors and cytokines in wound healing. *Wound Repair Regen* 16(5), pp. 585-601.

Barry, B. W. 2001. Novel mechanisms and devices to enable successful transdermal drug delivery. *Eur J Pharm Sci* 14(2), pp. 101-114.

Barry, M. E. et al. 1999. Role of endogenous endonucleases and tissue site in transfection and CpG-mediated immune activation after naked DNA injection. *Hum Gene Ther* 10(15), pp. 2461-2480.

Bartel, D. P. 2004. MicroRNAs: genomics, biogenesis, mechanism, and function. *Cell* 116(2), pp. 281-297.

Baskin, L. et al. 2008. A novel ex-vivo application of RNAi for neuroscience. *Biotechniques* 45(3), pp. 338-339.

Basner-Tschakarjan, E. et al. 2004. Uptake and trafficking of DNA in keratinocytes: evidence for DNA-binding proteins. *Gene Ther* 11(9), pp. 765-774.

Baxter, J. and Mitragotri, S. 2005. Jet-induced skin puncture and its impact on needle-free jet injections: experimental studies and a predictive model. *J Control Release* 106(3), pp. 361-373.

Beebe, D. J. et al. 2002. Physics and applications of microfluidics in biology. *Annu Rev Biomed Eng* 4, pp. 261-286.

Bernstein, E. et al. 2001. Role for a bidentate ribonuclease in the initiation step of RNA interference. *Nature* 409(6818), pp. 363-366.

Bickenbach, J. R. 2001. Stem Cells, Differentiation and Renewal Kinetics of Keratinocytes: Implications for Cutaneous Gene Therapy. In: Hengge, U.R. and Volc-Platzer, B. eds. *The Skin and Gene Therapy*. Berlin: Springer-Verlag, pp. 27-34.

Bierwagen, G. P. 1992. Film coating technologies and adhesion. *Electrochimica acta* 37(9), pp. 1471-1478.

Birchall, J. et al. 2006. Cutaneous gene expression of plasmid DNA in excised human skin following delivery via microchannels created by radio frequency ablation. *Int J Pharm* 312(1-2), pp. 15-23.

Birchall, J. et al. 2005. Cutaneous DNA delivery and gene expression in ex vivo human skin explants via wet-etch micro-fabricated micro-needles. *J Drug Target* 13(7), pp. 415-421.

Birchall, J. C. 2006. Microneedle array technology: the time is right but is the science ready? *Expert Rev Med Devices* 3(1), pp. 1-4.

Birchall, J. C. et al. 2000. Gene expression in an intact ex-vivo skin tissue model following percutaneous delivery of cationic liposome-plasmid DNA complexes. *Int J Pharm* 197(1-2), pp. 233-238.

Birnboim, H. C. and Doly, J. 1979. A rapid alkaline extraction procedure for screening recombinant plasmid DNA. *Nucleic Acids Res* 7(6), pp. 1513-1523.

Blaese, R. M. et al. 1995. T lymphocyte-directed gene therapy for ADA- SCID: initial trial results after 4 years. *Science* 270(5235), pp. 475-480.

Bos, J. D. and Meinardi, M. M. 2000. The 500 Dalton rule for the skin penetration of chemical compounds and drugs. *Exp Dermatol* 9(3), pp. 165-169.

Boukamp, P. et al. 1988. Normal keratinization in a spontaneously immortalized aneuploid human keratinocyte cell line. *J Cell Biol* 106(3), pp. 761-771.

Boukamp, P. et al. 1997. Sustained nontumorigenic phenotype correlates with a largely stable chromosome content during long-term culture of the human keratinocyte line HaCaT. *Genes Chromosomes Cancer* 19(4), pp. 201-214.

Boulais, N. and Misery, L. 2008. The epidermis: a sensory tissue. *Eur J Dermatol* 18(2), pp. 119-127.

Bourrguignon, L. Y. et al. 1995. Involvement of CD44 and its variant isoforms in membrane-cytoskeleton interaction, cell adhesion and tumor metastasis. *J Neurooncol* 26(3), pp. 201-208.

Boussif, O. et al. 1995. A versatile vector for gene and oligonucleotide transfer into cells in culture and in vivo: polyethylenimine. *Proc Natl Acad Sci U S A* 92(16), pp. 7297-7301.

Bouwstra, J. A. and Honeywell-Nguyen, P. L. 2002. Skin structure and mode of action of vesicles. *Adv Drug Deliv Rev* 54 Suppl 1, pp. S41-55.

Branski, L. K. et al. 2010. Pre-clinical evaluation of liposomal gene transfer to improve dermal and epidermal regeneration. *Gene Ther* 17(6), pp. 770-778.

Braverman, I. M. 1997. The cutaneous microcirculation: ultrastructure and microanatomical organization. *Microcirculation* 4(3), pp. 329-340.

Bressler, R. and Bressler, C. 1989. Functional anatomy of the skin. *Clinics in podiatric medicine and surgery* 6(2), p. 229.

Briggaman, R. and Wheeler, C. 1975. The epidermal-dermal junction. *Journal of Investigative Dermatology* 65(1), pp. 71-84.

Brock, R. et al. 1999. Comparison of fixation protocols for adherent cultured cells applied to a GFP fusion protein of the epidermal growth factor receptor. *Cytometry* 35(4), pp. 353-362.

Brown, M. B. et al. 2006. Dermal and transdermal drug delivery systems: current and future prospects. *Drug Deliv* 13(3), pp. 175-187.

Burgeson, R. and Christiano, A. 1997. The dermal--epidermal junction. *Current opinion in cell biology* 9(5), pp. 651-658.

Burnett, J. C. and Rossi, J. J. 2012. RNA-based therapeutics: current progress and future prospects. *Chem Biol* 19(1), pp. 60-71.

Bustin, S. A. 2000. Absolute quantification of mRNA using real-time reverse transcription polymerase chain reaction assays. *J Mol Endocrinol* 25(2), pp. 169-193.

Bystrova, S. and Luttge, R. 2011. Micromolding for ceramic microneedle arrays. *Microelectronic Engineering* 88(8), pp. 1681-1684.

Capecchi, M. R. 1980. High efficiency transformation by direct microinjection of DNA into cultured mammalian cells. *Cell* 22(2 Pt 2), pp. 479-488.

Caracciolo, G. et al. 2005. Multicomponent cationic lipid-DNA complex formation: role of lipid mixing. *Langmuir* 21(25), pp. 11582-11587.

Carralot, J. P. et al. 2009. Automated high-throughput siRNA transfection in raw 264.7 macrophages: a case study for optimization procedure. *J Biomol Screen* 14(2), pp. 151-160.

Carretero, M. et al. 2006. Skin gene therapy for acquired and inherited disorders. *Histol Histopathol* 21(11), pp. 1233-1247.

Castanotto, D. and Rossi, J. J. 2009. The promises and pitfalls of RNA-interference-based therapeutics. *Nature* 457(7228), pp. 426-433.

Cavazzana-Calvo, M. et al. 2000. Gene therapy of human severe combined immunodeficiency (SCID)-X1 disease. *Science* 288(5466), pp. 669-672.

Chabri, F. et al. 2004. Microfabricated silicon microneedles for nonviral cutaneous gene delivery. *Br J Dermatol* 150(5), pp. 869-877.

Chandrasekhar, S. et al. 2013. Microarrays and microneedle arrays for delivery of peptides, proteins, vaccines and other applications. *Expert Opin Drug Deliv* 10(8), pp. 1155-1170.

Chehtane, M. and Khaled, A. R. 2010. Interleukin-7 mediates glucose utilization in lymphocytes through transcriptional regulation of the hexokinase II gene. *Am J Physiol Cell Physiol* 298(6), pp. C1560-1571.

Chemin, I. et al. 1998. Liver-directed gene transfer: a linear polyethlenimine derivative mediates highly efficient DNA delivery to primary hepatocytes in vitro and in vivo. *J Viral Hepat* 5(6), pp. 369-375.

Chen, M. et al. 2003. An efficient gene transduction system for studying gene function in primary human dermal fibroblasts and epidermal keratinocytes. *Clin Exp Dermatol* 28(2), pp. 193-199.

Chen, T. et al. 1999. Charged microbeads are not transported across the human stratum corneum in vitro by short high-voltage pulses. *Bioelectrochem Bioenerg* 48(1), pp. 181-192.

Chen, W. Y. and Abatangelo, G. 1999. Functions of hyaluronan in wound repair. *Wound Repair Regen* 7(2), pp. 79-89.

Cherng, J. Y. et al. 1999. Long term stability of poly((2-dimethylamino)ethyl methacrylate)-based gene delivery systems. *Pharm Res* 16(9), pp. 1417-1423.

Choate, K. A. and Khavari, P. A. 1997. Direct cutaneous gene delivery in a human genetic skin disease. *Hum Gene Ther* 8(14), pp. 1659-1665.

Choi, M. J. et al. 2004. Effect of tape stripping on percutaneous penetration and topical vaccination. *Exogenous Dermatology* 2(5), pp. 262-269.

Choi, S. O. et al. 2010. An electrically active microneedle array for electroporation. *Biomed Microdevices* 12(2), pp. 263-273.

Chong, R. H. et al. 2013. Gene silencing following siRNA delivery to skin via coated steel microneedles: In vitro and in vivo proof-of-concept. *J Control Release* 166(3), pp. 211-219.

Christiano, A. and Uitto, J. 1996. Molecular complexity of the cutaneous basement membrane zone. *Experimental Dermatology* 5(1), pp. 1-11.

Christie, P. J. et al. 1987. Two conjugation systems associated with Streptococcus faecalis plasmid pCF10: identification of a conjugative transposon that transfers between S. faecalis and Bacillus subtilis. *J Bacteriol* 169(6), pp. 2529-2536.

Christophers, E. 1971. Cellular architecture of the stratum corneum. *J Invest Dermatol* 56(3), pp. 165-169.

Cichy, J. and Pure, E. 2003. The liberation of CD44. *J Cell Biol* 161(5), pp. 839-843.

Cideciyan, A. V. et al. 2013. Human retinal gene therapy for Leber congenital amaurosis shows advancing retinal degeneration despite enduring visual improvement. *Proc Natl Acad Sci U S A* 110(6), pp. E517-525.

Clemmensen, A. et al. 2009. Extraction of high-quality epidermal RNA after ammonium thiocyanate-induced dermo-epidermal separation of 4 mm human skin biopsies. *Exp Dermatol* 18(11), pp. 979-984.

ClontechLaboratories. 2002. pEGFP-N1 Vector Information.

ClontechLaboratories. 2004. pCMV-LacZ Vector Information.

Contag, C. H. and Bachmann, M. H. 2002. Advances in in vivo bioluminescence imaging of gene expression. *Annu Rev Biomed Eng* 4, pp. 235-260.

Cormier, M. et al. 2004. Transdermal delivery of desmopressin using a coated microneedle array patch system. *J Control Release* 97(3), pp. 503-511.

Coulman, S. 2006. *Gene delivery to human skin using microneedle arrays (PhD Thesis)*. Cardiff University.

Coulman, S. et al. 2006a. Microneedles and other physical methods for overcoming the stratum corneum barrier for cutaneous gene therapy. *Crit Rev Ther Drug Carrier Syst* 23(3), pp. 205-258.

Coulman, S. A. et al. 2006b. Minimally invasive cutaneous delivery of macromolecules and plasmid DNA via microneedles. *Curr Drug Deliv* 3(1), pp. 65-75.

Coulman, S. A. et al. 2011. In vivo, in situ imaging of microneedle insertion into the skin of human volunteers using optical coherence tomography. *Pharm Res* 28(1), pp. 66-81.

Crichton, M. L. et al. 2011. The viscoelastic, hyperelastic and scale dependent behaviour of freshly excised individual skin layers. *Biomaterials* 32(20), pp. 4670-4681.

Crick, F. 1970. Central dogma of molecular biology. *Nature* 227(5258), pp. 561-563.

Cross, S. E. and Roberts, M. S. 2004. Physical enhancement of transdermal drug application: is delivery technology keeping up with pharmaceutical development? *Curr Drug Deliv* 1(1), pp. 81-92.

Cui, Z. et al. 2003. Intradermal immunization with novel plasmid DNA-coated nanoparticles via a needle-free injection device. *J Biotechnol* 102(2), pp. 105-115.

Daniels, J. T. et al. 1996. Human keratinocyte isolation and cell culture: a survey of current practices in the UK. *Burns* 22(1), pp. 35-39.

Daud, A. I. et al. 2008. Phase I trial of interleukin-12 plasmid electroporation in patients with metastatic melanoma. *J Clin Oncol* 26(36), pp. 5896-5903.

Davis, S. P. et al. 2005. Hollow metal microneedles for insulin delivery to diabetic rats. *IEEE Trans Biomed Eng* 52(5), pp. 909-915.

De Paula, D. et al. 2007. Hydrophobization and bioconjugation for enhanced siRNA delivery and targeting. *RNA* 13(4), pp. 431-456.

De Smedt, S. C. et al. 2000. Cationic polymer based gene delivery systems. *Pharm Res* 17(2), pp. 113-126.

Deacon, B. and Abramowitz, J. 2006. Fear of needles and vasovagal reactions among phlebotomy patients. *J Anxiety Disord* 20(7), pp. 946-960.

Dean, D. A. et al. 2005. Nuclear entry of nonviral vectors. *Gene Ther* 12(11), pp. 881-890.

Dean, H. J. and Chen, D. 2004. Epidermal powder immunization against influenza. *Vaccine* 23(5), pp. 681-686.

Del Rio, M. et al. 2004. Current approaches and perspectives in human keratinocyte-based gene therapies. *Gene Ther* 11 Suppl 1, pp. S57-63.

Delalande, A. et al. 2013. Sonoporation: mechanistic insights and ongoing challenges for gene transfer. *Gene* 525(2), pp. 191-199.

Dellambra, E. et al. 2000. Toward epidermal stem cell-mediated ex vivo gene therapy of junctional epidermolysis bullosa. *Hum Gene Ther* 11(16), pp. 2283-2287.

Dickens, S. et al. 2010. Non-viral gene therapy strategies for keratinocytes, fibroblasts and endothelial progenitor cells for ex vivo gene transfer to skin wounds. *Tissue Eng Part C Methods* 16(6), pp. 1601-1608.

Dijkmans, P. A. et al. 2004. Microbubbles and ultrasound: from diagnosis to therapy. *Eur J Echocardiogr* 5(4), pp. 245-256.

Dileo, J. et al. 2003. Gene transfer to subdermal tissues via a new gene gun design. *Hum Gene Ther* 14(1), pp. 79-87.

Donnelly, R. F. et al. 2011. Design, optimization and characterisation of polymeric microneedle arrays prepared by a novel laser-based micromoulding technique. *Pharm Res* 28(1), pp. 41-57.

Donnelly, R. F. et al. 2009. Processing difficulties and instability of carbohydrate microneedle arrays. *Drug Dev Ind Pharm* 35(10), pp. 1242-1254.

Donnelly, R. F. et al. 2010. Microneedle-based drug delivery systems: microfabrication, drug delivery, and safety. *Drug Deliv* 17(4), pp. 187-207.

Drabick, J. J. et al. 2001. Cutaneous transfection and immune responses to intradermal nucleic acid vaccination are significantly enhanced by in vivo electropermeabilization. *Mol Ther* 3(2), pp. 249-255.

Dunne, J. et al. 2003. The apparent uptake of fluorescently labeled siRNAs by electroporated cells depends on the fluorochrome. *Oligonucleotides* 13(5), pp. 375-380.

Durieux, A. C. et al. 2004. In vivo gene electrotransfer into skeletal muscle: effects of plasmid DNA on the occurrence and extent of muscle damage. *J Gene Med* 6(7), pp. 809-816.

Eckert, R. L. 1989. Structure, function, and differentiation of the keratinocyte. *Physiol Rev* 69(4), pp. 1316-1346.

Eden, E. et al. 2011. Proteome half-life dynamics in living human cells. *Science* 331(6018), pp. 764-768.

Edmondson, J. et al. 1988. A rapid and simple MTT-based spectrophotometric assay for determining drug sensitivity in monolayer cultures. *Methods in Cell Science* 11(1), pp. 15-17.

Eichner, R. et al. 1986. The role of keratin subfamilies and keratin pairs in the formation of human epidermal intermediate filaments. *J Cell Biol* 102(5), pp. 1767-1777.

El Maghraby, G. M. et al. 2008. Liposomes and skin: from drug delivery to model membranes. *Eur J Pharm Sci* 34(4-5), pp. 203-222.

El Maghraby, G. M. and Williams, A. C. 2009. Vesicular systems for delivering conventional small organic molecules and larger macromolecules to and through human skin. *Expert Opin Drug Deliv* 6(2), pp. 149-163.

Elbashir, S. M. et al. 2001a. Duplexes of 21-nucleotide RNAs mediate RNA interference in cultured mammalian cells. *Nature* 411(6836), pp. 494-498.

Elbashir, S. M. et al. 2002. Analysis of gene function in somatic mammalian cells using small interfering RNAs. *Methods* 26(2), pp. 199-213.

Elbashir, S. M. et al. 2001b. RNA interference is mediated by 21- and 22-nucleotide RNAs. *Genes Dev* 15(2), pp. 188-200.

Elbashir, S. M. et al. 2001c. Functional anatomy of siRNAs for mediating efficient RNAi in Drosophila melanogaster embryo lysate. *EMBO J* 20(23), pp. 6877-6888.

Elias, P. M. 1983. Epidermal lipids, barrier function, and desquamation. *J Invest Dermatol* 80(1 Suppl), pp. 44s-49s.

Elias, P. M. 1988. Structure and function of the stratum corneum permeability barrier. *Drug Development Research* 13(2,Äê3), pp. 97-105.

Elias, P. M. et al. 1988. Membrane structural alterations in murine stratum corneum: relationship to the localization of polar lipids and phospholipases. *J Invest Dermatol* 91(1), pp. 3-10.

Elouahabi, A. and Ruysschaert, J. M. 2005. Formation and intracellular trafficking of lipoplexes and polyplexes. *Mol Ther* 11(3), pp. 336-347.

Enfield, J. et al. 2010. In-vivo dynamic characterization of microneedle skin penetration using optical coherence tomography. *J Biomed Opt* 15(4), p. 046001.

Erbacher, P. et al. 1998. Chitosan-based vector/DNA complexes for gene delivery: biophysical characteristics and transfection ability. *Pharm Res* 15(9), pp. 1332-1339.

Escoffre, J. M. et al. 2013. In-vivo gene delivery by sonoporation: recent progress and prospects. *Curr Gene Ther* 13(1), pp. 2-14.

Escriou, V. et al. 2001. Critical assessment of the nuclear import of plasmid during cationic lipid-mediated gene transfer. *J Gene Med* 3(2), pp. 179-187.

Evans, R. K. et al. 2000. Evaluation of degradation pathways for plasmid DNA in pharmaceutical formulations via accelerated stability studies. *J Pharm Sci* 89(1), pp. 76-87.

Falo Jr, L. 1999. Targeting the skin for genetic immunization. *Proceedings of the Association of American Physicians* 111(3), pp. 211-219.

Fattal, E. and Bochot, A. 2008. State of the art and perspectives for the delivery of antisense oligonucleotides and siRNA by polymeric nanocarriers. *Int J Pharm* 364(2), pp. 237-248.

Felgner, J. et al. 1994. Enhanced gene delivery and mechanism studies with a novel series of cationic lipid formulations. *Journal of biological Chemistry* 269(4), p. 2550.

Felgner, P. L. et al. 1987. Lipofection: a highly efficient, lipid-mediated DNA-transfection procedure. *Proc Natl Acad Sci U S A* 84(21), pp. 7413-7417.

Ferrari, S. et al. 2005. Gene therapy approaches for epidermolysis bullosa. *Clin Dermatol* 23(4), pp. 430-436.

Ferraro, B. et al. 2009. Intradermal delivery of plasmid VEGF(165) by electroporation promotes wound healing. *Mol Ther* 17(4), pp. 651-657.

Ferraro, B. et al. 2011. Evaluation of delivery conditions for cutaneous plasmid electrotransfer using a multielectrode array. *Gene Ther* 18(5), pp. 496-500.

Fire, A. et al. 1998. Potent and specific genetic interference by double-stranded RNA in Caenorhabditis elegans. *Nature* 391(6669), pp. 806-811.

Fischer, D. et al. 2003. In vitro cytotoxicity testing of polycations: influence of polymer structure on cell viability and hemolysis. *Biomaterials* 24(7), pp. 1121-1131.

Formanek, M. et al. 1996. Optimized growth medium for primary culture of human oral keratinocytes. *Int J Oral Maxillofac Surg* 25(2), pp. 157-160.

Fuchs, E. 1990. Epidermal differentiation: the bare essentials. *J Cell Biol* 111(6 Pt 2), pp. 2807-2814.

Funding, A. T. et al. 2006. Mitogen- and stress-activated protein kinase 1 is activated in lesional psoriatic epidermis and regulates the expression of pro-inflammatory cytokines. *J Invest Dermatol* 126(8), pp. 1784-1791.

Fynan, E. F. et al. 1993. DNA vaccines: protective immunizations by parenteral, mucosal, and gene-gun inoculations. *Proc Natl Acad Sci U S A* 90(24), pp. 11478-11482.

Gao, X. et al. 2007. Nonviral gene delivery: what we know and what is next. *AAPS J* 9(1), pp. E92-104.

Gary, D. J. et al. 2007. Polymer-based siRNA delivery: perspectives on the fundamental and phenomenological distinctions from polymer-based DNA delivery. *J Control Release* 121(1-2), pp. 64-73.

Germain, L. et al. 1995. Early basement membrane formation following the grafting of cultured epidermal sheets detached with thermolysin or Dispase. *Burns* 21(3), pp. 175-180.

Germain, L. et al. 1993. Improvement of human keratinocyte isolation and culture using thermolysin. *Burns* 19(2), pp. 99-104.

Gershon, H. et al. 1993. Mode of formation and structural features of DNA-cationic liposome complexes used for transfection. *Biochemistry* 32(28), pp. 7143-7151.

Gerstel, M. S. and Place, V. A. 1976. Drug delivery device. In: Patent, U.S. ed.

Geusens, B. et al. 2009a. Ultradeformable cationic liposomes for delivery of small interfering RNA (siRNA) into human primary melanocytes. *J Control Release* 133(3), pp. 214-220.

Geusens, B. et al. 2009b. Cutaneous short-interfering RNA therapy. *Expert Opin Drug Deliv* 6(12), pp. 1333-1349.

Geusens, B. et al. 2011. Lipid-mediated gene delivery to the skin. *Eur J Pharm Sci* 43(4), pp. 199-211.

Geusens, B. et al. 2010. Flexible Nanosomes (SECosomes) Enable Efficient siRNA Delivery in Cultured Primary Skin Cells and in the Viable Epidermis of ex vivo Human Skin. 20(23), pp. 4077-4090.

Gill, H. S. et al. 2008. Effect of microneedle design on pain in human volunteers. *Clin J Pain* 24(7), pp. 585-594.

Gill, H. S. and Prausnitz, M. R. 2007a. Coated microneedles for transdermal delivery. *J Control Release* 117(2), pp. 227-237.

Gill, H. S. and Prausnitz, M. R. 2007b. Coating formulations for microneedles. *Pharm Res* 24(7), pp. 1369-1380.

Gill, H. S. and Prausnitz, M. R. 2007c. Does needle size matter? *J Diabetes Sci Technol* 1(5), pp. 725-729.

Gill, H. S. et al. 2010. Cutaneous vaccination using microneedles coated with hepatitis C DNA vaccine. *Gene Ther* 17(6), pp. 811-814.

Godin, B. and Touitou, E. 2007. Transdermal skin delivery: predictions for humans from in vivo, ex vivo and animal models. *Adv Drug Deliv Rev* 59(11), pp. 1152-1161.

Gong, H. et al. 2005. The role of small RNAs in human diseases: potential troublemaker and therapeutic tools. *Med Res Rev* 25(3), pp. 361-381.

Gonzalez-Gonzalez, E. et al. 2011. Visualization of plasmid delivery to keratinocytes in mouse and human epidermis. *Sci Rep* 1, p. 158.

Gonzalez-Gonzalez, E. et al. 2009. siRNA silencing of keratinocyte-specific GFP expression in a transgenic mouse skin model. *Gene Ther* 16(8), pp. 963-972.

Gonzalez-Gonzalez, E. et al. 2010a. Increased interstitial pressure improves nucleic acid delivery to skin enabling a comparative analysis of constitutive promoters. *Gene Ther* 17(10), pp. 1270-1278.

Gonzalez-Gonzalez, E. et al. 2010b. Silencing of reporter gene expression in skin using siRNAs and expression of plasmid DNA delivered by a soluble protrusion array device (PAD). *Mol Ther* 18(9), pp. 1667-1674.

Goodison, S. et al. 1999. CD44 cell adhesion molecules. *Mol Pathol* 52(4), pp. 189-196.

Gothelf, A. and Gehl, J. 2010. Gene Electrotransfer to Skin; Review of Existing Literature and Clinical Perspectives. *Curr Gene Ther* 10(4), pp. 287-299.

Goula, D. et al. 1998. Size, diffusibility and transfection performance of linear PEI/DNA complexes in the mouse central nervous system. *Gene Ther* 5(5), pp. 712-717.

Green, H. et al. 1979. Growth of cultured human epidermal cells into multiple epithelia suitable for grafting. *Proc Natl Acad Sci U S A* 76(11), pp. 5665-5668.

Grimm, D. 2009. Small silencing RNAs: state-of-the-art. *Adv Drug Deliv Rev* 61(9), pp. 672-703.

Groves, R. B. et al. 2012. Quantifying the mechanical properties of human skin to optimise future microneedle device design. *Comput Methods Biomech Biomed Engin* 15(1), pp. 73-82.

Gruenbaum, Y. et al. 2000. Review: nuclear lamins - structural proteins with fundamental functions. *Journal of Structural Biology* 129(2-3), pp. 313-323.

Grunweller, A. et al. 2003. Cellular uptake and localization of a Cy3-labeled siRNA specific for the serine/threonine kinase Pim-1. *Oligonucleotides* 13(5), pp. 345-352.

Gupta, A. K. et al. 2010. Nonviral transfection of mouse calvarial organ in vitro using Accell-modified siRNA. *Plast Reconstr Surg* 125(2), pp. 494-501.

Gupta, J. et al. 2011. Kinetics of skin resealing after insertion of microneedles in human subjects. *J Control Release* 154(2), pp. 148-155.

Hacein-Bey-Abina, S. et al. 2008. Insertional oncogenesis in 4 patients after retrovirus-mediated gene therapy of SCID-X1. *J Clin Invest* 118(9), pp. 3132-3142.

Hacein-Bey-Abina, S. et al. 2003. LMO2-associated clonal T cell proliferation in two patients after gene therapy for SCID-X1. *Science* 302(5644), pp. 415-419.

Haensler, J. and Szoka, F. C., Jr. 1993. Polyamidoamine cascade polymers mediate efficient transfection of cells in culture. *Bioconjug Chem* 4(5), pp. 372-379.

Hamilton, A. J. and Baulcombe, D. C. 1999. A species of small antisense RNA in posttranscriptional gene silencing in plants. *Science* 286(5441), pp. 950-952.

Hammond, S. M. et al. 2000. An RNA-directed nuclease mediates post-transcriptional gene silencing in Drosophila cells. *Nature* 404(6775), pp. 293-296.

Hammond, S. M. et al. 2001. Argonaute2, a link between genetic and biochemical analyses of RNAi. *Science* 293(5532), pp. 1146-1150.

Hanas, R. 2004. Reducing injection pain in children and adolescents with diabetes: a review of indwelling catheters. *Pediatr Diabetes* 5(2), pp. 102-111.

Hansen, L. S. et al. 1984. The influence of the hair cycle on the thickness of mouse skin. *Anat Rec* 210(4), pp. 569-573.

Haq, M. I. et al. 2009. Clinical administration of microneedles: skin puncture, pain and sensation. *Biomed Microdevices* 11(1), pp. 35-47.

Hart, S. L. 2010. Multifunctional nanocomplexes for gene transfer and gene therapy. *Cell Biol Toxicol* 26(1), pp. 69-81.

Haynes, J. R. et al. 1996. Particle-mediated nucleic acid immunization. *J Biotechnol* 44(1-3), pp. 37-42.

Heller, R. et al. 2010. Electrically mediated delivery of plasmid DNA to the skin, using a multielectrode array. *Hum Gene Ther* 21(3), pp. 357-362.

Hengge, U. R. 2006. Gene therapy progress and prospects: the skin--easily accessible, but still far away. *Gene Ther* 13(22), pp. 1555-1563.

Hengge, U. R. et al. 1995. Cytokine gene expression in epidermis with biological effects following injection of naked DNA. *Nat Genet* 10(2), pp. 161-166.

Hengge, U. R. et al. 1996. Expression of naked DNA in human, pig, and mouse skin. *J Clin Invest* 97(12), pp. 2911-2916.

Henry, S. et al. 1998. Microfabricated microneedles: a novel approach to transdermal drug delivery. *J Pharm Sci* 87(8), pp. 922-925.

Hickerson, R. P. et al. 2011. Use of self-delivery siRNAs to inhibit gene expression in an organotypic pachyonychia congenita model. *J Invest Dermatol* 131(5), pp. 1037-1044.

Hickerson, R. P. et al. 2008. Stability study of unmodified siRNA and relevance to clinical use. *Oligonucleotides* 18(4), pp. 345-354.

Hilliges, M. et al. 1995. Ultrastructural evidence for nerve fibers within all vital layers of the human epidermis. *J Invest Dermatol* 104(1), pp. 134-137.

Hirao, L. A. et al. 2008. Intradermal/subcutaneous immunization by electroporation improves plasmid vaccine delivery and potency in pigs and rhesus macaques. *Vaccine* 26(3), pp. 440-448.

Hoeflich, K. P. et al. 2006. Oncogenic BRAF is required for tumor growth and maintenance in melanoma models. *Cancer Res* 66(2), pp. 999-1006.

Hoekstra, D. et al. 2007. Gene delivery by cationic lipids: in and out of an endosome. *Biochem Soc Trans* 35(Pt 1), pp. 68-71.

Hoerter, J. A. et al. 2011. siRNA-like double-stranded RNAs are specifically protected against degradation in human cell extract. *PLoS One* 6(5), p. e20359.

Holland, P. M. et al. 1991. Detection of specific polymerase chain reaction product by utilizing the 5'----3' exonuclease activity of Thermus aquaticus DNA polymerase. *Proc Natl Acad Sci U S A* 88(16), pp. 7276-7280.

Hosseinkhani, H. et al. 2004. Dextran-spermine polycation: an efficient nonviral vector for in vitro and in vivo gene transfection. *Gene Ther* 11(2), pp. 194-203.

Howarth, J. L. et al. 2010. Using viral vectors as gene transfer tools (Cell Biology and Toxicology Special Issue: ETCS-UK 1 day meeting on genetic manipulation of cells). *Cell Biol Toxicol* 26(1), pp. 1-20.

Howe, S. J. et al. 2008. Insertional mutagenesis combined with acquired somatic mutations causes leukemogenesis following gene therapy of SCID-X1 patients. *J Clin Invest* 118(9), pp. 3143-3150.

Hsu, T. and Mitragotri, S. 2011. Delivery of siRNA and other macromolecules into skin and cells using a peptide enhancer. *Proc Natl Acad Sci USA* 108(38), pp. 15816-15821.

Huang, D. et al. 1991. Optical coherence tomography. *Science* 254(5035), pp. 1178-1181.

Huzaira, M. et al. 2001. Topographic variations in normal skin, as viewed by in vivo reflectance confocal microscopy. *J Invest Dermatol* 116(6), pp. 846-852.

Hybbinette, S. et al. 1999. Enzymatic dissociation of keratinocytes from human skin biopsies for in vitro cell propagation. *Exp Dermatol* 8(1), pp. 30-38.

Idson, B. 1971. Biophysical factors in skin penetration. *J. Soc. Cosmet. Chem* 22, pp. 615-620.

Inoue, T. et al. 2007. Modulation of scratching behavior by silencing an endogenous cyclooxygenase-1 gene in the skin through the administration of siRNA. *J Gene Med* 9(11), pp. 994-1001.

Ishimoto, T. et al. 2008. Downregulation of monocyte chemoattractant protein-1 involving short interfering RNA attenuates hapten-induced contact hypersensitivity. *Mol Ther* 16(2), pp. 387-395.

Jacobi, U. et al. 2007. Porcine ear skin: an in vitro model for human skin. *Skin Res Technol* 13(1), pp. 19-24.

Jakobsen, M. et al. 2009. Amelioration of psoriasis by anti-TNF-alpha RNAi in the xenograft transplantation model. *Mol Ther* 17(10), pp. 1743-1753.

James, M. B. and Giorgio, T. D. 2000. Nuclear-associated plasmid, but not cell-associated plasmid, is correlated with transgene expression in cultured mammalian cells. *Mol Ther* 1(4), pp. 339-346.

Jeschke, M. G. et al. 2000. Biodistribution and feasibility of non-viral IGF-I gene transfers in thermally injured skin. *Lab Invest* 80(2), pp. 151-158.

Johansen, C. et al. 2006. Protein expression of TNF-alpha in psoriatic skin is regulated at a posttranscriptional level by MAPK-activated protein kinase 2. *J Immunol* 176(3), pp. 1431-1438.

Jones, S. et al. 2009. DNA vaccination protects against an influenza challenge in a double-blind randomised placebo-controlled phase 1b clinical trial. *Vaccine* 27(18), pp. 2506-2512.

Kalejta, R. F. et al. 1997. Use of a membrane-localized green fluorescent protein allows simultaneous identification of transfected cells and cell cycle analysis by flow cytometry. *Cytometry* 29(4), pp. 286-291.

Kaspar, R. L. et al. 2009. Achieving successful delivery of nucleic acids to skin: 6th Annual Meeting of the International Pachyonychia Congenita Consortium. *J Invest Dermatol* 129(9), pp. 2085-2087.

Kaur, P. and Li, A. 2000. Adhesive properties of human basal epidermal cells: an analysis of keratinocyte stem cells, transit amplifying cells, and postmitotic differentiating cells. *J Invest Dermatol* 114(3), pp. 413-420.

Kaushik, S. et al. 2001. Lack of pain associated with microfabricated microneedles. *Anesth Analg* 92(2), pp. 502-504.

Kendall, M. et al. 2004. Intradermal ballistic delivery of micro-particles into excised human skin for pharmaceutical applications. *J Biomech* 37(11), pp. 1733-1741.

Khalil, I. A. et al. 2006. Uptake pathways and subsequent intracellular trafficking in nonviral gene delivery. *Pharmacol Rev* 58(1), pp. 32-45.

Khandan, O. et al. 2012. Titanium-based, fenestrated, in-plane microneedles for passive ocular drug delivery. *Conf Proc IEEE Eng Med Biol Soc* 2012, pp. 6572-6575.

Khavari, P. A. et al. 2002. Cutaneous gene transfer for skin and systemic diseases. *J Intern Med* 252(1), pp. 1-10.

Kiernan, J. 2000. Formaldehyde, formalin, paraformaldehyde and glutaraldehyde: what they are and what they do. *Microscopy Today* 8, pp. 8-12.

Kikuchi, Y. et al. 2008. Cutaneous gene delivery. *J Dermatol Sci* 50(2), pp. 87-98.

Kim, H. J. et al. 1996. Ultrasound-mediated transfection of mammalian cells. *Hum Gene Ther* 7(11), pp. 1339-1346.

Kim, J. Y. et al. 2012a. siRNA-mediated knock-down of COX-2 in melanocytes suppresses melanogenesis. *Exp Dermatol* 21(6), pp. 420-425.

Kim, S. S. et al. 2009. Strategies for targeted nonviral delivery of siRNAs in vivo. *Trends Mol Med* 15(11), pp. 491-500.

Kim, Y.-C. et al. 2012b. Microneedles for drug and vaccine delivery. *Adv Drug Deliv Rev* 64(14), pp. 1547-1568.

Kim, Y. C. and Prausnitz, M. R. 2011. Enabling skin vaccination using new delivery technologies. *Drug Deliv Transl Res* 1(1), pp. 7-12.

Kim, Y. C. et al. 2010. Formulation and coating of microneedles with inactivated influenza virus to improve vaccine stability and immunogenicity. *J Control Release* 142(2), pp. 187-195.

Kitano, Y. and Okada, N. 1983. Separation of the epidermal sheet by dispase. *Br J Dermatol* 108(5), pp. 555-560.

Koch, S. et al. 2000. Ultrasound enhancement of liposome-mediated cell transfection is caused by cavitation effects. *Ultrasound Med Biol* 26(5), pp. 897-903.

Kwok, A. and Hart, S. L. 2011. Comparative structural and functional studies of nanoparticle formulations for DNA and siRNA delivery. *Nanomedicine* 7(2), pp. 210-219.

Lademann, J. et al. 1999. Penetration of titanium dioxide microparticles in a sunscreen formulation into the horny layer and the follicular orifice. *Skin Pharmacol Appl Skin Physiol* 12(5), pp. 247-256.

Lappalainen, K. et al. 1994. Comparison of cell proliferation and toxicity assays using two cationic liposomes. *Pharm Res* 11(8), pp. 1127-1131.

Lara, M. F. et al. 2012. Inhibition of CD44 gene expression in human skin models, using self-delivery short interfering RNA administered by dissolvable microneedle arrays. *Hum Gene Ther* 23(8), pp. 816-823.

Larregina, A. T. and Falo, L. D., Jr. 2005. Changing paradigms in cutaneous immunology: adapting with dendritic cells. *J Invest Dermatol* 124(1), pp. 1-12.

Layzer, J. M. et al. 2004. In vivo activity of nuclease-resistant siRNAs. *RNA* 10(5), pp. 766-771.

Leachman, S. A. et al. 2008. Therapeutic siRNAs for dominant genetic skin disorders including pachyonychia congenita. *J Dermatol Sci* 51(3), pp. 151-157.

Leachman, S. A. et al. 2009. First-in-human mutation-targeted siRNA phase Ib trial of an inherited skin disorder. *Mol Ther* 18(2), pp. 442-446.

Lechardeur, D. and Lukacs, G. L. 2006. Nucleocytoplasmic transport of plasmid DNA: a perilous journey from the cytoplasm to the nucleus. *Hum Gene Ther* 17(9), pp. 882-889.

Lechardeur, D. et al. 2005. Intracellular routing of plasmid DNA during non-viral gene transfer. *Adv Drug Deliv Rev* 57(5), pp. 755-767.

Lederberg, J. et al. 1952. Sex Compatibility in Escherichia Coli. *Genetics* 37(6), pp. 720-730.

Ledley, F. D. 1994. Non-viral gene therapy. *Curr Opin Biotechnol* 5(6), pp. 626-636.

Lee, K. Y. et al. 1998. Preparation of chitosan self-aggregates as a gene delivery system. *J Control Release* 51(2-3), pp. 213-220.

Lee, Y. and Hwang, K. 2002. Skin thickness of Korean adults. *Surg Radiol Anat* 24(3-4), pp. 183-189.

Leong, K. W. et al. 1998. DNA-polycation nanospheres as non-viral gene delivery vehicles. *J Control Release* 53(1-3), pp. 183-193.

Li, G. et al. 2009. In vitro transdermal delivery of therapeutic antibodies using maltose microneedles. *Int J Pharm* 368(1-2), pp. 109-115.

Li, S. D. et al. 2008. Efficient gene silencing in metastatic tumor by siRNA formulated in surface-modified nanoparticles. *J Control Release* 126(1), pp. 77-84.

Li, W. Z. et al. 2010. Super-short solid silicon microneedles for transdermal drug delivery applications. *Int J Pharm* 389(1-2), pp. 122-129.

Lin, M. et al. 2000. The gene gun: current applications in cutaneous gene therapy. *International journal of dermatology* 39(3), pp. 161-170.

Lin, W. et al. 2001. Transdermal delivery of antisense oligonucleotides with microprojection patch (Macroflux) technology. *Pharm Res* 18(12), pp. 1789-1793.

Lindahl, T. 1993. Instability and decay of the primary structure of DNA. *Nature* 362(6422), pp. 709-715.

Liu, F. et al. 1999. Hydrodynamics-based transfection in animals by systemic administration of plasmid DNA. *Gene Ther* 6(7), pp. 1258-1266.

Liu, L. J. et al. 2001. Topical application of HIV DNA vaccine with cytokine-expression plasmids induces strong antigen-specific immune responses. *Vaccine* 20(1-2), pp. 42-48.

Lombry, C. et al. 2000. Transdermal delivery of macromolecules using skin electroporation. *Pharm Res* 17(1), pp. 32-37.

Longin, A. et al. 1993. Comparison of anti-fading agents used in fluorescence microscopy: image analysis and laser confocal microscopy study. *J Histochem Cytochem* 41(12), pp. 1833-1840.

Lorenz, C. et al. 2004. Steroid and lipid conjugates of siRNAs to enhance cellular uptake and gene silencing in liver cells. *Bioorg Med Chem Lett* 14(19), pp. 4975-4977.

Lund, E. et al. 2004. Nuclear export of microRNA precursors. *Science* 303(5654), pp. 95-98.

Lungwitz, U. et al. 2005. Polyethylenimine-based non-viral gene delivery systems. *Eur J Pharm Biopharm* 60(2), pp. 247-266.

Luten, J. et al. 2008. Biodegradable polymers as non-viral carriers for plasmid DNA delivery. *J Control Release* 126(2), pp. 97-110.

Lv, H. et al. 2006. Toxicity of cationic lipids and cationic polymers in gene delivery. *J Control Release* 114(1), pp. 100-109.

Ma, B. et al. 2007. Lipoplex morphologies and their influences on transfection efficiency in gene delivery. *J Control Release* 123(3), pp. 184-194.

MacGregor, G. R. and Caskey, C. T. 1989. Construction of plasmids that express E. coli beta-galactosidase in mammalian cells. *Nucleic Acids Res* 17(6), p. 2365.

MacPhee, D. J. 2010. Methodological considerations for improving Western blot analysis. *J Pharmacol Toxicol Methods* 61(2), pp. 171-177.

Manche, L. et al. 1992. Interactions between double-stranded RNA regulators and the protein kinase DAI. *Mol Cell Biol* 12(11), pp. 5238-5248.

Mangelsdorf, S. et al. 2006. Ethnic variation in vellus hair follicle size and distribution. *Skin Pharmacol Physiol* 19(3), pp. 159-167.

Martin, C. J. et al. 2012. Low temperature fabrication of biodegradable sugar glass microneedles for transdermal drug delivery applications. *J Control Release* 158(1), pp. 93-101.

Masotti, A. et al. 2009. Comparison of different commercially available cationic liposome-DNA lipoplexes: Parameters influencing toxicity and transfection efficiency. *Colloids Surf B Biointerfaces* 68(2), pp. 136-144.

Matriano, J. A. et al. 2002. Macroflux microprojection array patch technology: a new and efficient approach for intracutaneous immunization. *Pharm Res* 19(1), pp. 63-70.

Matsumoto, G. et al. 2006. Cationized gelatin delivery of a plasmid DNA expressing small interference RNA for VEGF inhibits murine squamous cell carcinoma. *Cancer Sci* 97(4), pp. 313-321.

Mattaj, I. W. and Englmeier, L. 1998. Nucleocytoplasmic transport: the soluble phase. *Annu Rev Biochem* 67, pp. 265-306.

McCaffrey, A. P. et al. 2002. RNA interference in adult mice. *Nature* 418(6893), pp. 38-39.

McGrath, J. et al. 2004. Anatomy and organization of human skin. In: Burns, T. et al. eds. *Rook's textbook of dermatology*. 7th ed. Oxford: Blackwell Publishing, pp. 3.1-3.15.

McMahon, J. M. and Wells, D. J. 2004. Electroporation for gene transfer to skeletal muscles: current status. *BioDrugs* 18(3), pp. 155-165.

Meister, G. et al. 2004. Human Argonaute2 mediates RNA cleavage targeted by miRNAs and siRNAs. *Mol Cell* 15(2), pp. 185-197.

Meister, G. and Tuschl, T. 2004. Mechanisms of gene silencing by double-stranded RNA. *Nature* 431(7006), pp. 343-349.

Menon, G. K. 2002. New insights into skin structure: scratching the surface. *Adv Drug Deliv Rev* 54 Suppl 1, pp. S3-17.

Menon, G. K. and Elias, P. M. 2001. The Epidermal Barrier and Strategies for Surmounting It: An Overview. In: Hengge, U.R. and Volc-Platzer, B. eds. *The Skin and Gene Therapy*. Berlin: Springer-Verlag, pp. 3-26.

Menon, G. K. et al. 1992. Lamellar body secretory response to barrier disruption. *J Invest Dermatol* 98(3), pp. 279-289.

Meykadeh, N. et al. 2005. Topical application of plasmid DNA to mouse and human skin. *J Mol Med (Berl)* 83(11), pp. 897-903.

Middaugh, C. R. et al. 1998. Analysis of plasmid DNA from a pharmaceutical perspective. *J Pharm Sci* 87(2), pp. 130-146.

Mignet, N. et al. 2010. Cationic and anionic lipoplexes inhibit gene transfection by electroporation in vivo. *J Gene Med* 12(6), pp. 491-500.

Mikszta, J. A. et al. 2002. Improved genetic immunization via micromechanical disruption of skin-barrier function and targeted epidermal delivery. *Nat Med* 8(4), pp. 415-419.

Mitragotri, S. 2005. Immunization without needles. *Nat Rev Immunol* 5(12), pp. 905-916.

Mitragotri, S. 2006. Current status and future prospects of needle-free liquid jet injectors. *Nat Rev Drug Discov* 5(7), pp. 543-548.

Mitragotri, S. et al. 1995. Ultrasound-mediated transdermal protein delivery. *Science* 269(5225), pp. 850-853.

Molnar, M. J. et al. 2004. Factors influencing the efficacy, longevity, and safety of electroporation-assisted plasmid-based gene transfer into mouse muscles. *Mol Ther* 10(3), pp. 447-455.

Moore, C. B. et al. 2010. Short hairpin RNA (shRNA): design, delivery, and assessment of gene knockdown. *Methods Mol Biol* 629, pp. 141-158.

Morgan, K. E. et al. 2000. Experimental and theoretical evaluation of microbubble behavior: effect of transmitted phase and bubble size. *IEEE Trans Ultrason Ferroelectr Freq Control* 47(6), pp. 1494-1509.

Morgan, R. A. and Anderson, W. F. 1993. Human gene therapy. *Annu Rev Biochem* 62, pp. 191-217.

Mortimer, I. et al. 1999. Cationic lipid-mediated transfection of cells in culture requires mitotic activity. *Gene Ther* 6(3), pp. 403-411.

Morton, D. B. et al. 2001. Refining procedures for the administration of substances. Report of the BVAAWF/FRAME/RSPCA/UFAW Joint Working Group on Refinement. British Veterinary Association Animal Welfare Foundation/Fund for the Replacement of Animals in Medical Experiments/Royal Society for the Prevention of Cruelty to Animals/Universities Federation for Animal Welfare. *Lab Anim* 35(1), pp. 1-41.

Mulligan, R. C. 1993. The basic science of gene therapy. *Science* 260(5110), pp. 926-932.

Mumper, R. J. and Cui, Z. 2003. Genetic immunization by jet injection of targeted pDNA-coated nanoparticles. *Methods* 31(3), pp. 255-262.

Nagano, O. and Saya, H. 2004. Mechanism and biological significance of CD44 cleavage. *Cancer Sci* 95(12), pp. 930-935.

Naik, A. et al. 2000. Transdermal drug delivery: overcoming the skin's barrier function. *Pharm Sci Technolo Today* 3(9), pp. 318-326.

Nakai, N. et al. 2010. Mitf silencing cooperates with IL-12 gene transfer to inhibit melanoma in mice. *Int Immunopharmacol* 10(4), pp. 540-545.

Nakai, N. et al. 2007. Therapeutic RNA interference of malignant melanoma by electrotransfer of small interfering RNA targeting Mitf. *Gene Ther* 14(4), pp. 357-365.

Nakajima, H. et al. 2012. A rapid, targeted, neuron-selective, in vivo knockdown following a single intracerebroventricular injection of a novel chemically modified siRNA in the adult rat brain. *J Biotechnol* 157(2), pp. 326-333.

Nakamura, M. et al. 2008. Controlled delivery of T-box21 small interfering RNA ameliorates autoimmune alopecia (Alopecia Areata) in a C3H/HeJ mouse model. *Am J Pathol* 172(3), pp. 650-658.

Nanney, L. B. et al. 2000. Boosting epidermal growth factor receptor expression by gene gun transfection stimulates epidermal growth in vivo. *Wound Repair Regen* 8(2), pp. 117-127.

Nelson, W. G. and Sun, T. T. 1983. The 50- and 58-kdalton keratin classes as molecular markers for stratified squamous epithelia: cell culture studies. *J Cell Biol* 97(1), pp. 244-251.

Netzlaff, F. et al. 2005. The human epidermis models EpiSkin, SkinEthic and EpiDerm: an evaluation of morphology and their suitability for testing phototoxicity, irritancy, corrosivity, and substance transport. *Eur J Pharm Biopharm* 60(2), pp. 167-178.

Neumann, E. et al. 1982. Gene transfer into mouse lyoma cells by electroporation in high electric fields. *EMBO J* 1(7), pp. 841-845.

Newman, C. M. and Bettinger, T. 2007. Gene therapy progress and prospects: ultrasound for gene transfer. *Gene Ther* 14(6), pp. 465-475.

Ng, K. W. 2010. *Microneedles for Intraepidermal Hepatitis B Vaccination (PhD Thesis)*. Cardiff University.

Ng, K. W. et al. 2009. Development of an ex vivo human skin model for intradermal vaccination: tissue viability and Langerhans cell behaviour. *Vaccine* 27(43), pp. 5948-5955.

Nicolau, C. and Sene, C. 1982. Liposome-mediated DNA transfer in eukaryotic cells. Dependence of the transfer efficiency upon the type of liposomes used and the host cell cycle stage. *Biochim Biophys Acta* 721(2), pp. 185-190.

Niculescu-Duvaz, D. et al. 2003. Structure-activity relationship in cationic lipid mediated gene transfection. *Current Medicinal Chemistry* 10(14), pp. 1233-1261.

Nimesh, S. et al. 2006. Novel polyallylamine-dextran sulfate-DNA nanoplexes: highly efficient non-viral vector for gene delivery. *Int J Pharm* 320(1-2), pp. 143-149.

Nolan, T. et al. 2006. Quantification of mRNA using real-time RT-PCR. *Nat Protoc* 1(3), pp. 1559-1582.

Normand, J. and Karasek, M. A. 1995. A method for the isolation and serial propagation of keratinocytes, endothelial cells, and fibroblasts from a single punch biopsy of human skin. *In Vitro Cell Dev Biol Anim* 31(6), pp. 447-455.

O'Brien, J. and Lummis, S. C. 2002. An improved method of preparing microcarriers for biolistic transfection. *Brain Res Brain Res Protoc* 10(1), pp. 12-15.

Odell, I. D. and Cook, D. 2013. Immunofluorescence techniques. *J Invest Dermatol* 133(1), p. e4.

Odland, G. F. 1958. The fine structure of the interrelationship of cells in the human epidermis. *J Biophys Biochem Cytol* 4(5), pp. 529-538.

Ono, M. et al. 2001. Quantitative comparison of anti-fading mounting media for confocal laser scanning microscopy. *J Histochem Cytochem* 49(3), pp. 305-312.

Oshikawa, K. et al. 2001. Interleukin 12 gene transfer into skin distant from the tumor site elicits antimetastatic effects equivalent to local gene transfer. *Hum Gene Ther* 12(2), pp. 149-160.

Otberg, N. et al. 2008. The role of hair follicles in the percutaneous absorption of caffeine. *Br J Clin Pharmacol* 65(4), pp. 488-492.

Otberg, N. et al. 2004. Variations of hair follicle size and distribution in different body sites. *J Invest Dermatol* 122(1), pp. 14-19.

Park, J. H. et al. 2005. Biodegradable polymer microneedles: fabrication, mechanics and transdermal drug delivery. *J Control Release* 104(1), pp. 51-66.

Park, J. H. et al. 2010. A microneedle roller for transdermal drug delivery. *Eur J Pharm Biopharm* 76(2), pp. 282-289.

Park, J. H. et al. 2007. Tapered conical polymer microneedles fabricated using an integrated lens technique for transdermal drug delivery. *IEEE Trans Biomed Eng* 54(5), pp. 903-913.

Park, Y. J. et al. 2003. Low molecular weight protamine as an efficient and nontoxic gene carrier: in vitro study. *J Gene Med* 5(8), pp. 700-711.

Patel, G. K. et al. 2006. Numerous keratinocyte subtypes involved in wound re-epithelialization. *J Invest Dermatol* 126(2), pp. 497-502.

Patel, M. I. et al. 2005. A Pitfall of the 3-(4,5-dimethylthiazol-2-yl)-5(3-carboxymethonyphenol)-2-(4-sulfophenyl)-2H-tetra zolium (MTS) assay due to evaporation in wells on the edge of a 96 well plate. *Biotechnol Lett* 27(11), pp. 805-808.

Peachman, K. K. et al. 2003. Immunization with DNA through the skin. *Methods* 31(3), pp. 232-242.

Pearton, M. et al. 2008. Gene delivery to the epidermal cells of human skin explants using microfabricated microneedles and hydrogel formulations. *Pharm Res* 25(2), pp. 407-416.

Pearton, M. et al. 2010. Influenza virus-like particles coated onto microneedles can elicit stimulatory effects on Langerhans cells in human skin. *Vaccine* 28(37), pp. 6104-6113.

Pearton, M. et al. 2012. Microneedle delivery of plasmid DNA to living human skin: Formulation coating, skin insertion and gene expression. *J Control Release* 160(3), pp. 561-569.

Pedroso de Lima, M. C. et al. 2003. Cationic liposomes for gene delivery: from biophysics to biological applications. *Curr Med Chem* 10(14), pp. 1221-1231.

Pei, Y. and Tuschl, T. 2006. On the art of identifying effective and specific siRNAs. *Nat Methods* 3(9), pp. 670-676.

Pertmer, T. M. et al. 1995. Gene gun-based nucleic acid immunization: elicitation of humoral and cytotoxic T lymphocyte responses following epidermal delivery of nanogram quantities of DNA. *Vaccine* 13(15), pp. 1427-1430.

Petits, R. J. et al. 2009. Microneedle-based pen device for drug delivery and method for using same. In: Patent, U.S. ed.

Pfeiffer, S. et al. 2000. High-pressure freezing provides new information on human epidermis: simultaneous protein antigen and lamellar lipid structure preservation. Study on human epidermis by cryoimmobilization. *J Invest Dermatol* 114(5), pp. 1030-1038.

Ponta, H. et al. 1998. The CD44 protein family. *Int J Biochem Cell Biol* 30(3), pp. 299-305.

Poumay, Y. et al. 1994. Basal Detachment of the Epidermis Using Dispase: Tissue Spatial Organization and Fate of Integrin alpha6-beta4 and Hemidesmosomes. *Journal of Investigative Dermatology* 102(1), pp. 111-117.

Powell, J. S. et al. 2003. Phase 1 trial of FVIII gene transfer for severe hemophilia A using a retroviral construct administered by peripheral intravenous infusion. *Blood* 102(6), pp. 2038-2045.

Prausnitz, M. R. 2004. Microneedles for transdermal drug delivery. *Adv Drug Deliv Rev* 56(5), pp. 581-587.

Prausnitz, M. R. and Langer, R. 2008. Transdermal drug delivery. *Nat Biotechnol* 26(11), pp. 1261-1268.

Prazeres, D. M. et al. 1998. Preparative purification of supercoiled plasmid DNA using anion-exchange chromatography. *J Chromatogr A* 806(1), pp. 31-45.

Preat, V. and Dujardin, N. 2001. Topical delivery of nucleic acids in the skin. *STP pharma sciences* 11(1), pp. 57-68.

Ra, H. et al. 2011. In vivo imaging of human and mouse skin with a handheld dual-axis confocal fluorescence microscope. *J Invest Dermatol* 131(5), pp. 1061-1066.

Raghavachari, N. and Fahl, W. E. 2002. Targeted gene delivery to skin cells in vivo: a comparative study of liposomes and polymers as delivery vehicles. *J Pharm Sci* 91(3), pp. 615-622.

Raju, P. A. et al. 2006. Assessment of epidermal cell viability by near infrared multi-photon microscopy following ballistic delivery of gold micro-particles. *Vaccine* 24(21), pp. 4644-4647.

Rakhorst, H. A. et al. 2006. Mucosal keratinocyte isolation: a short comparative study on thermolysin and dispase. *Int J Oral Maxillofac Surg* 35(10), pp. 935-940.

Ramezani, M. et al. 2009. The influence of size, lipid composition and bilayer fluidity of cationic liposomes on the transfection efficiency of nanolipoplexes. *Colloids Surf B Biointerfaces* 72(1), pp. 1-5.

Rao, D. D. et al. 2009. siRNA vs. shRNA: similarities and differences. *Adv Drug Deliv Rev* 61(9), pp. 746-759.

Rao, N. M. 2010. Cationic lipid-mediated nucleic acid delivery: beyond being cationic. *Chem Phys Lipids* 163(3), pp. 245-252.

Raper, S. E. et al. 2003. Fatal systemic inflammatory response syndrome in a ornithine transcarbamylase deficient patient following adenoviral gene transfer. *Mol Genet Metab* 80(1-2), pp. 148-158.

Rehman, Z. et al. 2013. How cationic lipids transfer nucleic acids into cells and across cellular membranes: recent advances. *J Control Release* 166(1), pp. 46-56.

Rejman, J. et al. 2005. Role of clathrin- and caveolae-mediated endocytosis in gene transfer mediated by lipo- and polyplexes. *Mol Ther* 12(3), pp. 468-474.

Rheinwald, J. G. and Green, H. 1975. Serial cultivation of strains of human epidermal keratinocytes: the formation of keratinizing colonies from single cells. *Cell* 6(3), pp. 331-343.

Rheinwald, J. G. and Green, H. 1977. Epidermal growth factor and the multiplication of cultured human epidermal keratinocytes. *Nature* 265(5593), pp. 421-424.

Richards, S. et al. 2008. Development of defined media for the serum-free expansion of primary keratinocytes and human embryonic stem cells. *Tissue Eng Part C Methods* 14(3), pp. 221-232.

Ritprajak, P. et al. 2008. Topical application of cream-emulsified CD86 siRNA ameliorates allergic skin disease by targeting cutaneous dendritic cells. *Mol Ther* 16(7), pp. 1323-1330.

Roberts, L. K. et al. 2005. Clinical safety and efficacy of a powdered Hepatitis B nucleic acid vaccine delivered to the epidermis by a commercial prototype device. *Vaccine* 23(40), pp. 4867-4878.

Rudolph, C. et al. 2000. In vivo gene delivery to the lung using polyethylenimine and fractured polyamidoamine dendrimers. *J Gene Med* 2(4), pp. 269-278.

Ruiz, F. E. et al. 2001. A clinical inflammatory syndrome attributable to aerosolized lipid-DNA administration in cystic fibrosis. *Hum Gene Ther* 12(7), pp. 751-761.

Ruponen, M. et al. 2003. Extracellular and intracellular barriers in non-viral gene delivery. *J Control Release* 93(2), pp. 213-217.

Ruponen, M. et al. 1999. Interactions of polymeric and liposomal gene delivery systems with extracellular glycosaminoglycans: physicochemical and transfection studies. *Biochim Biophys Acta* 1415(2), pp. 331-341.

Sakurai, F. et al. 2000. Effect of DNA/liposome mixing ratio on the physicochemical characteristics, cellular uptake and intracellular trafficking of plasmid DNA/cationic liposome complexes and subsequent gene expression. *J Control Release* 66(2-3), pp. 255-269.

Sambrooks, J. and Russell, D. W. 2001. *Molecular Cloning: A Laboratory Manual*. 3rd ed. New York: Cold Spring Harbor Laboratory Press.

Sandby-Moller, J. et al. 2003. Epidermal thickness at different body sites: relationship to age, gender, pigmentation, blood content, skin type and smoking habits. *Acta Derm Venereol* 83(6), pp. 410-413.

Sauermann, K. et al. 2002. Age related changes of human skin investigated with histometric measurements by confocal laser scanning microscopy in vivo. *Skin Res Technol* 8(1), pp. 52-56.

Sawamura, D. et al. 1999. In vivo gene introduction into keratinocytes using jet injection. *Gene Ther* 6(10), pp. 1785-1787.

Sawamura, D. et al. 2002. The majority of keratinocytes incorporate intradermally injected plasmid DNA regardless of size but only a small proportion of cells can express the gene product. *J Invest Dermatol* 118(6), pp. 967-971.

Schatzlein, A. G. et al. 2005. Preferential liver gene expression with polypropylenimine dendrimers. *J Control Release* 101(1-3), pp. 247-258.

Scheule, R. K. et al. 1997. Basis of pulmonary toxicity associated with cationic lipid-mediated gene transfer to the mammalian lung. *Hum Gene Ther* 8(6), pp. 689-707.

Scheuplein, R. J. and Blank, I. H. 1971. Permeability of the skin. *Physiol Rev* 51(4), pp. 702-747.

Schramm-Baxter, J. and Mitragotri, S. 2004. Needle-free jet injections: dependence of jet penetration and dispersion in the skin on jet power. *J Control Release* 97(3), pp. 527-535.

Screaton, G. R. et al. 1992. Genomic structure of DNA encoding the lymphocyte homing receptor CD44 reveals at least 12 alternatively spliced exons. *Proc Natl Acad Sci U S A* 89(24), pp. 12160-12164.

Semizarov, D. et al. 2003. Specificity of short interfering RNA determined through gene expression signatures. *Proc Natl Acad Sci U S A* 100(11), pp. 6347-6352.

Serrano, F. et al. 2003. A comparison of targeting performance of oncoretroviral versus lentiviral vectors on human keratinocytes. *Hum Gene Ther* 14(16), pp. 1579-1585.

Seville, P. C. et al. 2002. Preparation of dry powder dispersions for non-viral gene delivery by freeze-drying and spray-drying. *J Gene Med* 4(4), pp. 428-437.

Shabalina, S. A. and Koonin, E. V. 2008. Origins and evolution of eukaryotic RNA interference. *Trends Ecol Evol* 23(10), pp. 578-587.

Sharma, A. et al. 2005. Mutant V599EB-Raf regulates growth and vascular development of malignant melanoma tumors. *Cancer Res* 65(6), pp. 2412-2421.

Singer, S. J. and Nicolson, G. L. 1972. The fluid mosaic model of the structure of cell membranes. *Science* 175(4023), pp. 720-731.

Singh, T. R. et al. 2011. Review of patents on microneedle applicators. *Recent Pat Drug Deliv Formul* 5(1), pp. 11-23.

Sintov, A. C. et al. 2003. Radiofrequency-driven skin microchanneling as a new way for electrically assisted transdermal delivery of hydrophilic drugs. *J Control Release* 89(2), pp. 311-320.

Siomi, H. and Siomi, M. C. 2009. On the road to reading the RNA-interference code. *Nature* 457(7228), pp. 396-404.

Sohn, R. L. et al. 2001. In-vivo particle mediated delivery of mRNA to mammalian tissues: ballistic and biologic effects. *Wound Repair Regen* 9(4), pp. 287-296.

Song, J. M. et al. 2010. Microneedle delivery of H5N1 influenza virus-like particles to the skin induces long-lasting B- and T-cell responses in mice. *Clin Vaccine Immunol* 17(9), pp. 1381-1389.

Song, Y. K. et al. 1997. Characterization of cationic liposome-mediated gene transfer in vivo by intravenous administration. *Hum Gene Ther* 8(13), pp. 1585-1594.

Sonnenberg, A. et al. 1991. Integrin alpha 6/beta 4 complex is located in hemidesmosomes, suggesting a major role in epidermal cell-basement membrane adhesion. *J Cell Biol* 113(4), pp. 907-917.

Soutschek, J. et al. 2004. Therapeutic silencing of an endogenous gene by systemic administration of modified siRNAs. *Nature* 432(7014), pp. 173-178.

Spagnou, S. et al. 2004. Lipidic carriers of siRNA: differences in the formulation, cellular uptake, and delivery with plasmid DNA. *Biochemistry* 43(42), pp. 13348-13356.

Spurr, S. J. and Gipson, I. K. 1985. Isolation of corneal epithelium with Dispase II or EDTA. Effects on the basement membrane zone. *Invest Ophthalmol Vis Sci* 26(6), pp. 818-827.

Staiano-Coico, L. et al. 1986. Human keratinocyte culture. Identification and staging of epidermal cell subpopulations. *J Clin Invest* 77(2), pp. 396-404.

Stark, G. R. et al. 1998. How cells respond to interferons. *Annu Rev Biochem* 67, pp. 227-264.

Steinstraesser, L. et al. 2007. Transient non-viral cutaneous gene delivery in burn wounds. *J Gene Med* 9(11), pp. 949-955.

Stoffler, D. et al. 1999. The nuclear pore complex: from molecular architecture to functional dynamics. *Curr Opin Cell Biol* 11(3), pp. 391-401.

Tachibana, K. and Tachibana, S. 2001. The use of ultrasound for drug delivery. *Echocardiography* 18(4), pp. 323-328.

Takanashi, M. et al. 2009. Therapeutic silencing of an endogenous gene by siRNA cream in an arthritis model mouse. *Gene Ther* 16(8), pp. 982-989.

Tang, D. C. et al. 1992. Genetic immunization is a simple method for eliciting an immune response. *Nature* 356(6365), pp. 152-154.

Tang, M. X. et al. 1996. In vitro gene delivery by degraded polyamidoamine dendrimers. *Bioconjug Chem* 7(6), pp. 703-714.

Tao, J. et al. 2005. Inhibiting the growth of malignant melanoma by blocking the expression of vascular endothelial growth factor using an RNA interference approach. *Br J Dermatol* 153(4), pp. 715-724.

Taylor, N. A. and Machado-Moreira, C. A. 2013. Regional variations in transepidermal water loss, eccrine sweat gland density, sweat secretion rates and electrolyte composition in resting and exercising humans. *Extrem Physiol Med* 2(1), p. 4.

Templeton, N. S. et al. 1997. Improved DNA: liposome complexes for increased systemic delivery and gene expression. *Nat Biotechnol* 15(7), pp. 647-652.

Teo, E. H. et al. 2009. Gene therapy in skin: choosing the optimal viral vector. *Ann Plast Surg* 62(5), pp. 576-580.

Thanik, V. D. et al. 2007. Topical matrix-based siRNA silences local gene expression in a murine wound model. *Gene Ther* 14(17), pp. 1305-1308.

Therkildsen, P. et al. 1998. Epidermal thickness measured by light microscopy: a methodological study. *Skin Research and Technology* 4(4), pp. 174-179.

ThermoScientific. 2011. *Thermo Scientific Dharmacon Accell siRNA A new world of RNAi discovery* [Online]. Thermo Fisher Scientific Inc. Available at: http://www.thermoscientificbio.com/uploadedFiles/Resources/accell-brochure-single-pg.pdf [Accessed: 6 August 2013].

Tomakidi, P. et al. 1999. Normalization of keratinocyte-type integrins during the establishment of the oral mucosa phenotype in vitro. *Ann Anat* 181(1), pp. 127-132.

Torrisi, B. M. et al. 2013. Pocketed microneedles for rapid delivery of a liquid-state botulinum toxin A formulation into human skin. *J Control Release* 165(2), pp. 146-152.

Towbin, H. et al. 1992. Electrophoretic transfer of proteins from polyacrylamide gels to nitrocellulose sheets: procedure and some applications. 1979. *Biotechnology* 24, pp. 145-149.

Tran, M. A. et al. 2008. Targeting V600EB-Raf and Akt3 using nanoliposomal-small interfering RNA inhibits cutaneous melanocytic lesion development. *Cancer Res* 68(18), pp. 7638-7649.

Tranchant, I. et al. 2004. Physicochemical optimisation of plasmid delivery by cationic lipids. *J Gene Med* 6 Suppl 1, pp. S24-35.

Trost, A. et al. 2007. Rapid, high-quality and epidermal-specific isolation of RNA from human skin. *Exp Dermatol* 16(3), pp. 185-190.

Trowell, O. A. 1954. A modified technique for organ culture in vitro. *Exp Cell Res* 6(1), pp. 246-248.

Tseng, W. C. et al. 1997. Transfection by cationic liposomes using simultaneous single cell measurements of plasmid delivery and transgene expression. *J Biol Chem* 272(41), pp. 25641-25647.

Tseng, Y. C. et al. 2009. Lipid-based systemic delivery of siRNA. *Adv Drug Deliv Rev* 61(9), pp. 721-731.

Tuan-Mahmood, T. M. et al. 2013. Microneedles for intradermal and transdermal drug delivery. *Eur J Pharm Sci* 50(5), pp. 623-637.

Turabelidze, A. et al. 2010. Importance of housekeeping gene selection for accurate reverse transcription-quantitative polymerase chain reaction in a wound healing model. *Wound Repair Regen* 18(5), pp. 460-466.

Tuting, T. et al. 1998. DNA immunization targeting the skin: molecular control of adaptive immunity. *J Invest Dermatol* 111(2), pp. 183-188.

Uitto, J. 2009. Progress in heritable skin diseases: translational implications of mutation analysis and prospects of molecular therapies*. *Acta Derm Venereol* 89(3), pp. 228-235.

Uitto, J. and Richard, G. 2004. Progress in epidermolysis bullosa: genetic classification and clinical implications. *Am J Med Genet C Semin Med Genet* 131C(1), pp. 61-74.

Usui, M. L. et al. 2005. Morphological evidence for the role of suprabasal keratinocytes in wound reepithelialization. *Wound Repair Regen* 13(5), pp. 468-479.

Vader, P. et al. 2010. A method for quantifying cellular uptake of fluorescently labeled siRNA. *J Control Release* 148(1), pp. 106-109.

Van Damme, P. et al. 2009. Safety and efficacy of a novel microneedle device for dose sparing intradermal influenza vaccination in healthy adults. *Vaccine* 27(3), pp. 454-459.

van der Maaden, K. et al. 2012. Microneedle technologies for (trans)dermal drug and vaccine delivery. *J Control Release* 161(2), pp. 645-655.

van Roessel, P. and Brand, A. H. 2002. Imaging into the future: visualizing gene expression and protein interactions with fluorescent proteins. *Nat Cell Biol* 4(1), pp. E15-20.

van Wamel, A. et al. 2006. Vibrating microbubbles poking individual cells: drug transfer into cells via sonoporation. *J Control Release* 112(2), pp. 149-155.

Vandermeulen, G. et al. 2009. Effect of tape stripping and adjuvants on immune response after intradermal DNA electroporation. *Pharm Res* 26(7), pp. 1745-1751.

Vannucci, L. et al. 2013. Viral vectors: a look back and ahead on gene transfer technology. *New Microbiol* 36(1), pp. 1-22.

Verbaan, F. J. et al. 2008. Improved piercing of microneedle arrays in dermatomed human skin by an impact insertion method. *J Control Release* 128(1), pp. 80-88.

Verbaan, F. J. et al. 2007. Assembled microneedle arrays enhance the transport of compounds varying over a large range of molecular weight across human dermatomed skin. *J Control Release* 117(2), pp. 238-245.

Vicentini, F. T. et al. 2013. Delivery systems and local administration routes for therapeutic siRNA. *Pharm Res* 30(4), pp. 915-931.

Villemejane, J. and Mir, L. M. 2009. Physical methods of nucleic acid transfer: general concepts and applications. *Br J Pharmacol* 157(2), pp. 207-219.

Vogel, J. C. 1999. A direct in vivo approach for skin gene therapy. *Proc Assoc Am Physicians* 111(3), pp. 190-197.

Voordouw, G. et al. 1978. Isolation and physical studies of the intact supercoiled:: The open circular and the linear forms of CoIE1-plasmid DNA. *Biophysical Chemistry* 8(2), pp. 171-189.

Walther, W. et al. 2009. Nonviral jet-injection technology for intratumoral in vivo gene transfer of naked DNA. *Methods Mol Biol* 542, pp. 195-208.

Walther, W. and Stein, U. 2000. Viral vectors for gene transfer: a review of their use in the treatment of human diseases. *Drugs* 60(2), pp. 249-271.

Walzer, C. et al. 1989. Thermolysin treatment: a new method for dermo-epidermal separation. *Journal of Investigative Dermatology* 92(1), pp. 78-81.

Wang, J. et al. 2010. Delivery of siRNA therapeutics: barriers and carriers. *AAPS J* 12(4), pp. 492-503.

Wang, P. M. et al. 2006. Precise microinjection into skin using hollow microneedles. *J Invest Dermatol* 126(5), pp. 1080-1087.

Wang, Q. et al. 2007. Delivery and inhibition of reporter genes by small interfering RNAs in a mouse skin model. *J Invest Dermatol* 127(11), pp. 2577-2584.

Wang, W. et al. 2013. Non-viral gene delivery methods. *Curr Pharm Biotechnol* 14(1), pp. 46-60.

Wasungu, L. and Hoekstra, D. 2006. Cationic lipids, lipoplexes and intracellular delivery of genes. *J Control Release* 116(2), pp. 255-264.

Watson, J. D. and Crick, F. H. 1953. Molecular structure of nucleic acids; a structure for deoxyribose nucleic acid. *Nature* 171(4356), pp. 737-738.

Watt, F. M. and Green, H. 1981. Involucrin synthesis is correlated with cell size in human epidermal cultures. *J Cell Biol* 90(3), pp. 738-742.

Wattiaux, R. et al. 2000. Endosomes, lysosomes: their implication in gene transfer. *Adv Drug Deliv Rev* 41(2), pp. 201-208.

Wells, D. J. 2010. Electroporation and ultrasound enhanced non-viral gene delivery in vitro and in vivo. *Cell Biol Toxicol* 26(1), pp. 21-28.

Wermeling, D. P. et al. 2008. Microneedles permit transdermal delivery of a skin-impermeant medication to humans. *Proc Natl Acad Sci U S A* 105(6), pp. 2058-2063.

Widera, G. et al. 2006. Effect of delivery parameters on immunization to ovalbumin following intracutaneous administration by a coated microneedle array patch system. *Vaccine* 24(10), pp. 1653-1664.

Wilke, M. et al. 1996. Efficacy of a peptide-based gene delivery system depends on mitotic activity. *Gene Ther* 3(12), pp. 1133-1142.

Wilkinson, K. D. 2000. Ubiquitination and deubiquitination: targeting of proteins for degradation by the proteasome. *Semin Cell Dev Biol* 11(3), pp. 141-148.

Wilson, G. L. et al. 1999. Nuclear import of plasmid DNA in digitonin-permeabilized cells requires both cytoplasmic factors and specific DNA sequences. *J Biol Chem* 274(31), pp. 22025-22032.

Wolff, J. A. and Budker, V. 2005. The mechanism of naked DNA uptake and expression. *Adv Genet* 54, pp. 3-20.

Wolff, J. A. et al. 1990. Direct gene transfer into mouse muscle in vivo. *Science* 247(4949 Pt 1), pp. 1465-1468.

Woodley, D. T. et al. 2004. Intradermal injection of lentiviral vectors corrects regenerated human dystrophic epidermolysis bullosa skin tissue in vivo. *Mol Ther* 10(2), pp. 318-326.

Wu, G. Y. and Wu, C. H. 1988. Receptor-mediated gene delivery and expression in vivo. *J Biol Chem* 263(29), pp. 14621-14624.

Wu, J. et al. 1998. Defects generated in human stratum corneum specimens by ultrasound. *Ultrasound Med Biol* 24(5), pp. 705-710.

Xu, L. and Anchordoquy, T. J. 2008. Cholesterol domains in cationic lipid/DNA complexes improve transfection. *Biochim Biophys Acta* 1778(10), pp. 2177-2181.

Xu, Y. et al. 1999. Physicochemical characterization and purification of cationic lipoplexes. *Biophys J* 77(1), pp. 341-353.

Xu, Y. and Szoka Jr, F. 1996. Mechanism of DNA Release from Cationic Liposome/DNA Complexes Used in Cell Transfection. *Biochemistry* 35(18), pp. 5616-5623.

Yadava, P. et al. 2008. Effect of lyophilization and freeze-thawing on the stability of siRNA-liposome complexes. *AAPS PharmSciTech* 9(2), pp. 335-341.

Yamano, S. et al. 2010. Comparison of transfection efficiency of nonviral gene transfer reagents. *Mol Biotechnol* 46(3), pp. 287-300.

Yan, G. et al. 2010. Evaluation needle length and density of microneedle arrays in the pretreatment of skin for transdermal drug delivery. *Int J Pharm* 391(1-2), pp. 7-12.

Yang, N. S. et al. 1990. In vivo and in vitro gene transfer to mammalian somatic cells by particle bombardment. *Proc Natl Acad Sci U S A* 87(24), pp. 9568-9572.

Yu, J. Y. et al. 2002. RNA interference by expression of short-interfering RNAs and hairpin RNAs in mammalian cells. *Proc Natl Acad Sci U S A* 99(9), pp. 6047-6052.

Yuzhakov, V. V. 2007. Microneedle array, patch and applicator for transdermal drug delivery. In: Patent, U.S. ed.

Yuzhakov, V. V. 2010. Microneedle array, patch and applicator for transdermal drug delivery. In: Patent, U.S. ed.

Zamore, P. D. et al. 2000. RNAi: double-stranded RNA directs the ATP-dependent cleavage of mRNA at 21 to 23 nucleotide intervals. *Cell* 101(1), pp. 25-33.

Zellmer, S. et al. 2001. Long-term expression of foreign genes in normal human epidermal keratinocytes after transfection with lipid/DNA complexes. *Histochem Cell Biol* 115(1), pp. 41-47.

Zellmer, S. and Reissig, D. 2002. Isolation, cultivation, and differentiation of normal human epidermal keratinocytes in serum-free medium. *Methods Mol Biol* 188, pp. 179-184.

Zhang, L. et al. 2002. Enhanced delivery of naked DNA to the skin by non-invasive in vivo electroporation. *Biochim Biophys Acta* 1572(1), pp. 1-9.

Zhang, S. et al. 2004. Cationic compounds used in lipoplexes and polyplexes for gene delivery. *J Control Release* 100(2), pp. 165-180.

Zhang, S. et al. 2007. Cationic lipids and polymers mediated vectors for delivery of siRNA. *J Control Release* 123(1), pp. 1-10.

Zhang, Y. and Anchordoquy, T. J. 2004. The role of lipid charge density in the serum stability of cationic lipid/DNA complexes. *Biochim Biophys Acta* 1663(1-2), pp. 143-157.

Zhao, J. Y. et al. 2013. Influence of hyaluronic acid on wound healing using composite porcine acellular dermal matrix grafts and autologous skin in rabbits. *Int Wound J* 10(5), pp. 562-572.

Zhao, M. et al. 2008. Lipofectamine RNAiMAX: an efficient siRNA transfection reagent in human embryonic stem cells. *Mol Biotechnol* 40(1), pp. 19-26.

Zhi, D. et al. 2010. Transfection efficiency of cationic lipids with different hydrophobic domains in gene delivery. *Bioconjug Chem* 21(4), pp. 563-577.

Zhou, J. et al. 1999. Growth and differentiation regulate CD44 expression on human keratinocytes. *In Vitro Cell Dev Biol Anim* 35(4), pp. 228-235.

Zhou, J. et al. 2013. Nanoparticle-Based Delivery of RNAi Therapeutics: Progress and Challenges. *Pharmaceuticals (Basel)* 6(1), pp. 85-107.

Zhou, Y. et al. 2009. The size of sonoporation pores on the cell membrane. *Ultrasound Med Biol* 35(10), pp. 1756-1760.

Zuhorn, I. S. et al. 2007. Gene delivery by cationic lipid vectors: overcoming cellular barriers. *Eur Biophys J* 36(4-5), pp. 349-362.

Appendix

Scientific paper

The following scientific paper was published during the post-graduate studies and is attached to the back of this thesis:

Chong, R. H. et al. 2013. Gene silencing following siRNA delivery to skin via coated steel microneedles: In vitro and in vivo proof-of-concept. *J Control Release* 166(3), pp. 211-219.

Journal of Controlled Release 166 (2013) 211–219

Contents lists available at SciVerse ScienceDirect

Journal of Controlled Release

journal homepage: www.elsevier.com/locate/jconrel

GENE DELIVERY

Gene silencing following siRNA delivery to skin *via* coated steel microneedles: *In vitro* and *in vivo* proof-of-concept

Rosalind H.E. Chong [a,b], Emilio Gonzalez-Gonzalez [c,1], Maria F. Lara [d], Tycho J. Speaker [d], Christopher H. Contag [c,e], Roger L. Kaspar [c,d], Sion A. Coulman [a], Rachel Hargest [b], James C. Birchall [a,*]

[a] School of Pharmacy and Pharmaceutical Sciences, Cardiff University, Cardiff, CF10 3NB, UK
[b] Academic Department of Surgery, University Hospital of Wales, Cardiff University, Cardiff, CF14 4XN, UK
[c] Department of Pediatrics, Stanford School of Medicine, and Molecular Imaging Program at Stanford, CA, USA
[d] Transderm Inc., Santa Cruz, CA, USA
[e] Departments of Radiology and Microbiology & Immunology, Stanford School of Medicine, Stanford, CA, USA

ARTICLE INFO

Article history:
Received 22 October 2012
Accepted 30 December 2012
Available online 8 January 2013

Keywords:
Microneedles
Coating
Lipoplex
Self-delivery siRNA
Keratinocytes
RNA interference

ABSTRACT

The development of siRNA-based gene silencing therapies has significant potential for effectively treating debilitating genetic, hyper-proliferative or malignant skin conditions caused by aberrant gene expression. To be efficacious and widely accepted by physicians and patients, therapeutic siRNAs must access the viable skin layers in a stable and functional form, preferably without painful administration. In this study we explore the use of minimally-invasive steel microneedle devices to effectively deliver siRNA into skin. A simple, yet precise microneedle coating method permitted reproducible loading of siRNA onto individual microneedles. Following recovery from the microneedle surface, lamin A/C siRNA retained full activity, as demonstrated by significant reduction in lamin A/C mRNA levels and reduced lamin A/C protein in HaCaT keratinocyte cells. However, lamin A/C siRNA pre-complexed with a commercial lipid-based transfection reagent (siRNA lipoplex) was less functional following microneedle coating. As Accell-modified "self-delivery" siRNA targeted against CD44 also retained functionality after microneedle coating, this form of siRNA was used in subsequent *in vivo* studies, where gene silencing was determined in a transgenic reporter mouse skin model. Self-delivery siRNA targeting the reporter (luciferase/GFP) gene was coated onto microneedles and delivered to mouse footpad. Quantification of reporter mRNA and intravital imaging of reporter expression in the outer skin layers confirmed functional *in vivo* gene silencing following microneedle delivery of siRNA. The use of coated metal microneedles represents a new, simple, minimally-invasive, patient-friendly and potentially self-administrable method for the delivery of therapeutic nucleic acids to the skin.

1. Introduction

The concept of RNA interference (RNAi) emerged in 1998 [1] and the functionality of a synthetic small interfering nucleic acid (siRNA) in mammalian cells was demonstrated in 2001 [2]. Breakthrough discoveries in recent years have led to a sustained interest in RNAi research and numerous publications have now established the potential of siRNA technology both *in vitro*, *in vivo* and in clinical trials (reviewed in [3,4]).

The skin has a large surface area and is the most accessible organ of the body, thus lending itself to gene modification approaches [5–7]. Well controlled treatment of a confined area of the skin is possible and any genetically modified region can be monitored and biopsied for functional improvement and/or removed surgically if unwanted side effects were to occur [8]. The successful development of siRNA therapies has significant potential for the treatment of skin conditions caused by aberrant gene expression, including allergic skin diseases [9–11], alopecia [12], skin cancer [13–20], psoriasis [16], hyperpigmentation [21] and pachyonychia congenita [22,23].

One of the most significant challenges in siRNA therapy is the effective transfer of nucleic acid across cellular membranes. This challenge is further compounded in the skin by the non-viable outermost barrier layer, the stratum corneum. Previous studies have used hypodermic needles for viable, intradermal delivery of therapeutic siRNA [22,23]; however the significant pain associated with localised injections into diseased tissue has hindered progress to the clinic [22]. To provide a less invasive method for overcoming the stratum corneum barrier, we investigate the use of steel microneedle devices for the functional delivery of siRNA into the skin. To interact effectively with the complex multi-layer structure of the skin, microneedles, typically comprising a plurality of projections of micron-sized dimension, are

* Corresponding author. Tel.: +44 2920875815.
E-mail address: birchalljc@cf.ac.uk (J.C. Birchall).
[1] Current address: The Andalusian Centre for Nanomedicine and Biotechnology, BIONAND, Malaga, Spain.

0168-3659/$ – see front matter © 2013 Elsevier B.V. All rights reserved.
http://dx.doi.org/10.1016/j.jconrel.2012.12.030

designed to create micron-sized channels within the epidermal layer through which therapeutic molecules and macromolecules can be delivered [24] in a pain-free manner [25–27].

Methods of microneedle-assisted drug delivery are commonly categorised into four general approaches: (i) pre-applying solid microneedles before drug application to "punch holes" in the stratum corneum barrier through which drugs can later pass, (ii) coating drugs onto microneedles, (iii) incorporating drug into dissolving or biodegradable microneedles, and (iv) injecting drugs through hollow microneedles [28]. In previous studies, delivery of functional unmodified siRNA through intradermal injection [29] and modified self-delivery siRNA through a microneedle-based delivery system called a biodegradable protrusion array device (PAD) [30] induced silencing of reporter gene expression in the epidermis of a transgenic mouse model. Steel microneedle devices have prospective clinical advantages of simple and cost-effective manufacture with high reproducibility, biocompatibility, reliable skin puncture and sufficient loading capacity for nucleic acid therapies [31,32]. Our aim is to evaluate the potential of stainless steel microneedles as a means to deliver surface-coated siRNA to the target region, the viable epidermis, of skin. Whilst we have recently demonstrated the utility of a similar microneedle system for plasmid DNA delivery to skin [32], this is the first study exploring the utility of this simple delivery system for siRNA delivery. The study confirms appropriate siRNA loading onto microneedles, siRNA deposition within skin and functionality, through demonstrable gene silencing *in vivo*.

2. Materials and methods

All reagents and laboratory equipment were purchased from Thermo Fisher Scientific (UK or USA) unless otherwise stated.

2.1. siRNA sequences

2.1.1. In vitro studies

The siRNA molecules used were a 19 + 2 format, synthesised with two 3′ deoxythymidine (dT) overhangs. An unmodified non-self-delivery (non-sd-) lamin A/C siRNA (lamin A/C non-sd-siRNA; sequence: 5′-CUGGACUUCCAGAAGAACA) targeting human lamin A/C mRNA was designed and synthesised by Eurofins MWG Operons (Ebersberg, Germany). A nonspecific unmodified green fluorescent protein (GFP) siRNA (control non-sd-siRNA; sequence: 5′-GGCUACG UCCAGGAGCGCACC) targeting the GFP mRNA not present in the human keratinocytes model was used as a control.

Accell modified self-delivery (sd-) CD44 siRNA (Accell CD44 sd-siRNA) and non-Accell modified non-sd-siRNA (siSTABLE CD44 non-sd-siRNA) targeting human CD44 mRNA (both siRNA sequence: 5′-GGCGCAGAUCGAUUUGAAU) [33] were designed and synthesised by Dharmacon Products, Thermo Fisher Scientific (Lafayette, CO, USA). A nonspecific self-delivery K6a_513a.12 siRNA (Accell control sd-siRNA) targeting a keratin 6a mutation not present in the human keratinocytes model or the mouse skin model was used as control [34].

2.1.2. In vivo studies

Accell modified sd-siRNA targeting the CBL coding region of transgenic hMGFP/CBL mouse mRNA (5′-UAACGAUCCACGACGUAAA; Accell CBL3 sd-siRNA) was designed and synthesised by Dharmacon Products, Thermo Fisher Scientific (Lafayette, CO, USA). Accell control sd-siRNA was used as control.

2.2. Microneedle fabrication and coating

2.2.1. Microneedle fabrication, coating and characterisation

Stainless steel microneedle devices (containing either 5 or 10 needles of 700 μm length and 200 μm base width) were fabricated from a stainless steel sheet by wire electrical discharge machining (EDM). A coating method was developed to coat siRNA onto the surface of the microneedles from a liquid formulation (Fig. 1A).

To determine the efficiency and reproducibility of the coating method, 3 μL of unmodified siRNA (Dharmacon Products, Thermo Fisher Scientific, Lafayette, CO, USA) (70 mg mL^{-1} in phosphate buffered saline; PBS) was loaded into a 20 μL pipette tip as a reservoir for coating. Microneedles (6 devices with 5 microneedles per array) were coated with siRNA using the method described in detail in Fig. 1A and were allowed to dry at 4 °C for either 1 or 20 h (3 devices for each drying time) to provide a *theoretical* loading of 35 μg siRNA coated onto each microneedle device. The method was repeated with another 6 devices with 10 microneedles per array. To determine *actual* loading, siRNA was recovered from the microneedle devices by washing in 150 μL siRNA buffer for 5 min and the nucleic acid concentration was quantified using the NanoDrop spectrophotometer (Thermo Fisher Scientific, USA).

To visually characterise siRNA coating onto microneedles, 1 μL of BLOCK-iT™ Alexa 647 fluorescent siRNA (1 mg mL^{-1} in PBS) (a gift from Dr. Xavier de Mollerat du Jeu, Life Technologies, USA) was loaded into a pipette tip and microneedles (10 microneedles per array) were coated with siRNA using the method described in Fig. 1A to provide a *theoretical* loading of 1 μg siRNA onto the microneedle device. The coated microneedles were imaged using the Leica DM IRB epifluorescence microscope and imaging system. Dry coated microneedles were manually inserted into excised human breast skin, obtained from surgical procedures with informed consent and full ethical approval, left seated for 10 min and then removed. The siRNA fluorescence remaining on the microneedles post-delivery was imaged.

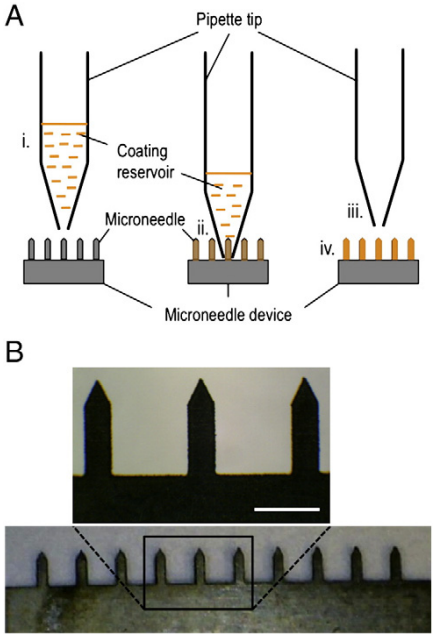

Fig. 1. (A) Simple and precise microneedle coating method. An illustration of siRNA coating onto the surface of steel microneedles. (i) A volume of siRNA of known concentration was loaded into a pipette tip as a reservoir for coating. (ii) Microneedles were coated with siRNA by repeated immersions of the needles into the reservoir, with 30 s of air-drying time between each immersion. (iii) Microneedles were coated until the reservoir was exhausted. (iv) The coated microneedles were allowed to further dry at 4 °C. (B) Microneedle morphology. An array of ten steel microneedles of 700 μm in length. The inset micrograph image shows the microneedle geometry in greater detail. (Bar = 500 μm).

2.2.2. Microneedle preparation for in vitro studies

Initial *in vitro* studies compared naked siRNA against siRNA complexed with a lipid-based transfection reagent (Lipofectamine™ RNAiMAX; Invitrogen, Life Technologies, UK), termed a "lipoplex." Using the coating method described in Fig. 1A, naked lamin A/C non-sd-siRNA pre-coating formulation (48 pmol in 8 μL PBS) or lamin A/C non-sd-siRNA lipoplex pre-coating formulation (48 pmol in 8 μL Lipofectamine™ RNAiMAX) was coated onto steel microneedle devices (4 devices per treatment group; each with 5 microneedles per array) to provide a *theoretical* loading of 12 pmol siRNA on each microneedle device. Coated microneedles were allowed to dry at 4 °C for 1 h before the siRNA was recovered by washing microneedles in 50 μL siRNA buffer for 5 min. The recovered siRNA solutions were used to treat cells as described in Section 2.3.2.

Accell control or Accell CD44 sd-siRNA was coated onto microneedle devices to determine the effect of microneedle coating on the stability of sd-siRNA. A *theoretical* loading of 1.5 nmol siRNA was coated onto each microneedle device, which was subsequently allowed to dry at 4 °C for 10 h before the siRNA was recovered by washing the microneedles in 60 μL siRNA buffer for 5 min. The recovered siRNA solutions (20 μL of recovered siRNA solution containing approximately 500 pmol siRNA) were used to treat cells as described in Section 2.3.2.

2.2.3. Microneedle preparation for in vivo studies

Two μL of siRNA coating solution (70 mg mL^{-1} for Accell sd-CBL3 and 80 mg mL^{-1} for Accell sd-Control) in PBS was loaded into a pipette tip reservoir for coating. The steel microneedle devices (4 devices per treatment group; each with 10 microneedles per array) were coated with siRNA using the coating method described in Fig. 1A to provide a *theoretical* loading of 35 μg and 40 μg Accell CBL3 and Accell control sd-siRNA coated onto each microneedle device, respectively. Coated microneedles were maintained at 4 °C for up to 18 h before use.

2.3. In vitro siRNA stability studies

2.3.1. HaCaT cell culture

Immortalised human keratinocyte cells (HaCaT cells) [35] were received as a gift from Dr. Mark Gumbleton (School of Pharmacy and Pharmaceutical Sciences, Cardiff University). Cells were cultured in a growth medium consisting of Dulbecco's modified Eagle medium (DMEM), supplemented with 10% foetal bovine serum (FBS), 100 unit mL^{-1} of penicillin and 100 mg mL^{-1} of streptomycin (all Life Technologies, UK) at 37 °C in a humidified atmosphere containing 5% CO_2.

2.3.2. Cell treatment

Before treatment, cells were seeded into 12-well plates at a density of 2.5×10^4 cells cm^{-2} in 1 mL growth medium and maintained for 24 h. Cell populations were then treated using (i) GFP non-sd-siRNA 10 nM lipoplex (non-targeting control), (ii) naked lamin A/C non-sd-siRNA 10 nM (non-lipoplex control), (iii) lamin A/C non-sd-siRNA lipoplex 10 nM (positive control), (iv) naked lamin A/C non-sd-siRNA pre-coating formulation diluted to 10 nM formed into lipoplex (naked siRNA pre-coat + lipo) (v) naked lamin A/C non-sd-siRNA recovered from microneedles and subsequently formed into lipoplex (naked siRNA coated + lipo), (vi) lamin A/C non-sd-siRNA lipoplex pre-coating formulation diluted to 10 nM (siRNA lipoplex pre-coat) (vii) lamin A/C non-sd-siRNA lipoplex formulation recovered from microneedles (siRNA lipoplex coated) and (viii) Opti-MEM® solution (untreated). The final concentration of lipoplexes in treatment groups with lipoplex was 1% v/v Lipofectamine™ RNAiMAX transfection reagent. Transfection complexes prepared according to the supplier's recommended protocol were diluted with Opti-MEM® solution (Life Technologies, UK) to a volume of 200 μL and added to the seeded cells to a final transfection volume of 1200 μL. The final concentration of siRNA across all treatment groups with siRNA was 10 nM (12 pmol in 1200 μL transfection volume). Cells were treated in quadruplicate transfection with triplicate sample for mRNA quantification by RT-qPCR and the remaining treatment sample for protein analysis by Western blotting. Treated cells were incubated at 37 °C in a humidified atmosphere containing 5% CO_2.

For the Accell sd-siRNA study, cells were seeded into 24-well plates at a density of 2.5×10^4 cells cm^{-2} in 0.5 mL growth medium and maintained for 24 h. Cell populations were then treated using (i) Accell control sd-siRNA 1 μM (Accell non-targeting control), (ii) siSTABLE CD44 non-sd-siRNA 1 μM (non-Accell CD44 control), (iii) Accell CD44 sd-siRNA 1 μM (Accell CD44 positive control), and (iv) Accell CD44 sd-siRNA recovered from microneedles 1 μM (Accell CD44 coated). HaCaT cells were treated with the siRNA diluted in serum-free Accell delivery media (ThermoFisher Scientific, UK) at a volume of 500 μL according to the supplier's recommended protocol. HaCaT cells were treated by replacing the seeding media with the delivery mixture containing siRNA. Due to the passive self-delivery nature of the Accell siRNA, a higher final siRNA concentration of 1 μM (500 pmol in 500 μL treatment volume) is required for efficient gene silencing *in vitro*. Treated cells were incubated at 37 °C in a humidified atmosphere containing 5% CO_2. After 24 h, the treatment media was replaced with DMEM supplemented with 10% FBS and the cells were incubated for a further 24 h. Cells were treated in triplicate transfection for mRNA quantification by RT-qPCR.

2.3.3. mRNA quantification

Forty-eight hours following treatment, total RNAs from lamin A/C non-sd-siRNA and Accell CD44 sd-siRNA treated cells were isolated using the Ambion® PureLink™ RNA Mini Kit (Life Technologies, UK), quantified (NanoVue spectrophotometer; GE Heathcare, UK) and stored at −80 °C. Reverse transcription converted total RNA into first-strand cDNA using random primers with the High Capacity cDNA Reverse Transcription system (Applied Biosystems, Life Technologies, UK). Quantitative PCR was performed using the ABI 7900HT Fast Real-Time PCR system with TaqMan® Fast Advanced Master Mix (Applied Biosystems). Target gene inhibition was measured using Taqman gene expression assays specific for lamin A/C (Hs00153462_m1) or CD44 (Hs00153304_m1) and the endogenous control GAPDH (Hs02758991_g1). All data points reported are the mean and standard error of three separate treatments each with three replicate qPCR assays.

2.3.4. Protein analysis

Following the transfection period (48 h), cells treated with lamin A/C non-sd-siRNA were washed and incubated with ice-cold lysis buffer (50 mM Tris–HCl, 150 mM NaCl, pH 8.0, 1% Triton X-100) containing protease inhibitor cocktail (Roche, UK). The lysates were incubated on ice for 10 min prior to centrifugation at 13 000 *g* at 4 °C for 10 min. Protein content was determined using a BCA (bicinchoninic acid) assay (Sigma Aldrich, UK). Samples containing 15 μg of protein were mixed with SDS sample buffer, heated at 95 °C for 5 min before being separated by electrophoresis on 10% resolving Mini-PROTEAN TGX precast gels (Bio-Rad, UK) using the Bio-Rad Mini Protean 3 system (Bio-Rad, UK). Proteins were transferred to nitrocellulose papers (Bio-Rad, UK) using the Trans-Blot® Turbo Transfer System™ (Bio-Rad, UK), probed with primary antibodies recognising lamin A/C (ab8984) (Abcam, UK) and α-tubulin (T9026) (Sigma Aldrich, UK) and detected using a HRP conjugated secondary antibody (32430) (Thermo Fisher Scientific, UK) and Super Signal West DURA solutions (Thermo Fisher Scientific, UK) developed onto Amersham Hyperfilm ECL (GE Healthcare, UK).

2.4. In vivo studies

2.4.1. Animal models

Tg CBL/hMGFP mice [29] were bred at Stanford University, Stanford, California, USA. Tg CBL/hMGFP mice were crossed with skh1 hairless

mice, purchased from Charles River (Wilmington, MA), to constitute the transgenic hairless reporter mouse Tg-h CBL/hMGFP. Mice were screened for reporter expression by intraperitoneal injection of luciferin (100 μL of 30 mg/mL; 150 mg/kg body weight) and the live anaesthetised (2% isoflurane) mice were imaged 10 min later using the IVIS 200 Imaging System (Caliper Life Sciences). All animals were treated according to the guidelines of both the National Institutes of Health and Stanford University.

2.4.2. Mouse paw treatment

Mice were anaesthetised with 2–3% isoflurane prior to microneedle administration. A group of four Tg-h CBL/hMGFP mice were treated on the right paw with microneedles (10 microneedles of 700 μm length) coated with Accell CBL3 sd-siRNA. The counterpart left paw was treated with identical microneedles loaded with Accell non-targeting control sd-siRNA. The microneedle devices were manually inserted into the middle region of the mouse paw (between the footpads) and held in place for 5 min. Devices remained in the skin for an additional 15 min (total insertion time 20 min) before being removed. Treatments were repeated at the same location daily for 10 days, except day 2. At day 10, the mice were sacrificed and the treated paw skin was removed by surgical dissection.

2.4.3. Quantification of siRNA deposition

The mass of siRNA loaded onto each microneedle device, prior to application, was estimated from the mass of siRNA in the known volume of coating formulation that was used to coat the microneedles. Following application, the microneedles were rinsed using a fixed volume of buffer (100 or 150 μL) for 5 min and the nucleic acid concentration was quantified using the NanoDrop spectrophotometer. The mass of nucleic acid deposited into the mouse skin during each treatment procedure was inferred by the mass balance between the loaded siRNA and the siRNA remaining on the microneedles after removal from mouse paws. Unpaired two-tailed t-tests were performed to determine the statistical difference of siRNA deposited in the control and CBL3 group.

2.4.4. Intravital fluorescence imaging and quantification

Prior to treatment, mice were anaesthetised with 2–3% isoflurane and imaged intravitally using the Maestro Optical imaging system (Caliper LifeSciences now part of Perkin Elmer, USA), as previously described [30,36]. Imaging was repeated on days 2, 4, 6, 8 and 10 of the treatment regimen. Each spectrum was set by unmixing the autofluorescence from a hairless skh1 negative non-hMGFP expressing mouse from the spectra of a Tg-h CBL/hMGFP positive mouse analysed in parallel. The conditions and subject positioning for image acquisition were standardized, facilitating meaningful comparison of data. Quantitative data was extracted using ImageJ software (National Institute of Health, USA) by selecting the treatment area and calculating the average signal (counts s^{-1} mm^{-1}) at the various time points. The ratio of average signal in the right (treatment) *versus* left (control) paws was determined in each mouse and was normalised to the pre-treatment levels.

2.4.5. Skin sectioning and immunofluorescence

Skin tissue from the region between the footpads of one mouse was excised, embedded in OCT and frozen on dry ice. Ten μm sections (Leica CM3050S Cryostat; Leica Microsystems (UK) Ltd, UK) were captured on microscope slides and mounted with VECTASHIELD® Mounting Medium containing 1.5 μg mL^{-1} 4,6-diamidino-2-phenylindole (DAPI; Vector Laboratories Ltd., UK) for nuclear staining. Transgene fluorescence was visualised using the Leica DM IRB epifluorescence microscope and imaging system (Leica Microsystems Ltd, UK).

2.4.6. Gene expression quantification

RNA was isolated from the skin tissue (obtained from three mice per cohort), reverse transcribed and subjected to qPCR as previously described [29]. A Taqman gene expression assay, specifically designed for hMGFP was used (hMGFP-F: 5′-CCCCAAGGACATCCCTGACT; hMGFP-R: TGCTTCGCTCCCACGAGTA and probe: 6FAM-TCAAGCAGA CCTTCCCCGA-MGBN FQ; Applied Biosystem, USA). TaqMan gene expression assay specific for CD44 (Hs00153304_m1) was used as the endogenous gene control. All data points reported are the mean and standard error of three replicate assays.

2.5. Data processing and statistical analysis

Graphs were generated and statistical analyses (unpaired two-tailed t-tests) performed using Prism® 5 for Mac OS X (GraphPad Software Inc. USA).

3. Results

3.1. Efficiency and reproducibility of siRNA coating onto microneedles

The pipette coating method, as shown in Fig. 1A, was used to coat stainless steel microneedles with siRNA. Two sets of microneedle devices of identical dimensions (Fig. 1B) but with different densities of microneedles per array (5 or 10 microneedles) were coated. The same volume and concentration of siRNA solution were used to coat each set of arrays. Fig. 2 shows that the pipette reservoir method for microneedle coating resulted in a meaningful and relatively reproducible (approximately 35 μg) mass of siRNA coated onto and recovered from each array of microneedles. The recovery of siRNA was not affected by prolonged (20 h) post-drying of the microneedles.

3.2. siRNA distribution on microneedles before and after skin insertion

To determine the extent of microneedle coating and subsequent *in situ* release of the siRNA, stainless steel microneedles were coated with a fluorescently-tagged siRNA, allowed to dry, imaged, applied to excised human skin and then re-imaged (Fig. 3). Fig. 3A shows a relatively uniform coating of siRNA on the surface of a single representative steel microneedle. Following a 10 min insertion into skin, the vast majority of the coating was removed from the microneedle surface (Fig. 3B).

3.3. Functionality of siRNA recovered from coated microneedles

In vitro cell studies were performed to determine whether siRNAs retain biological activity following coating on steel microneedles. Lamin A/C gene expression in HaCaT keratinocyte cells was analysed

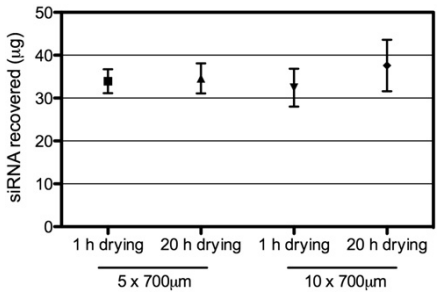

Fig. 2. siRNA coating onto steel microneedles. A theoretical mass of 35 μg of siRNA per microneedle device was loaded onto two sets of microneedle devices with different densities of microneedles per array (6 with 5 microneedles per array and 6 with 10 microneedles per array). siRNA from 3 devices was recovered from each set of microneedle devices at the drying time-points. (h = hour; n = 3; error bar = standard deviation).

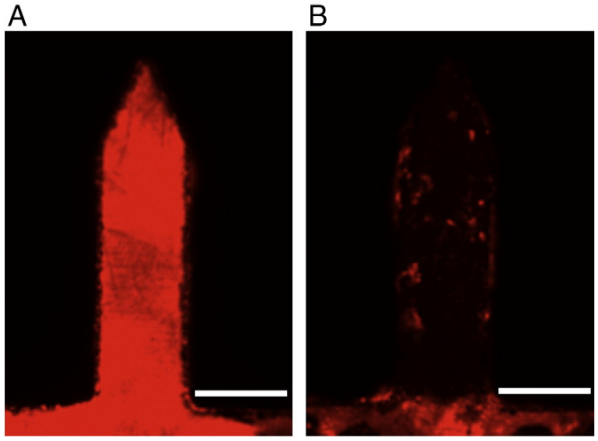

Fig. 3. Extent of siRNA coating pre- and post skin insertion. Fluorescence images of a microneedle coated with approximately 0.1 μg of fluorescent siRNA pre- (A) and post- (B) insertion into excised human breast skin. The images shown are representative of other microneedles analysed in the array. (Bar = 200 μm).

at both the mRNA (qPCR) (Fig. 4A) and protein (western blotting) levels (Fig. 4B). Lamin A/C mRNA levels were significantly ($p<0.0001$) reduced in cells treated with siRNA that had been previously coated onto microneedles, recovered and subsequently complexed with Lipofectamine™ RNAiMAX (naked siRNA coated + lipo) prior to treatment. The level of siRNA-mediated lamin A/C reduction (85.4%) was

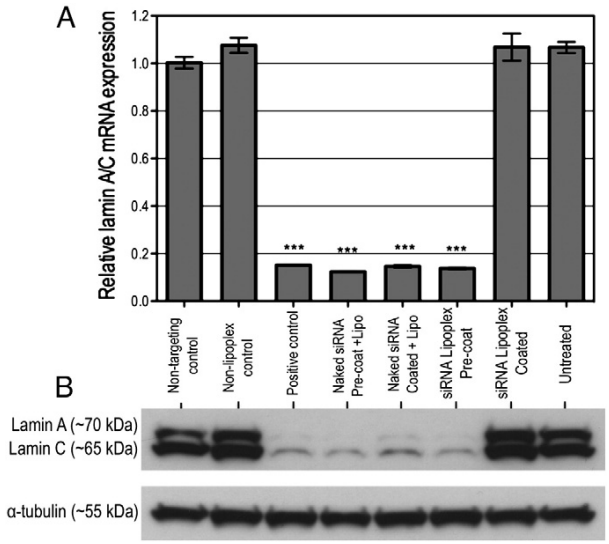

Fig. 4. Retention of siRNA functionality following microneedle coating. Lamin A/C mRNA (A) and protein (B) expression was determined in HaCaT cells 48 h post-treatment with siRNA. (A) Lamin A/C mRNA expressions were relative to the non-targeting negative control group and normalised to GAPDH endogenous control gene levels. (n = 3 transfection repeats, each with 3 qPCR assay replicates; ***significant reduction in mRNA expression compared with negative control, $p<0.0001$). (B) Lamin A/C protein expression with α-tubulin as the protein loading control. Lamin A/C siRNA recovered from microneedle devices (naked siRNA coated) was subsequently complexed with 1% v/v Lipofectamine™ RNAiMAX for transfection in HaCaT cells. The same amount of siRNA (10 nM) was used across all the treatment groups. (Non-targeting control = GFP siRNA 10nM + 1% v/v Lipofectamine™ RNAiMAX; non-lipoplex control = lamin A/C siRNA 10nM; positive control = lamin A/C siRNA 10 nM + 1% v/v Lipofectamine™ RNAiMAX; naked siRNA pre-coat + lipo = lamin A/C siRNA lipoplex pre-coating formulation diluted to 10nM + 1% v/v Lipofectamine™ RNAiMAX; siRNA lipoplex pre-coat = lamin A/C siRNA pre-coating formulation diluted to 10nM siRNA with 1% v/v Lipofectamine™ RNAiMAX; siRNA lipoplex coated = lamin A/C siRNA lipoplex formulation (10 nM siRNA + 1% v/v Lipofectamine™ RNAiMAX) recovered after coating onto microneedles).

comparable to that achieved with the positive control (non-coated siRNA lipoplex 10 nM; 85.2% reduction). When siRNA was pre-complexed with the transfection reagent prior to coating and recovery from microneedles (siRNA lipoplex coated) there was no reduction in mRNA synthesis. Lamin A/C protein expression studies were also performed to determine whether reduction in mRNA levels correlated to a reduction in protein expression. Fig. 4B confirms that the reduction in mRNA following treatment with lamin A/C siRNA, that has been coated and recovered from microneedles and subsequently complexed with transfection reagent (naked siRNA coated + lipo), translates to reduced lamin A/C protein expression in HaCaT cells. siRNA pre-complexed with a transfection reagent (siRNA lipoplex) prior to coating and recovery from microneedles (siRNA lipoplex coated) did not confer a reduction in protein expression.

Coating microneedles with a binary lipoplex appears to compromise the *in vitro* activity of the siRNA, which is likely to translate to limited gene silencing efficiency *in vivo*. Given the encouraging stability of naked siRNA coated onto microneedles, a further *in vitro* stability study was performed using modified "self-delivery" naked siRNA constructs. Accell sd-siRNAs enter cells passively without the need for lipid-based transfection reagents and are also modified for improved stability. CD44 mRNA expression in HaCaT keratinocyte cells treated with the modified sd-siRNA was analysed by RT-qPCR (Fig. 5). CD44 mRNA levels were significantly ($p<0.0001$) reduced in cells treated with both the sd-siRNA that had been previously coated onto microneedles and recovered (Accell CD44 coated; 67.4% reduction) and the Accell positive control (Accell CD44 sd-siRNA 1 μM; 74.5% reduction). Naked CD44 non-sd-siRNA did not reduce mRNA synthesis when applied to the cells in the absence of a transfection reagent (non-Accell CD44 control).

3.4. Delivery of microneedle coated sd-siRNA and gene silencing in transgenic mouse skin

Informed by the results of the *in vitro* siRNA stability studies, subsequent experiments examined the ability of Accell-modified sd-siRNA coated stainless steel microneedles (Fig. 2) to facilitate gene silencing *in vivo*. The central region of the CBL/hMGFP mouse paws was treated with Accell CBL3 sd-siRNA targeted against the CBL coding region of

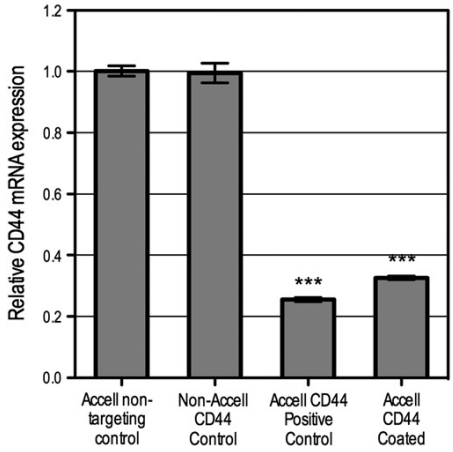

Fig. 5. Retention of Accell sd-siRNA functionality following microneedle coating. CD44 expression was determined in HaCaT cells 48 h post-treatment with siRNA. CD44 mRNA expressions were relative to the Accell non-targeting negative control group and normalised to GAPDH endogenous control gene levels. (n = 3 transfection repeats, each with 3 qPCR assay replicates; ***significant reduction in mRNA expression compared with Accell non-targeting control, $p<0.0001$). (Accell non-targeting control = Accell control sd-siRNA 1 μM; non-Accell CD44 control = siSTABLE CD44 non-sd-siRNA 1 μM; Accell CD44 positive control = Accell CD44 sd-siRNA 1 μM; Accell CD44 coated = Accell CD44 sd-siRNA recovered after coating onto microneedles, 1 μM).

the hMGFP/CBL mRNA. Treatments were conducted daily and the formulation was delivered as a dry coat. The doses of Accell control and CBL3 sd-siRNA were approximately 40 μg and 35 μg per microneedle device, respectively. The mass of siRNA deposited into the skin was relatively low (less than 15 μg) on day 1 (Fig. 6A). Thereafter, approximately 50% to 85% of loaded siRNA (in the range of 20–30 μg) was deposited in the mouse paws during each treatment. The dose of control siRNA that was deposited on day 1, 5 and 9 was significantly ($p<0.05$) higher than that of CBL3 siRNA but the delivery of functional siRNA was never significantly higher than the control siRNA.

At day 10, mice were sacrificed and the treated skin area was harvested from three mice for RT-qPCR analysis (Fig. 6B). The level of hMGFP mRNA was reduced in two out of three mice, with mouse 2 and mouse 3 showing a mean relative hMGFP mRNA reduction of 49% and 38%, respectively. No gene silencing was detectable at the mRNA level in Mouse 1.

Intravital fluorescence images were captured every other day throughout the treatment regime (Fig. 6C provides examples). The images captured using the Maestro imaging system were compared to determine the effect of siRNA treatment on hMGFP protein expression

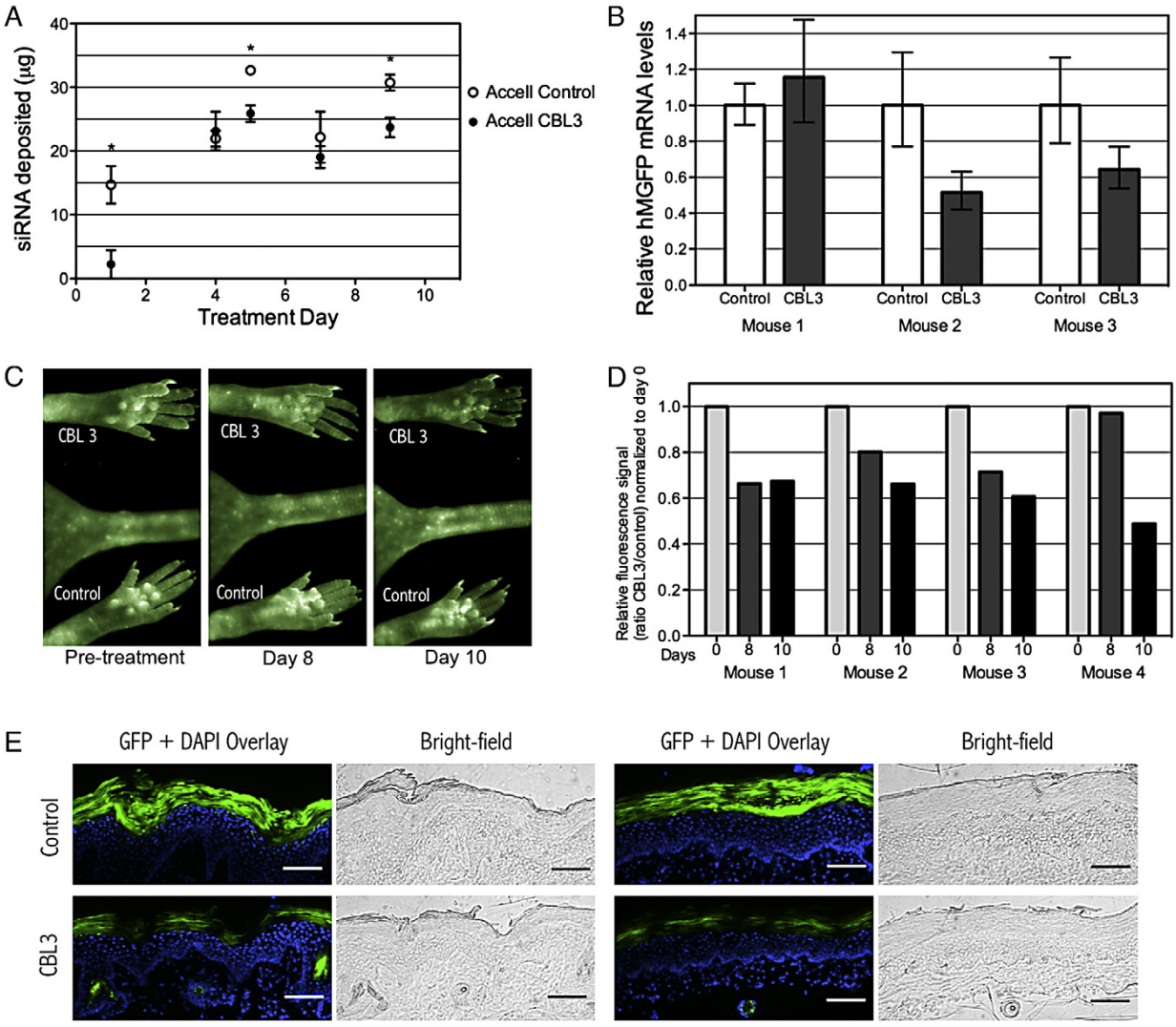

Fig. 6. hMGFP reporter gene and protein expression in transgenic CBL/hMGFP mouse paws microneedle treated with Accell CBL3 or control sd-siRNA over a 10-day treatment regime. (A) Mass of siRNA deposited in mouse paws from the dry-coated microneedle devices. siRNA deposition in skin was estimated by subtracting the quantity of siRNA remaining on the microneedle devices (10 microneedles) from the theoretical loaded quantity on treatment days 1, 4, 5, 7 and 9 of the 10-day regime. *Denotes a statistically significant ($p<0.05$; unpaired two-tailed t-test) difference between control and treatment groups. (B) RT-qPCR quantification of hMGFP mRNA expression. hMGFP mRNA levels from the CBL3 treated paw were quantified relative to the non-targeting control treated paw and normalised to CD44 endogenous gene control. Each column corresponds to the mean of three qPCR replicates and the error bars indicate standard error. (C) hMGFP expression in the paws of mouse 2 (as a representative example), imaged intravitally with the Maestro imaging system. Fluorescence is pseudocoloured green. (D) Quantification of hMGFP protein expression. Intravital images captured using the Maestro imaging system were processed through ImageJ and quantified. The ratio of the average signal of the CBL3 treated area and non-targeting control treated area is normalised to day 0 (pre-treatment). (E) Fluorescence microscopy of cross-sections (10 μm) of treated mouse paws following 10 days of treatment. hMGFP protein expression (or lack thereof) was visualised by fluorescence microscopy of samples from mouse paws treated with Accell non-targeting control (top panel) or CBL3 (bottom panel) sd-siRNA. Two sets of representative images are shown from different areas of the skin samples. In each set, the left panel shows the fluorescence overlay and the right panel shows the corresponding bright-field images. hMGFP fluorescence is pseudocoloured green. Nuclei were stained with DAPI and pseudocoloured blue. (Bar = 100 μm).

(Fig. 6D). The fluorescence signal intensity at the sites treated with microneedles coated with CBL3 siRNA showed a reduction in hMGFP protein expression after 8 and 10 days as compared to the paws administered with the non-targeting control siRNA. The reduction in signal intensity at day 10 ranged from 35% to 50%.

Paw skin from one mouse was also harvested and analysed using established histology methods to characterise the degree and depth of change in fluorescence signal intensity (Fig. 6E). Skin sections treated with the non-targeting control (upper panels of Fig. 6E) exhibit the intense GFP signal arising from the transgenic protein in the upper layers of the epidermis [29]. In the CBL3 treated paw (lower panels of Fig. 6E) the fluorescent signal is clearly reduced. These images, taken from two separate treatment areas, are representative of all the transverse sections of the analysed samples. Brightfield images (Fig. 6E) indicate that the stratum corneum is intact in the regions of low fluorescence, confirming that the depleted fluorescence is due to a reduction in protein rather than physical disruption of the skin.

4. Discussion

Greater understanding of the RNAi pathway is allowing researchers to study and modify gene function in an unprecedented way [4]. However, the lack of suitable and effective delivery tools for siRNA is a major barrier to clinical exploitation. For example, whilst siRNA has shown promise as an effective corrective therapy in severe genetic dermatological conditions, the conventional hypodermic needle and syringe delivery method was intolerable to patients [22]. Microneedles are able to penetrate the stratum corneum barrier of human skin in a minimally invasive manner [37,38] to enable effective nucleic acid delivery [31,32,39–44]. The use of steel microneedles to deliver molecules, macromolecules and vaccines, as a dried coating, is now well established [28,31,32,45,46]. However, this system has not previously been tested for the delivery of siRNA to skin.

In order for a coated microneedle delivery system to be effective, several factors need to be considered, including efficient and stable microneedle coating formulations and procedures, effective skin penetration performance and targeted and efficient drug deposition [28,45,47]. A drug formulation with sufficient viscosity and surface tension is important for uniform distribution of coated materials on the microneedle surface. A coating formulation that is sufficiently water-soluble is also important to enable the drug to dissolve quickly upon insertion of the microneedles into the skin [32]. Moreover, the mechanical strength and adhesive properties of a dried coating should be sufficient to retain contact with the microneedles during their insertion into skin [28]. siRNA is a small double-stranded RNA molecule that is highly water-soluble. Therefore, a simple aqueous formulation of fluorescently labelled siRNA was used to coat the surface of steel microneedles. The coating procedure, involving placing a formulation-loaded pipette tip over the microneedles, withdrawing, allowing 30 s for drying and then re-applying, led to a relatively reproducible and uniform coating of the microneedles. Using this method, we were able to load up to 40 μg of siRNA onto microneedles, which is an order of magnitude higher than the nanogram quantities of siRNA that have been loaded onto dissolvable microneedles in previous studies [30,33]. Following insertion into human skin and microscopic inspection of the microneedles, the coating dissolved leaving only residual fluorescence on the needle surface.

Having established a simple formulation and method to reproducibility coat appropriate quantities of siRNA onto steel microneedles, we further investigated the functional stability of the coated siRNA. Non-viral nucleic acid delivery commonly involves the use of lipid-based cationic transfection reagents to facilitate cell uptake and processing. The commercially available transfection reagent Lipofectamine™ RNAiMAX proved to be effective in transfecting the immortalised human keratinocyte cell line employed in this study, with no significant effect on cell toxicity (data not shown). This transfection reagent is also effective in transfecting cultured monolayer primary human keratinocyte cells isolated from excised human breast skin tissue (data not shown) and could potentially therefore be useful for *ex vivo* or *in vivo* applications.

When siRNA was coated onto microneedles, allowed to dry and recovered, the siRNA remained fully functional as evidenced by marked reduction of lamin A/C mRNA level and protein expression of lamin A/C in cells treated with siRNA. In contrast to this, the biological functionality of siRNA, when pre-complexed with Lipofectamine™ RNAiMAX diminished upon the microneedle coating, drying and recovery processes. We speculate that the coating and drying processes could result in a change in the structural conformation of the electrostatic lipoplex complex and/or compromised changes to the lipid reagent. It is known that nucleic acid–liposome complexes can form aggregates upon storage, resulting in reduced transfection efficiency and necessitating preparation of complexes immediately before administration [48]. A number of studies have however demonstrated the ability to freeze-dry, freeze-thaw or spray-dry siRNA-liposome and DNA–liposome complexes in the presence of sugars as lyoprotectants, with minimal effect on lipoplex functionality [48,49]. Indeed, as carbohydrate-enriched formulations have shown to improve the physical stability of nucleic acid, in this case plasmid DNA, upon microneedle coating [32,46], the value of these stability-enhancing formulations when coating siRNA onto steel microneedles is worthy of investigation in future studies.

Accell-modified “self-delivery” siRNA does not require a transfection agent to facilitate cell transfection. *In vitro* functionality studies revealed that following the coating and recovery process Accell sd-siRNA remained functional, as demonstrated by a significant reduction of CD44 mRNA expression in HaCaT cells treated with Accell sd-siRNA targeting the CD44 gene. Furthermore, as previous studies have shown gene silencing in skin treated with Accell sd-siRNA coated onto dissolvable microneedles [30,33] this form of sd-siRNA was used to assess the *in vivo* functionality of siRNA delivered *via* coated steel microneedles in a transgenic mouse model. The coating procedure described in this study was able to dry coat up to 40 μg of Accell sd-siRNA per array of 10 microneedles. Recovery and quantification of siRNA from microneedles following insertion into mouse model skin suggests that 50% to 85% of the coated siRNA was deposited in the mouse paw. The reduced deposition observed on treatment day 1 was likely attributable to inexperience in microneedle application in this model, leading to inadequate skin insertion. The delivery efficiency of nucleic acids from coated microneedles is a function of the coating formulation and its distribution on the needle, the depth of microneedle penetration into skin and the hydration status of the tissue proximal to the microneedles [32]. In this instance the major limitation is likely to be needle insertion depth, as it proved technically challenging to fully insert microneedles into the contoured footpad area. Moreover, the manual coating procedure inevitably results in some of the material being coated on the base of the microneedle device (Fig. 3). This material would not be deposited in the skin but would be quantifiable post-insertion. Nevertheless, both the actual dose and percentage deposited in the treatment area were significantly greater than previously reported, where an estimated dose of 120 ng siRNA (10% of coated dose) was administered using biodegradable microneedle arrays [30]. The greater utilization of coated material, with less wastage, could have important cost and efficacy implications when delivering expensive biological therapeutics using microneedles.

The transgenic mouse model used in the *in vivo* studies expresses GFP in the upper epidermis (granular layer and stratum corneum), enabling functional assessment of intradermally administered siRNA [29]. Visualisation and quantification of protein production, through fluorescence intensity, were used to determine gene silencing. Quantification of fluorescence intensity in the CBL3-treated mouse paw (but not the non-specific control-treated paw) indicates that microneedle

delivery of siRNA resulted in a discernible reduction in protein expression. The observed reduction in reporter protein signal was confirmed by fluorescence microscopy of skin sections, which illustrated a clear reduction in GFP signal in the upper regions of the epidermis, where the hMGFP protein is predominantly expressed in this model. Transverse sections confirmed that the reduction in fluorescence was not an artefact, *i.e.* it was attributable to reduced protein expression rather than physical disruption to the epidermis caused by the microneedle treatment. To determine siRNA gene silencing at the mRNA level, RT-qPCR quantification of hMGFP mRNA was performed from total RNA isolated from mice at the end of the 10-day treatment. The supportive, yet equivocal, nature of this mRNA data (a clear reduction of mRNA was seen in two out of the three mice tested) reflects the degree of challenge of inducing and analysing gene silencing *in vivo*. In *in vitro* studies, dividing cell monolayers can be exposed directly to high concentrations of siRNA and those cells can be easily recovered and characterised for gene expression. Accurately and reproducibly delivering siRNA to a three-dimensional tissue architecture and evaluating the functionality of the nucleic acid at a sub-cellular level within that tissue is a far greater challenge. Nevertheless, taken together, the protein and mRNA data presented in this study suggest that the siRNA coated onto, and released from, steel microneedles remains functional and can be effectively delivered to skin to facilitate localised gene silencing *in vivo*.

A major limiting factor for microneedle systems is the dosing capacity. Gonzalez-Gonzalez et al. have previously shown that delivery of Accell sd-siRNA from biodegradable microneedles can induce gene silencing in the paws of a similar transgenic CBL/hMGFP reporter mouse [30]. However, the loading capacity of these devices is restricted and thus dry-coated solid steel microneedles may provide an alternative for enhanced loading capacity [31,32]. The enhanced loading capacity of the steel microneedles did not translate to gene silencing efficiency above that observed in a previous microneedle study where an estimated 120 ng of siRNA was administered [30]. However, in the previous study, siRNA was delivered over a wider area using three separate arrays of 4×5 microneedles (60 in total) at each time-point compared to the single row of 10 microneedles that was employed in this study. It is possible that fewer microneedle penetrations could restrict the cell numbers exposed to the siRNA treatment, thus leading to a compromised gene silencing efficiency. It is also apparent however that publications targeting siRNAs to skin rarely observe a silencing effect in excess of 50% [29,30,33,50], regardless of siRNA dose or delivery method, and therefore a further reduction in gene expression may not be possible, even at greater delivered dose. Whilst the higher loading capacity achieved in our study lead to no obvious advantage in mouse skin over the biodegradable arrays used in this previous study, given the simplicity and improved loading capacity of steel microneedles, this may well be advantageous in human skin tissue in conditions where a larger dose of therapeutic siRNA needs to be delivered.

These results serve to demonstrate, for the first time, the ability to deliver siRNA using coated solid microneedles, resulting in reporter protein silencing *in vivo*. siRNA delivery using steel microneedles is attractive as such devices are simple and cost-effective for large-scale manufacture. Once coating formulations and processes are further optimised and automated, this system could provide a practical minimally invasive, patient-friendly, self-administration alternative for the delivery of therapeutic nucleic acids to the skin. Given these encouraging data the next stage is to determine the effectiveness of siRNA delivery using microneedles in human skin.

Acknowledgements

We would like to thank R.P. Hickerson for siRNA preparation and M.A. Flores for technical support (both *Transderm Inc*., *Santa Cruz*, *California*, *USA*). This work was funded in part through a grant from the NIH "GO Delivery!" Grant and Bowel Disease Research Foundation.

References

[1] A. Fire, S. Xu, M.K. Montgomery, S.A. Kostas, S.E. Driver, C.C. Mello, Potent and specific genetic interference by double-stranded RNA in *Caenorhabditis elegans*, Nature 391 (1998) 806–811.
[2] S.M. Elbashir, J. Harborth, W. Lendeckel, A. Yalcin, K. Weber, T. Tuschl, Duplexes of 21-nucleotide RNAs mediate RNA interference in cultured mammalian cells, Nature 411 (2001) 494–498.
[3] D. Guzman-Villanueva, I.M. El-Sherbiny, D. Herrera-Ruiz, A.V. Vlassov, H.D. Smyth, Formulation approaches to short interfering RNA and MicroRNA: challenges and implications, J. Pharm. Sci. 101 (2012) 4046–4066.
[4] D. Grimm, Small silencing RNAs: state-of-the-art, Adv. Drug Deliv. Rev. 61 (2009) 672–703.
[5] P.A. Khavari, O. Rollman, A. Vahlquist, Cutaneous gene transfer for skin and systemic diseases, J. Intern. Med. 252 (2002) 1–10.
[6] A. Naik, Y.N. Kalia, R.H. Guy, Transdermal drug delivery: overcoming the skin's barrier function, Pharm. Sci. Technol. Today 3 (2000) 318–326.
[7] V. Preat, N. Dujardin, Topical delivery of nucleic acids in the skin, S.T.P. Pharm. Sci. 11 (2001) 57–68.
[8] B. Geusens, N. Sanders, T. Prow, M. Van Gele, J. Lambert, Cutaneous short-interfering RNA therapy, Expert Opin. Drug Deliv. 6 (2009) 1333–1349.
[9] T. Ishimoto, Y. Takei, Y. Yuzawa, K. Hanai, S. Nagahara, Y. Tarumi, S. Matsuo, K. Kadomatsu, Downregulation of monocyte chemoattractant protein-1 involving short interfering RNA attenuates hapten-induced contact hypersensitivity, Mol. Ther. 16 (2008) 387–395.
[10] T. Inoue, M. Sugimoto, T. Sakurai, R. Saito, N. Futaki, Y. Hashimoto, Y. Honma, I. Arai, S. Nakaike, Modulation of scratching behavior by silencing an endogenous cyclooxygenase-1 gene in the skin through the administration of siRNA, J. Gene Med. 9 (2007) 994–1001.
[11] P. Ritprajak, M. Hashiguchi, M. Azuma, Topical application of cream-emulsified CD86 siRNA ameliorates allergic skin disease by targeting cutaneous dendritic cells, Mol. Ther. 16 (2008) 1323–1330.
[12] M. Nakamura, J. Jo, Y. Tabata, O. Ishikawa, Controlled delivery of T-box21 small interfering RNA ameliorates autoimmune alopecia (Alopecia Areata) in a C3H/HeJ mouse model, Am. J. Pathol. 172 (2008) 650–658.
[13] N. Nakai, T. Kishida, M. Shin-Ya, J. Imanishi, Y. Ueda, S. Kishimoto, O. Mazda, Therapeutic RNA interference of malignant melanoma by electrotransfer of small interfering RNA targeting Mitf, Gene Ther. 14 (2007) 357–365.
[14] N. Nakai, T. Kishida, G. Hartmann, N. Katoh, J. Imanishi, S. Kishimoto, O. Mazda, Mitf silencing cooperates with IL-12 gene transfer to inhibit melanoma in mice, Int. Immunopharmacol. 10 (2010) 540–545.
[15] K.P. Hoeflich, D.C. Gray, M.T. Eby, J.Y. Tien, L. Wong, J. Bower, A. Gogineni, J. Zha, M.J. Cole, H.M. Stern, L.J. Murray, D.P. Davis, S. Seshagiri, Oncogenic BRAF is required for tumor growth and maintenance in melanoma models, Cancer Res. 66 (2006) 999–1006.
[16] M. Jakobsen, K. Stenderup, C. Rosada, B. Moldt, S. Kamp, T.N. Dam, T.G. Jensen, J.G. Mikkelsen, Amelioration of psoriasis by anti-TNF-alpha RNAi in the xenograft transplantation model, Mol. Ther. 17 (2009) 1743–1753.
[17] M.A. Tran, R. Gowda, A. Sharma, E.J. Park, J. Adair, M. Kester, N.B. Smith, G.P. Robertson, Targeting V600EB-Raf and Akt3 using nanoliposomal-small interfering RNA inhibits cutaneous melanocytic lesion development, Cancer Res. 68 (2008) 7638–7649.
[18] A. Sharma, N.R. Trivedi, M.A. Zimmerman, D.A. Tuveson, C.D. Smith, G.P. Robertson, Mutant V599EB-Raf regulates growth and vascular development of malignant melanoma tumors, Cancer Res. 65 (2005) 2412–2421.
[19] G. Matsumoto, T. Kushibiki, Y. Kinoshita, U. Lee, Y. Omi, E. Kubota, Y. Tabata, Cationized gelatin delivery of a plasmid DNA expressing small interference RNA for VEGF inhibits murine squamous cell carcinoma, Cancer Sci. 97 (2006) 313–321.
[20] J. Tao, Y.T. Tu, C.Z. Huang, A.P. Feng, Q. Wu, Y.J. Lian, L.X. Zhang, X.P. Zhang, G.X. Shen, Inhibiting the growth of malignant melanoma by blocking the expression of vascular endothelial growth factor using an RNA interference approach, Br. J. Dermatol. 153 (2005) 715–724.
[21] J.Y. Kim, J.Y. Shin, M.R. Kim, S.K. Hann, S.H. Oh, siRNA-mediated knock-down of COX-2 in melanocytes suppresses melanogenesis, Exp. Dermatol. 21 (2012) 420–425.
[22] S.A. Leachman, R.P. Hickerson, M.E. Schwartz, E.E. Bullough, S.L. Hutcherson, K.M. Boucher, C.D. Hansen, M.J. Eliason, G.S. Srivatsa, D.J. Kornbrust, F.J. Smith, W.I. McLean, L.M. Milstone, R.L. Kaspar, First-in-human mutation-targeted siRNA phase Ib trial of an inherited skin disorder, Mol. Ther. 18 (2009) 442–446.
[23] S.A. Leachman, R.P. Hickerson, P.R. Hull, F.J. Smith, L.M. Milstone, E.B. Lane, S.J. Bale, D.R. Roop, W.H. McLean, R.L. Kaspar, Therapeutic siRNAs for dominant genetic skin disorders including pachyonychia congenita, J. Dermatol. Sci. 51 (2008) 151–157.
[24] S. Coulman, C. Allender, J. Birchall, Microneedles and other physical methods for overcoming the stratum corneum barrier for cutaneous gene therapy, Crit. Rev. Ther. Drug Carrier Syst. 23 (2006) 205–258.
[25] S. Kaushik, A.H. Hord, D.D. Denson, D.V. McAllister, S. Smitra, M.G. Allen, M.R. Prausnitz, Lack of pain associated with microfabricated microneedles, Anesth. Analg. 92 (2001) 502–504.
[26] M.I. Haq, E. Smith, D.N. John, M. Kalavala, C. Edwards, A. Anstey, A. Morrissey, J.C. Birchall, Clinical administration of microneedles: skin puncture, pain and sensation, Biomed. Microdevices 11 (2009) 35–47.
[27] H.S. Gill, D.D. Denson, B.A. Burris, M.R. Prausnitz, Effect of microneedle design on pain in human volunteers, Clin. J. Pain. 24 (2008) 585–594.
[28] Y.-C. Kim, J.H. Park, M.R. Prausnitz, Microneedles for drug and vaccine delivery, Adv. Drug Deliv. Rev. (2012), http://dx.doi.org/10.1016/j.addr.2012.1004.1005.

[29] E. Gonzalez-Gonzalez, H. Ra, R.P. Hickerson, Q. Wang, W. Piyawattanametha, M.J. Mandella, G.S. Kino, D. Leake, A.A. Avilion, O. Solgaard, T.C. Doyle, C.H. Contag, R.L. Kaspar, siRNA silencing of keratinocyte-specific GFP expression in a transgenic mouse skin model, Gene Ther. 16 (2009) 963–972.
[30] E. Gonzalez-Gonzalez, T.J. Speaker, R.P. Hickerson, R. Spitler, M.A. Flores, D. Leake, C.H. Contag, R.L. Kaspar, Silencing of reporter gene expression in skin using siRNAs and expression of plasmid DNA delivered by a soluble protrusion array device (PAD), Mol. Ther. 18 (2010) 1667–1674.
[31] E. Gonzalez-Gonzalez, Y.C. Kim, T.J. Speaker, R.P. Hickerson, R. Spitler, J.C. Birchall, M.F. Lara, R.H. Hu, Y. Liang, N. Kirkiles-Smith, M.R. Prausnitz, L.M. Milstone, C.H. Contag, R.L. Kaspar, Visualization of plasmid delivery to keratinocytes in mouse and human epidermis, Sci. Rep. 1 (2011) 158.
[32] M. Pearton, V. Saller, S.A. Coulman, C. Gateley, A.V. Anstey, V. Zarnitsyn, J.C. Birchall, Microneedle delivery of plasmid DNA to living human skin: Formulation coating, skin insertion and gene expression, J. Control. Release 160 (2012) 561–569.
[33] M.F. Lara, E. Gonzalez-Gonzalez, T.J. Speaker, R.P. Hickerson, D. Leake, L.M. Milstone, C.H. Contag, R.L. Kaspar, Inhibition of CD44 gene expression in human skin models, using self-delivery short interfering RNA administered by dissolvable microneedle arrays, Hum. Gene Ther. 23 (2012) 816–823.
[34] R.P. Hickerson, F.J. Smith, R.E. Reeves, C.H. Contag, D. Leake, S.A. Leachman, L.M. Milstone, W.H. McLean, R.L. Kaspar, Single-nucleotide-specific siRNA targeting in a dominant-negative skin model, J. Invest. Dermatol. 128 (2008) 594–605.
[35] P. Boukamp, R.T. Petrussevska, D. Breitkreutz, J. Hornung, A. Markham, N.E. Fusenig, Normal keratinization in a spontaneously immortalized aneuploid human keratinocyte cell line, J. Cell Biol. 106 (1988) 761–771.
[36] R.P. Hickerson, A.V. Vlassov, Q. Wang, D. Leake, H. Ilves, E. Gonzalez-Gonzalez, C.H. Contag, B.H. Johnston, R.L. Kaspar, Stability study of unmodified siRNA and relevance to clinical use, Oligonucleotides 18 (2008) 345–354.
[37] J.C. Birchall, Microneedle array technology: the time is right but is the science ready? Expert Rev. Med. Devices 3 (2006) 1–4.
[38] S.A. Coulman, J.C. Birchall, A. Alex, M. Pearton, B. Hofer, C. O'Mahony, W. Drexler, B. Povazay, In vivo, in situ imaging of microneedle insertion into the skin of human volunteers using optical coherence tomography, Pharm. Res. 28 (2011) 66–81.
[39] J. Birchall, S. Coulman, M. Pearton, C. Allender, K. Brain, A. Anstey, C. Gateley, N. Wilke, A. Morrissey, Cutaneous DNA delivery and gene expression in ex vivo human skin explants via wet-etch micro-fabricated micro-needles, J. Drug Target. 13 (2005) 415–421.
[40] J.C. Birchall, C. Marichal, L. Campbell, A. Alwan, J. Hadgraft, M. Gumbleton, Gene expression in an intact ex-vivo skin tissue model following percutaneous delivery of cationic liposome–plasmid DNA complexes, Int. J. Pharm. 197 (2000) 233–238.
[41] F. Chabri, K. Bouris, T. Jones, D. Barrow, A. Hann, C. Allender, K. Brain, J. Birchall, Microfabricated silicon microneedles for nonviral cutaneous gene delivery, Br. J. Dermatol. 150 (2004) 869–877.
[42] S.A. Coulman, D. Barrow, A. Anstey, C. Gateley, A. Morrissey, N. Wilke, C. Allender, K. Brain, J.C. Birchall, Minimally invasive cutaneous delivery of macromolecules and plasmid DNA via microneedles, Curr. Drug Deliv. 3 (2006) 65–75.
[43] K.W. Ng, M. Pearton, S. Coulman, A. Anstey, C. Gateley, A. Morrissey, C. Allender, J. Birchall, Development of an ex vivo human skin model for intradermal vaccination: tissue viability and Langerhans cell behaviour, Vaccine 27 (2009) 5948–5955.
[44] M. Pearton, C. Allender, K. Brain, A. Anstey, C. Gateley, N. Wilke, A. Morrissey, J. Birchall, Gene delivery to the epidermal cells of human skin explants using microfabricated microneedles and hydrogel formulations, Pharm. Res. 25 (2008) 407–416.
[45] H.S. Gill, M.R. Prausnitz, Coated microneedles for transdermal delivery, J. Control. Release 117 (2007) 227–237.
[46] Y.C. Kim, F.S. Quan, R.W. Compans, S.M. Kang, M.R. Prausnitz, Formulation and coating of microneedles with inactivated influenza virus to improve vaccine stability and immunogenicity, J. Control. Release 142 (2010) 187–195.
[47] H.S. Gill, M.R. Prausnitz, Coating formulations for microneedles, Pharm. Res. 24 (2007) 1369–1380.
[48] P.C. Seville, I.W. Kellaway, J.C. Birchall, Preparation of dry powder dispersions for non-viral gene delivery by freeze-drying and spray-drying, J. Gene Med. 4 (2002) 428–437.
[49] P. Yadava, M. Gibbs, C. Castro, J.A. Hughes, Effect of lyophilization and freeze-thawing on the stability of siRNA-liposome complexes, AAPS PharmSciTech 9 (2008) 335–341.
[50] T. Hsu, S. Mitragotri, Delivery of siRNA and other macromolecules into skin and cells using a peptide enhancer, Proc. Natl. Acad. Sci. U. S. A. 108 (2011) 15816–15821.